TRANSPORT OF THIOPEPTIDES ACROSS THE OUTER MEMBRANE

TONB-DEPENDENT TRANSPORT OF THIOPEPTIDE ANTIBIOTICS TO KILL GRAM-NEGATIVE PATHOGENS

By CHUK-KIN DEREK CHAN, B.Sc.

A Thesis Submitted to the School of Graduate Studies in Partial Fulfillment of the Requirements for the Degree Doctor of Philosophy

McMaster University DOCTOR OF PHILOSOPHY (2023) Hamilton, Ontario (Chemistry & Chemical Biology)

TITLE: TonB-Dependent Transport of Thiopeptide Antibiotics to Kill Gram-Negative Pathogens

AUTHOR: Chuk-Kin Derek Chan, B.Sc.

SUPERVISOR: Lori L. Burrows, Ph.D.

NUMBER OF PAGES: xix, 279

Foreword

Lay Abstract

Antibiotic resistance is a growing crisis that threatens modern medicine, and it is becoming more challenging to discover truly new antibiotics to combat this threat. Intrinsic resistance conferred by the outer membrane of Gram-negative bacteria restricts the entry of many antibiotics, especially larger antibiotics that would otherwise inhibit the growth of Gram-positive bacteria. Consequently, there are fewer treatment options for infections caused by Gram-negative bacteria and developing new antibiotics that can cross the outer membrane remains a significant challenge in drug discovery. My work describes the discovery of a class of antibiotics that can bypass the outer membrane using specific outer-membrane nutrient transporters. Using biochemical, structural biology, fluorescence microscopy, and molecular biology techniques, we uncover the molecular determinants of uptake of these antibiotics for their respective transporters. These results can inform the design of novel narrow-spectrum antibiotics that can overcome the outer membrane barrier to combat antimicrobial resistance.

Abstract

The outer membrane (OM) of *P. aeruginosa* is a semi-permeable barrier that contributes to antibiotic resistance by reducing uptake. Finding strategies to circumvent this barrier is a major challenge. One approach involves screening in physiologically relevant conditions to identify novel activity in existing molecules. We discovered that thiostrepton (TS), a thiopeptide antibiotic with no reported activity against Gram-negative bacteria, hijacks the pyoverdine siderophore transporters FpvA and FpvB to cross the OM under iron limitation to inhibit translation. Using TS, we subsequently showed that FpvB is not primarily a pyoverdine transporter, but rather a promiscuous transporter for siderophores ferrichrome and ferrioxamine B. Our work with TS suggested that other thiopeptides may use siderophore transporters for entry into the cell. This hypothesis led to a screen to identify other thiopeptides with activity against *P. aeruginosa*, uncovering two other thiopeptides, thiocillin and micrococcin, that use the ferrioxamine transporter FoxA for uptake. We discovered another siderophore, bisucaberin, could also use FoxA for uptake and our collaborators solved the crystal structure of bisucaberin bound to FoxA. Through biochemical approaches, we characterized how FoxA accommodates structurally distinct ligands. Finally, we screened known large natural product antibiotics with no pseudomonal activity under nutrient limitation and discovered that the glycopeptide vancomycin inhibits growth by blocking peptidoglycan crosslinking. This pilot screen emphasizes the importance of screening for antibiotics under physiologically relevant conditions to avoid overlooking potential hits. Overall, the findings from these studies can be used to guide medicinal chemistry efforts to develop novel siderophore-antibiotic conjugates for the treatment of *P. aeruginosa* infections. These results also help us gain a deeper understanding of the mechanism of binding and uptake through siderophore transporters and the range of substrates that can be taken up.

Acknowledgements

Lori – who would have thought that we would work on siderophores and iron transporters? Besides all the puns we could make, the project was fun and intellectually stimulating. Thank you for giving me the creative freedom to explore all the different avenues but reining me back in when I went on a tangent. Thank you for your tremendous support, enthusiasm, and advice over the past five years. I enjoyed our discussions trying to understand more about TonB-dependent transporters and your Slack messages with new ideas. It has been an absolute pleasure to have you as my supervisor. I am a better writer and communicator because of your help, which I will carry forward in my next role wherever it may be. To my committee members, Marie and Gerry, thank you for all of your advice, support, and enthusiasm for my work. Your questions and feedback pushed me further and have made me a better scientist and critical thinker.

My PhD journey would not have been possible without my present lab members Hanjong, Luke, Victoria, Ikram, Veronica, and Nathan. I enjoyed our nights bowling, skating, having dinner, and conversations. To Hanjeong, thank you for always being so willing to help whenever I had a roadblock and for teaching me so many things in lab and in life. I would be remiss to exclude Anne and Katie, who were a big part of my early graduate career. Finally, a big thank you to undergraduate senior thesis students, Irene, Mahrukh, and Katherine who helped tremendously on two papers. To my friends and family, none of this would have been possible without you. To my mom, thank you for your patience and support. Especially for driving me back to Hamilton on the weekends and packing extra food that I can't make myself. A big thank you is owed to Karen, who helped me edit a lot of my writing and listen to me rant. Finally, to my partner and best friend, Sherlyn, thank you for listening to me rant, for being supportive, and being happy for me even for the tiniest accomplishments. You were my greatest support.

Table of Contents

Foreword iii

Lay Abstract iii

Abstract iv

Acknowledgements v

Table of Contents vi

List of Figures xi

List of Tables xv

List of abbreviations xvii

Declaration of academic achievement xix

Chapter One: The Outer Membrane Barrier of *Pseudomonas aeruginosa* 1

Preface 2

Introduction 3

Lipopolysaccharides (LPS) 3
Porins 5
Efflux Pumps 6
TonB-Dependent Transporters (TBDTs) 7
Siderophores and TBDTs of *P. aeruginosa* 10
Exploiting TBDTs for uptake across the OM 11
Thiopeptide antibiotics 12

Purpose and goals of the thesis 19

References 21

Chapter Two: Thiostrepton Hijacks Siderophore Transporters to Cross the Outer Membrane of *P. aeruginosa* 30

Preface 31

Abstract 32

Introduction 33

Results 34

Thiostrepton stimulates *P. aeruginosa* biofilm formation 34
Growth in minimal media increases susceptibility of *P. aeruginosa* to TS 35
The ribosomal methyltransferase Tsr protects *P. aeruginosa* against TS 36
TS susceptibility increases in the presence of iron chelators 37
TS hijacks pyoverdine receptors FpvA and FpvB 40
TS is active against clinical isolates 42

Discussion 43

Methods 48

Bacterial strains and culture conditions....48
Growth curves....48
Biofilm modulation assay....49
Compounds screened....50
Construction of a *tsr* plasmid for expression in *P. aeruginosa*....51
Serum Preparation....51
MIC and checkboard assays....52
Clinical isolates testing....53
CAS Plate Assay....53
Generation of efflux mutants....53

Acknowledgements....54

References....55

Supplementary Figures....59

Supplementary Tables....63

Supplementary References....78

Chapter Three: *Pseudomonas aeruginosa* FpvB is a High-Affinity Transporter for Xenosiderophores Ferrichrome and Ferrioxamine B....79

Preface....80

Abstract....81

Introduction....82

Results....84

FpvB is a transporter for ferrichrome and ferrioxamine B....88
FpvB has higher affinity for ferrichrome and ferrioxamine B than pyoverdine....90
Molecular determinants of TS, ferrichrome, and ferrioxamine B uptake through FpvB....94

Discussion....101

Methods and Materials....106

Strains and primers....106
Compounds and media....106
Molecular biology....107
MIC assays....109
Checkerboard assays....109
Microscopy, fluorescence quenching, and recovery assay....110
Outer-membrane preparations, SDS PAGE, and Western Blots....111
Mutants resistant to TS....112
Structural Comparisons and Docking....113

References....114

Supplementary Figures....118

Supplementary Tables....124

Chapter Four: Thiocillin Exploits the Ferrioxamine Transporter for Uptake 128

Preface 129

Synopsis 130

Introduction 131

Results 134

Thiocillin activity against *P. aeruginosa* requires the FoxA receptor and the TonB system 134
Thiocillin acts through its canonical mechanism of protein synthesis inhibition 139
Thiocillin and Deferasirox Susceptibility is Strain- and Species-Specific 141

Discussion 144

Methods and Materials 146

Bacterial Strains and Culture Conditions 146
Chemicals and Compounds 147
Cloning and Transformation Procedures 147
Dose Response and Checkerboard Assays 147
IC_{50} Measurements 148
Isolation of Crude *B. cereus* Extracts 149
Mass Spectrometry 149

Acknowledgements 149

References 150

Supplementary Figures 153

Supplementary Tables 155

Chapter Five: Interactions of TonB-dependent Transporter FoxA with Siderophores and Antibiotics that Affect Binding, Uptake, and Signal Transduction 157

Preface 158

Abstract 159

Significance 159

Introduction 160

Results 163

Bisucaberin exclusively uses the FoxA receptor for uptake 163
At least five residues in FoxA are essential for thiocillin susceptibility 165
Siderophores compete with thiocillin for binding and uptake 169
Residues that impact thiocillin uptake are important for stimulation of FoxA expression by nocardamine 174
Sequence conservation of L8 is low and the loop is important for ligand uptake 177

Discussion 179

Material and Methods 181
MIC assays 182
Docking of ligands into FoxA 182
Checkerboard assays 183
Molecular Biology 183
Cysteine labeling, fluorescence quenching, and recovery assays 185
Microscopy 186
Promoter assays 186
Outer membrane preparations 187
SDS-PAGE and Western Blots 187
Thiocillin uptake assays, HPLC, and mass spectrometry 188
Bisucaberin-FoxA co-crystallization and data collection 189
Phylogenetic Tree, ortholog identification, and sequence alignments 190
Acknowledgements 191
References 192
Supporting Information 195
Chapter Six: Nutrient Limitation Sensitizes *P. aeruginosa* to Vancomycin 216
Preface 217
Abstract 218
Results 221
Vancomycin inhibits *P. aeruginosa* growth in an iron and copper-dependent manner 221
Activity is vancomycin-specific and not due to decreased outer membrane integrity 223
Loss of DacB and DacC leads to vancomycin resistance 226
Spontaneous vancomycin resistant mutants harbour mutations in the CpxSR two-component system 228
Activation of CpxS confers resistance to multiple classes of β-lactams 232
A WapR P164T vancomycin-resistant mutant has altered LPS composition and increased phage sensitivity in nutrient-limited media 234
Discussion 239
Conclusion 243
Methods 244
Media and Growth Conditions 244
Bacterial strains, phage, and plasmids 244
Molecular Biology 244
Compounds 244
MIC and Checkerboards assays 244
NPN assay 245
Fluorescence microscopy 245
Transposon library screening and WCC vancomycin susceptibility testing. 246

Spontaneous vancomycin-resistant *P. aeruginosa* 246
Genomic DNA isolation and sequencing 247
LPS isolation (whole cell and phenol/ethyl ether extraction) 247
SDS-PAGE and Western blot 248
Silver stain 248
Phage isolation, purification, and plaquing assays 249
Acknowledgments 250
References 251
Supplementary Information 258
Supplementary References 265
Chapter Seven: Discussion and future directions 266
References 277

List of Figures

Chapter One

Figure 1. The *P. aeruginosa* outer membrane is partly composed of LPS and proteins. 5

Figure 2. Architecture of TBDTs. 8

Figure 3. TBDTs of *P. aeruginosa* and the siderophore types they recognize. 10

Figure 4. Thiopeptide antibiotics are classified based on the number of members in the core macrocyclic ring. 13

Figure 5. The proposed mechanisms of action of 26- and 29-membered thiopeptide antibiotics. 15

Chapter Two

Figure 1. Thiostrepton stimulates *P. aeruginosa* biofilm formation. 35

Figure 2 Expression of Tsr *in trans* reduces susceptibility of *P. aeruginosa* to thiostrepton. 37

Figure 3. Thiostrepton activity is potentiated by iron chelators and serum. 39

Figure 4. Thiostrepton inhibits growth of clinical isolates. 43

Figure 5. Thiostrepton does not bind iron. 45

Supplementary Figure 1. Growth of *P. aeruginosa* PAO1 in various media. 59

Supplementary Figure 2. Thiostrepton susceptibility in Mueller-Hinton Broth versus 10:90. ..59

Supplementary Figure 3. Thiostrepton susceptibility is unaffected by addition of Mg^{2+} or casamino acids, or deletion of peptide transporters. 60

Supplementary Figure 4. Susceptibility of *P. aeruginosa* efflux mutants to thiostrepton. 61

Supplementary Figure 5. Checkerboard assays of various antibiotics with deferasirox (DSX).61

Supplementary Figure 6. *Acinetobacter baumannii* encodes homologs of *P. aeruginosa* FpvA and FpvB. 62

Chapter Three

Figure 1. Structures of compounds used in this study. 83

Figure 2. FpvB is required for growth with ferrichrome and ferrioxamine B in the absence of FiuA and FoxA. 87

Figure 3. FpvB interacts with ferrichrome, ferrioxamine B, and pyoverdine. 91

Figure 4. Molecular determinants of TS, ferrichrome, and ferrioxamine B uptake through FpvB. 96

Figure 5. FpvB single residue mutants are stably expressed but have reduced affinity for siderophores.....100

Figure 6. Model for thiopeptide and siderophore uptake through the TBDTs FpvA, FpvB, FoxA, and FiuA in P. aeruginosa. 103

Supplementary Figure 1......119

Supplementary Figure 2. Checkerboard assays of PA14 Δ*fpvA* Δ*fpvB* complemented with *fpvA* and *fpvB in trans* with TS and siderophores.....119

Supplementary Figure 3. Overlay of FpvA and FpvB showing residues mutated to cysteine for labeling with maleimide dyes.....120

Supplementary Figure 4......121

Supplementary Figure 5.....122

Supplementary Figure 6......123

Chapter Four

Figure 1. Structures of thiopeptides tested for activity against *P. aeruginosa*.....133

Figure 2. SM, TC, and MC checkerboards with DSX against PA14. 134

Figure 3. TC activity requires FoxA and the TonB system.....136

Figure 4. TC is potentiated by human serum through iron restriction. 138

Figure 5. Mutation at P26 of RplK protects *P. aeruginosa* against TC. 140

Figure 6. The effects of TC+DSX against *P. aeruginosa* clinical isolates.....142

Supplementary Figure 1. FoxA is specific for TC and FpvA is specific for TS. 153

Supplementary Figure 2. PA14, *exbB1*, and *exbB2* mutants challenged with TC+DSX. 154

Supplementary Figure 3. Serum-free controls.....154

Chapter Five

Figure 1. Thiocillin and siderophores use FoxA to cross the outer membrane. 162

Figure 2. Bisucaberin is taken up through FoxA. 164

Figure 3. Identifying FoxA residues important for thiocillin, nocardamine, and bisucaberin uptake. 169

Figure 4. Thiocillin competes with nocardamine-Fe^{3+} for FoxA. 171

Figure 5. FoxA single-residue mutants are defective in nocardamine signaling. 176

Figure 6. Conservation of amino acid sequences of FoxA orthologs at residues important for thiocillin susceptibility. 178

Supplementary Figure 1. OMIT electron density map for bisucaberin$_3$(blue)-$Fe^{3+}{}_2$ (orange)-FoxA (grey). 195

Supplementary Figure 2. Screening for permissive locations on FoxA for insertion of FLAG or V5 epitopes. 196

Supplementary Figure 3. Only nocardamine antagonizes thiocillin uptake. 197

Supplementary Figure 4. Screening for permissive cysteine-labeling sites for FoxA that allow WT responses to nocardamine. 199

Supplementary Figure 5. Labeled single residue mutants have reduced affinity for nocardamine-Fe^{3+} and addition of thiocillin further reduces the K_d. 200

Supplementary Figure 6. Confocal microscopy images of AlexaFluor 594 labeled FoxA A614C with amino acid mutations. 201

Supplementary Figure 7. Fluorescence quenching of labeled FoxA and FoxA mutants by bisucaberin with and without thiocillin. 202

Supplementary Figure 8. Summary of phenotypes of FoxA mutants. 202

Supplementary Figure 9. Raw and labeled blots. 203

Chapter Six

Figure 1. Vancomycin inhibits *P. aeruginosa* under nutrient-limited conditions. 223

Figure 2. Glycopeptide activity is vancomycin specific and vancomycin acts through its canonical mechanism of action. 225

Figure 3. Identifying genes important for vancomycin resistance. 227

Figure 4. Point mutations in CpxS confer resistance to vancomycin. 231

Figure 5. CpxSR activation confers resistance to β-lactams. 233

Figure 6. WapR P164T is resistant to vancomycin and azithromycin and has altered LPS profiles. 235

Figure 7. WapR P164T has larger plaques in LB and increased phage susceptibility in 10:90. 238

Supplementary Figure S1. Checkerboard assays of vancomycin with $MgCl_2$ and $CaCl_2$ against PA14. 258

Supplementary Figure S2. WapR P164T is not labeled by FITC-vancomycin.....259

Supplementary Figure S3. 260

Supplementary Figure S4. Vancomycin MIC assays with PA14 *cpxS*::Mar2xT7 with empty vector, expressing WT PA14 *cpxS*, and CpxS T163P in 10:90 + 0.25% arabinose.....260

Supplementary Figure S5. Checkerboard assays of vancomycin with $FeCl_3$ and $CuCl_2$ against Δ*cpxR*, CpxS T163P, and CpxS T163P Δ*cpxR*. 261

Supplementary Figure S6. WapR P164T mutant is not sensitized to pilus-specific phages in LB or 10:90.....261

Supplementary Figure S7. Growth curves of PA14, WapR P164T, *wapR*::Mar2xT7, Δ*pilA*, and CpxS T163P in 10:90. Results are averaged from three independent biological replicates.....262

Chapter Seven

Figure 1. The SURFAR Platform. 274

List of Tables

Chapter Two

Table 1. Susceptibility of *P. aeruginosa* PA14 mutants to thiostrepton in VBMM. 41

Supplementary Table 1. Hits from the screen 63

Supplementary Table 2. Antibiogram of WCC PA1 Clinical Isolates 72

Supplementary Table 3. Primers used to generate *P. aeruginosa* efflux mutants 77

Chapter Three

Supplementary Table 1. Strains used in this study 124

Supplementary Table 2. Primers used in this study 125

Chapter Four

Table 1. Summary of MIC values for wild type, mutant, and recombinant PA14 strains challenged with TC or TC+DSX. 137

Table 2. Thiopeptides inhibit protein synthesis in a coupled *in vitro* transcription/translation system using *E. coli* ribosomes 139

Table 3. Thiopeptide combinations are Pseudomonas specific with interstrain and interspecies differences in susceptibility 144

Supplementary Table 1. Strains used in this study. 155

Supplementary Table 2. Primers used in this study. 155

Supplementary Table 3. Accession numbers for *rplK, fpvA, foxA,* and *tonB1* 156

Supplementary Table 4. Panel of Transposon Mutants Used to Screen for TC and MC resistance. 156

Chapter Five

Supplementary Table 1. FoxA data collection and refinement statistics 204

S**upplementary Table 2.** Summary of K_d values from WT and mutants treated with nocardamine and thiocillin 205

Supplementary Table 3. List of Strains 205

Supplementary Table 4. List of Primers 210

Chapter Six

Supplementary Table S1. List of Compounds in the Initial Screen.....262

Supplementary Table S2. Strains used in this study.....263

Supplementary Table S3. Primers used in this study.....263

Supplementary Table S4. Compounds used in this study.....264

List of abbreviations

10:90	10% Lysogeny Broth: 90% Phosphate Buffered Saline
aatRNA	Aminoacyl-Transfer Ribonucleic Acid
AP	Alkaline Phosphatase
BCIP	5-Bromo-4-Chloro- 3-Indoyl Phosphate
CAA	Casamino Acids
CAS	Chrome Azurol S
CCCP	Carbonyl Cyanide-m-Chlorophenyl Hydrazone
CPA	Common Polysaccharide Antigen
DFP	Deferiprone
DHFR	Dihydrofolate Reductase
DI	Deionized
DIBI	Denying Iron to Bacterial Infections
DMSO	Dimethyl Sulfoxide
DNA	Deoxyribonucleic Acid
DSX	Deferasirox
DTT	Dithiothreitol
EDDHA	Ethylenediamine-N,N'-bis(2-hydroxyphentlacetic acid)
EF-4	Elongation Factor 4
EF-G	Elongation Factor G
EF-Tu	Elongation Factor Tu
FDA	Food and Drug Administration
FIC	Fractional Inhibitory Concentration
GDP	Guanosine Diphosphate
GTP	Guanosine Triphosphate
IC_{50}	Half-Maximal Inhibitory Concentration
IPTG	Isopropyl β-D-1-thiogalactopyranoside
K_d	Dissociation Constant
LB	Lysogeny Broth
LC MS	Liquid Chromatography Mass Spectrometry
LPS	Lipopolysaccharide
MC	Micrococcin
MHB	Mueller-Hinton Broth
MIC	Minimal Inhibitory Concentration
MOA	Mechanism of Action
MRSA	Methicillin-Resistant *Staphylococcus aureus*
NADPH	Reduced Nicotinamide Adenine Dinucleotide Phosphate
NBT	Nitro-Blue Tetrazolium
NPN	1-N-phenylnaphtylamide

NMR	Nuclear Magnetic Resonance
OSA	O-specific antigen
OM	Outer Membrane
PBP	Penicillin Binding Protein
PBS	Phosphate Buffered Saline
PCR	Polymerase Chain Reaction
PDB	Protein Data Bank
PIA	*Pseudomonas* Isolation Agar
RiPPs	Ribosomally Synthesized and Post-Translationally Modified Peptides
RNA	Ribonucleic Acid
RPM	Revolutions per Minute
SM	Siomycin
SURFAR Platform	Surface Receptor Platform
TBDT	TonB-Dependent Transporter
TBS	Tris buffered saline
TC	Thiocillin
TEV	Tobacco Etch Virus
TIP	Thiostrepton Induced Protein
TS	Thiostrepton
UDP-GluUA	Uridine-Diphosphate Glucuronic Acid
VBMM	Vogel Bonner Minimal Media
WT	Wild type
YT	Yeast Tryptone

Declaration of academic achievement

I have performed all the research in this body of work except where indicated in the preface of each chapter.

Chapter One: The Outer Membrane Barrier of *Pseudomonas aeruginosa*

Preface

The thiopeptide section presented in the following chapter has been published in:

Chan, D.C.K. and Burrows L. L. (2020). Thiopeptides with unique chemical structures and diverse biological activities. *The Journal of Antibiotics.* 74, 161-175.
https://doi.org/10.1038/s41429-020-00387-x

That material was shortened and modified for this introduction.

D.C. and L.L.B. wrote the manuscript.

Introduction

P. aeruginosa is a ubiquitous bacterium found naturally in the environment, but it can cause opportunistic disease in plants and animals, including humans. Its ability to thrive in nutrient-limiting conditions and across wide pH and temperature ranges allows it to colonize various sites of the body and cause disease. *P. aeruginosa* infections are typically treated with β-lactams alone – e.g. ceftazidime – or in combination with a β-lactamase inhibitor, e.g. piperacillin + tazobactam. Use of other antibiotic classes including quinolones (e.g. ciprofloxacin) or aminoglycosides (tobramycin) may be necessary. However, *P. aeruginosa* can quickly develop resistance to these antibiotics and many isolates already display resistance to most first-line antibiotics. In these cases, novel β-lactam + β-lactamase inhibitor combinations have been developed, including meropenem-vaborbactam that works against most isolates. However, in the case where an isolate is resistant to all standard of care antibiotics, last resort therapies such as colistin may be used, but these can have significant adverse effects on the patient. In addition to its adaptability, *P. aeruginosa* also forms prolific biofilm communities whose structure reduces antibiotic uptake. Extracellular DNA and anionic polysaccharides in the biofilm matrix also trap positively-charged antibiotics such as the aminoglycosides. The biofilm itself presents as a physical barrier which reduces drug penetration and physiological heterogeneity within a biofilm can also allow a subset of cells to survive, adapt, and grow in the presence of antibiotic.

Lipopolysaccharides (LPS)

One of the reasons that *P. aeruginosa* can exhibit resistance to so many antibiotics is due to its OM. The OM contributes to the intrinsic resistance of Gram-negative bacteria because it prevents the passive diffusion of charged and hydrophilic molecules, and molecules whose size

exceeds ~600 Da[1-4]. This characteristic reduces the concentration of antibiotic inside the cell – potentially at sub-lethal concentrations – which gives the bacteria time to activate different stress response mechanisms including increased expression of drug efflux pumps, mutate, and survive. The outer membrane is composed of an asymmetric bilayer with a phospholipid inner leaflet and a liposaccharide (LPS) outer leaflet. The OM of *P. aeruginosa* is especially formidable, being 100-fold less permeable compared to that of *Escherichia coli*[1–4]. The outer leaflet is embedded with a heterogeneous composition of LPS, porins, receptors, transporters, and efflux pumps (Figure 1). LPS is embedded in the outer leaflet of the OM through the hydrophobic lipid A component. Lipid A is composed of two glucosamine units in a β(1→6) linkage with one phosphate group on each sugar unit at the 1' and 4' positions and predominantly penta-acyl chains[5,6]. The core LPS consists of the inner and outer core. The relatively conserved inner core consists of two D-*manno*-oct-2-ulosonic acid and two L-*glycero*-D-*manno*-heptose residues. The two heptose residues are phosphorylated at the 2' and 4' positions of the first heptose and at the 6' end of the second. In *P. aeruginosa,* the outer core consists of one D-galactosamine bound to three or four D-glucose units and one L-rhamnose, which is specifically added by the glycosyltransferase WapR and is the site of O-antigen attachment or MigA, leading to an uncapped LPS core[7,8]. *P. aeruginosa* can make capped (with O antigen) or uncapped LPS cores. The length of the O-antigen can also vary between strains[5]; therefore, the overall composition of LPS on the cell surface is heterogeneous and changes in its chemistry can contribute to antibiotic resistance[9–12]. The phosphates of lipid A and LPS core contribute to the net negative charge of LPS and create repulsion between adjacent molecules. Divalent cations such as magnesium and calcium stabilize these interactions and are important for membrane integrity. Antibiotics that can compete with divalent cations, like cationic antimicrobial peptides, can permeabilize the OM[11]. In *P. aeruginosa,* mutations in the two-component sensor

PmrB lead to activation of multiple genes, including the *arn* operon which catalyzes the covalent addition of 4-amino-4-deoxy-L-arabinose to lipid A[11]. The addition of these sugars stabilizes the LPS and prevents cationic antimicrobial peptides from binding. In *E. coli*, mutations in the O-antigen ligase WaaL can lead to incorporation of peptidoglycan precursors that bind vancomycin, to prevent entry of the antibiotic into the cell[13].

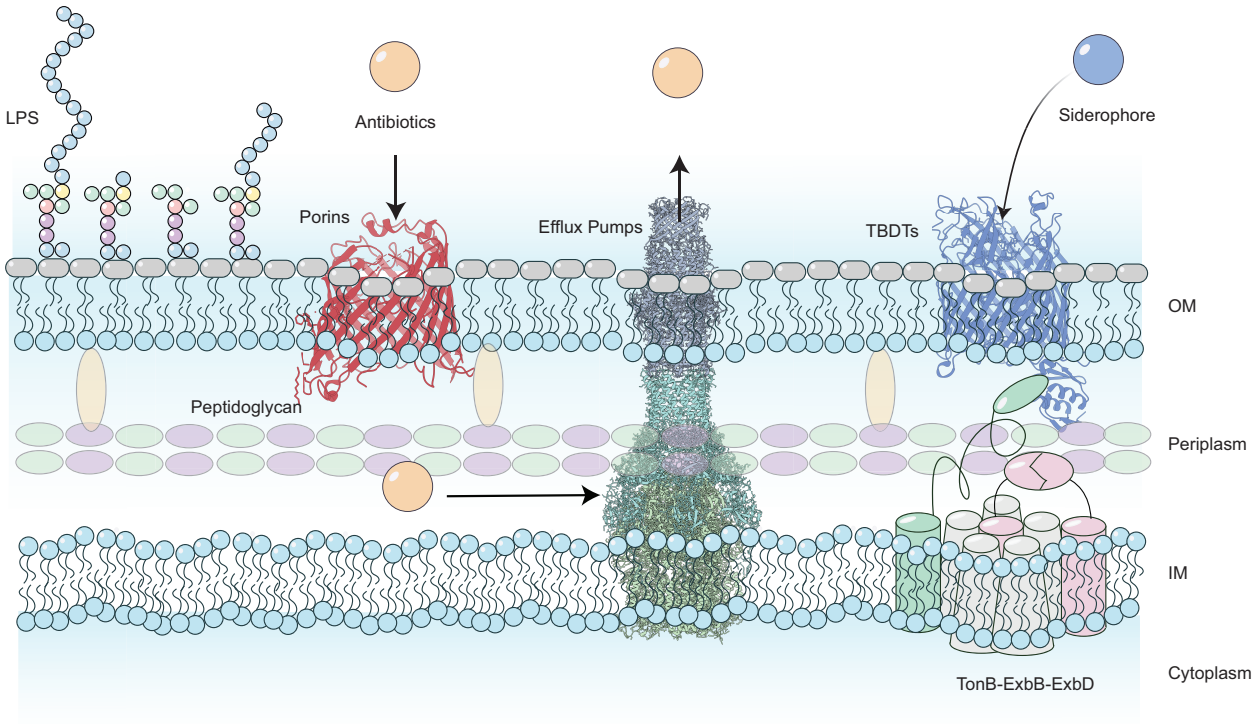

Figure 1. The *P. aeruginosa* outer membrane is partly composed of LPS and proteins. Representative structures of a porin from OprD (PDB: 3SY7), efflux pump from MexAB-OprM (PDB: 6TA5), and TBDT from FpvA (2IAH) are shown.

Porins

The ~600 Da size exclusion limit cut off was based on studies of the OmpF porin from *E. coli*[1,3,4,14–17] although more recent studies have shown that some porins in other bacteria can take up much larger molecules[2]. Nevertheless, porins are important for the uptake of various antibiotic classes due to their lack of specificity. Porins are β-barrel structures that vary in size (8-18 β-

strands) that form open water-filled channels in the OM to allow the diffusion of smaller solutes and antibiotics[18]. Specific porins such as the abundant OprF protein of *P. aeruginosa* can be in a "closed" state, which can limit the diffusion of molecules through the channel[19]. OprF also has a role in biofilm formation[20,21]. OprD is involved in carbapenem uptake, and resistance can arise from reduced OprD expression and amino acid mutations[22–25]. Despite this observation, a recent study using a *P. aeruginosa* isolate lacking all 40 porins suggested that antibiotics could still cross the OM and that OprD only played a small role in carbapenem uptake[26]. The addition of carboxylate groups to molecules reduced their uptake, consistent with the idea that charged molecules have difficulty crossing the OM.

Efflux Pumps

Efflux pumps are another important mechanism of resistance to antibiotics in *P. aeruginosa*. Antibiotics that enter the cell can be expelled via these systems. There are different classes of efflux pumps; however, among the best characterized systems are the resistance nodulation division type efflux pumps including MexAB-OprM, MexCD-OprJ, and MexXY-OprM, which extrude multiple classes of antibiotics[27]. MexB, D, or Y are inner membrane transporters that are linked to their respective OM channels (OprM/J) through an adaptor or fusion protein MexA, C, or X, forming a tripartite system. The membrane transporters form an asymmetric homotrimer with their respective hexameric adaptor protein that then is connected to the homotrimeric outer membrane channel[28,29]. The adaptor or fusion protein is important in pump assembly[30] and allows energy from the proton motive force to power extrusion[31]. Mutations in *nalD* can activate efflux pump expression constitutively, leading to resistance. Alternatively, mutations in the repressor MexR, which modulates expression of MexAB-OprM, can also lead to

constitutive expression of the efflux pump[32,33]. Additionally, activation of the two-component system CpxSR in *P. aeruginosa* increases expression of MexA[34]. Overall, the intracellular antibiotic concentration depends on the amount that can cross the OM and how much is effluxed out of the cell.

TonB-Dependent Transporters (TBDTs)

Also found in the outer membrane are specific proteins called TonB-dependent transporters (TBDTs). TBDTs are 22-stranded beta-barrels with a lumen occluded by a N-terminal plug (Figure 2)[35]. The plug prevents passive diffusion of large molecules through the transporter. Most of the best characterized transporters are involved in uptake of siderophores and xenosiderophores although some are involved in the uptake of vitamin B12[36], other metals[37–39], and carbohydrates[40]. Siderophores are natural products that have high affinity for iron[41]. Iron at physiologically relevant condition exists in its ferric form and is prone to formation of insoluble hydroxide complexes, making it poorly bioavailable. Therefore, siderophores function as diffusible iron-scavenging molecules. Siderophore-iron complexes are taken up through specific OM TBDTs. The number of TBDTs depends on the genus and species, but also the nature of the environment. In *P. aeruginosa*, there are 35 TBDTs whereas some *Bacteroides* spp. have over 100 predicted TBDTs. The specific functions of most are not known, although there appears to be a correlation between the number of TBDTs and the nutrient availability in an environment[42].

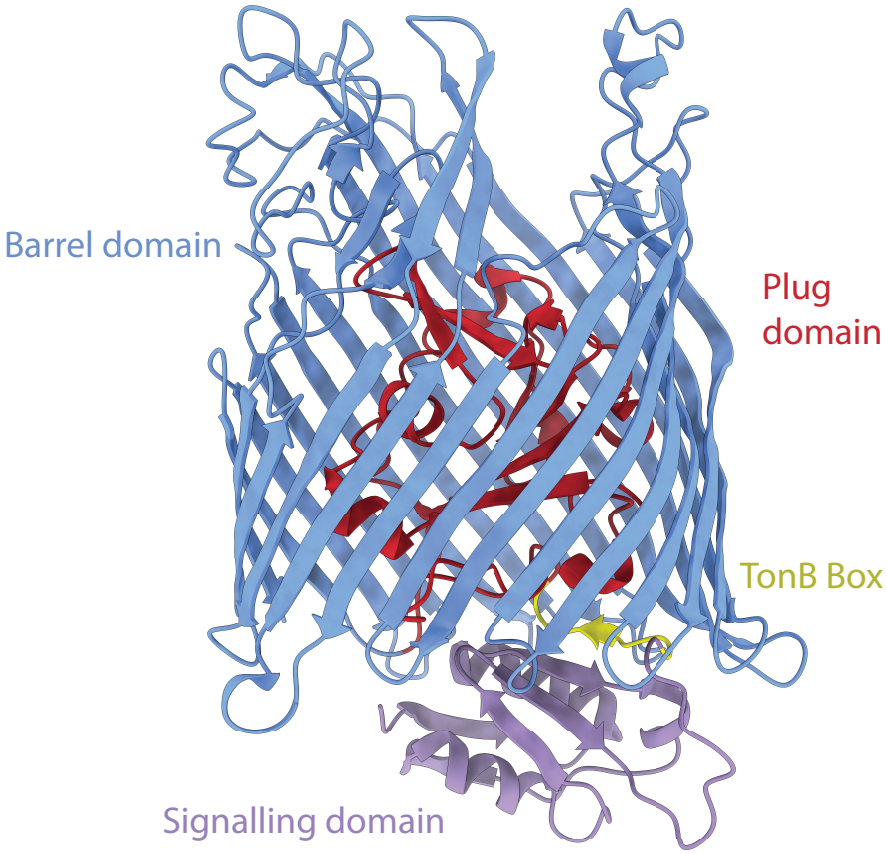

Figure 2. Architecture of TBDTs. Different domains are highlighted. As an example, FpvA from *P. aeruginosa* (PDB: 2W75) is shown. The signalling domain is not present in all TBDTs.

When a ligand specific for a transporter interacts with certain residues on the transporter, a series of conformational changes that are not fully understood occur, leading to the release of a short N-terminal periplasmic motif known as the TonB box (Figure 2) that forms hydrogen bonds with the C-terminus of TonB through beta-augmentation. TonB is part of an inner membrane complex with two other proteins, ExbB-ExbD (Figure 1). X-ray crystallography and cryo-electron microscopy structures of the ExbB-ExbD complex show that ExbB forms a pentamer around an ExbD dimer that functions as a proton channel, although other studies suggest that hexameric ExbB-trimeric ExbD complexes also exist, depending on pH[43,44]. The exact mechanism in which

protons pass through the channel is unknown; however, ExbD is hypothesized to act as a piston to "pump" electrons or undergoes a rotary motion that drives proton movement[43]. Overall, the proton motive force transferred via ExbB-ExbD drives conformational changes in TonB[35]. These conformational changes are then relayed to the transporter via the interaction between TonB and the TonB box and are thought to lead to the formation of a channel in the plug or complete removal of the plug to allow the substrate to enter. Both ideas are controversial as no studies have shown whether either of these events occur; however, there is evidence that supports both hypotheses[45,46].

The extracellular loops of the barrel and the plug itself are involved in ligand substrate specificity, but also in downstream signalling. Some transporters have an extended N-terminus with a signalling domain (Figure 2) that interacts with an inner membrane anti-sigma/sigma factor pair. Ligand uptake can lead to poorly characterized conformational changes in the transporter that leads to cleavage of the anti-sigma/sigma factor pair[47–49]. This event releases part of the complex from the inner membrane to the cytoplasm, where the sigma factor can bind upstream of the relevant transporter gene to recruit RNA polymerase and increase expression. The exact signaling determinants are unknown; however, uptake through a receptor can occur without triggering the signalling cascade[50,51].

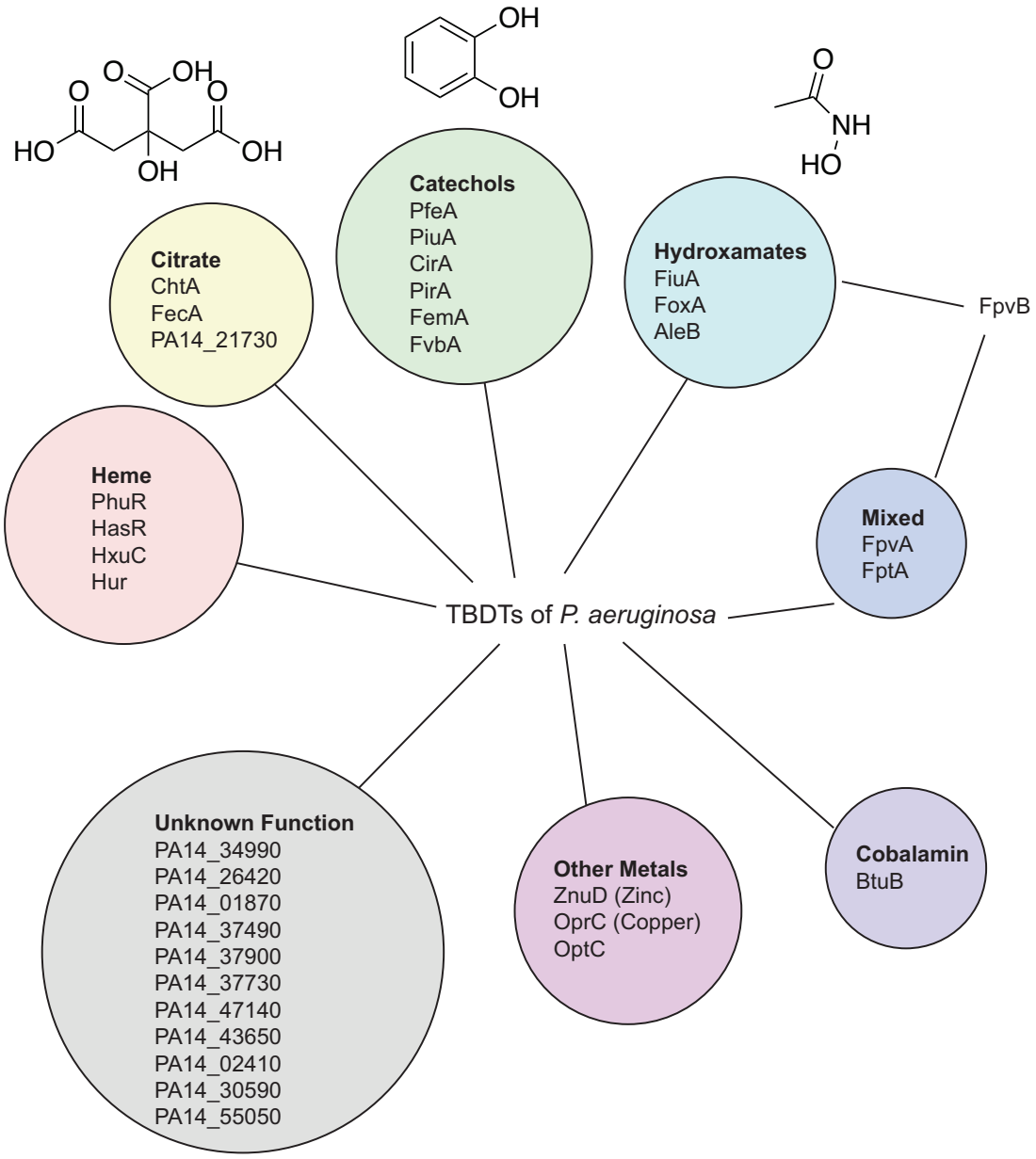

Figure 3. TBDTs of *P. aeruginosa* and the siderophore types they recognize. Structures for citrate, catechol, and hydroxamate type siderophores are shown. Our work has shown that FpvB recognizes siderophores with mixed chelating groups (hydroxamate + catechol from pyoverdine) and hydroxamate-type siderophores.

Siderophores and TBDTs of *P. aeruginosa*

P. aeruginosa makes two main siderophores, pyoverdine and pyochelin, with high and low affinity for iron respectively. Pyoverdine is taken up by at least two TBDTs, FpvA and FpvB (**f**erri-

pyo**v**erdine A and B)[52,53]. *P. aeruginosa* also encodes 33 other TBDTs that can presumably recognize xenosiderophores produced by other microbes (Figure 3). This arsenal includes FoxA and FiuA which take up the hydroxamate siderophores ferrioxamine, made by *Streptomyces* spp., and ferrichrome, made by fungi, respectively[49]. At least two transporters are responsible for the uptake of enterobactin, which is produced by Enterobacteriaceae, and belongs to the catechol group of siderophores[54,55]. The transporters for two other catechol siderophores mycobactin[56] and vibriobactin[57], are also known. ChtA, which was identified based on sequence similarity to the *E. coli* IutA transporter, takes up at least three siderophores of bacterial and fungal origin including aerobactin, rhizobactin, and schizokinen, which belong to the citrate-type siderophores[58]. Finally, four transporters have also been identified for heme[59–61]. Overall, while the substrates for some TBDTs are known, there are still substantial gaps in our understanding. We do not understand the function of the remaining transporters, nor do we understand the molecular details of substrate selectivity for TBDTs with known ligands.

Exploiting TBDTs for uptake across the OM

Some natural products have evolved to exploit TBDTs for uptake in a phenomenon known as the Trojan Horse strategy. For example, the lassopeptide microcin J25 uses the FhuA transporter of *E. coli* and some *Salmonella* spp. to cross the OM[62,63]. Rifabutin, a semi-synthetic rifamycin derivative, is taken up through FhuE of *Acinetobacter baumannii*[64]. Another rifamycin derivative, CGP 4382, uses FhuA for entry[65]. The sideromycins salmycin and albomycin exploit their resemblance to the hydroxamate siderophores[66]. Interestingly, they lack activity against *P. aeruginosa*. The pyocins, bacteriocins produced by Pseudomonads, can hijack the pyoverdine and heme transporters[46,61], and bacteriophages that target *E. coli* can use TBDTs for entry[67,68]. Natural

products have inspired the development of synthetic antibiotics that also mimic siderophores and many research groups have attempted to conjugate different siderophores to existing antibiotics. In 2019, the FDA approved the first siderophore-cephalosporin conjugate, cefiderocol, which is a combination of cefepime, ceftazidime, and a catechol moiety that binds iron[69]. Cefiderocol is taken up through the TBDTs PiuA and PirA in *P. aeruginosa*[70]. Overall, there is interest in the development of natural and synthetic antibiotics that can cross the OM via the Trojan Horse strategy.

Thiopeptide antibiotics

Another group of natural products that has been regaining interest is the thiopeptides, which have potent antibacterial activity against Gram-positive bacteria. Thiopeptides are thiazole-containing peptide antibiotics with complex structures of ribosomal origin (Figure 4). They belong to a larger class of natural products called ribosomally synthesized and posttranslationally modified peptides (RiPPs)[71]. They have three main components —a central pyridine ring, a core macrocyclic ring, and a tail. The tail extends from the central pyridine ring while the macrocyclic ring is connected by the central pyridine. The macrocyclic ring is decorated with various amino acids as well as thiazole, oxazole, and thiazoline substituents. Some thiopeptides have a secondary side ring with unique chemical moieties.

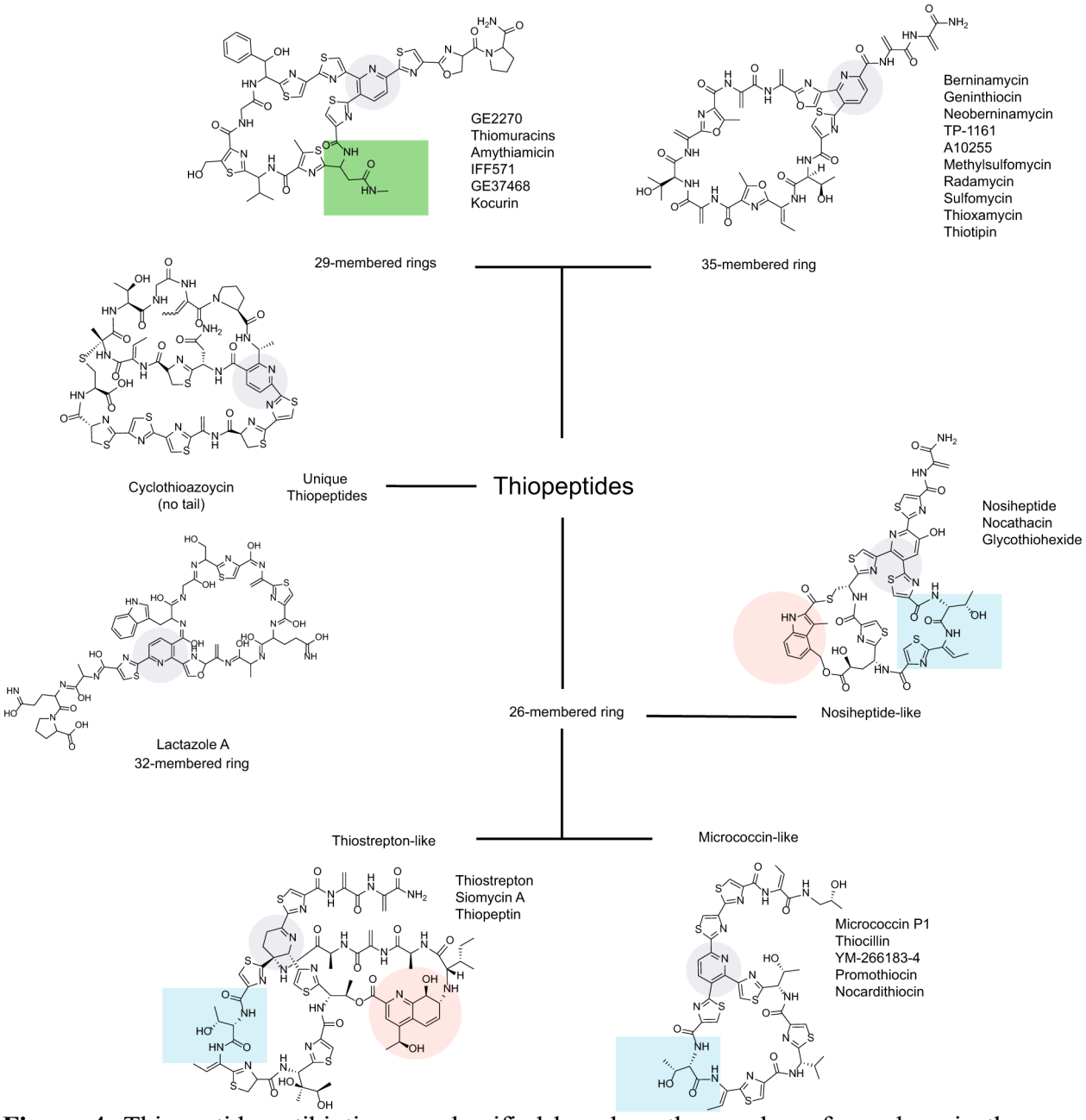

Figure 4. Thiopeptide antibiotics are classified based on the number of members in the core macrocyclic ring. Thiopeptides with 26-, 29-, and 35-membered macrocycles are grouped separately. The structure of thiostrepton is shown for the thiostrepton-like thiopeptides, micrococcin for the micrococcin-like thiopeptides, nosiheptide for the nosiheptide-like thiopeptides, GE2270 for those with 29-membered rings, and berninamycin for those with 35-membered rings. The names of structurally related thiopeptides are listed with each example. The unique quinaldic acid and indole moieties of thiostrepton and nosiheptide respectively are highlighted in red. The conserved Asn residue required for antibiotic activity in 29-membered thiopeptides is boxed in green. Conserved residues involved in TipA stimulation are boxed in blue. The central pyridine ring is highlighted in gray. Thiocillin is nearly identical to micrococcin with a 3-hydroxyvaline versus valine. Lactazole A has a 32-membered ring and lacks antibacterial activity.

Thiopeptides were first discovered in sewage samples by Su[72]. He identified a *Micrococcus* species that produced a compound with potent activity against other Gram-positive but not Gram-negative bacteria and named the compound micrococcin. Since then, over 100 thiopeptides have been discovered from a variety of marine and soil sources[73]. A recent study suggested there could be up to 400 distinct thiopeptides, based on the amino acid sequences of unique enzymes that perform [4 + 2] cycloadditions [13]. The [4 + 2] cycloaddition reaction is an essential step in biosynthesis and forms the central pyridine ring found in all thiopeptides (Figure 4, gray circles)[74–76]. Moreover, this enzyme differentiates them from closely related RiPPs, making this a selective method for identifying new thiopeptides[77]. Thiopeptides can be classified through two means. The first is a chemical identification system based on the oxidation state of the central pyridine ring—series a, b, c, d, and e[78]. The second classification is based on the number of residues in the core macrocyclic ring that encompasses the central pyridine, which can be 26, 29, 32, or 35-membered. The number of residues is related to a particular thiopeptide's biological activity and mechanism of action.

Despite their diversity, thiopeptides were never introduced in the clinic due to their low bioavailability, poor solubility, and complex synthesis. However, their potent in vitro and in vivo activity and complicated biosynthetic pathways have captivated many biochemists, while their challenging structures pose a significant challenge for organic chemists. Recent efforts to discover new thiopeptides through bioinformatics showed that there are many unique variants, including some with a Gram-negative origin, from *Serratia marcescens*[79,80]. None have yet been isolated to support those predictions.

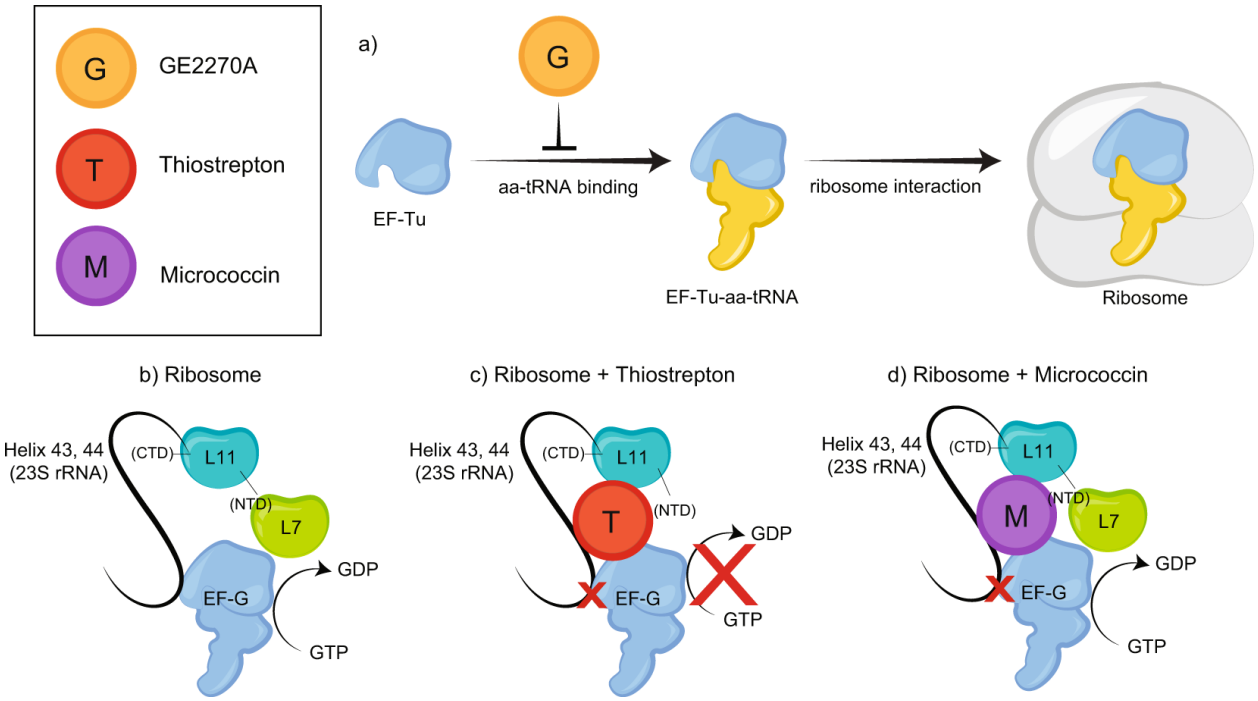

Figure 5. The proposed mechanisms of action of 26- and 29-membered thiopeptide antibiotics. a 29-membered antibiotics like GE2270A inhibit the formation of the EF-Tu–aa-tRNA complex. b The normal activity of a ribosome. The C-terminal domain (CTD) of L11 interacts with helix 43 and 44 of the 23S rRNA. The N-terminal domain is associated with L7. EF-G interacts with the NTD, L7 and helix 43 and 44. EF-G converts GTP to GDP for proper ribosomal activity. c Thiostrepton prevents binding of EF-G and inhibits the activity of EF-G. d Micrococcin does not prevent binding of EF-G to L7 and conversion of GTP to GDP occurs; however, the binding of EF-G to the helices is inhibited which prevents proper ribosomal activity.

Antibiotic activity, resistance, and additional biological activities

Thiopeptides are protein synthesis inhibitors whose exact mechanism of action depends on the number and type of residues in the core macrocycle[78]. Twenty six-membered macrocycles such as thiostrepton, nosiheptide, micrococcin, and thiocillin, as well as thirty five-membered macrocycles such as berninamycin and geninthiocin, bind at the interface of ribosomal protein L11 and the 23S rRNA (helix 43 and 44) of the bacterial 50S ribosomal subunit (Figure 5)[81–86]. This interaction affects GTPase elongation factor-G (EF-G), which is required for mRNA and tRNA translocation. However, the exact mechanism by which thiostrepton affects EF-G function is under debate. Early studies suggest that thiostrepton prevents stable binding of EF-G to the ribosome and

this is the general consensus[87,88]. This notion was contradicted by one group who showed that thiostrepton inhibits the turnover of EF-G, rather than its binding to the ribosome, preventing further processing after the initial round of GTP hydrolysis[89]. Another study revisiting the inhibitory mechanism renewed support for the idea that thiostrepton inhibits stable EF-G binding, and demonstrated inhibition of another elongation factor (EF-4)[85]. While more work is required to reconcile these discrepancies, it is generally agreed that EF-G binding is impacted (Figure 5). Conversely, micrococcin has a slightly different mechanism although it also belongs to the 26-membered group. Micrococcin treatment increased the conversion of GTP to GDP by EF-G[90]. Crystallographic studies revealed that micrococcin treatment prevents EF-G binding to helices 43 and 44 of the rRNA similar to thiostrepton; however, EF-G retains its GTPase activity and interacts with L7, which binds to the N-terminus of L11 (Figure 5)[90].

Streptomyces azureus, which produces thiostrepton, resists self-intoxication through methylation of the 23S rRNA at A1067[86,91,92]. Nucleotide substitutions at A1067 also confer resistance to micrococcin, and berninamycin-producing *Streptomyces* encode a RNA methylase similar to that of thiostrepton producers that makes them resistant[81,93,94]. Separate studies showed that thiostrepton has little to no inhibitory activity on eukaryotic ribosomes, promising for further development[95].

The 29-membered macrocycles such as GE2270 inhibit binding of elongation factor Tu (EF-Tu) to the aminoacyl-tRNA (aa-tRNA) (Fig. 3)[96]. Point mutations G257S or G257A in EF-Tu led to resistance[97]. The G257S mutation increases affinity for aa-tRNA, whereas the G257A mutation leads to decreased affinity for both EF-Tu and the antibiotic. Crystal structures of EF-Tu in complex with GTP and GE2270 showed steric clashes between the mutant residues and GE2270, and suggested that when GTP is bound, GE2270 is dislodged. The 29-membered

thiopeptides have a conserved Asn residue in the macrocyclic ring (Figure 4, green box). Codon randomization experiments showed that changing this position to other amino acids abolished antibacterial activity[98].

Since many *Streptomyces* spp. produce thiostrepton, the producers are resistant to the antibiotic, and it is used as a tool in *Streptomyces* genetics[99,100]. However, researchers noticed that thiostrepton induced the production of a number of proteins, which were termed thiostrepton-induced proteins (TIPs)[101,102]. TipAL is a transcriptional activator belonging to the MerR family, and interacts via its C-terminus with a dehydroalanine residue on thiostrepton. A second TIP, TipAS, is nearly identical to TipAL except it lacks 109 amino acids at the N-terminus, but still binds thiopeptides in the same manner[103,104]. TipAS and TipAL are encoded by the same open reading frame, but from different translational start sites. The N-terminus of TipAL binds to the *tipA* promoter. The TipAL–thiostrepton complex then activates the transcription of *tipA* leading to the increased production of TipAS[101,103,105]. Only a subset of thiopeptides induce *tipA* promoter expression, presumably due to differences in the thiopeptide tail and the pyridine ring[100]. TipA expression is common in *Streptomyces* that do not produce thiopeptides, whereas producers express the Tsr methyltransferease that blocks thiopeptide binding to ribosomes. TipA is thought to mediate drug resistance by sequestering thiopeptides and preventing them from reaching the target[106]. This phenomenon has been exploited in the search for novel thiopeptides, and screens of *tipA* promoter activity led to the discovery of promothiocins A and B[107]. The 26-membered thiopeptides have a conserved region (highlighted in blue, Fig. 2) that is responsible for stimulating TipA expression. The unique thiopeptides lactazole (32-membered) and radamycin (35-membered) lack antibacterial activity but while radamycin can activate TipA expression, this has not been reported for lactazole[108,109]. The production of thiopeptides lacking antibacterial activity

suggested that this family of antibiotics may also play a role in cell–cell signaling. This notion was supported by Bleich et al., who showed that thiocillin stimulated *B. subtilis* biofilm formation, independent of its antibacterial activity[110].

Thiocillin, a 26-membered thiopeptide, is produced by *Bacillus cereus*. Stimulation of biofilm formation in *B. subtilis*[110] was consistent with other studies showing that sub-minimal inhibitory concentrations (sub-MIC) of several classes of antibiotics have similar effects[111–114]. In *B. subtilis*, the biofilm stimulation response resulted from activation of both histidine kinase-dependent and -independent pathways by thiocillin. Thiopeptides may have a role in cell–cell signaling, while their limited aqueous solubility suggests that these molecules act in close proximity to the producer strain. Their precise biological role remains an avenue for future exploration.

Purpose and goals of the thesis

This body of work arose from a screen for compounds that stimulated *P. aeruginosa* biofilm formation at sub-inhibitory concentrations, suggesting that at higher concentrations, growth will be inhibited. The screen led to the discovery described in Chapter 2, where we showed that the stimulatory compound TS crosses the OM using the pyoverdine transporters FpvA and FpvB of *P. aeruginosa*, and inhibits growth through its canonical mechanism of action of ribosome inhibition. The general dogma for uptake through TBDTs was that individual transporters specifically recognize sets of structurally-related ligands, yet pyoverdine and TS share no structural similarities. This disconnect prompted the question: How is TS recognized by the FpvA and FpvB TBDTs? In Chapter 3, the project expanded to investigate how TS interacts with the transporters using molecular docking, site-directed mutagenesis, and fluorescence quenching. We found that while it was a poor pyoverdine transporter, FpvB was a high-affinity transporter for two hydroxamate xenosiderophores, ferrichrome and ferrioxamine B, whose uptake mechanisms were only partially understood. This work filled the gap in knowledge about the uptake of the two siderophores and corrected existing literature that stated FpvB was primarily a secondary pyoverdine transporter. We found that all uptake of all ligands relied on a single Tyr residue within an aromatic binding pocket, suggesting that structurally different ligands can bind and be taken up through TBDTs as long as certain interactions with the transporter are maintained.

Since TS is only one example of the thiopeptide family, we wondered if other thiopeptides could similarly hijack siderophore transporters to enter the cell. This led to the work in Chapter 4, where we discovered that TC uses the FoxA transporter for nocardamine to enter the cell. This was the first report of an antibiotic that can use the FoxA transporter of *P. aeruginosa*. In Chapter 5, we expanded on this discovery, identifying an additional xenosiderophore, bisucaberin, that could also use FoxA. We solved the co-crystal structure of bisucaberin bound to FoxA and identified

residues important for binding and uptake of bisucaberin, thiocillin, and the native ligand nocardamine. Binding and uptake for most TBDTs is incompletely understood, and our work revealed how these three ligands can each interact in slightly different ways with FoxA. Another poorly understood characteristic of TBDTs is the signalling response that leads to increased expression in the presence of relevant ligands, because only a subset of TBDTs have a signalling domain. Through this work, we found that the signalling response occurs as early as the initial binding event and that signalling can be uncoupled from uptake, as thiocillin failed to trigger signalling despite being taken up through FoxA.

The discovery of thiostrepton and thiocillin activity against *P. aeruginosa* under nutrient-limited conditions described in Chapters 2 and 4 prompted a screen in low iron media of other large natural product antibiotics reported to lack Gram negative activity. Among the resulting hits was the glycopeptide, vancomycin, which exhibited low micromolar activity that was dependent on LPS composition. These data supported our hypothesis that the potential anti-Pseudomonal activity of many antibiotics was overlooked because they were initially screened in nutrient-replete conditions, while bacteria normally grow in more nutrient-limiting conditions.

Chapter 7 brings together the major findings and outlines future directions for strategies to understand the substrate specificity of various TBDTs, how thiopeptides cross the IM, considerations for developing new siderophore-antibiotic conjugates, and emphasizes the advantages of screening in nutrient-limited media for the discovery of novel activity from existing antibiotics. To address the limited understanding of the range of substrates that can be taken up through TBDTs, we created a panel of *P. aeruginosa* TBDT-overexpression strains (SURFAR, for Surface Receptors). SURFAR has potential use for characterizing uptake pathways for bacteriophages, bacteriocins, siderophores, metals, and other nutrients.

References

(1) Yoshimura, F.; Nikaido, H. Permeability of *Pseudomonas aeruginosa* Outer Membrane to Hydrophilic Solutes. *J Bacteriol* **1982**, *152* (2), 636–642.
(2) van den Berg, B.; Prathyusha Bhamidimarri, S.; Dahyabhai Prajapati, J.; Kleinekathöfer, U.; Winterhalter, M. Outer-Membrane Translocation of Bulky Small Molecules by Passive Diffusion. *Proceedings of the National Academy of Sciences* **2015**, *112* (23), E2991–E2999. https://doi.org/10.1073/pnas.1424835112.
(3) Nikaido, H. Molecular Basis of Bacterial Outer Membrane Permeability Revisited. *Microbiology and Molecular Biology Reviews* **2003**, *67* (4), 593–656. https://doi.org/10.1128/MMBR.67.4.593-656.2003.
(4) Cowan, S.; Garavito, R.; Jansonius, J.; Jenkins, J.; Karlsson, R.; König, N.; Pai, E.; Pauptit, R.; Rizkallah, P.; Rosenbusch, J.; Rummel, G.; Schirmer, T. The Structure of OmpF Porin in a Tetragonal Crystal Form. *Structure* **1995**, *3* (10), 1041–1050. https://doi.org/10.1016/S0969-2126(01)00240-4.
(5) Huszczynski, S. M.; Lam, J. S.; Khursigara, C. M. The Role of *Pseudomonas aeruginosa* Lipopolysaccharide in Bacterial Pathogenesis and Physiology. *Pathogens* **2019**, *9* (1), 6. https://doi.org/10.3390/pathogens9010006.
(6) Pier, G. B. *Pseudomonas aeruginosa* Lipopolysaccharide: A Major Virulence Factor, Initiator of Inflammation and Target for Effective Immunity. *Int J Med Microbiol* **2007**, *297* (5), 277–295. https://doi.org/10.1016/j.ijmm.2007.03.012.
(7) Poon, K. K. H.; Westman, E. L.; Vinogradov, E.; Jin, S.; Lam, J. S. Functional Characterization of MigA and WapR: Putative Rhamnosyltransferases Involved in Outer Core Oligosaccharide Biosynthesis of *Pseudomonas aeruginosa*. *J Bacteriol* **2008**, *190* (6), 1857–1865. https://doi.org/10.1128/JB.01546-07.
(8) Kocíncová, D.; Ostler, S. L.; Anderson, E. M.; Lam, J. S. Rhamnosyltransferase Genes MigA and WapR Are Regulated in a Differential Manner To Modulate the Quantities of Core Oligosaccharide Glycoforms Produced by *Pseudomonas aeruginosa*. *Journal of Bacteriology* **2012**, *194* (16), 4295–4300. https://doi.org/10.1128/JB.05741-11.
(9) Manioglu, S.; Modaresi, S. M.; Ritzmann, N.; Thoma, J.; Overall, S. A.; Harms, A.; Upert, G.; Luther, A.; Barnes, A. B.; Obrecht, D.; Müller, D. J.; Hiller, S. Antibiotic Polymyxin Arranges Lipopolysaccharide into Crystalline Structures to Solidify the Bacterial Membrane. *Nat Commun* **2022**, *13* (1), 6195. https://doi.org/10.1038/s41467-022-33838-0.
(10) Imamura, Y.; Higashiyama, Y.; Tomono, K.; Izumikawa, K.; Yanagihara, K.; Ohno, H.; Miyazaki, Y.; Hirakata, Y.; Mizuta, Y.; Kadota, J.; Iglewski, B. H.; Kohno, S. Azithromycin Exhibits Bactericidal Effects on *Pseudomonas aeruginosa* through Interaction with the Outer Membrane. *Antimicrob Agents Chemother* **2005**, *49* (4), 1377–1380. https://doi.org/10.1128/AAC.49.4.1377-1380.2005.
(11) Chen, H. D.; Groisman, E. A. The Biology of the PmrA/PmrB Two-Component System: The Major Regulator of Lipopolysaccharide Modifications. *Annual Review of Microbiology* **2013**, *67* (1), 83–112. https://doi.org/10.1146/annurev-micro-092412-155751.
(12) Stokes, J. M.; French, S.; Ovchinnikova, O. G.; Bouwman, C.; Whitfield, C.; Brown, E. D. Cold Stress Makes *Escherichia coli* Susceptible to Glycopeptide Antibiotics by Altering Outer Membrane Integrity. *Cell Chemical Biology* **2016**, *23* (2), 267–277. https://doi.org/10.1016/j.chembiol.2015.12.011.

(13) Grabowicz, M.; Andres, D.; Lebar, M. D.; Malojčić, G.; Kahne, D.; Silhavy, T. J. A Mutant *Escherichia coli* That Attaches Peptidoglycan to Lipopolysaccharide and Displays Cell Wall on Its Surface. *eLife* **2014**, *3*, e05334. https://doi.org/10.7554/eLife.05334.
(14) Cowan, S. W. Bacterial Porins: Lessons from Three High-Resolution Structures: Current Opinion in Structural Biology 1993, 3:501–507. *Current Opinion in Structural Biology* **1993**, *3* (4), 501–507. https://doi.org/10.1016/0959-440X(93)90075-V.
(15) Schulz, G. E. Bacterial Porins: Structure and Function. *Current Opinion in Cell Biology* **1993**, *5* (4), 701–707. https://doi.org/10.1016/0955-0674(93)90143-E.
(16) Nikaido, H.; Saier, M. H. Transport Proteins in Bacteria: Common Themes in Their Design. *Science* **1992**, *258* (5084), 936–942. https://doi.org/10.1126/science.1279804.
(17) Jap, B. K.; Walian, P. J. Biophysics of the Structure and Function of Porins. *Quarterly Reviews of Biophysics* **1990**, *23* (4), 367–403. https://doi.org/10.1017/S003358350000559X.
(18) Chevalier, S.; Bouffartigues, E.; Bodilis, J.; Maillot, O.; Lesouhaitier, O.; Feuilloley, M. G. J.; Orange, N.; Dufour, A.; Cornelis, P. Structure, Function and Regulation of *Pseudomonas aeruginosa* Porins. *FEMS Microbiology Reviews* **2017**, *41* (5), 698–722. https://doi.org/10.1093/femsre/fux020.
(19) Sugawara, E.; Nestorovich, E. M.; Bezrukov, S. M.; Nikaido, H. *Pseudomonas aeruginosa* Porin OprF Exists in Two Different Conformations*. *Journal of Biological Chemistry* **2006**, *281* (24), 16220–16229. https://doi.org/10.1074/jbc.M600680200.
(20) Bouffartigues, E.; Moscoso, J. A.; Duchesne, R.; Rosay, T.; Fito-Boncompte, L.; Gicquel, G.; Maillot, O.; Bénard, M.; Bazire, A.; Brenner-Weiss, G.; Lesouhaitier, O.; Lerouge, P.; Dufour, A.; Orange, N.; Feuilloley, M. G. J.; Overhage, J.; Filloux, A.; Chevalier, S. The Absence of the *Pseudomonas aeruginosa* OprF Protein Leads to Increased Biofilm Formation through Variation in C-Di-GMP Level. *Frontiers in Microbiology* **2015**, *6*.
(21) Cassin, E. K.; Tseng, B. S. Pushing beyond the Envelope: The Potential Roles of OprF in *Pseudomonas aeruginosa* Biofilm Formation and Pathogenicity. *Journal of Bacteriology* **2019**, *201* (18), e00050-19. https://doi.org/10.1128/JB.00050-19.
(22) Shu, J.-C.; Kuo, A.-J.; Su, L.-H.; Liu, T.-P.; Lee, M.-H.; Su, I.-N.; Wu, T.-L. Development of Carbapenem Resistance in *Pseudomonas aeruginosa* Is Associated with OprD Polymorphisms, Particularly the Amino Acid Substitution at Codon 170. *Journal of Antimicrobial Chemotherapy* **2017**, *72* (9), 2489–2495. https://doi.org/10.1093/jac/dkx158.
(23) Shen, J.; Pan, Y.; Fang, Y. Role of the Outer Membrane Protein OprD2 in Carbapenem-Resistance Mechanisms of *Pseudomonas aeruginosa*. *PLOS ONE* **2015**, *10* (10), e0139995. https://doi.org/10.1371/journal.pone.0139995.
(24) Skurnik, D.; Roux, D.; Cattoir, V.; Danilchanka, O.; Lu, X.; Yoder-Himes, D. R.; Han, K.; Guillard, T.; Jiang, D.; Gaultier, C.; Guerin, F.; Aschard, H.; Leclercq, R.; Mekalanos, J. J.; Lory, S.; Pier, G. B. Enhanced in Vivo Fitness of Carbapenem-Resistant OprD Mutants of *Pseudomonas aeruginosa* Revealed through High-Throughput Sequencing. *Proceedings of the National Academy of Sciences* **2013**, *110* (51), 20747–20752. https://doi.org/10.1073/pnas.1221552110.
(25) Quale, J.; Bratu, S.; Gupta, J.; Landman, D. Interplay of Efflux System, AmpC, and OprD Expression in Carbapenem Resistance of *Pseudomonas aeruginosa* Clinical Isolates. *Antimicrobial Agents and Chemotherapy* **2006**, *50* (5), 1633–1641. https://doi.org/10.1128/AAC.50.5.1633-1641.2006.
(26) Ude, J.; Tripathi, V.; Buyck, J. M.; Söderholm, S.; Cunrath, O.; Fanous, J.; Claudi, B.; Egli, A.; Schleberger, C.; Hiller, S.; Bumann, D. Outer Membrane Permeability: Antimicrobials and

Diverse Nutrients Bypass Porins in *Pseudomonas aeruginosa*. *Proc Natl Acad Sci U S A* **2021**, *118* (31), e2107644118. https://doi.org/10.1073/pnas.2107644118.
(27) Masuda, N.; Sakagawa, E.; Ohya, S.; Gotoh, N.; Tsujimoto, H.; Nishino, T. Substrate Specificities of MexAB-OprM, MexCD-OprJ, and MexXY-OprM Efflux Pumps in *Pseudomonas aeruginosa*. *Antimicrob Agents Chemother* **2000**, *44* (12), 3322–3327.
(28) Tsutsumi, K.; Yonehara, R.; Ishizaka-Ikeda, E.; Miyazaki, N.; Maeda, S.; Iwasaki, K.; Nakagawa, A.; Yamashita, E. Structures of the Wild-Type MexAB–OprM Tripartite Pump Reveal Its Complex Formation and Drug Efflux Mechanism. *Nat Commun* **2019**, *10* (1), 1520. https://doi.org/10.1038/s41467-019-09463-9.
(29) Glavier, M.; Puvanendran, D.; Salvador, D.; Decossas, M.; Phan, G.; Garnier, C.; Frezza, E.; Cece, Q.; Schoehn, G.; Picard, M.; Taveau, J.-C.; Daury, L.; Broutin, I.; Lambert, O. Antibiotic Export by MexB Multidrug Efflux Transporter Is Allosterically Controlled by a MexA-OprM Chaperone-like Complex. *Nat Commun* **2020**, *11* (1), 4948. https://doi.org/10.1038/s41467-020-18770-5.
(30) Symmons, M. F.; Bokma, E.; Koronakis, E.; Hughes, C.; Koronakis, V. The Assembled Structure of a Complete Tripartite Bacterial Multidrug Efflux Pump. *Proceedings of the National Academy of Sciences* **2009**, *106* (17), 7173–7178. https://doi.org/10.1073/pnas.0900693106.
(31) Sennhauser, G.; Bukowska, M. A.; Briand, C.; Grütter, M. G. Crystal Structure of the Multidrug Exporter MexB from *Pseudomonas aeruginosa*. *Journal of Molecular Biology* **2009**, *389* (1), 134–145. https://doi.org/10.1016/j.jmb.2009.04.001.
(32) Srikumar, R.; Paul, C. J.; Poole, K. Influence of Mutations in the MexR Repressor Gene on Expression of the MexA-MexB-OprM Multidrug Efflux System of *Pseudomonas aeruginosa*. *J Bacteriol* **2000**, *182* (5), 1410–1414.
(33) Adewoye, L.; Sutherland, A.; Srikumar, R.; Poole, K. The MexR Repressor of the MexAB-OprM Multidrug Efflux Operon in *Pseudomonas aeruginosa*: Characterization of Mutations Compromising Activity. *J Bacteriol* **2002**, *184* (15), 4308–4312. https://doi.org/10.1128/JB.184.15.4308-4312.2002.
(34) Tian, Z.-X.; Yi, X.-X.; Cho, A.; O'Gara, F.; Wang, Y.-P. CpxR Activates MexAB-OprM Efflux Pump Expression and Enhances Antibiotic Resistance in Both Laboratory and Clinical NalB-Type Isolates of *Pseudomonas aeruginosa*. *PLoS Pathog* **2016**, *12* (10), e1005932. https://doi.org/10.1371/journal.ppat.1005932.
(35) Noinaj, N.; Guillier, M.; Barnard, T. J.; Buchanan, S. K. TonB-Dependent Transporters: Regulation, Structure, and Function. *Annual Review of Microbiology* **2010**, *64* (1), 43–60. https://doi.org/10.1146/annurev.micro.112408.134247.
(36) Gudmundsdottir, A.; Bell, P. E.; Lundrigan, M. D.; Bradbeer, C.; Kadner, R. J. Point Mutations in a Conserved Region (TonB Box) of *Escherichia coli* Outer Membrane Protein BtuB Affect Vitamin B12 Transport. *J Bacteriol* **1989**, *171* (12), 6526–6533.
(37) Bhamidimarri, S. P.; Young, T. R.; Shanmugam, M.; Soderholm, S.; Baslé, A.; Bumann, D.; Berg, B. van den. Acquisition of Ionic Copper by the Bacterial Outer Membrane Protein OprC through a Novel Binding Site. *PLOS Biology* **2021**, *19* (11), e3001446. https://doi.org/10.1371/journal.pbio.3001446.
(38) Rodionov, D. A.; Hebbeln, P.; Gelfand, M. S.; Eitinger, T. Comparative and Functional Genomic Analysis of Prokaryotic Nickel and Cobalt Uptake Transporters: Evidence for a Novel Group of ATP-Binding Cassette Transporters. *Journal of Bacteriology* **2006**, *188* (1), 317–327. https://doi.org/10.1128/JB.188.1.317-327.2006.

(39) Schauer, K.; Gouget, B.; Carrière, M.; Labigne, A.; de Reuse, H. Novel Nickel Transport Mechanism across the Bacterial Outer Membrane Energized by the TonB/ExbB/ExbD Machinery. *Mol Microbiol* **2007**, *63* (4), 1054–1068. https://doi.org/10.1111/j.1365-2958.2006.05578.x.
(40) Blanvillain, S.; Meyer, D.; Boulanger, A.; Lautier, M.; Guynet, C.; Denancé, N.; Vasse, J.; Lauber, E.; Arlat, M. Plant Carbohydrate Scavenging through TonB-Dependent Receptors: A Feature Shared by Phytopathogenic and Aquatic Bacteria. *PLOS ONE* **2007**, *2* (2), e224. https://doi.org/10.1371/journal.pone.0000224.
(41) Kramer, J.; Özkaya, Ö.; Kümmerli, R. Bacterial Siderophores in Community and Host Interactions. *Nat Rev Microbiol* **2020**, *18* (3), 152–163. https://doi.org/10.1038/s41579-019-0284-4.
(42) Schauer, K.; Rodionov, D. A.; de Reuse, H. New Substrates for TonB-Dependent Transport: Do We Only See the 'Tip of the Iceberg'? *Trends in Biochemical Sciences* **2008**, *33* (7), 330–338. https://doi.org/10.1016/j.tibs.2008.04.012.
(43) Celia, H.; Botos, I.; Ni, X.; Fox, T.; De Val, N.; Lloubes, R.; Jiang, J.; Buchanan, S. K. Cryo-EM Structure of the Bacterial Ton Motor Subcomplex ExbB–ExbD Provides Information on Structure and Stoichiometry. *Commun Biol* **2019**, *2* (1), 1–6. https://doi.org/10.1038/s42003-019-0604-2.
(44) Maki-Yonekura, S.; Matsuoka, R.; Yamashita, Y.; Shimizu, H.; Tanaka, M.; Iwabuki, F.; Yonekura, K. Hexameric and Pentameric Complexes of the ExbBD Energizer in the Ton System. *eLife* **2018**, *7*, e35419. https://doi.org/10.7554/eLife.35419.
(45) Hickman, S. J.; Cooper, R. E. M.; Bellucci, L.; Paci, E.; Brockwell, D. J. Gating of TonB-Dependent Transporters by Substrate-Specific Forced Remodelling. *Nat Commun* **2017**, *8* (1), 14804. https://doi.org/10.1038/ncomms14804.
(46) White, P.; Joshi, A.; Rassam, P.; Housden, N. G.; Kaminska, R.; Goult, J. D.; Redfield, C.; McCaughey, L. C.; Walker, D.; Mohammed, S.; Kleanthous, C. Exploitation of an Iron Transporter for Bacterial Protein Antibiotic Import. *Proceedings of the National Academy of Sciences* **2017**, *114* (45), 12051–12056. https://doi.org/10.1073/pnas.1713741114.
(47) Josts, I.; Veith, K.; Tidow, H. Ternary Structure of the Outer Membrane Transporter FoxA with Resolved Signalling Domain Provides Insights into TonB-Mediated Siderophore Uptake. *eLife* **2019**, *8*, e48528. https://doi.org/10.7554/eLife.48528.
(48) Bastiaansen, K. C.; van Ulsen, P.; Wijtmans, M.; Bitter, W.; Llamas, M. A. Self-Cleavage of the *Pseudomonas aeruginosa* Cell-Surface Signaling Anti-Sigma Factor FoxR Occurs through an N-O Acyl Rearrangement. *J Biol Chem* **2015**, *290* (19), 12237–12246. https://doi.org/10.1074/jbc.M115.643098.
(49) Llamas, M. A.; Sparrius, M.; Kloet, R.; Jiménez, C. R.; Vandenbroucke-Grauls, C.; Bitter, W. The Heterologous Siderophores Ferrioxamine B and Ferrichrome Activate Signaling Pathways in *Pseudomonas aeruginosa*. *J Bacteriol* **2006**, *188* (5), 1882–1891. https://doi.org/10.1128/JB.188.5.1882-1891.2006.
(50) Chan, D. C. K.; Josts, I.; Koteva, K.; Wright, G. D.; Tidow, H.; Burrows, L. L. A Single Extracellular Loop of FoxA Controls Ligand Specificity, Uptake, and Signaling in *Pseudomonas aeruginosa*. bioRxiv November 18, 2022, p 2022.11.18.517105. https://doi.org/10.1101/2022.11.18.517105.
(51) Ferguson, A. D.; Amezcua, C. A.; Halabi, N. M.; Chelliah, Y.; Rosen, M. K.; Ranganathan, R.; Deisenhofer, J. Signal Transduction Pathway of TonB-Dependent Transporters. *Proceedings of the National Academy of Sciences* **2007**, *104* (2), 513–518. https://doi.org/10.1073/pnas.0609887104.

(52) Chan, D. C. K.; Burrows, L. L. *Pseudomonas aeruginosa* FpvB Is a High-Affinity Transporter for Xenosiderophores Ferrichrome and Ferrioxamine B. *mBio* **2022**, *0* (0), e03149-22. https://doi.org/10.1128/mbio.03149-22.
(53) Ghysels, B.; Dieu, B. T. M.; Beatson, S. A.; Pirnay, J.-P.; Ochsner, U. A.; Vasil, M. L.; Cornelis, P. FpvB, an Alternative Type I Ferripyoverdine Receptor of *Pseudomonas aeruginosa*. *Microbiology* **2004**, *150* (6), 1671–1680. https://doi.org/10.1099/mic.0.27035-0.
(54) Moynié, L.; Milenkovic, S.; Mislin, G. L. A.; Gasser, V.; Malloci, G.; Baco, E.; McCaughan, R. P.; Page, M. G. P.; Schalk, I. J.; Ceccarelli, M.; Naismith, J. H. The Complex of Ferric-Enterobactin with Its Transporter from *Pseudomonas aeruginosa* Suggests a Two-Site Model. *Nat Commun* **2019**, *10* (1), 3673. https://doi.org/10.1038/s41467-019-11508-y.
(55) Ghysels, B.; Ochsner, U.; Möllman, U.; Heinisch, L.; Vasil, M.; Cornelis, P.; Matthijs, S. The *Pseudomonas aeruginosa* PirA Gene Encodes a Second Receptor for Ferrienterobactin and Synthetic Catecholate Analogues. *FEMS Microbiol Lett* **2005**, *246* (2), 167–174. https://doi.org/10.1016/j.femsle.2005.04.010.
(56) Llamas, M. A.; Mooij, M. J.; Sparrius, M.; Vandenbroucke-Grauls, C. M. J. E.; Ratledge, C.; Bitter, W. Characterization of Five Novel *Pseudomonas aeruginosa* Cell-Surface Signalling Systems. *Molecular Microbiology* **2008**, *67* (2), 458–472. https://doi.org/10.1111/j.1365-2958.2007.06061.x.
(57) Elias, S.; Degtyar, E.; Banin, E. FvbA Is Required for Vibriobactin Utilization in *Pseudomonas aeruginosa*. *Microbiology* **2011**, *157* (7), 2172–2180. https://doi.org/10.1099/mic.0.044768-0.
(58) Cuív, P. Ó.; Clarke, P.; O'Connell, M. Identification and Characterization of an Iron-Regulated Gene, ChtA, Required for the Utilization of the Xenosiderophores Aerobactin, Rhizobactin 1021 and Schizokinen by *Pseudomonas aeruginosa*. *Microbiology* **2006**, *152* (4), 945–954. https://doi.org/10.1099/mic.0.28552-0.
(59) Ghequire, M. G. K.; Öztürk, B. A Colicin M-Type Bacteriocin from *Pseudomonas aeruginosa* Targeting the HxuC Heme Receptor Requires a Novel Immunity Partner. *Appl Environ Microbiol* **2018**, *84* (18), e00716-18. https://doi.org/10.1128/AEM.00716-18.
(60) Cornelis, P.; Dingemans, J. *Pseudomonas aeruginosa* Adapts Its Iron Uptake Strategies in Function of the Type of Infections. *Frontiers in Cellular and Infection Microbiology* **2013**, *3*.
(61) Atanaskovic, I.; Mosbahi, K.; Sharp, C.; Housden, N. G.; Kaminska, R.; Walker, D.; Kleanthous, C. Targeted Killing of *Pseudomonas aeruginosa* by Pyocin G Occurs via the Hemin Transporter Hur. *J Mol Biol* **2020**, *432* (13), 3869–3880. https://doi.org/10.1016/j.jmb.2020.04.020.
(62) Salomón, R. A.; Farías, R. N. Microcin 25, a Novel Antimicrobial Peptide Produced by *Escherichia coli*. *J Bacteriol* **1992**, *174* (22), 7428–7435.
(63) Destoumieux-Garzón, D.; Duquesne, S.; Peduzzi, J.; Goulard, C.; Desmadril, M.; Letellier, L.; Rebuffat, S.; Boulanger, P. The Iron–Siderophore Transporter FhuA Is the Receptor for the Antimicrobial Peptide Microcin J25: Role of the Microcin Val11–Pro16 β-Hairpin Region in the Recognition Mechanism. *Biochem J* **2005**, *389* (Pt 3), 869–876. https://doi.org/10.1042/BJ20042107.
(64) Luna, B.; Trebosc, V.; Lee, B.; Bakowski, M.; Ulhaq, A.; Yan, J.; Lu, P.; Cheng, J.; Nielsen, T.; Lim, J.; Ketphan, W.; Eoh, H.; McNamara, C.; Skandalis, N.; She, R.; Kemmer, C.; Lociuro, S.; Dale, G. E.; Spellberg, B. A Nutrient-Limited Screen Unmasks Rifabutin Hyperactivity for Extensively Drug-Resistant *Acinetobacter baumannii*. *Nat Microbiol* **2020**, *5* (9), 1134–1143. https://doi.org/10.1038/s41564-020-0737-6.

(65) Ferguson, A. D.; Ködding, J.; Walker, G.; Bös, C.; Coulton, J. W.; Diederichs, K.; Braun, V.; Welte, W. Active Transport of an Antibiotic Rifamycin Derivative by the Outer-Membrane Protein FhuA. *Structure* **2001**, *9* (8), 707–716. https://doi.org/10.1016/S0969-2126(01)00631-1.
(66) Braun, V.; Pramanik, A.; Gwinner, T.; Köberle, M.; Bohn, E. Sideromycins: Tools and Antibiotics. *Biometals* **2009**, *22* (1), 3–13. https://doi.org/10.1007/s10534-008-9199-7.
(67) Langenscheid, J.; Killmann, H.; Braun, V. A FhuA Mutant of *Escherichia coli* Is Infected by Phage T1-Independent of TonB. *FEMS Microbiology Letters* **2004**, *234* (1), 133–137. https://doi.org/10.1111/j.1574-6968.2004.tb09524.x.
(68) Rabsch, W.; Ma, L.; Wiley, G.; Najar, F. Z.; Kaserer, W.; Schuerch, D. W.; Klebba, J. E.; Roe, B. A.; Laverde Gomez, J. A.; Schallmey, M.; Newton, S. M. C.; Klebba, P. E. FepA- and TonB-Dependent Bacteriophage H8: Receptor Binding and Genomic Sequence. *J Bacteriol* **2007**, *189* (15), 5658–5674. https://doi.org/10.1128/JB.00437-07.
(69) Ito, A.; Nishikawa, T.; Matsumoto, S.; Yoshizawa, H.; Sato, T.; Nakamura, R.; Tsuji, M.; Yamano, Y. Siderophore Cephalosporin Cefiderocol Utilizes Ferric Iron Transporter Systems for Antibacterial Activity against *Pseudomonas aeruginosa*. *Antimicrob Agents Chemother* **2016**, *60* (12), 7396–7401. https://doi.org/10.1128/AAC.01405-16.
(70) Luscher, A.; Moynié, L.; Auguste, P. S.; Bumann, D.; Mazza, L.; Pletzer, D.; Naismith, J. H.; Köhler, T. TonB-Dependent Receptor Repertoire of *Pseudomonas aeruginosa* for Uptake of Siderophore-Drug Conjugates. *Antimicrob Agents Chemother* **2018**, *62* (6), e00097-18. https://doi.org/10.1128/AAC.00097-18.
(71) Arnison, P. G.; Bibb, M. J.; Bierbaum, G.; Bowers, A. A.; Bugni, T. S.; Bulaj, G.; Camarero, J. A.; Campopiano, D. J.; Challis, G. L.; Clardy, J.; Cotter, P. D.; Craik, D. J.; Dawson, M.; Dittmann, E.; Donadio, S.; Dorrestein, P. C.; Entian, K.-D.; Fischbach, M. A.; Garavelli, J. S.; Göransson, U.; Gruber, C. W.; Haft, D. H.; Hemscheidt, T. K.; Hertweck, C.; Hill, C.; Horswill, A. R.; Jaspars, M.; Kelly, W. L.; Klinman, J. P.; Kuipers, O. P.; Link, A. J.; Liu, W.; Marahiel, M. A.; Mitchell, D. A.; Moll, G. N.; Moore, B. S.; Müller, R.; Nair, S. K.; Nes, I. F.; Norris, G. E.; Olivera, B. M.; Onaka, H.; Patchett, M. L.; Piel, J.; Reaney, M. J. T.; Rebuffat, S.; Ross, R. P.; Sahl, H.-G.; Schmidt, E. W.; Selsted, M. E.; Severinov, K.; Shen, B.; Sivonen, K.; Smith, L.; Stein, T.; Süssmuth, R. D.; Tagg, J. R.; Tang, G.-L.; Truman, A. W.; Vederas, J. C.; Walsh, C. T.; Walton, J. D.; Wenzel, S. C.; Willey, J. M.; van der Donk, W. A. Ribosomally Synthesized and Post-Translationally Modified Peptide Natural Products: Overview and Recommendations for a Universal Nomenclature. *Nat Prod Rep* **2013**, *30* (1), 108–160. https://doi.org/10.1039/c2np20085f.
(72) Su, T. L. Micrococcin. An Antibacterial Substance Formed by a Strain of *Micrococcus*. *Br J Exp Pathol* **1948**, *29* (5), 473–481.
(73) Li, J.; Qu, X.; He, X.; Duan, L.; Wu, G.; Bi, D.; Deng, Z.; Liu, W.; Ou, H.-Y. ThioFinder: A Web-Based Tool for the Identification of Thiopeptide Gene Clusters in DNA Sequences. *PLoS One* **2012**, *7* (9), e45878. https://doi.org/10.1371/journal.pone.0045878.
(74) Cogan, D. P.; Hudson, G. A.; Zhang, Z.; Pogorelov, T. V.; van der Donk, W. A.; Mitchell, D. A.; Nair, S. K. Structural Insights into Enzymatic [4+2] Aza-Cycloaddition in Thiopeptide Antibiotic Biosynthesis. *Proceedings of the National Academy of Sciences* **2017**, *114* (49), 12928–12933. https://doi.org/10.1073/pnas.1716035114.
(75) Fleming, S. R.; Bartges, T. E.; Vinogradov, A. A.; Kirkpatrick, C. L.; Goto, Y.; Suga, H.; Hicks, L. M.; Bowers, A. A. Flexizyme-Enabled Benchtop Biosynthesis of Thiopeptides. *J. Am. Chem. Soc.* **2019**, *141* (2), 758–762. https://doi.org/10.1021/jacs.8b11521.

(76) Little, R.; Paiva, F. C. R.; Jenkins, R.; Hong, H.; Sun, Y.; Demydchuk, Y.; Samborskyy, M.; Tosin, M.; Leeper, F. J.; Dias, M. V. B.; Leadlay, P. F. Unexpected Enzyme-Catalysed [4+2] Cycloaddition and Rearrangement in Polyether Antibiotic Biosynthesis. *Nat Catal* **2019**, *2* (11), 1045–1054. https://doi.org/10.1038/s41929-019-0351-2.
(77) Schwalen, C. J.; Hudson, G. A.; Kille, B.; Mitchell, D. A. Bioinformatic Expansion and Discovery of Thiopeptide Antibiotics. *J Am Chem Soc* **2018**, *140* (30), 9494–9501. https://doi.org/10.1021/jacs.8b03896.
(78) Bagley, M. C.; Dale, J. W.; Merritt, E. A.; Xiong, X. Thiopeptide Antibiotics. *Chem. Rev.* **2005**, *105* (2), 685–714. https://doi.org/10.1021/cr0300441.
(79) Cheng, T. H.; Saidin, J.; Danish-Daniel, M.; Gan, H. M.; Mat Isa, M. N.; Abu Bakar, M. F.; Ismail, N. Genome Sequence of *Serratia marcescens* Subsp. *sakuensis* Strain *K27,* a Marine Bacterium Isolated from Sponge (*Haliclona amboinensis*). *Genome Announcements* **2018**, *6* (6), e00022-18. https://doi.org/10.1128/genomeA.00022-18.
(80) Khilyas, I. V.; Tursunov, K. A.; Shirshikova, T. V.; Kamaletdinova, L. K.; Matrosova, L. E.; Desai, P. T.; McClelland, M.; Bogomolnaya, L. M. Genome Sequence of Pigmented Siderophore-Producing Strain *Serratia marcescens* SM6. *Microbiology Resource Announcements* **2019**, *8* (18), e00247-19. https://doi.org/10.1128/MRA.00247-19.
(81) Thompson, J.; Cundliffe, E.; Stark, M. J. R. The Mode of Action of Berninamycin and the Mechanism of Resistance in the Producing Organism, *Streptomyces bernensis*. *Microbiology* **1982**, *128* (4), 875–884. https://doi.org/10.1099/00221287-128-4-875.
(82) Cundliffe, E.; Thompson, J. The Mode of Action of Nosiheptide (Multhiomycin) and the Mechanism of Resistance in the Producing Organism. *Microbiology* **1981**, *126* (1), 185–192. https://doi.org/10.1099/00221287-126-1-185.
(83) Naaktgeboren, N.; Roobol, K.; Gubbens, J.; Voorma, H. O. The Mode of Action of Thiostrepton in the Initiation of Protein Synthesis. *European Journal of Biochemistry* **1976**, *70* (1), 39–47. https://doi.org/10.1111/j.1432-1033.1976.tb10953.x.
(84) Polikanov, Y. S.; Aleksashin, N. A.; Beckert, B.; Wilson, D. N. The Mechanisms of Action of Ribosome-Targeting Peptide Antibiotics. *Frontiers in Molecular Biosciences* **2018**, *5*.
(85) Walter, J. D.; Hunter, M.; Cobb, M.; Traeger, G.; Spiegel, P. C. Thiostrepton Inhibits Stable 70S Ribosome Binding and Ribosome-Dependent GTPase Activation of Elongation Factor G and Elongation Factor 4. *Nucleic Acids Research* **2012**, *40* (1), 360–370. https://doi.org/10.1093/nar/gkr623.
(86) Bowen, W. S.; Dyke, N. V.; Murgola, E. J.; Lodmell, J. S.; Hill, W. E. Interaction of Thiostrepton and Elongation Factor-G with the Ribosomal Protein L11-Binding Domain *. *Journal of Biological Chemistry* **2005**, *280* (4), 2934–2943. https://doi.org/10.1074/jbc.M407008200.
(87) Bodley, J. W.; Lin, L.; Highland, J. H. Studies on Translocation VI: Thiostrepton Prevents the Formation of a Ribosome-G Factor-Guanine Nucleotide Complex. *Biochemical and Biophysical Research Communications* **1970**, *41* (6), 1406–1411. https://doi.org/10.1016/0006-291X(70)90543-7.
(88) Highland, J. H.; Lin, L.; Bodley, J. W. Translocation. VIII. Protection of Ribosomes Frm Thiostrepton Inactivation by the Binding of G Factor and Guanosine Diphosphate. *Biochemistry* **1971**, *10* (24), 4404–4409. https://doi.org/10.1021/bi00800a009.
(89) Rodnina, M. V.; Savelsbergh, A.; Matassova, N. B.; Katunin, V. I.; Semenkov, Y. P.; Wintermeyer, W. Thiostrepton Inhibits the Turnover but Not the GTPase of Elongation Factor G

on the Ribosome. *Proceedings of the National Academy of Sciences* **1999**, *96* (17), 9586–9590. https://doi.org/10.1073/pnas.96.17.9586.
(90) Harms, J. M.; Wilson, D. N.; Schluenzen, F.; Connell, S. R.; Stachelhaus, T.; Zaborowska, Z.; Spahn, C. M. T.; Fucini, P. Translational Regulation via L11: Molecular Switches on the Ribosome Turned On and Off by Thiostrepton and Micrococcin. *Molecular Cell* **2008**, *30* (1), 26–38. https://doi.org/10.1016/j.molcel.2008.01.009.
(91) Bechthold, A.; Floss, H. G. Overexpression of the Thiostrepton-Resistance Gene from *Streptomyces azureus* in *Escherichia coli* and Characterization of Recognition Sites of the 23S RRNA A1067 2′-Methyltransferase in the Guanosine Triphosphatase Center of 23S Ribosomal RNA. *European Journal of Biochemistry* **1994**, *224* (2), 431–437. https://doi.org/10.1111/j.1432-1033.1994.00431.x.
(92) Thompson, J.; Schmidt, F.; Cundliffe, E. Site of Action of a Ribosomal RNA Methylase Conferring Resistance to Thiostrepton. *Journal of Biological Chemistry* **1982**, *257* (14), 7915–7917. https://doi.org/10.1016/S0021-9258(18)34268-6.
(93) Yin, S.; Jiang, H.; Chen, D.; Murchie, A. I. H. Substrate Recognition and Modification by the Nosiheptide Resistance Methyltransferase. *PLoS One* **2015**, *10* (4), e0122972. https://doi.org/10.1371/journal.pone.0122972.
(94) Rosendahl, G.; Douthwaite, S. The Antibiotics Micrococcin and Thiostrepton Interact Directly with 23S RRNA Nucleotides 1067A and 1095A. *Nucleic Acids Res* **1994**, *22* (3), 357–363.
(95) Lentzen, G.; Klinck, R.; Matassova, N.; Aboul-ela, F.; Murchie, A. I. H. Structural Basis for Contrasting Activities of Ribosome Binding Thiazole Antibiotics. *Chemistry & Biology* **2003**, *10* (8), 769–778. https://doi.org/10.1016/S1074-5521(03)00173-X.
(96) Parmeggiani, A.; Krab, I. M.; Okamura, S.; Nielsen, R. C.; Nyborg, J.; Nissen, P. Structural Basis of the Action of Pulvomycin and GE2270 A on Elongation Factor Tu,. *Biochemistry* **2006**, *45* (22), 6846–6857. https://doi.org/10.1021/bi0525122.
(97) Zuurmond, A.-M.; Martien de Graaf, J.; Olsthoorn-Tieleman, L. N.; van Duyl, B. Y.; Mörhle, V. G.; Jurnak, F.; Mesters, J. R.; Hilgenfeld, R.; Kraal, B. GE2270A-Resistant Mutations in Elongation Factor Tu Allow Productive Aminoacyl-TRNA Binding to EF-Tu·GTP·GE2270A Complexes. *Journal of Molecular Biology* **2000**, *304* (5), 995–1005. https://doi.org/10.1006/jmbi.2000.4260.
(98) Young, T. S.; Dorrestein, P. C.; Walsh, C. T. Codon Randomization for Rapid Exploration of Chemical Space in Thiopeptide Antibiotic Variants. *Chem Biol* **2012**, *19* (12), 1600–1610. https://doi.org/10.1016/j.chembiol.2012.10.013.
(99) Fouces, R.; Rodríguez, M.; Mellado, E.; Díez, B.; Barredo, J. L. Conjugation and Transformation of *Streptomyces* Species by Tylosin Resistance. *FEMS Microbiology Letters* **2000**, *186* (2), 319–325. https://doi.org/10.1111/j.1574-6968.2000.tb09124.x.
(100) Mugweru, J.; Makafe, G.; Cao, Y.; Zhang, Y.; Wang, B.; Huang, S.; Njire, M.; Chhotaray, C.; Tan, Y.; Li, X.; Liu, J.; Tan, S.; Deng, J.; Zhang, T. A Cassette Containing Thiostrepton, Gentamicin Resistance Genes, and Dif Sequences Is Effective in Construction of Recombinant Mycobacteria. *Front Microbiol* **2017**, *8*, 468. https://doi.org/10.3389/fmicb.2017.00468.
(101) Chiu, M. L.; Folcher, M.; Griffin, P.; Holt, T.; Klatt, T.; Thompson, C. J. Characterization of the Covalent Binding of Thiostrepton to a Thiostrepton-Induced Protein from *Streptomyces lividans*. *Biochemistry* **1996**, *35* (7), 2332–2341. https://doi.org/10.1021/bi952073e.

(102) Murakami, T.; Holt, T. G.; Thompson, C. J. Thiostrepton-Induced Gene Expression in *Streptomyces lividans*. *Journal of Bacteriology* **1989**, *171* (3), 1459–1466. https://doi.org/10.1128/jb.171.3.1459-1466.1989.
(103) Holmes, D. j.; Caso, J. l.; Thompson, C. j. Autogenous Transcriptional Activation of a Thiostrepton-Induced Gene in *Streptomyces lividans*. *The EMBO Journal* **1993**, *12* (8), 3183–3191. https://doi.org/10.1002/j.1460-2075.1993.tb05987.x.
(104) Chiu, M. L.; Viollier, P. H.; Katoh, T.; Ramsden, J. J.; Thompson, C. J. Ligand-Induced Changes in the *Streptomyces lividans* TipAL Protein Imply an Alternative Mechanism of Transcriptional Activation for MerR-Like Proteins. *Biochemistry* **2001**, *40* (43), 12950–12958. https://doi.org/10.1021/bi010328k.
(105) Chiu, M. L.; Folcher, M.; Katoh, T.; Puglia, A. M.; Vohradsky, J.; Yun, B.-S.; Seto, H.; Thompson, C. J. Broad Spectrum Thiopeptide Recognition Specificity of The*Streptomyces lividans* TipAL Protein and Its Role in Regulating Gene Expression. *Journal of Biological Chemistry* **1999**, *274* (29), 20578–20586. https://doi.org/10.1074/jbc.274.29.20578.
(106) Myers, C. L.; Harris, J.; Yeung, J. C. K.; Honek, J. F. Molecular Interactions between Thiostrepton and the TipAS Protein from *Streptomyces lividans*. *ChemBioChem* **2014**, *15* (5), 681–687. https://doi.org/10.1002/cbic.201300724.
(107) Yun, B.-S.; Hidaka, T.; Furihata, K.; Seto, H. PROMOTHIOCINS A AND B, NOVEL THIOPEPTIDES WITH A Tip A PROMOTER INDUCING ACTIVITY PRODUCED BY *Streptomyces Sp. SF2741*. *J. Antibiot.* **1994**, *47* (4), 510–514. https://doi.org/10.7164/antibiotics.47.510.
(108) Hayashi, S.; Ozaki, T.; Asamizu, S.; Ikeda, H.; Ōmura, S.; Oku, N.; Igarashi, Y.; Tomoda, H.; Onaka, H. Genome Mining Reveals a Minimum Gene Set for the Biosynthesis of 32-Membered Macrocyclic Thiopeptides Lactazoles. *Chemistry & Biology* **2014**, *21* (5), 679–688. https://doi.org/10.1016/j.chembiol.2014.03.008.
(109) González Holgado, G.; Castro Rodríguez, J.; Cañedo Hernández, L. M.; Díaz, M.; Fernández-Abalos, J. M.; Trujillano, I.; Santamaría, R. I. Radamycin, a Novel Thiopeptide Produced by Streptomyces Sp. RSP9. I. Taxonomy, Fermentation, Isolation and Biological Activities. *J Antibiot (Tokyo)* **2002**, *55* (4), 383–390. https://doi.org/10.7164/antibiotics.55.383.
(110) Bleich, R.; Watrous, J. D.; Dorrestein, P. C.; Bowers, A. A.; Shank, E. A. Thiopeptide Antibiotics Stimulate Biofilm Formation in *Bacillus subtilis*. *Proceedings of the National Academy of Sciences* **2015**, *112* (10), 3086–3091. https://doi.org/10.1073/pnas.1414272112.
(111) Szczuka, E.; Jabłońska, L.; Kaznowski, A. Effect of Subinhibitory Concentrations of Tigecycline and Ciprofloxacin on the Expression of Biofilm-Associated Genes and Biofilm Structure of *Staphylococcus epidermidis*. *Microbiology (Reading)* **2017**, *163* (5), 712–718. https://doi.org/10.1099/mic.0.000453.
(112) Hoffman, L. R.; D'Argenio, D. A.; MacCoss, M. J.; Zhang, Z.; Jones, R. A.; Miller, S. I. Aminoglycoside Antibiotics Induce Bacterial Biofilm Formation. *Nature* **2005**, *436* (7054), 1171–1175. https://doi.org/10.1038/nature03912.
(113) Jin, Y.; Guo, Y.; Zhan, Q.; Shang, Y.; Qu, D.; Yu, F. Subinhibitory Concentrations of Mupirocin Stimulate *Staphlyococcus aureus* Biofilm Formation by Upregulating CidA. *Antimicrobial Agents and Chemotherapy* **2020**, *64* (3), e01912-19. https://doi.org/10.1128/AAC.01912-19.
(114) Gotoh, H.; Zhang, Y.; Dallo, S. F.; Hong, S.; Kasaraneni, N.; Weitao, T. *Pseudomonas aeruginosa*, under DNA Replication Inhibition, Tends to Form Biofilms via Arr. *Research in Microbiology* **2008**, *159* (4), 294–302. https://doi.org/10.1016/j.resmic.2008.02.002.

Chapter Two: Thiostrepton Hijacks Siderophore Transporters to Cross the Outer Membrane of *P. aeruginosa*

Preface

The work presented in the following chapter has been published in:

Ranieri, M. R. M., Chan, D. C. K., Yaeger, L. N., Rudolph, M., Karabelas-Pittman S., Abdo, H., Chee, J., Harvey, H., Nguyen, U., and Burrows, L. L. (2019). Thiostrepton Hijacks Pyoverdine Receptors to Inhibit Growth of *Pseudomonas aeruginosa*. *Antimicrob. Agents. Chemother.* 63(9), e00472-19. https://doi.org/10.1128/AAC.00472-19.

M.R.M.R. performed experiments and wrote the first draft. D.C.K.C. performed experiments, generated new figures, edited multiple drafts, and completed all experiments for revisions. L.N.Y. provided input on multiple drafts. M.R. performed high throughput screening and confirmatory assays. S.K. performed high throughput screening and confirmatory assays. H.A. repeated some key studies. J.C. performed high throughput screening and confirmatory assays. H.H. assisted with the molecular biology experiments. U.N. performed the original high throughput screen. L.L.B. provided funding, designed experiments, guided data analysis, wrote and edited multiple drafts.

Abstract

Pseudomonas aeruginosa is a biofilm-forming opportunistic pathogen and intrinsically resistant to many antibiotics. In a high-throughput screen for molecules that modulate biofilm formation, we discovered that the thiopeptide antibiotic, thiostrepton (TS) - considered inactive against Gram-negative bacteria - stimulated *P. aeruginosa* biofilm formation in a dose-dependent manner. This phenotype is characteristic of exposure to antimicrobial compounds at sub-inhibitory concentrations, suggesting that TS was active against *P. aeruginosa.* Supporting this observation, TS inhibited growth of a panel of 96 multidrug-resistant (MDR) *P. aeruginosa* clinical isolates at low micromolar concentrations. TS also had activity against *Acinetobacter baumannii* clinical isolates. Expression of Tsr - a 23S rRNA-modifying methyltransferase from TS producer, *Streptomyces azureus* - in trans conferred TS resistance, confirming that the drug acted via its canonical mode of action, inhibition of ribosome function. Deletion of oligopeptide permease systems used by other peptide antibiotics for uptake failed confer TS resistance. TS susceptibility was inversely proportional to iron availability, suggesting that TS exploits uptake pathways whose expression is increased under iron starvation. Consistent with this finding, TS activity against *P. aeruginosa* and *A. baumannii* was potentiated by FDA-approved iron chelators deferiprone and deferasirox. Screening of *P. aeruginosa* mutants for TS resistance revealed that it exploits pyoverdine receptors FpvA and FpvB to cross the outer membrane. Our data show that the biofilm stimulation phenotype can reveal cryptic sub-inhibitory antibiotic activity, and that TS has activity against select multidrug resistant Gram-negative pathogens under iron-limited growth conditions, similar to those encountered at sites of infection.

Introduction

Bacterial pathogens are rapidly evolving resistance to available antibiotics, creating an urgent need for new therapies. Gram-negative bacteria are particularly challenging to treat because their outer membranes limit the access of many drugs to intracellular targets (1). Resistance arises when bacteria accumulate target mutations, acquire specific resistance determinants, increase drug efflux, and/or enter antibiotic-tolerant dormant or biofilm modes of growth (2). Biofilms consist of surface-associated bacteria surrounded by self-produced extracellular polymeric substances (EPS). Biofilm architecture allows for development of phenotypic heterogeneity that leads to variations in susceptibility as well as the formation of drug-tolerant persister cells (3). Approaches with the potential to preserve current antibiotics include combining them with biofilm inhibitors, resistance blockers (e.g. ampicillin with clavulanic acid or piperacillin with tazobactam), efflux inhibitors (e.g. PAβN), outer membrane permeabilizers, or coupling them to molecules such as siderophores that are actively imported, so-called Trojan horses (4).

Among the bacterial pathogens deemed most problematic by the World Health Organization is the Gram-negative opportunist, *Pseudomonas aeruginosa* (5). It infects immunocompromised patients – particularly those with medical devices – and is a major problem for people with severe burns or cystic fibrosis (6). It is intrinsically resistant to many antibiotics and readily forms biofilms, further enhancing its ability to evade therapy (7). The low permeability of its outer membrane and expression of multiple efflux pumps that extrude a wide variety of substrates, coupled with its propensity to form biofilms, limit the repertoire of effective anti-*Pseudomonas* antibiotics (8-10). Here with the aim of identifying potential modulators of *P. aeruginosa* biofilm formation, we screened a collection of bioactive molecules, including previously FDA-approved off-patent drugs, at 10 μM. During this work, we identified 60 growth inhibitors, plus an additional

60 molecules that stimulated biofilm formation beyond our arbitrary cutoff of 200% of the vehicle control, a phenotype associated with exposure to sub-MIC antibiotics (11, 12). Investigation of one such stimulatory compound, thiostrepton (TS), revealed that it had low micromolar activity against *P. aeruginosa* in minimal medium. Through a series of investigations, we showed that TS gains access to its ribosomal targets by exploiting iron limitation-dependent uptake pathways. These data show that the biofilm stimulation phenotype can reveal cryptic antibiotic activity when concentrations are too low (or growth conditions not conducive) to inhibit growth.

Results

Thiostrepton stimulates *P. aeruginosa* biofilm formation

We used a previously described *P. aeruginosa* biofilm assay (13) to screen a bespoke collection of 3921 bioactive molecules that includes ~1100 FDA-approved, off-patent drugs and antibiotics (14). The molecules were screened in duplicate at 10 μM in a dilute growth medium consisting of 10% lysogeny broth (LB), 90% phosphate buffered saline (henceforth, 10:90) to identify molecules capable of modulating biofilm formation. This medium was chosen to minimize the amount of biofilm formed in the presence of the vehicle control, so that molecules stimulating biofilm formation could be more easily identified. The hits were divided into planktonic growth inhibitors (60 compounds), biofilm inhibitors (defined as those resulting in ≤50% of vehicle control biofilm, 8 compounds), or biofilm stimulators (those resulting in ≥200% of vehicle-treated control biofilm, 60 compounds) (**Supplementary Table S1**). The hit rate of ~3% was relatively high for a primary screen, but all the molecules in this curated collection have biological activity. The hits belonged to a variety of chemical classes and included drugs with nominally eukaryotic targets.

Multiple studies showed that sub-inhibitory concentrations of antibiotics from a variety of classes and with different mechanisms of action (MOA) stimulate *P. aeruginosa* biofilm formation, although the specific pathways underlying this response remain unclear (11, 12, 15-18). Among the molecules in our screen that stimulated biofilm formation was the thiopeptide antibiotic, thiostrepton (TS; **Fig 1A**). This response intrigued us because TS was reported to be ineffective against Gram-negative bacteria (19, 20), likely due to the impermeability of the outer membrane (OM) to large hydrophobic compounds. In light of the need for new therapeutics for *P. aeruginosa*, we decided to further investigate its possible anti-*Pseudomonas* activity. In dose-response experiments in 10:90 medium, biofilm levels increased while planktonic cell density decreased with increasing TS concentrations to 10 μM (17 μg/ml), the maximum that could be tested due to its limited solubility (**Fig 1B)**.

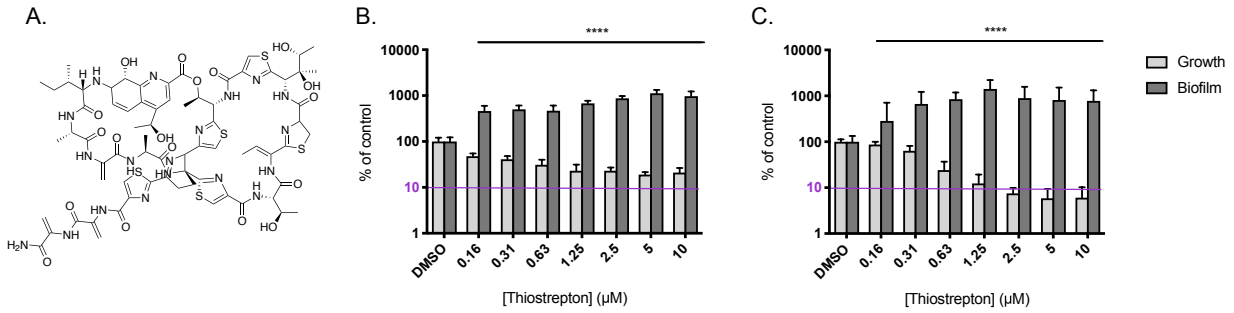

Figure 1. Thiostrepton stimulates *P. aeruginosa* biofilm formation. **A.** Structure of thiostrepton (TS). **B.** TS stimulated biofilm formation (absorbance of eluted crystal violet at 600 nm, plotted as percent of the DMSO control on a log10 scale) of *P. aeruginosa* PAO1 and decreased planktonic cell density (optical density at 600 nm, plotted as percent of the DMSO control on a log10 scale) in 10:90 medium in a dose-dependent manner, up to its maximum soluble concentration of 10 μM (17 μg/ml). **C.** In VBMM, PAO1 biofilm formation was stimulated by TS, while planktonic cell density decreased below the level of detection at concentrations above 1.25 μM. The 10% value is highlighted with a purple line. Assays were performed at least 3 times in triplicate. **** $p<0.0001$.

Growth in minimal media increases susceptibility of *P. aeruginosa* to TS

Environmental conditions can modulate the expression or essentiality of antibiotic targets or alter the availability of particular nutrients (21), leading to changes in susceptibility. We hypothesized that the biofilm response of *P. aeruginosa* to TS may be the result of nutrient deficiency in 10:90, which was more limiting to *P. aeruginosa* growth than M9 minimal medium (**Supplementary Fig S1**). Consistent with this idea, growth of *P. aeruginosa* in nutrient-rich Mueller-Hinton broth (MHB) reduced susceptibility to TS (**Supplementary Fig S2**). Growth rates in Vogel Bonner Minimal Media (VBMM) in the absence of TS were similar to those in 10:90 (**Supplementary Fig S1**) but in the presence of TS, planktonic cell density decreased to below the level of detection at concentrations above ~1.25μM (**Fig 1C**). These data suggested that nutrient limitation enhances susceptibility of *P. aeruginosa* to TS.

The ribosomal methyltransferase Tsr protects *P. aeruginosa* against TS

The established MOA for TS antibacterial activity is inhibition of protein translation through direct binding to bacterial ribosomes (22). However, because TS also has anti-parasitic and anti-neoplastic activities (23, 24) we considered the possibility that it might inhibit *P. aeruginosa* growth in a novel way. To validate the MOA, we expressed a resistance gene, *tsr,* from a plasmid in *P. aeruginosa* strains PAO1 and PA14. *tsr* encodes a 23s rRNA methyltransferase, used by TS producer *Streptomyces azureus* to prevent self-intoxication (25). Tsr methylates the conserved A1067 residue of 23s rRNA, impairing the binding of TS to its target (26). Expression of *tsr* in trans increased TS resistance of both PAO1 and PA14 compared to vector-only controls (**Fig 2AB**). PAO1 was resistant up to the maximum soluble TS concentration of 10 μM, while resistance of PA14 was significantly increased compared to control, although not to the same

extent as PAO1. These results suggest that TS inhibits growth via its canonical MOA of ribosome binding, implying that it crosses the *P. aeruginosa* OM to access the bacterial cytoplasm.

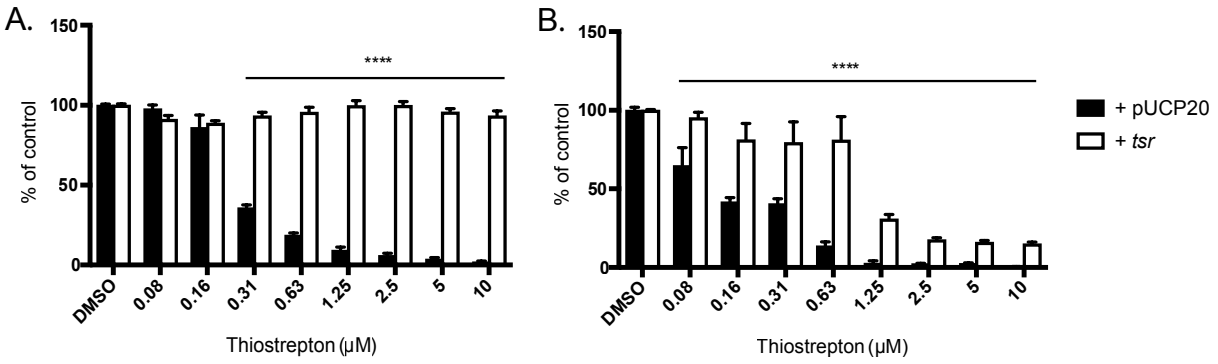

Figure 2 Expression of Tsr in trans reduces susceptibility of *P. aeruginosa* to thiostrepton. Expression of the *tsr* gene from *Streptomyces azureus* in trans from pUCP20 in two strains of *P. aeruginosa* reduced susceptibility to TS in VBMM, suggesting it inhibits growth via its canonical mode of action, disrupting translation. A. Growth of PAO1 (OD_{600} plotted as percent of the DMSO control); B. Growth of PA14. Each assay was performed at least 3 times in triplicate. **** $p<0.0001$

TS susceptibility increases in the presence of iron chelators

To understand the reason for increased TS susceptibility of *P. aeruginosa* in VBMM compared to 10:90, we considered the differences in nutrient availability between the two media types. The primary carbon source in 10% LB is amino acids (27) while the carbon source in VBMM is citrate (28). Citrate can chelate divalent cations including calcium and magnesium, which are important for OM integrity. We hypothesized that this chelation effect may increase OM permeability. To stabilize the OM, we repeated the dose response assay in VBMM supplemented with 100 mM $MgCl_2$ but saw no effect on susceptibility (**Supplementary Fig S3A**). Since TS is a thiopeptide, we next hypothesized that amino acid limitation during growth in VBMM may increase uptake of TS, leading to growth inhibition. To test this, we supplemented VBMM with 0.1% casamino acids, but saw no change in TS susceptibility (**Supplementary Fig 3B**). Further, simultaneous deletion of components of the Opp (Npp) peptide transport system, exploited by

other peptide antibiotics for entry (29, 30), and a homologous system, Spp, had no effect on TS susceptibility (**Supplementary Fig S3C**).

We next considered that VBMM was more iron-limited than 10:90, which contains trace iron from yeast extract and peptone. Under iron limitation, bacteria secrete siderophores into the extracellular milieu to scavenge the metal. Specialized receptors then transport siderophore-iron complexes back into the cell. Some antimicrobials, including sideromycins, pyocins, and bacteriocins, use siderophore receptors to access intracellular targets (31-34), and we hypothesized that TS may use this strategy. We compared *P. aeruginosa* PAO1 grown in 10:90 with increasing concentrations of TS alone (**Fig 3A**) or with 0.1μM EDDHA, a membrane-impermeable iron chelator (35) (**Fig 3B**). Addition of EDDHA shifted biofilm stimulation and growth inhibition to lower concentrations of TS compared to 10:90 alone, while supplementation of 10:90 plus 0.1μM EDDHA with 100μM $FeCl_3$ increased planktonic cell density and reduced biofilm stimulation (**Fig 3C**). These data suggest that TS susceptibility is inversely proportional to iron availability, and that TS may exploit siderophore receptors to cross the OM of *P. aeruginosa*.

The poor solubility of TS has hampered its development as a therapeutic, but these data suggested that its effective concentration could be reduced in the presence of iron chelators. We tested the FDA-approved iron chelators deferiprone (DFP) and deferasirox (DSX) for potential synergy with TS. Checkerboard assays revealed that while neither chelator had activity against *P. aeruginosa*, both potentiated TS activity (**Fig 3DE**) at concentrations well below those used to safely treat patients, up to 28 mg/kg/day for DSX or 99 mg/kg/day for DFP (36).

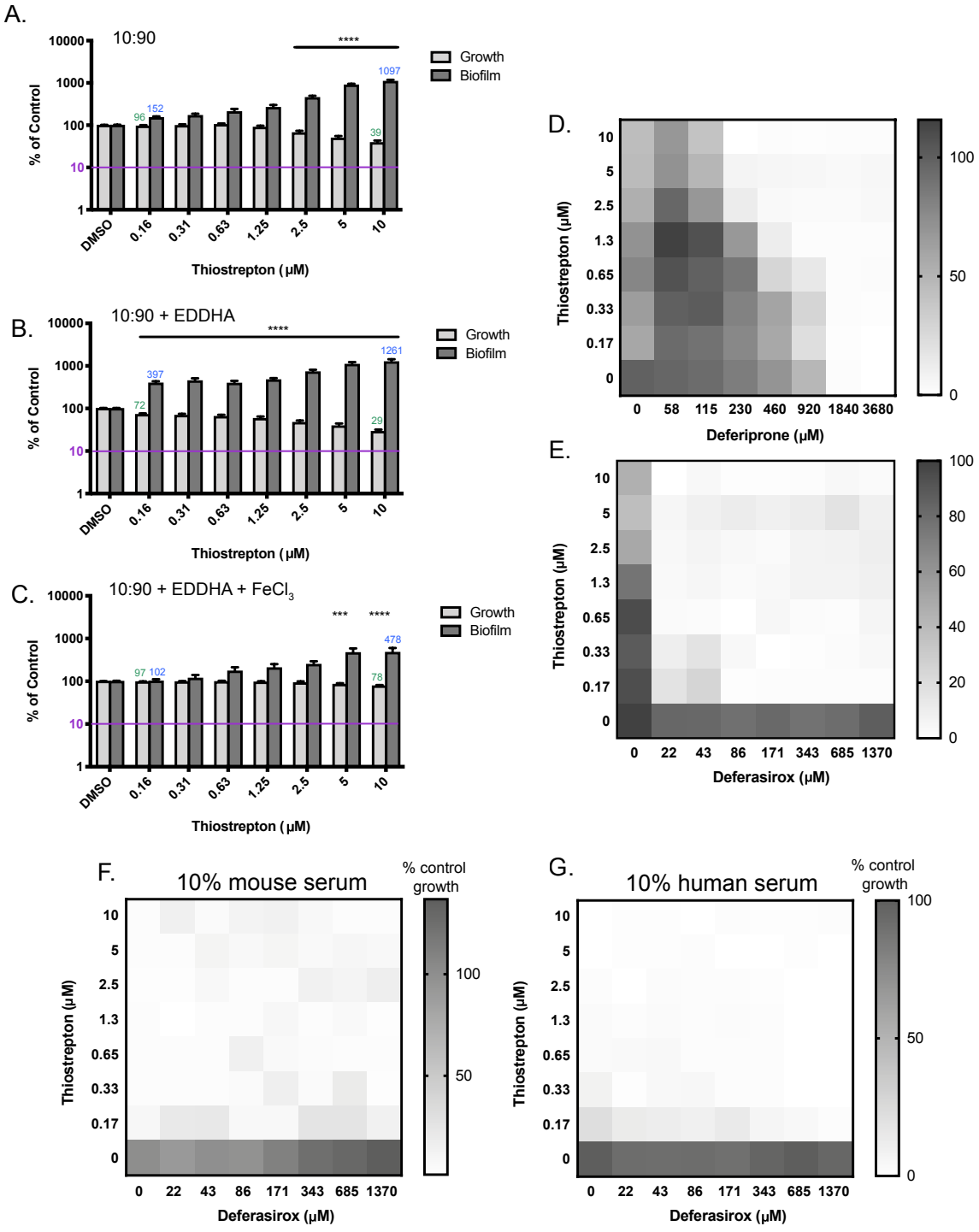

Figure 3. Thiostrepton activity is potentiated by iron chelators and serum. Biofilm stimulation by TS in 10:90 medium increased with addition of 0.1 μM EDDHA, a cell-impermeant iron chelator, while further addition of 100 μM $FeCl_3$ increased the concentration of TS required for biofilm stimulation and growth inhibition. **A.** PAO1 growth (OD_{600}) and biofilm (absorbance of CV at 600 nm) in 10:90 medium alone plotted as percent of DMSO control on a log_{10} scale, with 10% of

control indicated by a purple line; **B.** 10:90 plus 0.1μM EDDHA; **C.** 10:90 plus 0.1μM EDDHA and 100 μM $FeCl_3$. Average growth and biofilm values for the lowest and highest concentrations of TS tested are shown in green and blue numerals, respectively, to emphasize shifts caused by manipulation of iron availability. TS activity against PAO1 was also potentiated in 10:90 by FDA-approved iron chelators, **D.** deferiprone and **E.** deferasirox, or by 10% heat-inactivated **F.** mouse or **G.** human serum. Checkerboard assays were plotted as percent growth of the DMSO control (0,0 μM at lower left). The highest concentrations of DFP (3680 μM) and DSX (1370 μM) are each equal to 512 μg/ml. The Each assay was performed at least 3 times. *** $p<0.001$; **** $p<0.0001$

High-affinity iron chelation by transferrin, hemoglobin, and lactoferrin is a common strategy used by mammals to restrict the growth of microorganisms (37, 38). We investigated whether serum could also potentiate TS activity. Interestingly, addition of 10% heat-inactivated mouse or human serum to 10:90 markedly decreased the concentration of TS required to inhibit growth, regardless of the presence of DSX (**Fig 3FG**), suggesting the levels of iron were already very low under these conditions.

TS hijacks pyoverdine receptors FpvA and FpvB

To identify the route of iron-limitation dependent TS entry into *P. aeruginosa*, we tested the susceptibility of mutants from the ordered PA14 transposon library (39) with insertions in genes encoding known siderophore receptors, as well as mutants with insertions in uncharacterized OM proteins homologous to siderophore receptors. In VBMM, most mutants had TS MICs similar to the parental strain (**Table 1**). In contrast, an *fpvA* mutant, encoding the type I pyoverdine receptor, had an MIC of 10 μM. Growth inhibition was still observed at the highest TS concentration, indicating that the *fpvA* mutant remained partially susceptible. *P. aeruginosa* encodes two type I pyoverdine receptors, FpvA and FpvB, with ~39% amino acid identity (71% similarity). The *fpvB* mutant was also less susceptible to TS than the parent strain, with an MIC of 2.5 μM. Based on these patterns of susceptibility, we speculated that TS may use both FpvA and

FpvB, but that FpvA was the preferred receptor. When we deleted *fpvA* in the *fpvB* background, the double mutant was more resistant to TS than the single mutants (**Table 1**). Complementation of the *fpvAB* mutant with *fpvB* on a plasmid restored TS susceptibility to levels similar to those of the single *fpvA* mutant (**Table 1**). Together, these data suggest that TS exploits both pyoverdine receptors for entry.

Table 1. Susceptibility of *P. aeruginosa* PA14 mutants to thiostrepton in VBMM.

Strain/mutant	**Gene(s)**	**Function**	**MIC (μM)[a]**
PA14 (wild type)	N/A	N/A	0.60
fpvA::Mar2xT7	PA2398	Type 1 ferripyoverdine receptor	10
fpvB::Mar2xT7	PA4168	L-ornithine N5-oxygenase	2.5
pvdA::Mar2xT7	PA2386	Alternate Type 1 ferripyoverdine receptor	0.26
fpvA *fpvB*::Mar2xT7	PA2398, PA4168	Type I ferripyoverdine receptor, Alternate type I ferripyoverdine receptor	>10
fpvA *fpvB*::Mar2xT7 + pUCP20	PA2398, PA4168	Type I ferripyoverdine receptor, Alternate type I ferripyoverdine receptor	>10
fpvA *fpvB*::Mar2xT7 + pUCP20-*fpvB*	PA2398, PA4168	Type I ferripyoverdine receptor, Alternate type I ferripyoverdine receptor	6.6
fptA::Mar2xT7	PA4221	Pyochelin receptor	0.36
PA1322::Mar2xT7	PA1322	Probable TonB-dependent receptor	1.1
PA4837::Mar2xT7	PA4837	Probable outer membrane protein precursor	0.72
foxA::Mar2xT7	PA2466	Ferrioxamine receptor FoxA	0.60
fiuA::Mar2xT7	PA0470	Ferrichrome receptor FiuA	0.82
pirA::Mar2xT7	PA0931	Alternate enterobactin receptor	0.60
pfeA::Mar2xT7	PA2688	Enterobactin receptor	0.82
hasR::Mar2xT7	PA3408	Heme uptake outer membrane receptor	0.60
fvbA::Mar2xT7	PA4516	Vibriobactin receptor	0.60
piuA::Mar2xT7	PA4514	Hydroxamate-type ferrisiderophore receptor	0.60
PA0151::Mar2xT7	PA0151	Probable TonB-dependent receptor	0.27
chtA::Mar2xT7	PA4675	Aerobactin, Rhizobactin 1021, Schizokinen receptor	0.22
phuR::Mar2xT7	PA4710	Heme/Hemoglobin uptake receptor precursor	0.21

[a]Minimal inhibitory concentration in VBMM (average of 3 replicates). The maximum soluble concentration of TS is 10 μM, equivalent to 17 μg/ml.

TS is active against clinical isolates

To test whether TS could inhibit growth of a broader range of *P. aeruginosa* strains, particularly those for which there are fewer antibiotic options, we tested 96 recent clinical isolates for susceptibility to TS in 10:90. While approximately 1 in 10 of those strains had an MIC ≥5μM TS (**Fig 4A**), a combination of 5 μM TS (8.3 μg/ml) plus 86 μM DSX (32 μg/ml) reduced growth of most isolates to less than 10% of the DMSO control (**Fig 4A**). We next tested the activity of TS against another MDR Gram-negative pathogen that causes severe infections, *Acinetobacter baumannii* (40). *A. baumannii* encodes FpvA and FpvB homologs (**Supplementary Fig S4**), suggesting it may be susceptible to the thiopeptide. Growth of 6 of 10 *A. baumannii* strains in 10:90 was reduced to ≤50% of control with 5 μM TS, while the combination of 5μM TS and 86 μM DSX reduced growth of 8/9 clinical isolates of *A. baumanii* below 10% of control (**Fig 4B**). As reported previously (41), growth of *E. coli* – which lacks FpvAB homologs – was unaffected even at the maximum soluble concentration of 10 μM TS (**Supplementary Fig S2**). The growth of methicillin-resistant *Staphylococcus aureus* USA 300 was inhibited by 32-64 ng/ml of TS in both 10:90 and MHB, showing that iron limitation has little effect on susceptibility in the absence of an outer membrane.

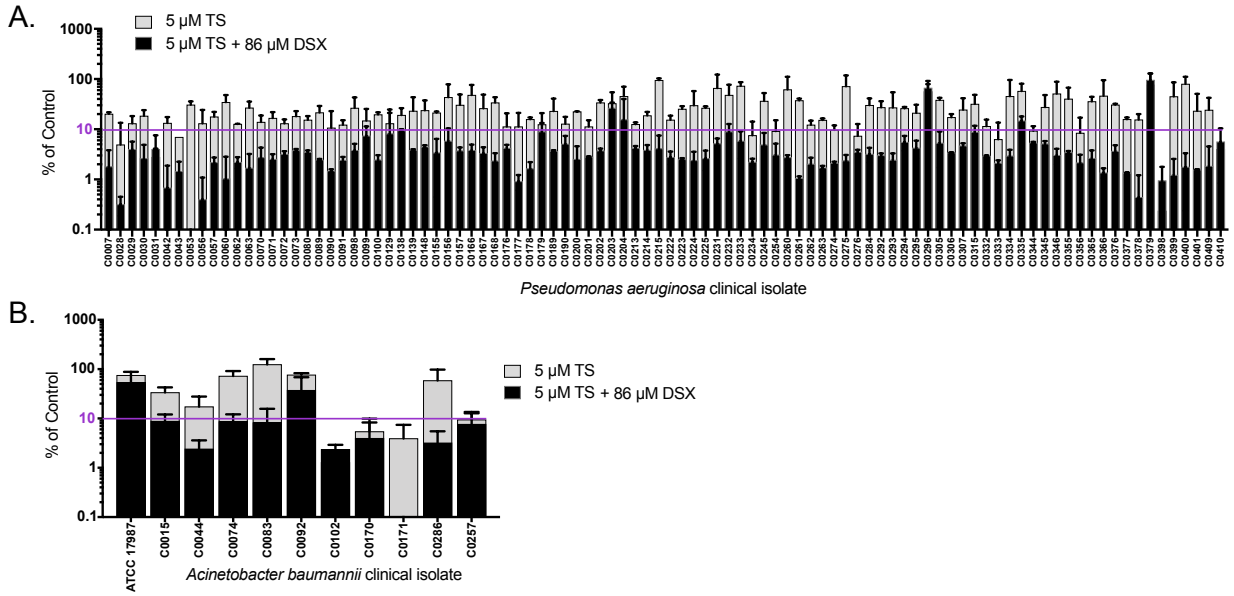

Figure 4. Thiostrepton inhibits growth of clinical isolates. The growth of most clinical isolates of **A.** *P. aeruginosa* and **B.** *Acinetobacter baumannii* (see **Supplementary Table S2** for antibiograms) was inhibited by 5 µM (8.3 µg/ml) TS in 10:90 medium (grey bars). TS activity was potentiated by the addition of 86 µM deferasirox (DSX; 32 µg/ml; black bars). Each assay was performed at least 3 times and the results plotted as percent of the DMSO-only growth control (OD_{600}) on a $\log_{10}$ scale. The 10% value is indicated with a purple line. Error bars equal one standard deviation.

Discussion

The natural role of antibiotics has been broadly debated (15, 17): are they signaling molecules that are toxic at high concentrations, or weapons used by bacteria to gain an advantage over competitors in their environment? The biofilm stimulation response to sub-inhibitory concentrations of antibiotics is consistent with both views. At concentrations too low to elicit damage, bacteria show little phenotypic response to antibiotic exposure. As concentrations approach the MIC, the bacteria respond in a dose-dependent manner by ramping up the amount of biofilm produced – detecting either the antibiotics or their effects – which may protect a subpopulation of cells. Above the MIC, antibiotics fall into the deadly weapons category. Biofilm

stimulation by sub-inhibitory concentrations of antibiotics is a common phenomenon among multiple Gram-positive and Gram-negative species, and is induced by several drug classes, suggesting it is not necessarily linked to a specific MOA (11, 17, 42). As demonstrated here, this phenomenon can be used to identify potential antibiotic activity in the absence of overt killing, a useful feature when screening at a single arbitrary concentration that may be below the MIC for a particular drug-organism combination. Interestingly, we and others (43) found that many drugs intended for eukaryotic targets can impact bacterial growth and biofilm formation (**Supplementary Table S1**), implying that they have deleterious effects on prokaryotic physiology. With a new appreciation of the role of the human microbiome in health and disease, these potential effects should be considered during drug development.

TS, a complex cyclic thiopeptide made by *Streptomyces azureus, S. hawaiiensis,* and *S. laurantii,* is experiencing a resurgence of research interest due to its broad anti-bacterial, anti-malarial, and anti-cancer activities (23, 24). It is a member of the RiPP (ribosomally-synthesized and post-translationally modified peptides) class of natural products (44), derived from a 42-amino acid precursor, TsrA (45). Although the mechanism of its antibacterial activity (inhibition of translation by binding to helices H43/H44 of 23S rRNA) and resistance (methylation of 23S rRNA residue A1067) have been deciphered (26, 46), the way in which this ~1.7 kDa molecule enters target bacteria is unknown. Our data suggest that TS is actively imported into *P. aeruginosa* under iron-restricted conditions. Its large mass would impede passive diffusion through the outer membrane, and single, double, or triple mutants lacking the outer membrane components of major efflux systems MexAB-OprM, MexCD-OprJ, and MexEF-OpmD have wild-type TS susceptibility (**Supplementary Fig S5**).

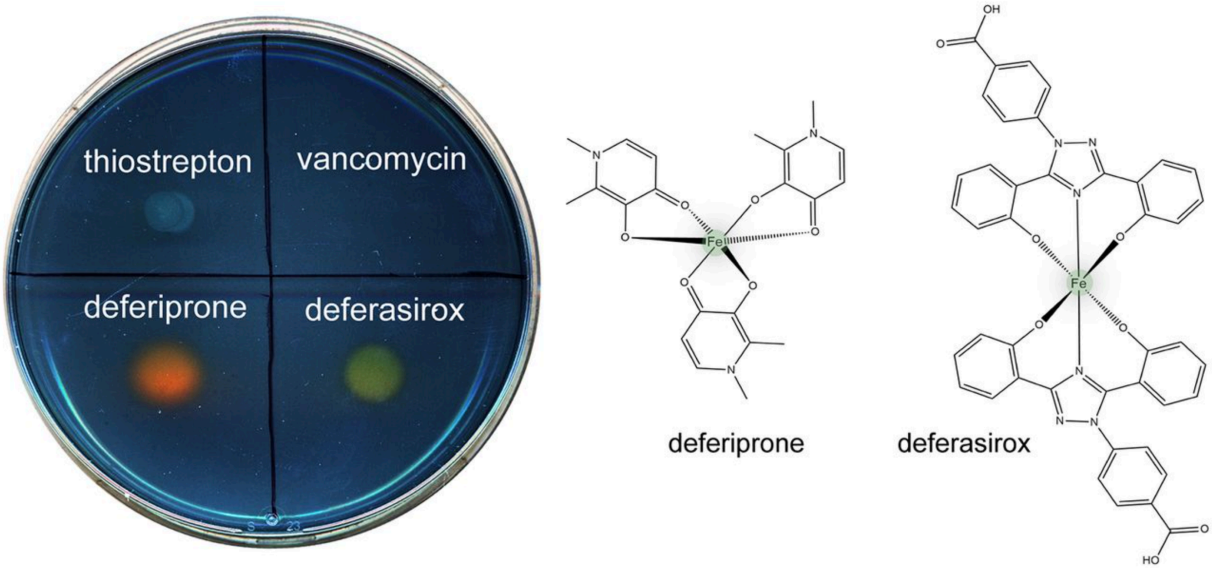

Figure 5. Thiostrepton does not bind iron. To determine whether the uptake of TS by pyoverdine receptors depends on formation of a ferric complex, its ability to decolorize chrome azurol S (CAS) agar was tested. No color change for TS (5 µl of 2 mg/ml) indicates that in contrast to chelators deferiprone and deferasirox, it is unlikely to chelate iron. The glycopeptide antibiotic vancomycin was used as a negative control. Five µl of each compound at 2 mg/ml was spotted onto CAS agar and the plate incubated at room temperature for 1 h.

There are multiple examples of molecules that exploit iron uptake pathways to enter bacteria. Class I microcins – narrow-spectrum antibiotics produced by some gram negative species – bind to siderophore receptors and share many of TS's properties. They are RiPPs, less than 5 kDa in mass, and cyclic (giving them the nickname 'lasso peptides'). Notably, binding of iron by microcins is not a prerequisite for uptake, as some interact with siderophore receptors in an iron-free state. For example, MccJ25, produced by *E. coli* (47), interacts with siderophore receptor FhuA by mimicking the structure of ferrichrome (48). Although TS has multiple hydroxyls positioned in a manner that could potentially coordinate metals (**Fig 1A**), it is unlikely to bind iron based on its inability to decolorize chrome azural agar in comparison to known chelators, DFP and DSX (**Fig 5**). Further, its structure has been solved both by X-ray crystallography and NMR, and no bound metals were reported (49, 50). The FpvA receptor is also exploited by S-pyocins, 40-80

kDa peptide antibiotics produced by competing *P. aeruginosa* strains, showing that it is an important promiscuous access point for diverse molecules in addition to its ligand, pyoverdine (33, 34, 51).

Our discovery that TS exploits FpvA and FpvB for uptake into the periplasm explains the resistance of gram-negative species such as *E. coli* to this antibiotic, as they lack those proteins. Bioinformatic searches show FpvAB homologs are expressed by *P. aeruginosa* and related pathogens – including *A. baumannii* (**Supplementary Fig S4**) – suggesting that TS could have utility as a narrow-spectrum agent. Use of multiple pyoverdine receptors by TS may reduce the probability of resistance arising through mutation of a single receptor, although genome analysis of clinical isolate C0379 that was most resistant to the combination of TS and DSX (**Fig 4A**) revealed a wild type copy of *fpvA* coupled with an ~800 bp deletion encompassing the 5' region of *fpvB*. Multiple single nucleotide polymorphisms with unknown effects on function were present in other strains, both TS susceptible and resistant isolates. A more detailed investigation of *P. aeruginosa* strains resistant to TS will be needed to understand the most likely routes by which it occurs.

Although TS uses siderophore receptors to cross the *P. aeruginosa* OM, the way in which this compound transits the cytoplasmic membranes of gram-positive and gram-negative bacteria to reach its ribosomal targets remains undefined. Expression of *tsr* in *P. aeruginosa* conferred resistance, confirming that TS acts at least in part via its canonical bacteriostatic MOA. While PA14 expressing Tsr was significantly more resistant to TS than the control, it was more sensitive than PAO1. This difference is not due to nucleotide polymorphism at the Tsr methylation site on the rRNA, as these residues are conserved between PAO1 and PA14. The reasons for strain-

specific differences in susceptibility are unclear, but our data confirm that most clinical *P. aeruginosa* isolates tested are susceptible to TS, especially when combined with DSX (**Fig 4A**).

TS's major liability is its poor solubility (52). Smaller, more soluble fragments that retain activity against gram-positive bacteria and have reduced toxicity for eukaryotic cells have been identified (53) but it is not clear if they would be active against *P. aeruginosa* or *A. baumannii* if uptake by the FpvAB receptors requires the intact molecule. Another way to circumvent solubility issues is to reduce the concentration required to kill. Our data show that co-administration of TS with FDA-approved iron chelators DFP or DSX markedly reduces its MIC against *P. aeruginosa* and *A. baumannii* (**Fig 3DE, Fig 4AB**). These effects are specific for TS, as DSX failed to synergize with other antibiotics that do not depend on iron availability for uptake (**Supplementary Fig S6**). The true potential of TS as an anti-infective may be underestimated, as MIC evaluations are typically performed in rich, iron-replete media. Many host environments are iron-restricted, particularly in the presence of infection and inflammation (54-56). Our data show that TS is active at low micromolar concentrations against *P. aeruginosa* in 10% mouse and human serum, even in the absence of added chelator (**Fig 3FG**). The combination of TS with DSX may be useful at sites such as in chronically-infected lungs, where iron is more abundant (57).

In summary, we showed that biofilm stimulation can be used in high-throughput small molecule screening to report on sub-inhibitory antibiotic activity that may otherwise be missed using the usual metric of growth inhibition. In a small screen of less than 4000 molecules at a fixed concentration of 10 μM, we doubled the number of potential antimicrobials identified, finding 60 growth inhibitors plus another 60 molecules that stimulated biofilm formation. This phenotype can indicate potential antimicrobial activity at higher concentrations, or under different growth conditions, as demonstrated here for TS. Stimulation of biofilm matrix production by TS in the

gram-positive genus *Bacillus* was reported previously, and that phenotype leveraged to identify novel thiopeptide producers in co-cultures (58). Those studies, and the data presented here, suggest that monitoring biofilm stimulation (or an easily assayed proxy thereof, such as increased expression from biofilm matrix promoters) could allow for more sensitive detection of molecules with potential antibacterial activity during screening, making it a useful addition to the antimicrobial discovery toolkit.

Methods

Bacterial strains and culture conditions

The bacterial strains and plasmids used in this study are listed in **Table 1** and **Supplementary Table S2**. Bacterial cultures were grown in Lysogeny Broth (LB), 10:90 (10% LB and 90% phosphate buffered saline), M9 medium, Vogel Bonner minimal medium (VBMM), or cation-adjusted Mueller-Hinton broth (MHB) as indicated. Where solid media were used, plates were solidified with 1.5% agar. DFP (Sigma-Aldrich) and DSX (Cayman Chemicals) were stored at 4°C until use. TS was stored at -20˚C. A 60 mg/mL stock solution of DFP was made in 6M HCl and Milli-Q H_2O (DFP solvent) in a ratio of 3:50. A 20 mg/mL stock solution of DSX was made in DMSO. A 20mM stock solution of TS was made in DMSO.

Growth curves

PAO1-KP was inoculated from a -80°C stock into 5 ml LB broth and grown with shaking at 200 rpm, 16h, 37°C. The overnight culture was subcultured at 1:500 into 5 different media (LB, 10:90, M9, Mueller-Hinton (MH), and VBMM) – incubated at 37°C for 6h with shaking at 200 rpm. Each subculture was standardized to $OD_{600} \sim 0.1$ (Biomate 3 Spectrophotometer) then diluted

1:500 into the same medium. Six replicates of 200 µl of each sample were added to a 96 well plate, which was incubated at 37°C for 24 h with shaking at 200 rpm (Tecan Ultra Evolution plate reader). The OD_{612} was read every 15 min for 24 h. The data for the six replicates of each sample were averaged and the experiment was repeated 3 times. The final data with standard deviations were plotted using Prism (Graphpad).

Biofilm modulation assay

Biofilm formation was assayed as described in (13), with modifications. Briefly, *P. aeruginosa* was inoculated in 5 mL of LB and grown at 37°C overnight, shaking at 200 rpm, and subsequently standardized to an OD_{600} of ~ 0.1 in 10:90. For the initial screen, 1 mM compound stocks in DMSO were diluted 1:100 in standardized cell suspension (1.5 µL of compound stock in 148.5 µL of cell suspension) to a final concentration of 10 µM. Control wells contained 10:90 plus 1% DMSO (sterility control) or standardized cell suspension plus 1% DMSO (growth control). Biofilms were formed on polystyrene peg lids (Nunc). After placement of the peg lid, the plate was sealed with parafilm to prevent evaporation and incubated for 16 h at 37°C, 200 rpm. Following incubation, the 96-peg lid was removed and planktonic density in the 96 well plate measured at OD_{600} to assess the effect of test compounds on bacterial growth. The lid was transferred to a new microtiter plate containing 200 µl of 1X phosphate-buffered saline (PBS) per well for 10 min to wash off any loosely adherent bacterial cells, then to a microtiter plate containing 200 µL of 0.1% (wt/vol) CV per well for 15 min. Following staining, the lid was washed with 70 mL of dH_2O, in a single well tray, for 10 min. This step was repeated four times to ensure complete removal of excess CV. The lid was transferred to a 96-well plate containing 200 µL of 33% (vol/vol) acetic acid per well for 5 min to elute the bound CV. The absorbance of the eluted CV

was measured at 600 nm (BioTek ELx800), and the results plotted as percent of the DMSO control using Prism (Graphpad). Screens were performed in duplicate. Compounds that resulted in <50% of control biofilm were defined as biofilm inhibitors, while compounds that resulted in >200% of control biofilm were defined as biofilm stimulators. Compounds of interest were further evaluated using the same assay but over a wider range of concentrations (dose-response assay).

For TS dose response assays, TS stock solutions were diluted in DMSO and 2µL of the resulting solutions plus 148µL of a bacterial suspension standardized to an OD_{600} of ~ 0.1 in 10:90 were added to a 96 well plate in triplicate, as described above. Control wells contained 148µL of 10:90 + 1.3% DMSO (sterility control) or standardized bacterial suspension + 1.3% DMSO (growth control). For EDDHA alone or with $FeCl_3$ experiments, 2µL of each were added as aqueous solutions to reach final concentrations of 0.1µM EDDHA and 100µM $FeCl_3$, and the amount of bacterial suspension adjusted to keep the total well volume at 150µL. Controls for EDDHA and $FeCl_3$ were 2µL of sterile dH_20. Biofilms were grown for 16h at 37˚C, 200 rpm, then stained and quantified as described above. Assays were performed in triplicate and results were graphed using Prism (Graphpad) as a percentage of the DMSO control.

Compounds screened

The biofilm modulation assay was used to screen the McMaster Bioactives compound collection. This curated collection includes off-patent, FDA-approved drugs from the Prestwick Chemical Library (Prestwick Chemical, Illkirch, France), purified natural products from the Screen-Well Natural Products Library (Enzo Life Sciences, Inc., Farmingdale, NY, USA), drug-like molecules from the Lopac^{1280} (International Version) collection (Sigma-Aldrich Canada Ltd., Oakville, ON, Canada) and the Spectrum Collection (MicroSource Discovery Systems, Inc.,

Gaylordsville, CT, USA) which includes off patent drugs, natural products, and other biologically active compounds. In total, the collection is 3921 unique compounds.

Construction of a *tsr* plasmid for expression in *P. aeruginosa*

The *tsr* gene from pIJ6902 (59) was PCR-amplified using primers 5' GAATCCCGGGCGGTAGGACGACCATGAC 3' and 5' CTTCAAGCTTTTATCGGTTGGCCGCGAG 3'. Both the PCR product and pUCP20 vector were digested with SmaI and HindIII, gel-purified, and ligated at a 1:3 molar ratio using T4 DNA ligase. The ligated DNA was transformed into *E. coli* DH5a and transformants selected on LB agar containing 100 μg/mL ampicillin and 5-bromo-4-chloro-3-indolyl-β-D-galactopyranoside for blue-white selection. Plasmids from white colonies were purified using a GeneJet Plasmid Miniprep kit (Thermo Scientific) following the manufacturer's protocols. After verification by restriction digest and DNA sequencing, pUCP20 and pUCP20-tsr were each introduced into *P. aeruginosa* PAO1 and PA14 by electroporation. Transformants were selected on LB agar containing 200 μg/mL carbenicillin.

Serum Preparation

Human serum (Corning) and mouse serum (Equitech-Bio) were stored at -20°C. Serum was aliquoted into 5 mL culture tubes by thawing once at 37°C for 30mins with occasional gentle mixing to maintain uniformity. Culture tubes were frozen at -20°C until use. To make 10% serum solutions, serum was thawed for 10 mins at 37°C and then heat-inactivated at 57°C for 30mins. 2mL of heat-inactivated serum was added to 18mL 10:90 and gently mixed. This 10% serum solution was used for checkerboard assays.

MIC and checkboard assays

MICs were determined with microbroth dilution assays in Nunc 96-well plates. Vehicle controls consisted of 1:75 dilutions of DMSO in 10:90 inoculated with PA14 or its mutants as described in Growth Curves. Sterile controls consisted of 1:75 dilutions of DMSO in 10:90. Seven serially diluted concentrations of TS – with 17 μg/mL being the highest final concentration – was set up in triplicate. Tests were done with 1:75 dilutions of each TS concentration in 10:90 inoculated with PA14 or its mutants as described in Growth Curves. Plates were sealed to prevent evaporation and incubated with shaking at 200 rpm, 16h, 37°C. The OD_{600} of the plates was read (Multiskan Go - Thermo Fisher Scientific) and used to determine the MIC. The final volume of each well was 150 μL and each experiment was repeated at least three times.

Checkerboard assays were set-up using Nunc 96-well plates in an 8-well by 8-well format. Two columns were allocated for vehicle controls and two columns for sterility controls. Vehicle controls contained 2 μL DMSO + 2 μL DFP solvent for checkerboards with TS and DFP or 4 μL DMSO for TS and DSX. 146 μL of 10:90 or 10% serum was then inoculated with PA14 or PAO1-KP as described in Growth Curves and added to the wells. Sterile controls contained the same components in 10:90 or 10% serum, without cells. Serial dilutions of TS – with 17 μg/mL being the highest final concentration – was added along the ordinate of the checkerboard (increasing concentration from bottom to top) whereas serial dilutions of DFP or DSX – with 512 μg/mL being the highest final concentration – was added along the abscissa (increasing concentration from left to right). The final volume of each well was 150 μL and each checkerboard was repeated at least three times. Plates were incubated and the final OD_{600} determined as detailed above.

Clinical isolates testing

Clinical isolates of *P. aeruginosa* and *A. baumannii* were inoculated from -80°C stocks into 200 µL LB broth and grown with shaking at 200 rpm, 16h, 37°C. in Nunc 96-well plates. The overnight cultures were subcultured (1:25 dilution) into 10:90 and grown with shaking at 200 rpm, 2h, 37°C**.** Vehicle controls consisted of 4 µL of DMSO, 144µL 10:90 and 2 µL of subculture. Sterile controls consisted of 4 µL of DMSO and 146µL 10:90. Test samples consisted of 2 µL of TS (final concentration of 5 µM, 8.3 µg/ml), 2 µL of DMSO (or DSX, final concentration of 86 µM, 32 µg/mL), 144 µL 10:90 and 2 µL of subculture. The final volume of each well was 150 µL and each checkerboard was repeated at least three times. Plates were incubated with shaking at 200 rpm, 16h, 37°C and OD_{600} was measured (Multiskan Go - Thermo Fisher Scientific). The results were plotted as percent of control (wells containing only DMSO) using Prism (GraphPad).

CAS Plate Assay

CAS agar plates were prepared as described by Louden et al. All components were purchased from Sigma except for agar, NaOH, NaCl (BioShop), casamino acids (Becton Dickinson), and glucose (EMD Millipore). Stock solutions of TS, vancomycin (VAN), DSX, and DFP were standardized to 2 mg/mL. Five µL of 2 mg/mL compound was spotted on a plate and incubated at room temperature for one hour.

Generation of efflux mutants

Deletion mutants lacking the outer membrane components of the 4 major RND efflux systems of *P. aeruginosa* (MexAB-OprM, MexXY-OprM, MexCD-OprJ, and MexEF-OpmD) were generated as reported previously. Briefly, the pairs of primers listed in Supplementary Table

S3 were used to amplify regions up and downstream of the gene to be deleted. The PCR products were digested with the restriction enzymes indicated in the primer sequences and the resulting fragments ligated into the suicide vector, pEX18Gm. After DNA sequencing validation of the constructs, they were introduced into *E. coli* SM10 for biparental mating into *P. aeruginosa* PAO1. Mating mixtures were plated on Pseudomonas Isolation Agar containing 200 μg/ml Gm to counter-select the donor. Gm-sensitive double recombinants were selected on LB agar, no salt, plus 5% w/v sucrose. Gm-sensitive deletion mutants were identified by PCR and validated by DNA sequencing of the deletion junction.

Acknowledgements

We thank Gerry Wright for access to strains from the Wright Clinical Collection, David Heinrichs for the gift of EDDHA and helpful discussions, and Neha Sharma, Andrew Hogan, Amanda Veri, and Victor Yang for assistance with method development. This work was supported by a Natural Sciences and Engineering Research (NSERC) grant RGPIN-2016-06521, and by Ontario Research Fund grant RE07-048. MRR and UN held Ontario Graduate Scholarships, MR was supported by an NSERC Undergraduate Summer Research Award, SKP was supported by a Summer Studentship from GlycoNet, and HA was supported by a Summer Studentship from Cystic Fibrosis Canada.

References

1. Zabawa TP, Pucci MJ, Parr TR, Jr., Lister T. 2016. Treatment of Gram-negative bacterial infections by potentiation of antibiotics. *Curr Opin Microbiol* 33:7-12.
2. Blair JM, Webber MA, Baylay AJ, Ogbolu DO, Piddock LJ. 2015. Molecular mechanisms of antibiotic resistance. *Nat Rev Microbiol* 13:42-51.
3. Hall CW, Mah TF. 2017. Molecular mechanisms of biofilm-based antibiotic resistance and tolerance in pathogenic bacteria. *FEMS Microbiol Rev* 41:276-301.
4. Kalan L, Wright GD. 2011. Antibiotic adjuvants: multicomponent anti-infective strategies. *Expert Rev Mol Med* 13:e5.
5. Tacconelli E, Carrara E, Savoldi A, Harbarth S, Mendelson M, Monnet DL, Pulcini C, Kahlmeter G, Kluytmans J, Carmeli Y, Ouellette M, Outterson K, Patel J, Cavaleri M, Cox EM, Houchens CR, Grayson ML, Hansen P, Singh N, Theuretzbacher U, Magrini N, Group WHOPPLW. 2018. Discovery, research, and development of new antibiotics: the WHO priority list of antibiotic-resistant bacteria and tuberculosis. *Lancet Infect Dis* 18:318-327.
6. Fothergill JL, Winstanley C, James CE. 2012. Novel therapeutic strategies to counter *Pseudomonas aeruginosa* infections. *Expert Rev Anti Infect Ther* 10:219-35.
7. Rybtke M, Hultqvist LD, Givskov M, Tolker-Nielsen T. 2015. *Pseudomonas aeruginosa* Biofilm Infections: Community Structure, Antimicrobial Tolerance and Immune Response. J Mol Biol 427:3628-45.
8. Burrows LL. 2018. The Therapeutic Pipeline for *Pseudomonas aeruginosa* Infections. ACS Infect Dis 4:1041-1047.
9. Nguyen L, Garcia J, Gruenberg K, MacDougall C. 2018. Multidrug-Resistant *Pseudomonas* Infections: Hard to Treat, But Hope on the Horizon? *Curr Infect Dis Rep* 20:23.
10. Page MG, Heim J. 2009. Prospects for the next anti-*Pseudomonas* drug. *Curr Opin Pharmacol* 9:558-65.
11. Ranieri MR, Whitchurch CB, Burrows LL. 2018. Mechanisms of biofilm stimulation by subinhibitory concentrations of antimicrobials. *Curr Opin Microbiol* 45:164-169.
12. Hoffman LR, D'Argenio DA, MacCoss MJ, Zhang Z, Jones RA, Miller SI. 2005. Aminoglycoside antibiotics induce bacterial biofilm formation. *Nature* 436:1171-5.
13. Wenderska IB, Chong M, McNulty J, Wright GD, Burrows LL. 2011. Palmitoyl-DL-carnitine is a multitarget inhibitor of *Pseudomonas aeruginosa* biofilm development. *Chembiochem* 12:2759-66.
14. Ejim L, Farha MA, Falconer SB, Wildenhain J, Coombes BK, Tyers M, Brown ED, Wright GD. 2011. Combinations of antibiotics and nonantibiotic drugs enhance antimicrobial efficacy. *Nat Chem Biol* 7:348-50.
15. Linares JF, Gustafsson I, Baquero F, Martinez JL. 2006. Antibiotics as intermicrobial signaling agents instead of weapons. *Proc Natl Acad Sci U S A* 103:19484-9.
16. Jones C, Allsopp L, Horlick J, Kulasekara H, Filloux A. 2013. Subinhibitory concentration of kanamycin induces the *Pseudomonas aeruginosa* type VI secretion system. PLoS One 8:e81132.
17. Oliveira NM, Martinez-Garcia E, Xavier J, Durham WM, Kolter R, Kim W, Foster KR. 2015. Biofilm Formation As a Response to Ecological Competition. PLoS Biol 13:e1002191.
18. Ahmed MN, Porse A, Sommer MOA, Hoiby N, Ciofu O. 2018. Evolution of Antibiotic Resistance in Biofilm and Planktonic *Pseudomonas aeruginosa* Populations Exposed to Subinhibitory Levels of Ciprofloxacin. *Antimicrob Agents Chemother* 62.

19. Delcour AH. 2009. Outer membrane permeability and antibiotic resistance. *Biochim Biophys Acta* 1794:808-16.
20. Cox G, Wright GD. 2013. Intrinsic antibiotic resistance: mechanisms, origins, challenges and solutions. *Int J Med Microbiol* 303:287-92.
21. Zlitni S, Ferruccio LF, Brown ED. 2013. Metabolic suppression identifies new antibacterial inhibitors under nutrient limitation. *Nat Chem Biol* 9:796-804.
22. Weisblum B, Demohn V. 1970. Thiostrepton, an inhibitor of 5OS ribosome subunit function. *J Bacteriol* 101:1073-5.
23. Gartel AL. 2008. FoxM1 inhibitors as potential anticancer drugs. *Expert Opin Ther Targets* 12:663-5.
24. Aminake MN, Schoof S, Sologub L, Leubner M, Kirschner M, Arndt HD, Pradel G. 2011. Thiostrepton and derivatives exhibit antimalarial and gametocytocidal activity by dually targeting parasite proteasome and apicoplast. *Antimicrob Agents Chemother* 55:1338-48.
25. Bibb MJ, Bibb MJ, Ward JM, Cohen SN. 1985. Nucleotide sequences encoding and promoting expression of three antibiotic resistance genes indigenous to *Streptomyces. Mol Gen Genet* 199:26-36.
26. Dunstan MS, Hang PC, Zelinskaya NV, Honek JF, Conn GL. 2009. Structure of the thiostrepton resistance methyltransferase.S-adenosyl-L-methionine complex and its interaction with ribosomal RNA. *J Biol Chem* 284:17013-20.
27. Sezonov G, Joseleau-Petit D, D'Ari R. 2007. *Escherichia coli* physiology in Luria-Bertani broth. *J Bacteriol* 189:8746-9.
28. Vogel HJ, Bonner DM. 1956. Acetylornithinase of *Escherichia coli*: partial purification and some properties. *J Biol Chem* 218:97-106.
29. Pletzer D, Braun Y, Dubiley S, Lafon C, Kohler T, Page MGP, Mourez M, Severinov K, Weingart H. 2015. The *Pseudomonas aeruginosa* PA14 ABC Transporter NppA1A2BCD Is Required for Uptake of Peptidyl Nucleoside Antibiotics. *J Bacteriol* 197:2217-2228.
30. Pletzer D, Braun Y, Weingart H. 2016. Swarming motility is modulated by expression of the putative xenosiderophore transporter SppR-SppABCD in *Pseudomonas aeruginosa* PA14. *Antonie Van Leeuwenhoek* 109:737-53.
31. Grinter R, Milner J, Walker D. 2013. Beware of proteins bearing gifts: protein antibiotics that use iron as a Trojan horse. *FEMS Microbiol Lett* 338:1-9.
32. Braun V, Pramanik A, Gwinner T, Koberle M, Bohn E. 2009. Sideromycins: tools and antibiotics. *Biometals* 22:3-13.
33. Denayer S, Matthijs S, Cornelis P. 2007. Pyocin S2 (Sa) kills *Pseudomonas aeruginosa* strains via the FpvA type I ferripyoverdine receptor. *J Bacteriol* 189:7663-8.
34. Elfarash A, Wei Q, Cornelis P. 2012. The soluble pyocins S2 and S4 from *Pseudomonas aeruginosa* bind to the same FpvAI receptor. *Microbiologyopen* 1:268-75.
35. Poole K, Neshat S, Heinrichs D. 1991. Pyoverdine-mediated iron transport in *Pseudomonas aeruginosa*: involvement of a high-molecular-mass outer membrane protein. *FEMS Microbiol Lett* 62:1-5.
36. Kwiatkowski JL. 2016. Current recommendations for chelation for transfusion-dependent thalassemia. *Ann N Y Acad Sci* 1368:107-14.
37. Skaar EP. 2010. The battle for iron between bacterial pathogens and their vertebrate hosts. *PLoS Pathog* 6:e1000949.

38. Rajamaki A, Irjala K, Aitio A. 1979. Immunochemical determination of serum transferrin. Reference values, correlation with serum total iron-binding capacity and value in the diagnosis of iron deficiency anaemia and anaemia of chronic disorders. *Scand J Haematol* 23:227-31.
39. Liberati NT, Urbach JM, Miyata S, Lee DG, Drenkard E, Wu G, Villanueva J, Wei T, Ausubel FM. 2006. An ordered, nonredundant library of *Pseudomonas aeruginosa* strain PA14 transposon insertion mutants. *Proc Natl Acad Sci U S A* 103:2833-8.
40. Harding CM, Hennon SW, Feldman MF. 2018. Uncovering the mechanisms of *Acinetobacter baumannii* virulence. *Nat Rev Microbiol* 16:91-102.
41. Singer ME, Finnerty WR. 1988. Construction of an *Escherichia coli-Rhodococcus* shuttle vector and plasmid transformation in *Rhodococcus* spp. *J Bacteriol* 170:638-45.
42. Townsley L, Shank EA. 2017. Natural-Product Antibiotics: Cues for Modulating Bacterial Biofilm Formation. *Trends Microbiol* 25:1016-1026.
43. Maier L, Pruteanu M, Kuhn M, Zeller G, Telzerow A, Anderson EE, Brochado AR, Fernandez KC, Dose H, Mori H, Patil KR, Bork P, Typas A. 2018. Extensive impact of non-antibiotic drugs on human gut bacteria. *Nature* 555:623-628.
44. Arnison PG, Bibb MJ, Bierbaum G, Bowers AA, Bugni TS, Bulaj G, Camarero JA, Campopiano DJ, Challis GL, Clardy J, Cotter PD, Craik DJ, Dawson M, Dittmann E, Donadio S, Dorrestein PC, Entian KD, Fischbach MA, Garavelli JS, Goransson U, Gruber CW, Haft DH, Hemscheidt TK, Hertweck C, Hill C, Horswill AR, Jaspars M, Kelly WL, Klinman JP, Kuipers OP, Link AJ, Liu W, Marahiel MA, Mitchell DA, Moll GN, Moore BS, Muller R, Nair SK, Nes IF, Norris GE, Olivera BM, Onaka H, Patchett ML, Piel J, Reaney MJ, Rebuffat S, Ross RP, Sahl HG, Schmidt EW, Selsted ME, et al. 2013. Ribosomally synthesized and post-translationally modified peptide natural products: overview and recommendations for a universal nomenclature. *Nat Prod Rep* 30:108-60.
45. Kelly WL, Pan L, Li C. 2009. Thiostrepton biosynthesis: prototype for a new family of bacteriocins. *J Am Chem Soc* 131:4327-34.
46. Baumann S, Schoof S, Bolten M, Haering C, Takagi M, Shin-ya K, Arndt HD. 2010. Molecular determinants of microbial resistance to thiopeptide antibiotics. *J Am Chem Soc* 132:6973-81.
47. Asensio C, Perez-Diaz JC. 1976. A new family of low molecular weight antibiotics from enterobacteria. *Biochem Biophys Res Commun* 69:7-14.
48. Mathavan I, Zirah S, Mehmood S, Choudhury HG, Goulard C, Li Y, Robinson CV, Rebuffat S, Beis K. 2014. Structural basis for hijacking siderophore receptors by antimicrobial lasso peptides. *Nat Chem Biol* 10:340-2.
49. Anderson B, Hodgkin DC, Viswamitra MA. 1970. The structure of thiostrepton. *Nature* 225:233-5.
50. Jonker HR, Baumann S, Wolf A, Schoof S, Hiller F, Schulte KW, Kirschner KN, Schwalbe H, Arndt HD. 2011. NMR structures of thiostrepton derivatives for characterization of the ribosomal binding site. *Angew Chem Int Ed Engl* 50:3308-12.
51. White P, Joshi A, Rassam P, Housden NG, Kaminska R, Goult JD, Redfield C, McCaughey LC, Walker D, Mohammed S, Kleanthous C. 2017. Exploitation of an iron transporter for bacterial protein antibiotic import. *Proc Natl Acad Sci U S A* 114:12051-12056.
52. Zhang F, Kelly WL. 2012. In vivo production of thiopeptide variants. *Methods Enzymol* 516:3-24.

53. Nicolaou KC, Zak M, Rahimipour S, Estrada AA, Lee SH, O'Brate A, Giannakakou P, Ghadiri MR. 2005. Discovery of a biologically active thiostrepton fragment. J *Am Chem Soc* 127:15042-4.
54. Schaible UE, Kaufmann SH. 2004. Iron and microbial infection. *Nat Rev Microbiol* 2:946-53.
55. Nairz M, Schroll A, Sonnweber T, Weiss G. 2010. The struggle for iron - a metal at the host-pathogen interface. *Cell Microbiol* 12:1691-702.
56. Cassat JE, Skaar EP. 2013. Iron in infection and immunity. *Cell Host Microbe* 13:509-519.
57. Reid DW, Carroll V, O'May C, Champion A, Kirov SM. 2007. Increased airway iron as a potential factor in the persistence of *Pseudomonas aeruginosa* infection in cystic fibrosis. *Eur Respir J* 30:286-92.
58. Bleich R, Watrous JD, Dorrestein PC, Bowers AA, Shank EA. 2015. Thiopeptide antibiotics stimulate biofilm formation in *Bacillus subtilis. Proc Natl Acad Sci U S A* 112:3086-91.
59. Huang J, Shi J, Molle V, Sohlberg B, Weaver D, Bibb MJ, Karoonuthaisiri N, Lih CJ, Kao CM, Buttner MJ, Cohen SN. 2005. Cross-regulation among disparate antibiotic biosynthetic pathways of *Streptomyces coelicolor. Mol Microbiol* 58:1276-87.

Supplementary Figures

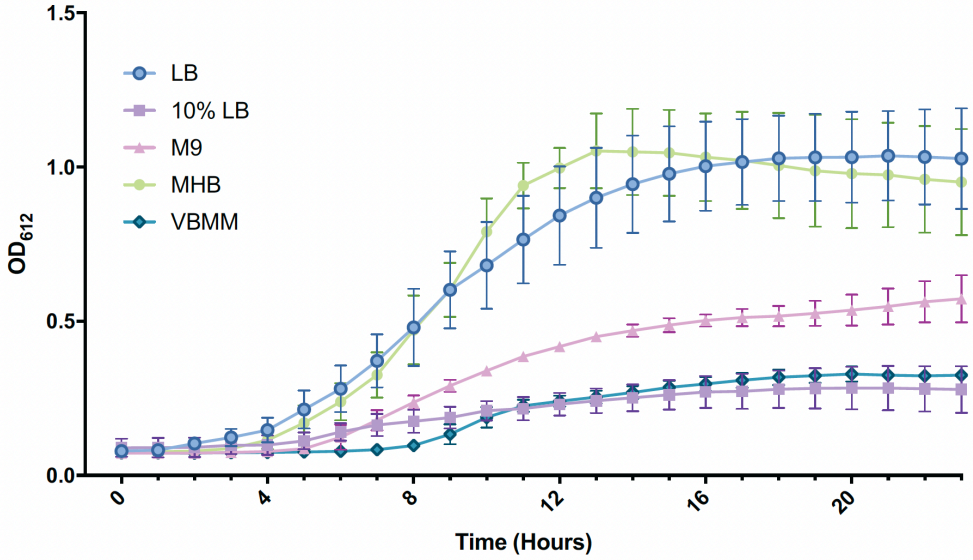

Supplementary Figure 1. Growth of *P. aeruginosa* PAO1 in various media. The growth (OD_{612}) of strain PAO1 in various media was monitored for 24 h. Growth in 10:90 (10% LB, 90% PBS) was similar to that in VBMM (Vogel Bronner Minimal Medium) (1). The experiment was performed 3 times in triplicate.

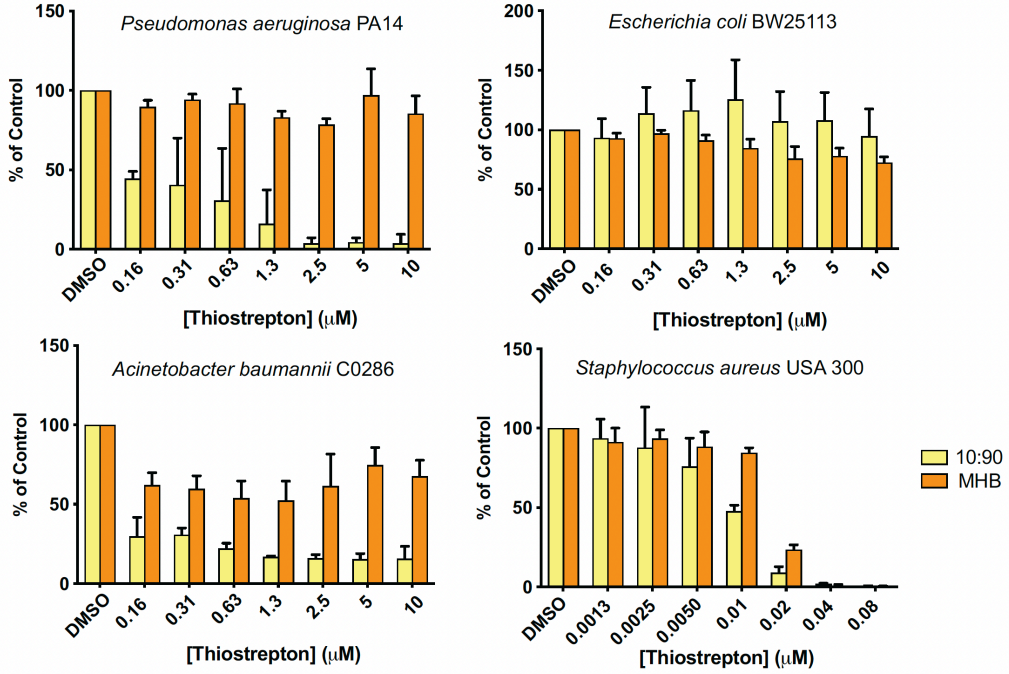

Supplementary Figure 2. Thiostrepton susceptibility in Mueller-Hinton Broth versus 10:90. The susceptibility of *P. aeruginosa* PA14 (2), *E. coli* BW25113 (3), *A. baumannii* C0286 (this study), and *S. aureus* USA300 (4) was compared in MHB verus 10:90 medium. E. coli lacks FpvAB and is resistant to TS in both media. S. aureus is highly susceptible to TS in both media, suggesting that TS uptake by Gram-positive bacteria is independent of iron levels.

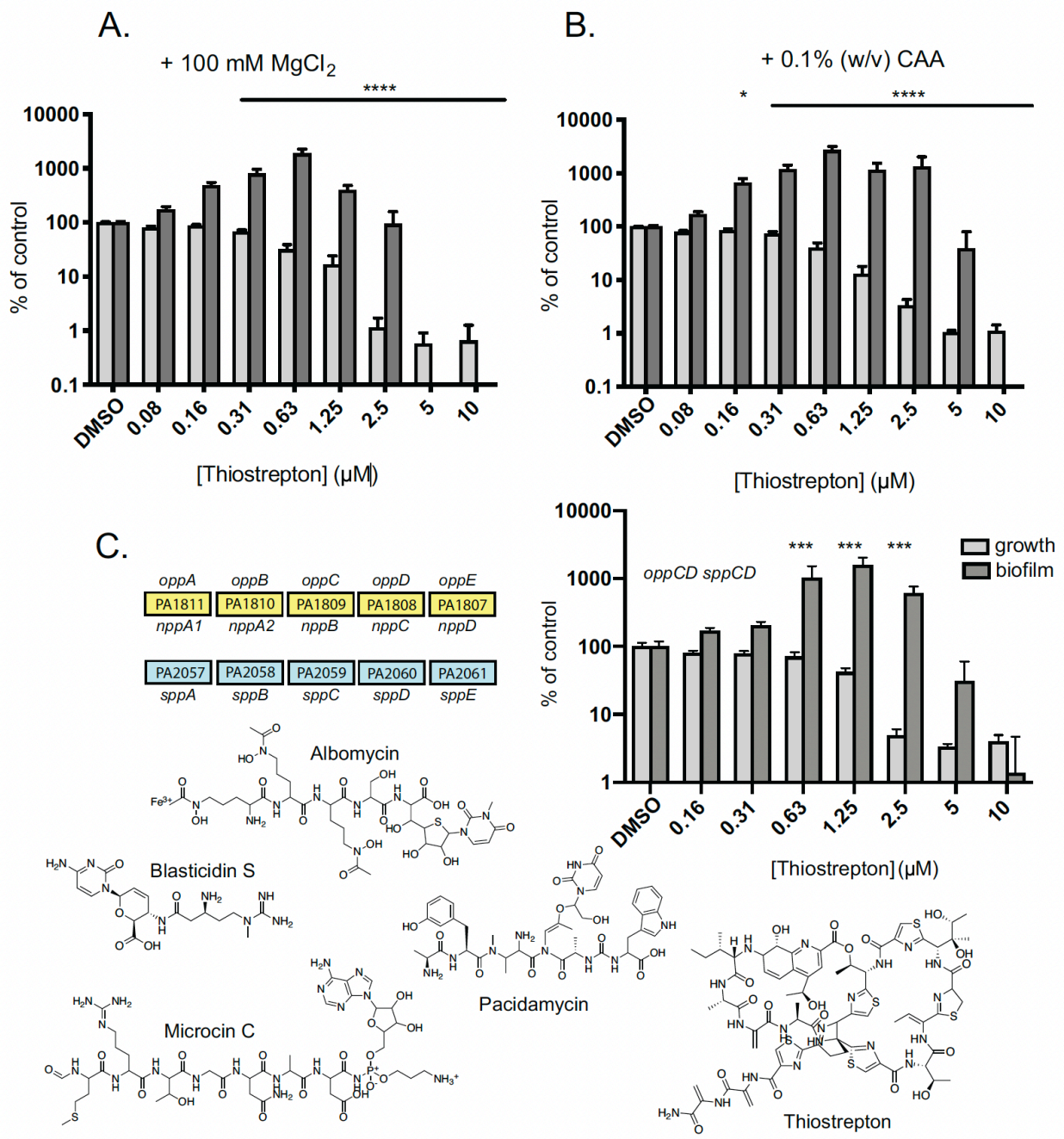

Supplementary Figure 3. Thiostrepton susceptibility is unaffected by addition of Mg^{2+} or casamino acids, or deletion of peptide transporters. **A.** To rule out increased susceptibility to TS due to enhanced outer membrane permeability from chelation of divalent cations by citrate – the carbon source in VBMM – the medium was supplemented with 100 mM MgCl2. Growth and biofilm formation are plotted as percent of the DMSO control on a log10 scale. **B.** Supplementation of VBMM with 0.1% (w/v) casamino acids did not affect susceptibility of PAO1 to TS. **C.** Deletion of the C and D components of peptide transport systems Opp (also called Npp) used by other peptide antibiotics including pacidamycin, blasticidin S, microcin C, and albomycin for uptake (5, 6) and a homologous system Spp (7), had no effect on TS susceptibility.

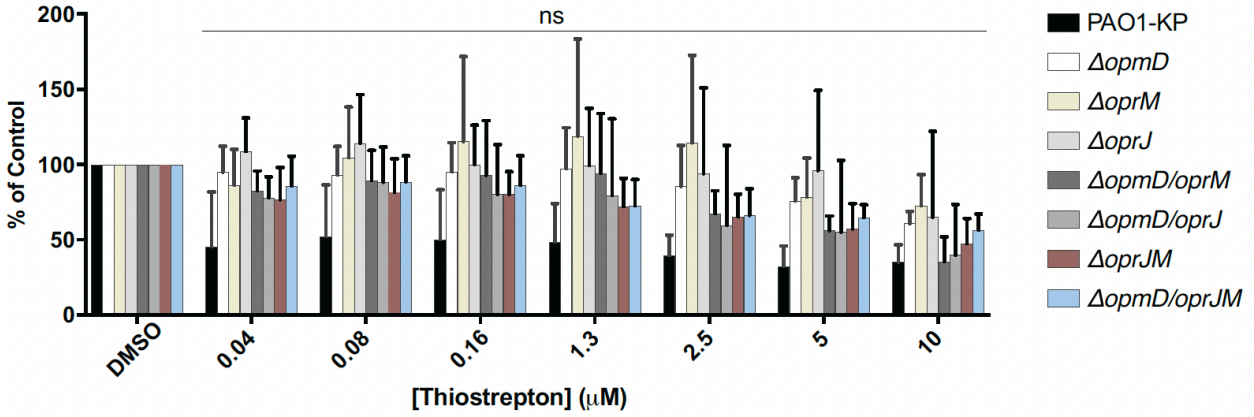

Supplementary Figure 4. Susceptibility of *P. aeruginosa* efflux mutants to thiostrepton. Mutants of strain PAO1 in which the gene(s) encoding the outer membrane component of the major efflux systems MexAB-OprM (shared with MexXY), MexCD-OprJ, and MexGH-OpmD (8) were deleted singly or in combination as described in the Methods were tested for susceptibility to thiostrepton. There were no significant differences in susceptibility compared to the wild-type parent.

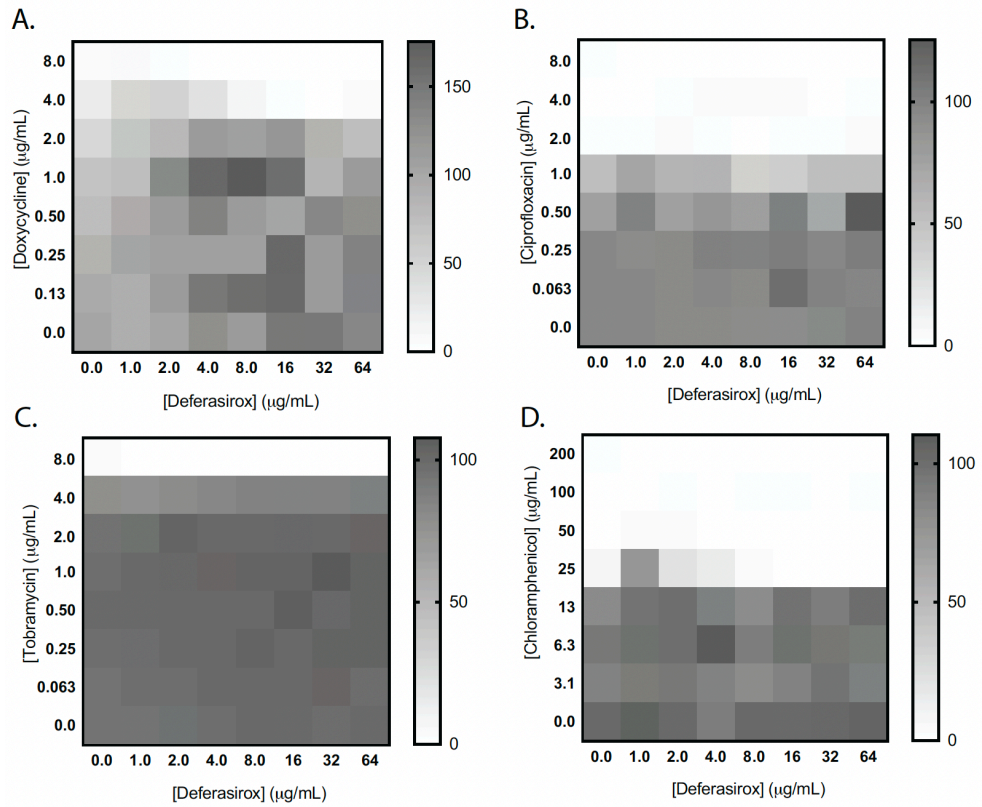

Supplementary Figure 5. Checkerboard assays of various antibiotics with deferasirox (DSX). To test whether DSX could potentiate the activity of antibiotics besides thiostrepton against *P. aeruginosa* PA14, checkboard assays of DSX with **A.** doxycycline, **B.** ciprofloxacin, **C.** tobramycin, or **D.** chloramphenicol were performed. No synergy with these antibiotics was observed, suggesting that their activity is not potentiated by DSX.

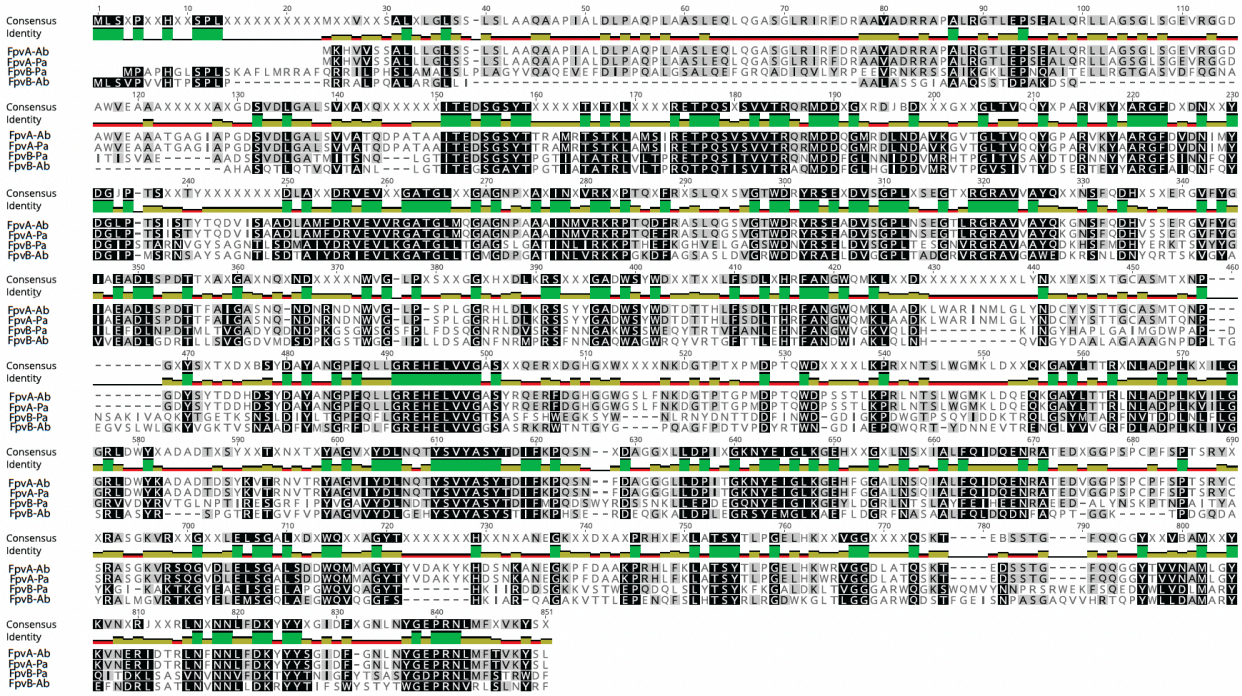

Supplementary Figure 6. *Acinetobacter baumannii* encodes homologs of *P. aeruginosa* FpvA and FpvB. The amino acid sequences of *P. aeruginosa* FpvA and FpvB were aligned with their closest homologs in *A. baumannii* using MUSCLE (Genious). The FpvA-Pa and FpvA-Ab homologs share ~44% identity, while the FpvB homologs from the two species are nearly identical (99%). FpvA-Pa, PA2398 (9); FpvB-Pa, PA4168 (9); FpvA-Ab, GenBank: SSM88576.1; FpvB-Ab, GenBank: SCZ16661.1.

Supplementary Tables

Supplementary Table 1. Hits from the screen

COMPOUND	VENDOR	CAT#	FORMULA	MW	SMILES
GROWTH INHIBITORS					
Coumermycin A1	BIOMOL	GR-317	C55H59N5O20	1110.0785	CO[C@H]1[C@H](OC(=O)c2ccc(C)[nH]2)[C@H](O)C(Oc2ccc3c(O)c(NC(=O)c4c[nH]c(C(=O)Nc5c(O)c6ccc(OC7OC(C)(C)[C@H](OC)[C@@H](OC(=O)c8ccc(C)[nH]8)[C@H]7O)c(C)c6oc5=O)c4C)c(=O)oc3c2C)OC1(C)C
Patulin	BIOMOL	NP-223	C7H6O4	154.1201	OC1OCC=C2OC(=O)C=C12
Harmane	BIOMOL	NP-122	C12H10N2	182.2212	Cc1nccc2c3ccccc3[nH]c12
Echinomycin	BIOMOL	NP-090	C51H64N12O12S2	1101.257	CSC1SC[C@@H]2N(C)C(=O)[C@H](C)NC(=O)[C@@H](COC(=O)[C@H](C(C)C)N(C)C(=O)[C@@H]1N(C)C(=O)[C@H](C)NC(=O)[C@@H](COC(=O)[C@H](C(C)C)N(C)C2=O)NC(=O)c1cnc2ccccc2n1)NC(=O)c1cnc2ccccc2n1
4-chloromercuribenzoic acid	LOPAC	C 5913	C7H5ClHgO2	357.16	OC(=O)c1ccc([Hg]Cl)cc1
Diphenyleneiodonium chloride	LOPAC	D 2926	C12H8ClI	314.549	[Cl-].[I+]1c2ccccc2-c2ccccc12
Doxycycline hydrochloride	LOPAC	D 9891	C22H25ClN2O8	480.896	Cl.[H][C@@]12[C@@H](C)c3cccc(O)c3C(=O)C1=C(O)[C@]1(O)C(=O)C(C(N)=O)=C(O)[C@@H](N(C)C)[C@]1([H])[C@H]2O
Demeclocycline hydrochloride	LOPAC	D 6140	C21H22Cl2N2O8	501.314	Cl.[H][C@]12C[C@@]3([H])[C@H](N(C)C)C(O)=C(C(N)=O)C(=O)[C@@]3(O)C(O)=C1C(=O)c1c(O)ccc(Cl)c1[C@H]2O
Lomefloxacin hydrochloride	LOPAC	L 2906	C17H20ClF2N3O3	387.809	Cl.CCn1cc(C(O)=O)c(=O)c2cc(F)c(N3CCNC(C)C3)c(F)c12
Mitoxantrone	LOPAC	M 6545	C22H30Cl2N4O6	517.403	Cl.Cl.OCCNCCNc1ccc(NCCNCCO)c2C(=O)c3c(O)ccc(O)c3C(=O)c12
Ofloxacin	LOPAC	O 8757	C18H20FN3O4	361.3675	CC1COc2c(N3CCN(C)CC3)c(F)cc3c2n1cc(C(O)=O)c3=O
Ruthenium red	LOPAC	R 2751	Cl6H42N14O2Ru3	786.35	[Cl-].[Cl-].[Cl-].[Cl-].[Cl-].[Cl-].[NH3+][Ru]([NH3+])([NH

					3+])([NH3+])([NH3+])O[Ru]([NH3+])([NH3+])([NH3+])([NH3+])O[Ru]([NH3+])([NH3+])([NH3+])([NH3+])[NH3+]
Trimethoprim	LOPAC	T 7883	C14H18N4O3	290.31 77	COc1cc(Cc2cnc(N)nc2N)cc(OC)c1OC
Peucenin	MICROSOUR CE	100528	C15H16O4	260.28 51	CC(C)=CCc1c(O)cc2oc(C)c c(=O)c2c1O
Koparin	MICROSOUR CE	200422	C16H12O6	300.26 29	COc1ccc(c(O)c1O)- c1coc2cc(O)ccc2c1=O
Pomiferin	MICROSOUR CE	201580	C25H24O6	420.45 45	CC(C)=CCc1c(O)c2c(occ(- c3ccc(O)c(O)c3)c2=O)c2C= CC(C)(C)Oc12
Osajin	MICROSOUR CE	201595	C25H24O5	404.45 51	CC(C)=CCc1c(O)c2c(occ(- c3ccc(O)cc3)c2=O)c2C=CC(C)(C)Oc12
Theaflavin digallate	MICROSOUR CE	201515	C43H32O20	868.70 22	Oc1cc(O)c2C[C@@H](OC(=O)c3cc(O)c(O)c(O)c3)[C@ H](Oc2c1)c1cc(O)c(O)c2c1c c(cc(O)c2=O)[C@H]1Oc2cc (O)cc(O)c2C[C@H]1OC(=O)c1cc(O)c(O)c(O)c1
Purpurin	MICROSOUR CE	1505300	C14H8O5	256.21 03	Oc1cc(O)c2C(=O)c3ccccc3 C(=O)c2c1O
Polymyxin b sulfate	MICROSOUR CE	1500492	C56H100N16 O17S	1301.5 55	OS(O)(=O)=O.CCC(C)CCC CC(=O)NC(CCN)C(=O)NC(C(C)O)C(=O)NC(CCN)C(= O)NC1CCNC(=O)C(NC(=O)C(CCN)NC(=O)C(CCN)N C(=O)C(CC(C)C)NC(=O)C(Cc2ccccc2)NC(=O)C(CCN) NC1=O)C(C)O
Tetracycline hydrochloride	MICROSOUR CE	1500566	C22H25ClN2 O8	480.89 6	Cl.CN(C)[C@H]1[C@@H]2 C[C@H]3C(=C(O)[C@]2(O)C(=O)C(C(N)=O)=C1O)C(=O)c1c(O)cccc1[C@@]3(C) O
Colistin sulfate	MICROSOUR CE	1505955	C52H102N16 O21S2	1351.5 91	OS(O)(=O)=O.OS(O)(=O)= O.CCC(C)C1NC(=O)C(CC N)NC(=O)C(CCNC(=O)C(N C(=O)C(CCN)NC(=O)C(CC N)NC(=O)C(NC1=O)C(C)C C)C(C)O)NC(=O)C(CCN)N C(=O)C(NC(=O)C(CCN)NC (=O)CCCCC(C)C)C(C)O
Pyrithione zinc	MICROSOUR CE	1500260	C10H9N2O2S 2Zn	318.73	S=C1CC=CC=[N]1O[Zn]On 1ccccc1=S
Minocycline hydrochloride	MICROSOUR CE	1500414	C23H28ClN3 O7	493.93 7	Cl.[H][C@@]12Cc3c(ccc(O)c3C(=O)C1=C(O)[C@]1(O)C(=O)C(C(N)=O)=C(O)[C @@H](N(C)C)[C@]1([H])C 2)N(C)C
Oxytetracycline	MICROSOUR CE	1500457	C22H25ClN2 O9	496.89 5	Cl.CN(C)[C@H]1[C@@H]2 [C@@H](O)[C@H]3C(=C(

					O)[C@]2(O)C(=O)C(C(N)=O)=C1O)C(=O)c1c(O)cccc1[C@@]3(C)O
Sulfadiazine	MICROSOURCE	1500546	C10H10N4O2S	250.277	Nc1ccc(cc1)S(=O)(=O)Nc1ncccn1
Thimerosal	MICROSOURCE	1500572	C9H9HgNaO2S	404.81	[Na+].CC[Hg]Sc1ccccc1C([O-])=O
Phenylmercuric acetate	MICROSOURCE	1500644	C8H8HgO2	336.74	CC(=O)O[Hg]c1ccccc1
Merbromin	MICROSOURCE	1500637	C20H8Br2HgNa2O6	750.65	[Na+].[Na+].O[Hg]c1c([O-])c(Br)cc2c(-c3ccccc3C([O-])=O)c3cc(Br)c(=O)cc3oc12
Meclocycline sulfosalicylate	MICROSOURCE	1501118	C29H27ClN2O14S	695.048	OC(=O)c1cc(ccc1O)S(O)(=O)=O.CN(C)[C@H]1[C@@H]2[C@@H](O)[C@@H]3C(=C)c4c(Cl)ccc(O)c4C(=O)C3=C(O)[C@]2(O)C(=O)C(C(N)=O)=C1O
Cetrimonium bromide	MICROSOURCE	1503200	C19H42BrN	364.447	[Br-].CCCCCCCCCCCCCCCC[N+](C)(C)C
Chloroxine	MICROSOURCE	1503202	C9H5Cl2NO	214.048	Oc1c(Cl)cc(Cl)c2cccnc12
Clioquinol	MICROSOURCE	1505114	C9H5ClINO	305.5	Oc1c(I)cc(Cl)c2cccnc12
Acrisorcin	MICROSOURCE	1504218	C25H28N2O2	388.502	CCCCCCc1ccc(O)cc1O.Nc1c2ccccc2nc2ccccc12
Gatifloxacin	MICROSOURCE	1504272	C19H22FN3O4	375.3941	COc1c(N2CCNC(C)C2)c(F)cc2c1n(cc(C(O)=O)c2=O)C1CC1
Moxifloxacin hydrochloride	MICROSOURCE	1504303	C23H29ClFN3O4	465.945	Cl.COc1c(CN2CC[C@@H]3CCCN[C@@H]3C2)c(F)cc2c1n(cc(C(O)=O)c2=O)C1CC1
Rifaximin	MICROSOURCE	1505321	C43H51N3O11	785.8785	CO[C@H]1\C=C\O[C@@]2(C)Oc3c(C2=O)c2c4nc5cc(C)ccn5c4c(NC(=O)\C(C)=C/C=C/[C@H](C)[C@H](O)[C@@H](C)C(O)[C@@H](C)[C@H](OC(C)=O)[C@@H]1C)c(O)c2c(O)c3C
Pefloxacine mesylate	MICROSOURCE	1505305	C18H24FN3O6S	429.463	CS(O)(=O)=O.CCn1cc(C(O)=O)c(=O)c2cc(F)c(cc12)N1CCN(C)CC1
Bismuth subsalicylate	MICROSOURCE	1505412	C7H5BiO4	362.0926	O[Bi]1OC(=O)c2ccccc2O1
Sarafloxacin hydrochloride	MICROSOURCE	1505314	C20H18ClF2N3O3	421.825	Cl.OC(=O)c1cn(-c2ccc(F)cc2)c2cc(N3CCNCC3)c(F)cc2c1=O
Gemifloxacin mesylate	MICROSOURCE	1505802	C19H24FN5O7S	485.487	CS(O)(=O)=O.CO\N=C1/CN(CC1CN)c1nc2n(cc(C(O)=O)c(=O)c2cc1F)C1CC1
Colistimethate sodium	MICROSOURCE	1500206	C57H103N16Na5O28S5	1735.792	[Na+].[Na+].[Na+].[Na+].[Na+].CCC(C)C1NC(=O)C(CCNCS([O-

					])(=O)=O)NC(=O)C(CCNC(=O)C(NC(=O)C(CCNCS([O-])(=O)=O)NC(=O)C(CCNCS([O-])(=O)=O)NC(=O)C(NC1=O)C(C)CC)C(C)O)NC(=O)C(CCNCS([O-])(=O)=O)NC(=O)C(NC(=O)C(CCNCS([O-])(=O)=O)NC(=O)CCCCC(C)C)C(C)O
Alexidine hydrochloride	MICROSOURCE	1503074	C26H58Cl2N10	581.712	Cl.Cl.CCCCC(CC)CNC(=N)NC(=N)NCCCCCCNC(=N)NC(=N)NCC(CC)CCCC
Dibenzoylmethane	MICROSOURCE	1505311	C15H12O2	224.2546	O=C(CC(=O)c1ccccc1)c1ccccc1
Broxyquinoline	MICROSOURCE	1500623	C9H5Br2NO	302.95	Oc1c(Br)cc(Br)c2cccnc12
Tetrachloroisophthalonitrile	MICROSOURCE	1504101	C8Cl4N2	265.911	Clc1c(Cl)c(C#N)c(Cl)c(C#N)c1Cl
Auranofin	MICROSOURCE	1505744	C20H34AuO9PS	678.484	CCP(CC)(CC)=[Au]S[C@@H]1O[C@H](COC(C)=O)[C@@H](OC(C)=O)[C@H](OC(C)=O)[C@H]1OC(C)=O
Dobutamine hydrochloride	MICROSOURCE	1503212	C18H24ClNO3	337.841	Cl.CC(CNCCc1ccc(O)c(O)c1)Cc1cccc(O)c1
Ciprofloxacin hydrochloride	PRESTWICK	Prestw-113	C17H21ClFN3O4	385.818	O.Cl.OC(=O)c1cn(C2CC2)c2cc(N3CCNCC3)c(F)cc2c1=O
Chlorhexidine	PRESTWICK	Prestw-143	C22H30Cl2N10	505.447	Clc1ccc(NC(=N)NC(=N)NCCCCCNC(=N)NC(=N)Nc2ccc(Cl)cc2)cc1
Aztreonam	PRESTWICK	Prestw-185	C13H17N5O8S2	435.433	C[C@H]1[C@H](NC(=O)C(=N/OC(C)(C)C(O)=O)\c2csc(N)n2)C(=O)N1S(O)(=O)=O
Norfloxacin	PRESTWICK	Prestw-221	C16H18FN3O3	319.3308	CCn1cc(C(O)=O)c(=O)c2cc(F)c(cc12)N1CCNCC1
Minocycline hydrochloride	PRESTWICK	Prestw-315	C23H28ClN3O7	493.937	Cl.CN(C)[C@@H]1C2CC3Cc4c(ccc(O)c4C(=O)C3=C(O)[C@@]2(O)C(=O)C(C(N)=O)=C1O)N(C)C
Cefoperazone dihydrate	PRESTWICK	Prestw-327	C25H31N9O10S2	681.698	O.O.[H][C@]12SCC(CSc3nnnn3C)=C(N1C(=O)[C@@]2([H])NC(=O)[C@H](NC(=O)N1CCN(CC)C(=O)C1=O)c1ccc(O)cc1)C(O)=O
Zaprinast	PRESTWICK	Prestw-335	C13H13N5O2	271.2746	CCCOc1ccccc1-c1nc(=O)c2[nH]nnc2[nH]1
Amikacin hydrate	PRESTWICK	Prestw-395	C22H47N5O15	621.6331	O.O.NCC[C@H](O)C(=O)N[C@@H]1C[C@H](N)[C@@H](O[C@H]2O[C@H](CN)[C@@H](O)[C@H](O)[C@H]2O)[C@H](O)[C@H]1O[C@H]1O[C@H](CO)[C

					@@H](O)[C@H](N)[C@H]1O
Piperacillin sodium salt	PRESTWICK	Prestw-755	C23H26N5NaO7S	539.537	[Na+].[H][C@]12SC(C)(C)[C@@H](N1C(=O)[C@@]2([H])NC(=O)[C@H](NC(=O)N1CCN(CC)C(=O)C1=O)c1ccccc1)C([O-])=O
Merbromin	PRESTWICK	Prestw-787	C20H14Br2HgNa2O9	804.7	O.O.O.[Na+].[Na+].O[Hg]c1c([O-])c(Br)cc2c1Oc1cc([O-])c(Br)cc1C21OC(=O)c2ccccc12
Azlocillin sodium salt	PRESTWICK	Prestw-821	C20H22N5NaO6S	483.473	[Na+].[H][C@@]1(NC(=O)[C@H](NC(=O)N2CCNC2=O)c2ccccc2)C(=O)N2[C@@H](C([O-])=O)C(C)(C)S[C@]12[H]
Doxycycline hyclate	PRESTWICK	Prestw-852	C22H25ClN2O8	480.896	Cl.[H][C@@]12[C@@H](C)c3cccc(O)c3C(=O)C1=C(O)C1(O)C(=O)C(C(N)=O)=C(O)[C@@H](N(C)C)[C@]1([H])[C@H]2O
BIOFILM STIMULATORS (>200% DMSO CONTROL BIOFILM)					
Geranylgeranoic acid	BIOMOL	AP-307	C20H32O2	304.4669	CC(C)=CCC\C(C)=C\CC\C(C)=C\CC\C(C)=C\C(O)=O
Calmidazolium chloride	LOPAC	C 3930	C31H23Cl7N2O	687.698	[Cl-].Clc1ccc(cc1)C(c1ccc(Cl)cc1)[n+]1ccn(CC(OCc2ccc(Cl)cc2Cl)c2ccc(Cl)cc2Cl)c1
Daphnetin	LOPAC	D 5564	C9H6O4	178.1415	Oc1ccc2ccc(=O)oc2c1O
4-diphenylacetoxy-n-(2-chloroethyl)piperidine hydrochloride	LOPAC	D-142	C21H25Cl2NO2	394.335	Cl.ClCCN1CCC(CC1)OC(=O)C(c1ccccc1)c1ccccc1
S-(+)-fluoxetine hydrochloride	LOPAC	F 1553	C17H19ClF3NO	345.787	Cl.CNCC[C@H](Oc1ccc(cc1)C(F)(F)F)c1ccccc1
Fluphenazine dihydrochloride	LOPAC	F 4765	C22H28Cl2F3N3OS	510.443	Cl.Cl.OCCN1CCN(CCCN2c3ccccc3Sc3ccc(cc23)C(F)(F)F)CC1
5-hydroxyindolacetic acid	LOPAC	H 8876	C10H9NO3	191.1834	OC(=O)Cc1c[nH]c2ccc(O)cc12
Loperamide hydrochloride	LOPAC	L 4762	C29H34Cl2N2O2	513.498	Cl.CN(C)C(=O)C(CCN1CCC(O)(CC1)c1ccc(Cl)cc1)(c1ccccc1)c1ccccc1
Maprotiline hydrochloride	LOPAC	M 9651	C20H24ClN	313.864	Cl.CNCCCC12CCC(c3ccccc13)c1ccccc21
Ci-976 (2,2-dimethyl-n-(2,4,6-trimethoxyphenyl)dodecanamide)	LOPAC	C3743	C23H39NO4	393.5601	CCCCCCCCCCCC(C)(C)C(=O)Nc1c(OC)cc(OC)cc1OC
Niclosamide	LOPAC	N 3510	C13H8Cl2N2O4	327.12	Oc1ccc(Cl)cc1C(=O)Nc1ccc(cc1Cl)[N+]([O-])=O

Pimozide	LOPAC	P 1793	C28H29F2N3O	461.5462	Fc1ccc(cc1)C(CCCN1CCC(CC1)n1c2ccccc2[nH]c1=O)c1ccc(F)cc1
Bay 11-7082	LOPAC	B 5556	C10H9NO2S	207.249	Cc1ccc(cc1)S(=O)(=O)\C=C\C#N
Tyrphostin a9	LOPAC	T-182	C18H22N2O	282.3801	CC(C)(C)c1cc(C=C(C#N)C#N)cc(c1O)C(C)(C)C
Khayanthone	MICROSOURCE	100049	C32H42O9	570.6705	CC(=O)O[C@@H]1C[C@H](OC(C)=O)[C@]2(C)C3CC[C@@]4(C)[C@@H](C(=O)[C@H]5O[C@@]45[C@]3(C)[C@@H](CC2C1(C)C)OC(C)=O)c1ccoc1
Atranorin	MICROSOURCE	200034	C19H18O8	374.3414	COC(=O)c1c(C)cc(OC(=O)c2c(C)cc(O)c(C=O)c2O)c(C)c1O
Epicatechin monogallate	MICROSOURCE	210238	C22H18O10	442.3723	Oc1cc(O)c2C[C@@H](OC(=O)c3cc(O)c(O)c(O)c3)[C@H](Oc2c1)c1ccc(O)c(O)c1
Retusin 7-methyl ether	MICROSOURCE	240645	C17H14O5	298.2901	COc1ccc(cc1)-c1coc2c(O)c(OC)ccc2c1=O
Larixol	MICROSOURCE	300056	C20H34O2	306.4828	C[C@](O)(CCC1C(=C)C[C@H](O)C2C(C)(C)CCCC12C)C=C
Chrysanthemic acid, ethyl ester	MICROSOURCE	310019	C12H20O2	196.286	CCOC(=O)C1C(C=C(C)C)C1(C)C
Larixinic acid	MICROSOURCE	310025	C6H6O3	126.11	Cc1occc(=O)c1O
Chaulmoogric acid	MICROSOURCE	310016	C18H32O2	280.4455	OC(=O)CCCCCCCCCCCCC1CCC=C1
Harmol hydrochloride	MICROSOURCE	1502237	C12H11ClN2O	234.682	Cl.Cc1nccc2c3ccc(O)cc3[nH]c12
Hederagenin	MICROSOURCE	1504016	C30H48O4	472.6997	CC1(C)CC[C@@]2(CC[C@]3(C)C(=CCC4[C@@]5(C)CC[C@H](O)[C@@](C)(CO)C5CC[C@@]34C)C2C1)C(O)=O
Cytisine	MICROSOURCE	1504027	C11H14N2O	190.2417	O=c1cccc2C3CNC[C@@H](C3)Cn12
Fraxetin	MICROSOURCE	1504069	C10H8O5	208.1675	COc1cc2ccc(=O)oc2c(O)c1O
Ursolic acid	MICROSOURCE	1800031	C30H48O3	456.7003	C[C@@H]1CC[C@@]2(CC[C@]3(C)C(=CCC4[C@@]5(C)CC[C@H](O)C(C)(C)C5CC[C@@]34C)C2[C@H]1C)C(O)=O
Diallyl sulfide	MICROSOURCE	1505293	C6H10S	114.209	C=CCSCC=C
Deferoxamine mesylate	MICROSOURCE	1500224	C26H52N6O11S	656.79	CS(O)(=O)=O.CC(=O)N(O)CCCCCNC(=O)CCC(=O)N(O)CCCCCNC(=O)CCC(=O)N(O)CCCCCN
Chlortetracycline hydrochloride	MICROSOURCE	1500186	C22H24Cl2N2O8	515.341	Cl.CN(C)[C@H]1[C@@H]2C[C@H]3C(=C(O)[C@]2(O)C(=O)C(C(N)=O)=C1O)C(

					=O)c1c(O)ccc(Cl)c1[C@@]3(C)O
Hexachlorophene	MICROSOURCE	1500328	C13H6Cl6O2	406.904	Oc1c(Cl)cc(Cl)c(Cl)c1Cc1c(O)c(Cl)cc(Cl)c1Cl
Gramicidin	MICROSOURCE	1500319	C60H92N12O10	1141.4469	CC(C)CC1NC(=O)C(CCCN)NC(=O)C(NC(=O)C2CCCN2C(=O)C(Cc2ccccc2)NC(=O)C(CC(C)C)NC(=O)C(CCCN)NC(=O)C(NC(=O)C2CCCN2C(=O)C(Cc2ccccc2)NC1=O)C(C)C)C(C)C
Mechlorethamine	MICROSOURCE	1500375	C5H11Cl2N	156.054	CN(CCCl)CCCl
Piperacillin sodium	MICROSOURCE	1500489	C23H26N5NaO7S	539.537	[Na+].CCN1CCN(C(=O)NC(C(=O)N[C@H]2[C@H]3SC(C)(C)[C@@H](N3C2=O)C([O-])=O)c2ccccc2)C(=O)C1=O
Sulfapyridine	MICROSOURCE	1500551	C11H11N3O2S	249.289	Nc1ccc(cc1)S(=O)(=O)Nc1ccccn1
Sulfathiazole	MICROSOURCE	1500553	C9H9N3O2S2	255.317	Nc1ccc(cc1)S(=O)(=O)Nc1nccs1
Thiamphenicol	MICROSOURCE	1503136	C12H15Cl2NO5S	356.222	CS(=O)(=O)c1ccc(cc1)[C@@H](O)[C@@H](CO)NC(=O)C(Cl)Cl
Azithromycin	MICROSOURCE	1503679	C38H72N2O12	748.9845	CC[C@H]1OC(=O)[C@H](C)[C@@H](O[C@H]2C[C@@](C)(OC)[C@@H](O)[C@H](C)O2)[C@H](C)[C@@H](O[C@@H]2O[C@H](C)C[C@@H]([C@H]2O)N(C)C)[C@](C)(O)C[C@@H](C)CN(C)[C@H](C)[C@@H](O)[C@]1(C)O
Thiram	MICROSOURCE	1503322	C6H12N2S4	240.433	CN(C)C(=S)SSC(=S)N(C)C
Dirithromycin	MICROSOURCE	1504144	C42H78N2O14	835.0737	CC[C@H]1OC(=O)[C@H](C)[C@@H](O[C@H]2C[C@@](C)(OC)[C@@H](O)[C@H](C)O2)[C@H](C)[C@@H](O[C@@H]2O[C@H](C)C[C@@H]([C@H]2O)N(C)C)[C@](C)(O)C[C@@H](C)[C@@H]2N[C@@H](COCCOC)O[C@H]([C@H]2C)[C@]1(C)O
Telithromycin	MICROSOURCE	1505265	C43H65N5O10	812.0037	CCC1OC(=O)[C@H](C)C(=O)[C@H](C)[C@@H](OC2O[C@H](C)C[C@@H]([C@H]2O)N(C)C)[C@@](C)(C[C@@H](C)C(=O)[C@H](C)[C@H]2N(CCCCn3cnc(c3)-c3cccnc3)C(=O)OC12C)OC

Thiostrepton	MICROSOURCE	1505111	C72H85N19O18S5	1664.887	CCC(C)C1NC2C=Cc3c(cc(nc3C2O)C(=O)OC(C)C2NC(=O)c3csc(n3)C(NC(=O)C3CSC(=N3)\C(NC(=O)C(NC(=O)c3csc(n3)C3(CCC(=NC3c3csc2n3)c2nc(cs2)C(=O)NC(=C)C(=O)NC(=C)C(N)=O)NC(=O)C(C)NC(=O)C(=C)NC(=O)C(C)NC1=O)C(C)O)=C/C)C(C)(O)C(C)O)C(C)O
Triclosan	MICROSOURCE	1505465	C12H7Cl3O2	289.542	Oc1cc(Cl)ccc1Oc1ccc(Cl)cc1Cl
Trientine hydrochloride	MICROSOURCE	1505675	C6H20Cl2N4	219.156	Cl.Cl.NCCNCCNCCN
Bromperidol	MICROSOURCE	1505972	C21H23BrFNO2	420.315	OC1(CCN(CCCC(=O)c2ccc(F)cc2)CC1)c1ccc(Br)cc1
Lipoamide	MICROSOURCE	1505740	C8H15NOS2	205.341	NC(=O)CCCCC1CCSS1
Aliskiren hemifumarate	MICROSOURCE	1505710	C34H57N3O10	667.8305	OC(=O)\C=C\C(O)=O.COCCCOc1cc(C[C@@H](C[C@H](N)[C@@H](O)C[C@@H](C(C)C)C(=O)NCC(C)(C)C(N)=O)C(C)C)ccc1OC
Chloramphenicol hemisuccinate	MICROSOURCE	1500173	C15H16Cl2N2O8	423.202	[H][C@](COC(=O)CCC(O)=O)(NC(=O)C(Cl)Cl)[C@]([H])(O)c1ccc(cc1)[N+]([O-])=O
Thioctic acid	MICROSOURCE	1503941	C8H14O2S2	206.326	OC(=O)CCCCC1CCSS1
Pipemidic acid	MICROSOURCE	1502024	C14H17N5O3	303.3165	CCn1cc(C(O)=O)c(=O)c2cnc(nc12)N1CCNCC1
Carmofur	MICROSOURCE	1505317	C11H16FN3O3	257.2614	CCCCCCNC(=O)n1cc(F)c(=O)[nH]c1=O
Hygromycin b	MICROSOURCE	1505362	C20H37N3O13	527.5201	CN[C@H]1C[C@@H](N)[C@H](O)[C@@H](O[C@@H]2O[C@H](CO)[C@@H]3OC4(O[C@@H]3[C@@H]2O)O[C@H](C(N)CO)[C@H](O)[C@H](O)[C@H]4O)[C@@H]1O
Dichlorophene	MICROSOURCE	1500626	C13H10Cl2O2	269.123	Oc1ccc(Cl)cc1Cc1cc(Cl)ccc1O
Rosmarinic acid	MICROSOURCE	1502094	C18H16O8	360.3148	OC(=O)C(Cc1ccc(O)c(O)c1)OC(=O)\C=C\c1ccc(O)c(O)c1
Dropropizine	MICROSOURCE	1501004	C13H20N2O2	236.3101	OCC(O)CN1CCN(CC1)c1ccccc1
2,4-dichlorophenoxyacetic acid, isooctyl ester	MICROSOURCE	330048	C16H22Cl2O3	333.25	CCCCCCCC(C)OC(=O)COc1ccc(Cl)cc1Cl
Atracurium besylate	PRESTWICK	Prestw-5	C65H82N2O18S2	1243.479	[O-]S(=O)(=O)c1ccccc1.[O-]S(=O)(=O)c1ccccc1.COc1ccc(CC2c3cc(OC)c(OC)cc3C

					C[N+]2(C)CCC(=O)OCCCCCOC(=O)CC[N+]2(C)CCc3cc(OC)c(OC)cc3C2Cc2ccc(OC)c(OC)c2)cc1OC
Chloramphenicol	PRESTWICK	Prestw-31	C11H12Cl2N2O5	323.129	OC[C@@H](NC(=O)C(Cl)Cl)[C@H](O)c1ccc(cc1)[N+]([O-])=O
Dihydrostreptomycin sulfate	PRESTWICK	Prestw-159	C42H88N14O36S3	1461.415	OS(O)(=O)=O.OS(O)(=O)=O.OS(O)(=O)=O.CN[C@H]1[C@H](O)[C@@H](O)[C@H](CO)O[C@H]1O[C@H]1[C@H](O[C@@H]2[C@@H](O)[C@H](O)[C@@H](NC(N)=N)[C@H](O)[C@H]2NC(N)=N)O[C@@H](C)[C@]1(O)CO.CN[C@H]1[C@H](O)[C@@H](O)[C@H](CO)O[C@H]1O[C@H]1[C@H](O[C@@H]2[C@@H](O)[C@H](O)[C@@H](NC(N)=N)[C@H](O)[C@H]2NC(N)=N)O[C@@H](C)[C@]1(O)CO
Cefotetan	PRESTWICK	Prestw-473	C17H17N7O8S4	575.619	[H][C@]12SCC(CSc3nnnn3C)=C(N1C(=O)[C@]2(NC(=O)C1SC(S1)=C(C(N)=O)C(O)=O)OC)C(O)=O
Dacarbazine	PRESTWICK	Prestw-574	C6H10N6O	182.1832	CN(C)N=Nc1[nH]cnc1C(N)=O
Roxithromycin	PRESTWICK	Prestw-854	C41H76N2O15	837.0465	[H][C@@]1(O[C@@H]2[C@@H](C)[C@H](OC3C[C@@](C)(OC)[C@@H](O)[C@H](C)O3)[C@@H](C)C(=O)O[C@H](CC)[C@@](C)(O)[C@H](O)[C@@H](C)\C(=N\OCOCCOC)[C@H](C)C[C@@]2(C)O)O[C@H](C)C[C@@H]([C@H]1O)N(C)C
Thonzonium bromide (soap)	PRESTWICK	Prestw-925	C32H55BrN4O	591.709	[Br-].CCCCCCCCCCCCCCCC[N+](C)(C)CCN(Cc1ccc(OCcc1)c1ncccn1
Flucytosine	PRESTWICK	Prestw-934	C4H4FN3O	129.0925	Nc1nc(=O)[nH]cc1F
Florfenicol	PRESTWICK	Prestw-955	C12H14Cl2FNO4S	358.213	CS(=O)(=O)c1ccc(cc1)[C@@H](O)[C@@H](CF)NC(=O)C(Cl)Cl
Apramycin	PRESTWICK	Prestw-1005	C21H41N5O11	539.5771	[H][C@]12C[C@@H](N)[C@@H](O[C@]3([H])[C@@H](N)C[C@@H](N)[C@H](O)[C@H]3O)OC1[C@H](O)[C@H](NC)C(O[C@@]1([H])O[C@H](CO)[C@@H](N)[C@H](O)[C@H]1O)O2

Ramipril	PRESTWICK	Prestw-1107	C23H32N2O5	416.5106	[H][C@@]12CCC[C@]1([H])N(C(C2)C(O)=O)C(=O)[C@H](C)N[C@@H](CCc1ccccc1)C(=O)OCC
Cefepime hydrochloride	PRESTWICK	Prestw-1118	C19H27ClN6O6S2	535.037	O.[Cl-].[H][C@@]1(NC(=O)C(=N/OC)\c2csc(N)n2)C(=O)N2C(C(O)=O)=C(C[N+]3(C)CCCC3)CS[C@]12[H]
BIOFILM INHIBITORS (<50% DMSO CONTROL BIOFILM)					
L-3,4-dihydroxyphenylalanine methyl ester hydrochloride	LOPAC	D 1507	C10H14ClNO4	247.675	Cl.COC(=O)[C@@H](N)Cc1ccc(O)c(O)c1
R(-)-propylnorapomorphine hydrochloride	LOPAC	D-027	C19H22ClNO2	331.836	Cl.[H][C@]12Cc3ccc(O)c(O)c3-c3cccc(CCN1CCC)c23
Nordihydroguaiaretic acid from *Larrea divaricata* (creosote bush)	LOPAC	N 5023	C18H22O4	302.3649	C[C@@H](Cc1ccc(O)c(O)c1)[C@H](C)Cc1ccc(O)c(O)c1
N-oleoyldopamine	LOPAC	O 2139	C26H43NO3	417.6245	CCCCCCCC\C=C/CCCCCCCC(=O)NCCc1ccc(O)c(O)c1
Curcumin	MICROSOURCE	1505345	C21H20O6	368.3799	COc1cc(\C=C\C(\O)=C\C(=O)\C=C\c2ccc(O)c(OC)c2)ccc1O
3,5-dihydroxyflavone	MICROSOURCE	1505147	C15H10O4	254.2375	Oc1cccc2oc(-c3ccccc3)c(O)c(=O)c12
3-hydroxy-3',4'-dimethoxyflavone	MICROSOURCE	1505278	C17H14O5	298.2901	COc1ccc(cc1OC)-c1oc2ccccc2c(=O)c1O
Limonin	MICROSOURCE	1800018	C26H30O8	470.5116	CC1(C)O[C@H]2CC(=O)OC[C@@]22[C@H]1CC(=O)[C@]1(C)[C@@H]2CC[C@@]2(C)[C@@H](OC(=O)[C@H]3O[C@@]123)c1ccoc1

Supplementary Table 2. Antibiogram of WCC PA1 Clinical Isolates

Strain number	Resistant to:[a]
***P. aeruginosa* clinical isolates (Wright Clinical Collection[b])**	
C0007	ampicillin, amoxicillin clavulanic acid, cefazolin, cefalotin, cefixime, ceftazidime, nitrofuratoin, piperacillin tazobactam, tetracycline, trimethoprim sulfamethoxazole, cefoxitin, ceftriaxone
C0028	ampicillin, amoxicillin clavulanic acid, cefazolin, cefalotin, ciprofloxacin, cefixime, metropenem, nitrofuratoin, tetracycline, trimethoprim sulfamethoxazole, cefoxitin, ceftriaxone
C0029	ampicillin, amoxicillin clavulanic acid, cefazolin, cefalotin, cefixime, ceftazidime, nitrofuratoin, piperacillin tazobactam, tetracycline, trimethoprim sulfamethoxazole, cefoxitin, ceftriaxone

C0030	ampicillin, amoxicillin clavulanic acid, cefazolin, cefalotin, cefixime, nitrofuratoin, tetracycline, trimethoprim sulfamethoxazole, cefoxitin, ceftriaxone
C0031	ampicillin, amoxicillin clavulanic acid, cefazolin, cefalotin, cefixime, nitrofuratoin, tetracycline, trimethoprim sulfamethoxazole, cefoxitin, ceftriaxone
C0042	ampicillin, amoxicillin clavulanic acid, cefazolin, cefalotin, nitrofuratoin, tetracycline, trimethoprim sulfamethoxazole, cefoxitin, ceftriaxone
C0043	ampicillin, amoxicillin clavulanic acid, cefazolin, cefalotin, cefixime, nitrofuratoin, tetracycline, trimethoprim sulfamethoxazole, cefoxitin, ceftriaxone
C0053	cefazolin, cefalotin, cefixime, nitrofuratoin, tetracycline
C0056	ampicillin, amoxicillin clavulanic acid, cefazolin, cefalotin, cefixime, nitrofuratoin, tetracycline, trimethoprim sulfamethoxazole, cefoxitin, ceftriaxone
C0057	ampicillin, amoxicillin clavulanic acid, cefazolin, cefalotin, cefixime, nitrofuratoin, tetracycline, trimethoprim sulfamethoxazole, cefoxitin, ceftriaxone
C0060	ampicillin, amoxicillin clavulanic acid, cefazolin, cefalotin, ciprofloxacin, cefixime, gentamicin, nitrofuratoin, tetracycline, trimethoprim sulfamethoxazole, cefoxitin, ceftriaxone
C0062	ampicillin, amoxicillin clavulanic acid, cefazolin, cefalotin, cefixime, nitrofuratoin, tetracycline, trimethoprim sulfamethoxazole, cefoxitin, ceftriaxone
C0063	ampicillin, amoxicillin clavulanic acid, cefazolin, cefalotin, cefixime, ceftazidime, metropenem, nitrofuratoin, piperacillin tazobactam, tetracycline, trimethoprim sulfamethoxazole, cefoxitin, ceftriaxone
C0070	ampicillin, amoxicillin clavulanic acid, cefazolin, cefalotin, cefixime, nitrofuratoin, tetracycline, trimethoprim sulfamethoxazole, cefoxitin, ceftriaxone
C0071	ampicillin, amoxicillin clavulanic acid, cefazolin, cefalotin, cefixime, nitrofuratoin, tetracycline, trimethoprim sulfamethoxazole, cefoxitin, ceftriaxone
C0072	ampicillin, amoxicillin clavulanic acid, cefazolin, cefalotin, cefixime, nitrofuratoin, tetracycline, trimethoprim sulfamethoxazole, cefoxitin, ceftriaxone
C0073	ampicillin, amoxicillin clavulanic acid, cefazolin, cefalotin, cefixime, nitrofuratoin, tetracycline, trimethoprim sulfamethoxazole, cefoxitin, ceftriaxone
C0080	nitrofuratoin, tetracycline
C0089	ampicillin, amoxicillin clavulanic acid, cefazolin, cefalotin, ciprofloxacin, cefixime, nitrofuratoin, tetracycline, trimethoprim sulfamethoxazole, cefoxitin, ceftriaxone
C0090	ampicillin, amoxicillin clavulanic acid, cefazolin, cefalotin, cefixime, ceftazidime, nitrofuratoin, piperacillin tazobactam, tetracycline, trimethoprim sulfamethoxazole, cefoxitin, ceftriaxone
C0091	ampicillin, amoxicillin clavulanic acid, cefazolin, cefalotin, cefixime, ceftazidime, nitrofuratoin, piperacillin tazobactam, tetracycline, trimethoprim sulfamethoxazole, cefoxitin, ceftriaxone
C0098	ampicillin, amoxicillin clavulanic acid, cefazolin, cefalotin, cefixime, nitrofuratoin, tetracycline, trimethoprim sulfamethoxazole, cefoxitin, ceftriaxone
C0099	ampicillin, amoxicillin clavulanic acid, cefazolin, cefalotin, cefixime, nitrofuratoin, tetracycline, trimethoprim sulfamethoxazole, cefoxitin, ceftriaxone
C0100	ampicillin, amoxicillin clavulanic acid, cefazolin, cefalotin, cefixime, nitrofuratoin, tetracycline, trimethoprim sulfamethoxazole, cefoxitin, ceftriaxone
C0129	ampicillin, amoxicillin clavulanic acid, cefazolin, cefalotin, cefixime, nitrofuratoin, tetracycline, cefoxitin, ceftriaxone
C0138	ampicillin, amoxicillin clavulanic acid, cefazolin, cefalotin, cefixime, nitrofuratoin, tetracycline, trimethoprim sulfamethoxazole, cefoxitin, ceftriaxone
C0139	ampicillin, amoxicillin clavulanic acid, cefazolin, cefalotin, cefixime, nitrofuratoin, tetracycline, trimethoprim sulfamethoxazole, cefoxitin, ceftriaxone

C0148	ampicillin, amoxicillin clavulanic acid, cefazolin, cefalotin, cefixime, nitrofuratoin, tetracycline, trimethoprim sulfamethoxazole, cefoxitin, ceftriaxone
C0155	ampicillin, amoxicillin clavulanic acid, cefazolin, cefalotin, cefixime, nitrofuratoin, tetracycline, trimethoprim sulfamethoxazole, cefoxitin, ceftriaxone
C0156	ampicillin, amoxicillin clavulanic acid, cefazolin, cefalotin, cefixime, nitrofuratoin, piperacillin tazobactam, tetracycline, trimethoprim sulfamethoxazole, cefoxitin, ceftriaxone
C0157	ampicillin, amoxicillin clavulanic acid, cefazolin, cefalotin, cefixime, nitrofuratoin, tetracycline, trimethoprim sulfamethoxazole, cefoxitin, ceftriaxone
C0166	ampicillin, amoxicillin clavulanic acid, cefazolin, cefalotin, cefixime, nitrofuratoin, tetracycline, trimethoprim sulfamethoxazole, cefoxitin, ceftriaxone
C0167	ampicillin, amoxicillin clavulanic acid, cefazolin, cefalotin, cefixime, nitrofuratoin, tetracycline, trimethoprim sulfamethoxazole, cefoxitin, ceftriaxone
C0168	ampicillin, amoxicillin clavulanic acid, cefazolin, cefalotin, cefixime, nitrofuratoin, tetracycline, trimethoprim sulfamethoxazole, cefoxitin, ceftriaxone
C0176	ampicillin, amoxicillin clavulanic acid, cefazolin, cefalotin, cefixime, ceftazidime, nitrofuratoin, piperacillin tazobactam, tetracycline, trimethoprim sulfamethoxazole, cefoxitin, ceftriaxone
C0177	ampicillin, amoxicillin clavulanic acid, cefazolin, cefalotin, ciprofloxacin, cefixime, metropenem, nitrofuratoin, piperacillin tazobactam, tetracycline, trimethoprim sulfamethoxazole, cefoxitin, ceftriaxone
C0178	ampicillin, amoxicillin clavulanic acid, cefazolin, cefalotin, cefixime, nitrofuratoin, tetracycline, trimethoprim sulfamethoxazole, cefoxitin, ceftriaxone
C0179	ampicillin, amoxicillin clavulanic acid, cefazolin, cefalotin, cefixime, nitrofuratoin, tetracycline, trimethoprim sulfamethoxazole, cefoxitin, ceftriaxone
C0189	ampicillin, amoxicillin clavulanic acid, cefazolin, cefalotin, cefixime, nitrofuratoin, tetracycline, trimethoprim sulfamethoxazole, cefoxitin, ceftriaxone
C0190	ampicillin, amoxicillin clavulanic acid, cefazolin, cefalotin, cefixime, nitrofuratoin, tetracycline, trimethoprim sulfamethoxazole, cefoxitin, ceftriaxone
C0200	ampicillin, amoxicillin clavulanic acid, cefazolin, cefalotin, cefixime, nitrofuratoin, tetracycline, trimethoprim sulfamethoxazole, cefoxitin, ceftriaxone
C0201	ampicillin, amoxicillin clavulanic acid, cefazolin, cefalotin, cefixime, nitrofuratoin, tetracycline, trimethoprim sulfamethoxazole, cefoxitin, ceftriaxone
C0202	ampicillin, amoxicillin clavulanic acid, cefazolin, cefalotin, cefixime, nitrofuratoin, tetracycline, trimethoprim sulfamethoxazole, cefoxitin, ceftriaxone
C0203	ampicillin, amoxicillin clavulanic acid, cefazolin, cefalotin, cefixime, nitrofuratoin, tetracycline, trimethoprim sulfamethoxazole, cefoxitin, ceftriaxone
C0204	ampicillin, amoxicillin clavulanic acid, cefazolin, cefalotin, cefixime, ceftazidime, nitrofuratoin, piperacillin tazobactam, tetracycline, trimethoprim sulfamethoxazole, cefoxitin, ceftriaxone
C0213	ampicillin, amoxicillin clavulanic acid, cefazolin, cefalotin, cefixime, nitrofuratoin, tetracycline, trimethoprim sulfamethoxazole, cefoxitin, ceftriaxone
C0214	ampicillin, amoxicillin clavulanic acid, cefazolin, cefalotin, ciprofloxacin, cefixime, nitrofuratoin, tetracycline, trimethoprim sulfamethoxazole, cefoxitin, ceftriaxone
C0215	ampicillin, amoxicillin clavulanic acid, cefazolin, cefalotin, cefixime, nitrofuratoin, tetracycline, trimethoprim sulfamethoxazole, cefoxitin, ceftriaxone
C0222	ampicillin, amoxicillin clavulanic acid, cefazolin, cefalotin, ciprofloxacin, cefixime, nitrofuratoin, tetracycline, trimethoprim sulfamethoxazole, cefoxitin, ceftriaxone
C0223	ampicillin, amoxicillin clavulanic acid, cefazolin, cefalotin, ciprofloxacin, cefixime, nitrofuratoin, tetracycline, trimethoprim sulfamethoxazole, cefoxitin, ceftriaxone

C0224	ampicillin, amoxicillin clavulanic acid, cefazolin, cefalotin, ciprofloxacin, cefixime, nitrofuratoin, tetracycline, trimethoprim sulfamethoxazole, cefoxitin, ceftriaxone
C0225	ampicillin, amoxicillin clavulanic acid, cefazolin, cefalotin, cefixime, nitrofuratoin, tetracycline, trimethoprim sulfamethoxazole, cefoxitin, ceftriaxone
C0231	ampicillin, amoxicillin clavulanic acid, cefazolin, cefalotin, cefixime, nitrofuratoin, tetracycline, trimethoprim sulfamethoxazole, cefoxitin, ceftriaxone
C0232	ampicillin, amoxicillin clavulanic acid, cefazolin, cefalotin, cefixime, nitrofuratoin, tetracycline, trimethoprim sulfamethoxazole, cefoxitin, ceftriaxone
C0233	ampicillin, amoxicillin clavulanic acid, cefazolin, cefalotin, ciprofloxacin, cefixime, nitrofuratoin, tetracycline, trimethoprim sulfamethoxazole, cefoxitin, ceftriaxone
C0234	ampicillin, amoxicillin clavulanic acid, cefazolin, cefalotin, cefixime, nitrofuratoin, tetracycline, trimethoprim sulfamethoxazole, cefoxitin, ceftriaxone
C0245	ampicillin, amoxicillin clavulanic acid, cefazolin, cefalotin, cefixime, nitrofuratoin, tetracycline, trimethoprim sulfamethoxazole, cefoxitin, ceftriaxone
C0254	ampicillin, amoxicillin clavulanic acid, cefazolin, cefalotin, cefixime, nitrofuratoin, tetracycline, trimethoprim sulfamethoxazole, cefoxitin, ceftriaxone
C0260	ampicillin, amoxicillin clavulanic acid, cefazolin, cefalotin, cefixime, nitrofuratoin, piperacillin tazobactam, tetracycline, trimethoprim sulfamethoxazole, cefoxitin, ceftriaxone
C0261	ampicillin, amoxicillin clavulanic acid, cefazolin, cefalotin, cefixime, nitrofuratoin, tetracycline, trimethoprim sulfamethoxazole, cefoxitin, ceftriaxone
C0262	ampicillin, amoxicillin clavulanic acid, cefazolin, cefalotin, cefixime, nitrofuratoin, tetracycline, trimethoprim sulfamethoxazole, cefoxitin, ceftriaxone
C0263	ampicillin, amoxicillin clavulanic acid, cefazolin, cefalotin, cefixime, metropenem, nitrofuratoin, tetracycline, trimethoprim sulfamethoxazole, cefoxitin, ceftriaxone
C0274	ampicillin, amoxicillin clavulanic acid, cefazolin, cefalotin, cefixime, nitrofuratoin, tetracycline, trimethoprim sulfamethoxazole, cefoxitin, ceftriaxone
C0275	ampicillin, amoxicillin clavulanic acid, cefazolin, cefalotin, cefixime, nitrofuratoin, tetracycline, trimethoprim sulfamethoxazole, cefoxitin, ceftriaxone
C0276	ampicillin, amoxicillin clavulanic acid, cefazolin, cefalotin, cefixime, nitrofuratoin, tetracycline, trimethoprim sulfamethoxazole, cefoxitin, ceftriaxone
C0284	ampicillin, amoxicillin clavulanic acid, cefazolin, cefalotin, cefixime, nitrofuratoin, tetracycline, trimethoprim sulfamethoxazole, cefoxitin, ceftriaxone
C0292	ampicillin, amoxicillin clavulanic acid, cefazolin, cefalotin, ciprofloxacin, cefixime, ceftazidime, metropenem, nitrofuratoin, piperacillin tazobactam, tetracycline, trimethoprim sulfamethoxazole, cefoxitin, ceftriaxone
C0293	ampicillin, amoxicillin clavulanic acid, cefazolin, cefalotin, cefixime, nitrofuratoin, piperacillin tazobactam, tetracycline, trimethoprim sulfamethoxazole, cefoxitin, ceftriaxone
C0294	ampicillin, amoxicillin clavulanic acid, cefazolin, cefalotin, cefixime, nitrofuratoin, tetracycline, trimethoprim sulfamethoxazole, cefoxitin, ceftriaxone
C0295	ampicillin, amoxicillin clavulanic acid, cefazolin, cefalotin, cefixime, nitrofuratoin, tetracycline, trimethoprim sulfamethoxazole, cefoxitin, ceftriaxone
C0296	ampicillin, amoxicillin clavulanic acid, cefazolin, cefalotin, cefixime, nitrofuratoin, tetracycline, trimethoprim sulfamethoxazole, cefoxitin, ceftriaxone
C0305	ampicillin, amoxicillin clavulanic acid, cefazolin, cefalotin, cefixime, nitrofuratoin, tetracycline, trimethoprim sulfamethoxazole, cefoxitin, ceftriaxone
C0306	ampicillin, amoxicillin clavulanic acid, cefazolin, cefalotin, cefixime, nitrofuratoin, tetracycline, trimethoprim sulfamethoxazole, cefoxitin, ceftriaxone

C0307	ampicillin, amoxicillin clavulanic acid, cefazolin, cefalotin, cefixime, nitrofuratoin, tetracycline, trimethoprim sulfamethoxazole, cefoxitin, ceftriaxone
C0315	ampicillin, amoxicillin clavulanic acid, cefazolin, cefalotin, cefixime, nitrofuratoin, piperacillin tazobactam, tetracycline, trimethoprim sulfamethoxazole, cefoxitin, ceftriaxone
C0332	ampicillin, amoxicillin clavulanic acid, cefazolin, cefalotin, cefixime, nitrofuratoin, tetracycline, trimethoprim sulfamethoxazole, cefoxitin, ceftriaxone
C0333	ampicillin, amoxicillin clavulanic acid, cefazolin, cefalotin, cefixime, nitrofuratoin, tetracycline, trimethoprim sulfamethoxazole, cefoxitin, ceftriaxone
C0334	ampicillin, amoxicillin clavulanic acid, cefazolin, cefalotin, cefixime, ceftazidime, metropenem, nitrofuratoin, piperacillin tazobactam, tetracycline, trimethoprim sulfamethoxazole, cefoxitin, ceftriaxone
C0335	ampicillin, amoxicillin clavulanic acid, cefazolin, cefalotin, cefixime, nitrofuratoin, tetracycline, trimethoprim sulfamethoxazole, cefoxitin, ceftriaxone
C0344	ampicillin, amoxicillin clavulanic acid, cefazolin, cefalotin, cefixime, nitrofuratoin, tetracycline, trimethoprim sulfamethoxazole, cefoxitin, ceftriaxone
C0345	ampicillin, amoxicillin clavulanic acid, cefazolin, cefalotin, cefixime, nitrofuratoin, piperacillin tazobactam, tetracycline, trimethoprim sulfamethoxazole, cefoxitin, ceftriaxone
C0346	ampicillin, amoxicillin clavulanic acid, cefazolin, cefalotin, cefixime, nitrofuratoin, tetracycline, trimethoprim sulfamethoxazole, cefoxitin, ceftriaxone
C0355	ampicillin, amoxicillin clavulanic acid, cefazolin, cefalotin, cefixime, nitrofuratoin, tetracycline, trimethoprim sulfamethoxazole, cefoxitin, ceftriaxone
C0356	ampicillin, amoxicillin clavulanic acid, cefazolin, cefalotin, cefixime, ceftazidime, nitrofuratoin, piperacillin tazobactam, tetracycline, trimethoprim sulfamethoxazole, cefoxitin, ceftriaxone
C0365	ampicillin, amoxicillin clavulanic acid, cefazolin, cefalotin, cefixime, nitrofuratoin, tetracycline, trimethoprim sulfamethoxazole, cefoxitin, ceftriaxone
C0366	ampicillin, amoxicillin clavulanic acid, cefazolin, cefalotin, cefixime, nitrofuratoin, piperacillin tazobactam, tetracycline, trimethoprim sulfamethoxazole, cefoxitin, ceftriaxone
C0376	ampicillin, amoxicillin clavulanic acid, cefazolin, cefalotin, cefixime, nitrofuratoin, tetracycline, trimethoprim sulfamethoxazole, cefoxitin, ceftriaxone
C0377	ampicillin, amoxicillin clavulanic acid, cefazolin, cefalotin, cefixime, nitrofuratoin, tetracycline, trimethoprim sulfamethoxazole, cefoxitin, ceftriaxone
C0378	ampicillin, amoxicillin clavulanic acid, cefazolin, cefalotin, cefixime, nitrofuratoin, tetracycline, trimethoprim sulfamethoxazole, cefoxitin, ceftriaxone
C0379	ampicillin, amoxicillin clavulanic acid, cefazolin, cefalotin, cefixime, nitrofuratoin, tetracycline, trimethoprim sulfamethoxazole, cefoxitin, ceftriaxone
C0398	ampicillin, amoxicillin clavulanic acid, cefazolin, cefalotin, cefixime, nitrofuratoin, tetracycline, trimethoprim sulfamethoxazole, cefoxitin, ceftriaxone
C0399	ampicillin, amoxicillin clavulanic acid, cefazolin, cefalotin, ciprofloxacin, cefixime, nitrofuratoin, piperacillin tazobactam, tetracycline, trimethoprim sulfamethoxazole, cefoxitin, ceftriaxone
C0400	ampicillin, amoxicillin clavulanic acid, cefazolin, cefalotin, ciprofloxacin, cefixime, nitrofuratoin, tetracycline, trimethoprim sulfamethoxazole, cefoxitin, ceftriaxone
C0401	ampicillin, amoxicillin clavulanic acid, cefazolin, cefalotin, cefixime, nitrofuratoin, tetracycline, trimethoprim sulfamethoxazole, cefoxitin, ceftriaxone
C0409	ampicillin, amoxicillin clavulanic acid, cefazolin, cefalotin, cefixime, nitrofuratoin, tetracycline, trimethoprim sulfamethoxazole, cefoxitin, ceftriaxone

C0410	ampicillin, amoxicillin clavulanic acid, cefazolin, cefalotin, ciprofloxacin, cefixime, metropenem, nitrofuratoin, tetracycline, trimethoprim sulfamethoxazole, cefoxitin, ceftriaxone
***Acinetobacter baumannii* clinical isolates (Wright Clinical Collection)**	
C0015	ampicillin, amoxicillin clavulanic acid, cefazolin, cefalotin, cefixime, nitrofuratoin, cefoxitin
C0044	ampicillin, amoxicillin clavulanic acid, cefazolin, cefalotin, cefixime, nitrofuratoin, cefoxitin, ceftriaxone
C0074	ampicillin, amoxicillin clavulanic acid, amikacin, cefazolin, cefalotin, ciprofloxacin, cefixime, ceftazidime, gentamicin, metropenem, nitrofuratoin, tetracycline, tobramycin, trimethoprim sulfamethoxazole, cefoxitin, ceftriaxone
C0083	ampicillin, amoxicillin clavulanic acid, cefazolin, cefalotin, cefixime, nitrofuratoin, cefoxitin
C0092	ampicillin, amoxicillin clavulanic acid, amikacin, cefazolin, cefalotin, ciprofloxacin, cefixime, ceftazidime, gentamicin, metropenem, nitrofuratoin, tetracycline, tobramycin, trimethoprim sulfamethoxazole, cefoxitin, ceftriaxone
C0102	ampicillin, amoxicillin clavulanic acid, cefazolin, cefalotin, cefixime, nitrofuratoin, tetracycline, cefoxitin
C0170	ampicillin, amoxicillin clavulanic acid, cefazolin, cefalotin, cefixime, nitrofuratoin, trimethoprim sulfamethoxazole, cefoxitin
C0171	ampicillin, amoxicillin clavulanic acid, cefazolin, cefalotin, cefixime, nitrofuratoin, cefoxitin
C0267	ampicillin, amoxicillin clavulanic acid, cefazolin, cefalotin, cefixime, nitrofuratoin, cefoxitin, ceftriaxone
C0286	ampicillin, amoxicillin clavulanic acid, amikacin, cefazolin, cefalotin, ciprofloxacin, cefixime, ceftazidime, gentamicin, metropenem, nitrofuratoin, tetracycline, tobramycin, trimethoprim sulfamethoxazole, cefoxitin, ceftriaxone

[a] based on CLSI breakpoints for *P. aeruginosa* or *A. baumannii*, respectively
[b] the Wright Clinical Collection is an internal collection of clinical isolates sourced from Hamilton, ON hospitals in the last 2 years. Patient identifiers for these strains were removed to comply with privacy requirements and strains assigned local reference numbers.

Supplementary Table 3. Primers used to generate *P. aeruginosa* efflux mutants

Primer Name	Sequence (restriction sites underlined and bolded)
Del-oprM-Eco-F1	5’-CGTTG**GAATTC**CTGGACCGGCCTGTCCTAC-3’
Del-oprM-Sac-R1	5’-GGCCG**GAGCTC**CGCCGCGCCGGTGTTCTGC-3’
Del-oprM-Sac-F2	5’-CGCTC**GAGCTC**GTTCACCGCGCAGCAGCAA-3’
Del-oprM-Hind-R2	5’-CGGCC**AAGCTT**AATCGGCCGCCGGAAGTCG-3’
Del-oprJ-Eco-F1	5’-GCCG**GAATTC**GGCTACGAGTGGACCGGCCT-3’
Del-oprJ-Sac-R1	5’-CTCC**GAGCTC**GTCGGCCACCGGCGCGGCGG-3’
Del-oprJ-Sac-F2	5’-CGAT**GAGCTC**CGCAGCAGCTTCCTCAACGA-3’
Del-oprJ-Hind-R2	5’-TCTCG**AAGCTT**CAGCGCCAACCCCGTCGT-3’
Del-opmD-Eco-F1	5’-GACTG**GAATTC**CGACTCGCGGCAATACAC-3’
Del-opmD-Sac-R1	5’-CGCTG**GAGCTC**GGGGCCGACGCTGCAGGC-3’
Del-opmD-Sac-F2	5’-ACCA**GAGCTC**CGCGAGGAACTGGCGCAGGC-3’
Del-opmD-Hind-R2	5’-CCTG**AAGCTT**GCTGCCCGGATGCCGGCCG-3’

Supplementary References

1. Vogel HJ, Bonner DM. 1956. Acetylornithinase of *Escherichia coli*: partial purification and some properties. *J Biol Chem* 218:97-106.
2. Liberati NT, Urbach JM, Miyata S, Lee DG, Drenkard E, Wu G, Villanueva J, Wei T, Ausubel FM. 2006. An ordered, nonredundant library of *Pseudomonas aeruginosa* strain PA14 transposon insertion mutants. *Proc Natl Acad Sci U S A* 103:2833-8.
3. Baba T, Ara T, Hasegawa M, Takai Y, Okumura Y, Baba M, Datsenko KA, Tomita M, Wanner BL, Mori H. 2006. Construction of *Escherichia coli K-12* in-frame, single-gene knockout mutants: the Keio collection. *Mol Syst Biol* 2:2006 0008.
4. Carrel M, Perencevich EN, David MZ. 2015. USA300 Methicillin-Resistant *Staphylococcus aureus*, United States, 2000-2013. *Emerg Infect Dis* 21:1973-80.
5. Mistry A, Warren MS, Cusick JK, Karkhoff-Schweizer RR, Lomovskaya O, Schweizer HP. 2013. High-level pacidamycin resistance in *Pseudomonas aeruginosa* is mediated by an opp oligopeptide permease encoded by the *opp-fabI* operon. *Antimicrob Agents Chemother* 57:5565-71.
6. Pletzer D, Braun Y, Dubiley S, Lafon C, Kohler T, Page MGP, Mourez M, Severinov K, Weingart H. 2015. The *Pseudomonas aeruginosa* PA14 ABC Transporter NppA1A2BCD Is Required for Uptake of Peptidyl Nucleoside Antibiotics. *J Bacteriol* 197:2217-2228.
7. Pletzer D, Braun Y, Weingart H. 2016. Swarming motility is modulated by expression of the putative xenosiderophore transporter SppR-SppABCD in *Pseudomonas aeruginosa* PA14. *Antonie Van Leeuwenhoek* 109:737-53.
8. Poole K. 2001. Multidrug efflux pumps and antimicrobial resistance in *Pseudomonas aeruginosa* and related organisms. *J Mol Microbiol Biotechnol* 3:255-64.
9. Winsor GL, Griffiths EJ, Lo R, Dhillon BK, Shay JA, Brinkman FS. 2016. Enhanced annotations and features for comparing thousands of *Pseudomonas* genomes in the *Pseudomonas* genome database. *Nucleic Acids Res* 44:D646-53.

Chapter Three: *Pseudomonas aeruginosa* FpvB is a High-Affinity Transporter for Xenosiderophores Ferrichrome and Ferrioxamine B

Preface

The work presented in the following chapter has been published in:

Chan D. C. K., and Burrows, L. L. (2022). *Pseudomonas aeruginosa* FpvB is a High-Affinity Transporter for Xenosiderophores Ferrichrome and Ferrioxamine B. *Mbio.* e03149-22. https://doi.org/10.1128/mbio.03149-22

D.C.K.C. and L.L.B. conceived the study and designed the experiments. D.C.K.C. and L.L.B. wrote the manuscript.

Abstract

Iron is essential for many biological functions in bacteria but its poor solubility is a limiting factor for growth. Bacteria produce siderophores, soluble natural products that bind iron with high affinity, to overcome this challenge. Siderophore-iron complexes return to the cell through specific outer-membrane transporters. The opportunistic pathogen Pseudomonas aeruginosa makes multiple transporters that recognize its own siderophores, pyoverdine and pyochelin, and xenosiderophores produced by other bacteria, which gives it a competitive advantage. Some antibiotics exploit these transporters to bypass the membrane to reach their intercellular targets – including the thiopeptide antibiotic, thiostrepton (TS), which uses the pyoverdine transporters FpvA and FpvB to cross the outer membrane. Here, we assessed TS susceptibility in the presence of various siderophores and discovered that ferrichrome and ferrioxamine B antagonized TS uptake via FpvB. Unexpectedly, we found that FpvB transports ferrichrome and ferrioxamine B with higher affinity than pyoverdine. Site-directed mutagenesis of FpvB coupled with competitive growth inhibition and affinity label quenching studies suggested that the siderophores and antibiotic share a common binding site in an aromatic pocket formed by the plug and barrel domains but have differences in their binding mechanism and molecular determinants for uptake. This work describes an alternative uptake pathway for ferrichrome and ferrioxamine B in *P. aeruginosa* and emphasizes the promiscuity of siderophore transporters, with implications for Gram-negative antibiotic development via the Trojan horse approach.

Introduction

Iron is an essential micronutrient for bacteria, but has poor aqueous solubility at neutral pH and consequently, low bioavailability (1, 2). At sites of infection, bacteria also compete with host-defense proteins that sequester iron. To overcome these limitations, Gram-negative bacteria secrete siderophores, small molecules with high affinity for iron. Once outside the cell, siderophores scavenge iron and return through specific outer-membrane transporters on the cell surface (3). The architecture of siderophore transporters is conserved, consisting of a 22-stranded beta-barrel with a plug domain that occludes the lumen to prevent passive diffusion (3). The extracellular loops of the transporters are important for siderophore recognition and uptake. The periplasmic N-terminus contains a short motif known as the TonB box (3–5), which interacts with the inner membrane protein TonB. Together with the inner membrane proteins ExbB-ExbD, TonB harnesses the proton motive force to actively transport ligands through the transporters via a mechanism that remains incompletely understood (2, 3). Although TonB-dependent transporters (TBDTs) are considered ligand-specific, they can be exploited by antimicrobial compounds, bacteriophages, and bacteriocins for uptake, making them of interest for drug delivery across the outer membrane of Gram negatives (6–14).

The opportunistic bacterial pathogen, *Pseudomonas aeruginosa* encodes ~35 predicted TBDTs for different ligands including siderophores, cobalamin, and other metal complexes (2, 4, 8, 15–17). *P. aeruginosa* makes two main siderophores, pyoverdine and pyochelin, which are taken up via FpvA and FpvB, and FptA, respectively (18–22) (Figure 1). Pyoverdine has higher affinity for iron than pyochelin (23, 24) and has roles in tolerance to antibiotics, biofilm formation, and virulence factor production (25, 26). *P. aeruginosa* can also take up siderophores produced by other microorganisms, including ferrioxamine E and B (produced by *Streptomyces spp.*) and

ferrichrome (produced by fungal species) via the FoxA and FiuA TBDTs, respectively (2, 17, 27) (Figure 1).

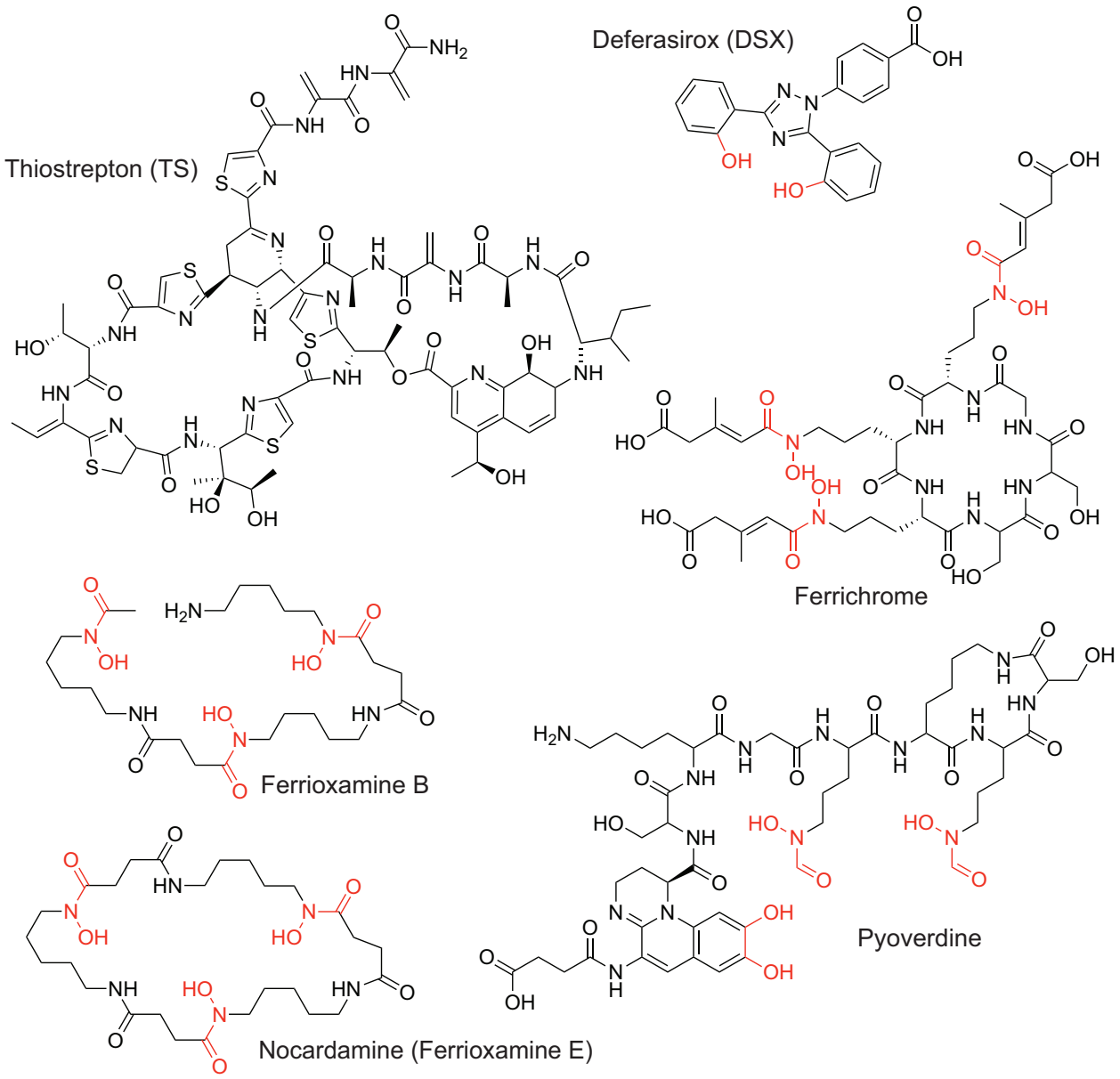

Figure 1. Structures of compounds used in this study. Iron chelating groups are highlighted in red.

Understanding the range of ligands that can be taken up by TBDTs is important as there is growing interest in designing novel antibiotics that can exploit these transporters for uptake. However, our understanding of the substrate range for individual TBDTs is lacking. Even for those

with known ligands, there may be substrates that have yet to be discovered. For example, ferrioxamine E exclusively uses FoxA to enter *P. aeruginosa* (27). However, after *foxA* or *fiuA* are deleted, the bacteria still grow in iron-limited media when supplied with ferrioxamine B or ferrichrome, respectively, suggesting these siderophores can also be recognized by other transporters (27).

Previously we showed that the large thiopeptide antibiotics thiostrepton (TS) and thiocillin use TBDTs to enter *P. aeruginosa* to access their cytoplasmic target, the ribosome. TS exploits the pyoverdine transporters, FpvA and FpvB, while thiocillin uses the ferrioxamine transporter, FoxA (Figure 1) (13, 14, 28). Here we further characterized the interaction of TS with the pyoverdine transporters. We discovered that the secondary transporter FpvB has high affinity for ferrichrome and ferrioxamine B but is a poor pyoverdine transporter. FpvB is a promiscuous transporter as it can recognize structurally distinct ligands using different binding modes. Overall, this work expands our understanding of TBDT function and fills in the missing details of ferrichrome and ferrioxamine B uptake in *P. aeruginosa*.

Results

Exogenous pyoverdine poorly rescues iron-restricted growth of a PA14 Δ*fpvA* mutant

Previously we showed that TS synergized with the FDA-approved iron chelator deferasirox (DSX) against PA14, and that susceptibility required the FpvA and FpvB pyoverdine transporters (Figure 1) (13). DSX lacks antimicrobial activity against wild type (WT) cells since they produce pyoverdine, which competes with DSX for iron. Therefore, WT PA14, a Δ*fpvA* mutant, and a Δ*fpvB* mutant are each expected to be susceptible to TS and grow in the presence of DSX since they still encode functional pyoverdine transporters. A Δ*fpvA* Δ*fpvB* mutant is resistant to TS and inhibited by DSX (13, 14).

We first confirmed these phenotypes via minimal inhibitory concentration (MIC) assays. The WT and Δ*fpvA* mutant were susceptible to TS in iron-limited medium (Figure 2A). The Δ*fpvB* mutant was resistant to TS although its growth was reduced at the maximum soluble TS concentration of 17 µg/mL. The Δ*fpvA* Δ*fpvB* mutant was resistant to TS with no observable decrease in growth. The MIC of DSX against the Δ*fpvA* Δ*fpvB* mutant was 8 µg/mL (Figure 2B), but unexpectedly, DSX also inhibited the growth of the Δ*fpvA* mutant, with the same MIC. This result was surprising, since the Δ*fpvA* mutant has WT susceptibility to TS, suggesting that FpvB is expressed in that background. To confirm that FpvB was expressed in the Δ*fpvA* mutant, we tagged FpvB chromosomally with a C-terminal FLAG tag in both WT and the Δ*fpvA* mutant and blotted for expression. FpvB was detected in the tagged WT and Δ*fpvA* mutant but not in the untagged strains (Supplementary Figure 1A). FpvA is also expressed in WT cells (Supplementary Figure 1B). As a loading control, we monitored expression of PilF, an outer membrane lipoprotein required for multimerization and localization of the *P. aeruginosa* type IV pilus secretin (29). Taken together, these results suggested that the role of FpvB in pyoverdine transport needed to be revisited.

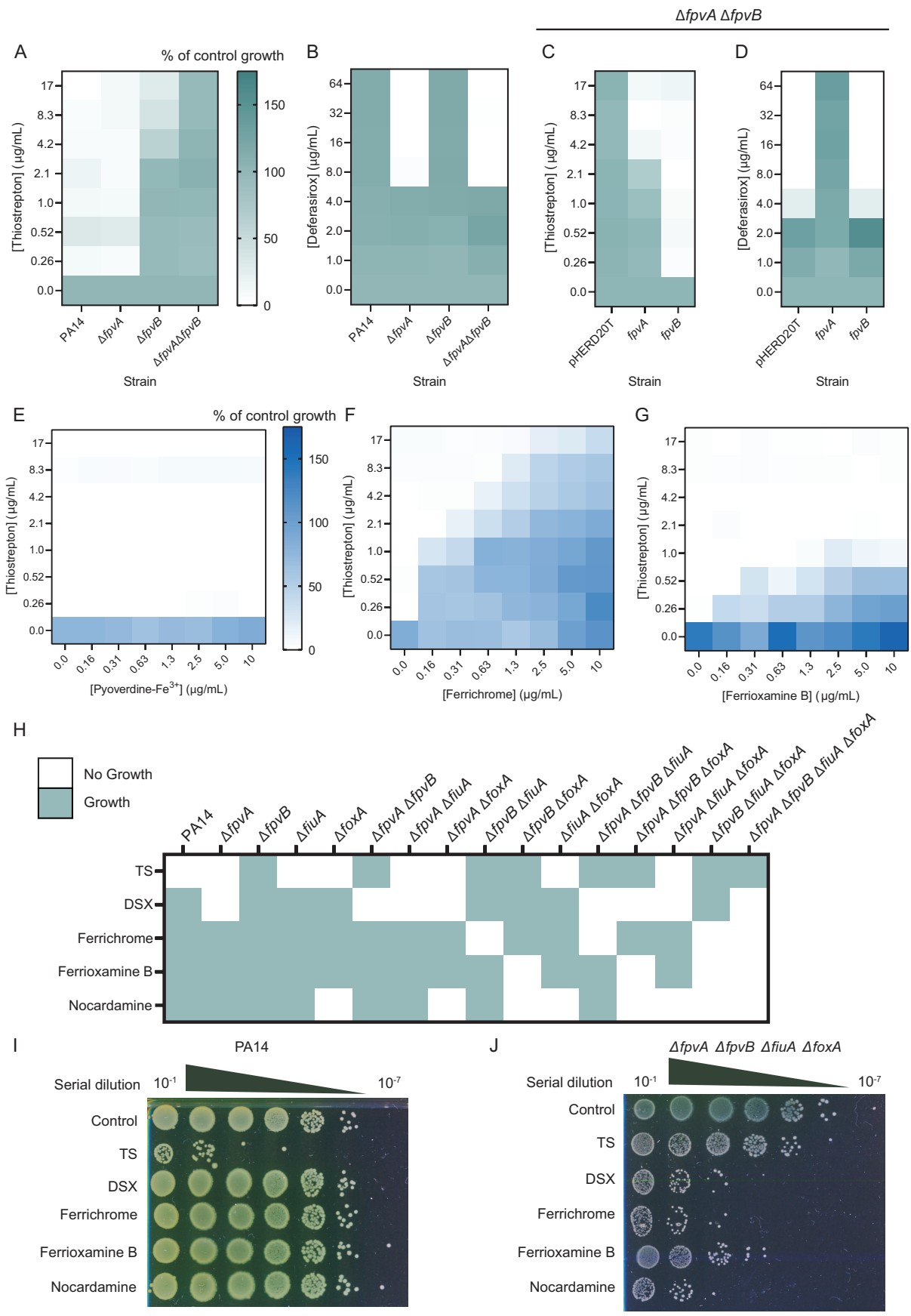
ΔfpvA ΔfpvB
A
% of control growth
[Thiostrepton] (μg/mL)
17
8.3
4.2
2.1
1.0
0.52
0.26
0.0
150
100
50
0
PA14
ΔfpvA
ΔfpvB
ΔfpvAΔfpvB
Strain
B
[Deferasirox] (μg/mL)
64
32
16
8.0
4.0
2.0
1.0
0.0
C
pHERD20T
fpvA
fpvB
D
E
[Pyoverdine-Fe3+] (μg/mL)
0.0
0.16
0.31
0.63
1.3
2.5
5.0
10
F
[Ferrichrome] (μg/mL)
G
[Ferrioxamine B] (μg/mL)
H
No Growth
Growth
PA14
ΔfpvA
ΔfpvB
ΔfiuA
ΔfoxA
ΔfpvA ΔfpvB
ΔfpvA ΔfiuA
ΔfpvA ΔfoxA
ΔfpvB ΔfiuA
ΔfpvB ΔfoxA
ΔfiuA ΔfoxA
ΔfpvA ΔfpvB ΔfiuA
ΔfpvA ΔfpvB ΔfoxA
ΔfpvA ΔfiuA ΔfoxA
ΔfpvB ΔfiuA ΔfoxA
ΔfpvA ΔfpvB ΔfiuA ΔfoxA
TS
DSX
Ferrichrome
Ferrioxamine B
Nocardamine
I
PA14
Serial dilution
10-1
10-7
Control
TS
DSX
Ferrichrome
Ferrioxamine B
Nocardamine
J
ΔfpvA ΔfpvB ΔfiuA ΔfoxA

Figure 2. FpvB is required for growth with ferrichrome and ferrioxamine B in the absence of FiuA and FoxA. PA14, Δ*fpvA,* Δ*fpvB,* and Δ*fpvA* Δ*fpvB* treated with (A) TS and (B) DSX in 10:90. Green indicates growth and white indicates lack of growth. Growth is expressed as percent of control. PA14 Δ*fpvA* Δ*fpvB* complemented with pHERD20T, *fpvA*, or *fpvB* treated with (C) TS and (D) DSX in 10:90. Checkerboard assays of PA14 Δ*fpvA* Δ*fpvB* pHERD20T-*fpvB* treated with TS and (E) pyoverdine-Fe^{3+}, (F) ferrichrome, and (G) ferrioxamine B. All experiments are averaged from three independent biological replicates. Blue indicates growth and white indicates no growth. (H) Summary of growth phenotypes of WT PA14 and combinations of single, double, triple, and quadruple deletion mutants in *fpvA*, *fpvB*, *fiuA*, and *foxA*. Strains were treated with 17 μg/mL TS, 64 μg/mL DSX, 10 μg/mL ferrichrome, 10 μg/mL ferrioxamine B, or 10 μg/mL nocardamine in 10:90. Green indicates growth whereas no growth is indicated in white. Serial 10-fold dilutions of PA14 (I) and the quadruple mutant (J) treated with 17 μg/mL TS, 64 μg/mL DSX, 10 μg/mL ferrichrome, 10 μg/mL ferrioxamine B, or 10 μg/mL nocardamine in 10:90 spotted onto LB 1.5% agar plates and grown overnight at 37°C. Representative plates are shown.

Another explanation for the susceptibility of the Δ*fpvA* mutant to DSX is that the mutant produces less pyoverdine compared to WT cells due to loss of the signalling cascade that controls siderophore production in response to its binding to FpvA (25). To differentiate whether the *fpvA* mutant was susceptible to DSX because of reduced pyoverdine production or because FpvB was a poor pyoverdine transporter, we treated WT, Δ*fpvA*, Δ*fpvB,* and Δ*fpvA* Δ*fpvB* with DSX (64 μg/mL), without and with exogenous pyoverdine (10 μg/mL) for 20 h (Figure 1, Supplementary Figure 1C). Growth of the Δ*fpvA* mutant should be restored if there are functional pyoverdine transporters. For WT and the Δ*fpvB* mutant*,* growth was similar between the control and DSX conditions. Pyoverdine or DSX + pyoverdine treatment increased growth. For the Δ*fpvA* mutant, DSX inhibited growth and pyoverdine supplementation delayed growth. DSX + pyoverdine treatment restored growth compared to DSX alone, but also further delayed growth compared to the pyoverdine-alone treatment. The growth of the Δ*fpvA* Δ*fpvB* mutant was inhibited by DSX and pyoverdine, confirming previously published results (18). Taken together, this suggests that the FpvB is a less efficient pyoverdine transporter than FpvA.

As a control, a Δ*pvdA* Δ*pchA* mutant unable to make pyoverdine and pyochelin was also tested. Growth of this mutant was inhibited by DSX. We showed previously that a *pvdA* mutant remains susceptible to TS, indicating that it makes functional pyoverdine transporters even though the signalling cascade controlled by FpvA is disrupted in the absence of ligand production (13). As expected, pyoverdine restored growth of the mutant in the presence of DSX (Supplementary Figure 1C). As additional controls, Δ*fpvA,* Δ*fpvA* Δ*fpvB,* and Δ*pvdA* Δ*pchA* were treated with DSX in the presence of the xenosiderophores ferrichrome and ferrioxamine B, which use FiuA and FoxA for uptake (Supplementary Figure 1D,E) (17). The two xenosiderophores rescued growth of all three mutants in the presence of DSX within a 20 h incubation period, without the delay in growth seen with pyoverdine. Taken together, these data suggest that FpvB is a poor pyoverdine transporter.

The Δ*fpvA* Δ*fpvB* mutant was complemented *in trans* with pHERD20T-*fpvA* or pHERD20T-*fpvB*. pHERD20T is an arabinose-inducible vector with expression driven by the P_{BAD} promoter under control of AraC (30). Complementation with *fpvA* or *fpvB* and induction with arabinose restored TS susceptibility, although susceptibility was greater with *fpvB* (Figure 2C). However, only complementation with *fpvA* restored growth with DSX (Figure 2D). Since *fpvB* could not restore growth of the double mutant in the presence of DSX, we hypothesized that FpvB is a poor transporter of pyoverdine but may transport other siderophores.

FpvB is a transporter for ferrichrome and ferrioxamine B

We investigated this hypothesis by treating the Δ*fpvA* Δ*fpvB* mutant complemented with *fpvA* or *fpvB* with TS and pyoverdine-Fe^{3+}. If pyoverdine competes with TS for the same binding site in the transporter, a reduction in TS susceptibility would be expected as competition would

decrease entry of the antibiotic into the cell. TS susceptibility decreased >8-fold with increasing concentrations of pyoverdine-Fe^{3+} when FpvA was expressed (Supplementary Figure 2A). However, pyoverdine-Fe^{3+} did not impact TS susceptibility when FpvB was expressed under the same conditions (Figure 2E). These results show that pyoverdine is a poor competitor for FpvB binding. As controls, we tested TS with ferrichrome, ferrioxamine B, enterobactin, ferrioxamine E, and arthrobactin, siderophores not expected to use FpvA or FpvB for uptake (Supplementary Figure 2B-F). None of those siderophores reduced TS susceptibility when FpvA was expressed, showing that only pyoverdine competes with TS for FpvA binding.

Surprisingly, ferrichrome and ferrioxamine B, but not other siderophores, antagonized TS susceptibility when FpvB was expressed (Figure 2F,G, Supplementary Figure 2G-I). These data suggested that FpvB may transport these two xenosiderophores. We generated 15 single, double, triple, and quadruple knockout mutants lacking different combinations of *fpvA, fpvB, foxA,* and *fiuA* and assessed their growth in the presence of 64 µg/mL DSX, 10 µg/mL ferrichrome, 10 µg/mL ferrioxamine B, and 10 µg/mL ferrioxamine E to determine ligand specificity (Figure 2H). If there were no transporters for a particular siderophore, the mutant would fail to grow due to iron restriction. TS was used as a control at 17 µg/mL since Δ*fpvB* and Δ*fpvA* Δ*fpvB* mutants are resistant to the antibiotic (Figure 2A). Δ*fpvA* mutants were unable to grow in the presence of DSX, consistent with previous results (Figure 1B, Supplementary Figure 1C). Growth of any mutant combination that included Δ*foxA* was inhibited by ferrioxamine E, confirming previous work showing that ferrioxamine E exclusively uses FoxA as a transporter in *P. aeruginosa* (27). Δ*fpvB* Δ*foxA* mutants failed to grow in the presence of ferrioxamine B, while Δ*fpvB* Δ*fiuA* mutants failed to grow with ferrichrome. The quadruple mutant, Δ*fpvA* Δ*fpvB* Δ*fiuA* Δ*foxA*, failed to grow with DSX, ferrioxamine B, ferrioxamine E, or ferrichrome and was resistant to TS. These results

suggest that ferrichrome can be taken up via FpvB and FiuA, whereas ferrioxamine B can be taken up via FpvB and FoxA. The siderophores and chelators were bacteriostatic rather than bactericidal, as serial dilution onto non-selective media of PA14 and Δ*fpvA* Δ*fpvB* Δ*fiuA* Δ*foxA* after treatment with the different compounds resulted in regrowth (Figure 2I,J).

FpvB has higher affinity for ferrichrome and ferrioxamine B than pyoverdine

To determine the affinity of the siderophores for FpvA and FpvB, we adapted the method from Chakravorty et al., to generate a whole-cell sensor where fluorescence quenching serves as an indicator of ligand interaction (31). Siderophore binding triggers conformational changes at the extracellular loops of the TBDT (Figure 3A). Cys substitutions were introduced at the loops and labeled with a fluorescent maleimide dye. When a ligand binds the transporter, the loops fold inwards towards the lumen of the barrel, and changes in the chemical environment surrounding the fluorophore lead to quenching (31, 32). Fluorescence recovery occurs once the siderophore is taken up and the loop returns to its original conformation.

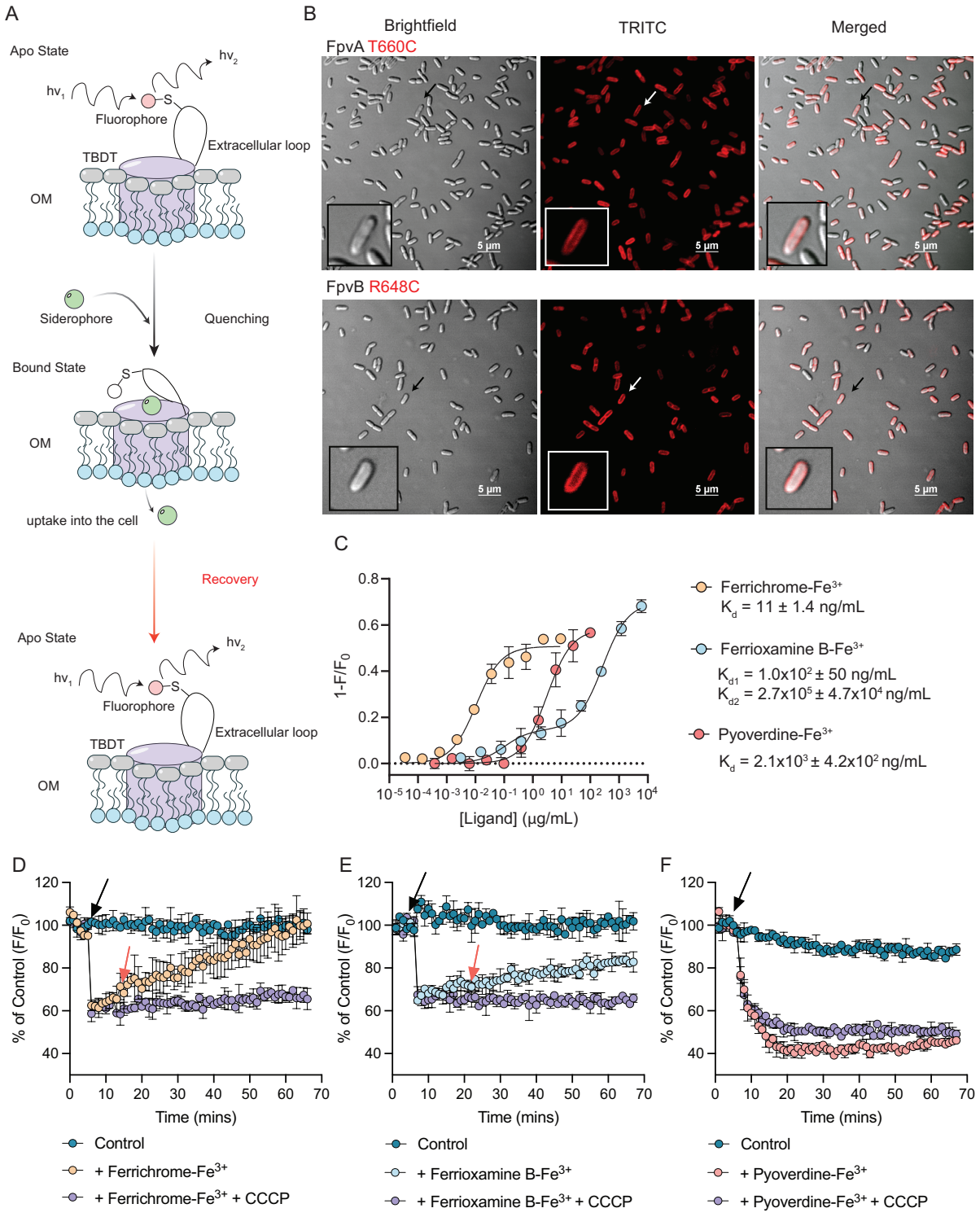

Figure 3. FpvB interacts with ferrichrome, ferrioxamine B, and pyoverdine. (A) Schematic for fluorescence quenching of site-directed labeling of TBDT Cys mutants. A Cys residue is introduced in the extracellular loops of a TBDT of interest and labeled with maleimide dye. A siderophore recognized by the TBDT binds the transporter, inducing conformational changes at the labeled extracellular loop. Changes in the chemical environment surrounding the fluorophore

quenches fluorescence. Uptake of the siderophore into the cell restores fluorescence as the loop returns to its original conformation. (B) Fluorescence microscopy images of PA14 ΔfpvA ΔfpvB pHERD20T-fpvA T660C and fpvB R684C labeled with AlexaFluor 594. Inset: zoomed in view of a single labeled cell. Scale bar is 5 μm. (C) Fluorescence quenching of labeled FpvB R648C by ferrichrome-Fe^{3+} (blue circles), ferrioxamine B-Fe^{3+} (red circles), or pyoverdine-Fe^{3+} (orange circles). K_d values are shown for ferrichrome-Fe^{3+} and pyoverdine-Fe^{3+}. Quenching experiments were conducted in PBS. Fluorescence recovery of labeled FpvB R648C at ½ K_d for (D) ferrichrome-Fe^{3+} (orange circles), (E) ferrioxamine B-Fe^{3+} (blue circles), and (F) pyoverdine-Fe^{3+} (red circles). Teal circles represent vehicle controls and purple circles represent siderophores + 20 μM CCCP. The black arrow indicates when each siderophore complex was added. The red arrow highlights when recovery is observed. No recovery was observed at any pyoverdine-Fe^{3+} concentration. Recovery assays were conducted in PBS + 0.4% glucose. All results are averaged from three independent biological replicates except for the microscopy images where a representative image is shown.

FpvA T660C was used previously to measure pyoverdine-Fe^{3+} binding affinity (32). However, this technique has not been applied to FpvB. A high-confidence structural model of FpvB was generated using AlphaFold2 (33, 34) and aligned with the structure of FpvA (PDB:2O5P) to identify a residue suitable for labeling, with the assumption that FpvA and FpvB undergo similar conformational changes upon ferrisiderophore binding (Supplementary Figure 3A-C). Based on this analysis, FpvB R648 was mutated to Cys. FpvA T660C and FpvB R648C were each expressed *in trans* in the Δ*fpvA* Δ*fpvB* mutant. FpvB R648C had WT susceptibility to TS and growth in the presence of DSX (Supplementary Figure 3D). Expression of FpvA T660C increased susceptibility to TS by 4-fold compared to WT FpvA and restored growth with DSX. We could also detect expression by fluorescence microscopy, with peripheral labeling consistent with expression in the outer membrane (Figure 3B). Labeling was undetectable in empty vector and WT controls (Supplementary Figure 4A).

Ferrichrome-Fe^{3+}, ferrioxamine B-Fe^{3+}, and pyoverdine-Fe^{3+}, were titrated at increasing concentrations into cells expressing FpvA T660C and FpvB R648C labeled with fluorescein-5-maleimide. TS was omitted from these studies because it quenched fluorescence (~20%) of the dye in the absence of cells (Supplementary Figure 4B). In the absence of protein, none of the three

siderophores quenched fluorescence of the dye at the highest concentrations tested. Quenching curves were then generated and used to calculate the K_d. Pyoverdine-Fe^{3+} strongly quenched fluorescence of cells expressing FpvA T660C, with a K_d of 10 ± 1.6 ng/mL (8.2 ± 1.2 nM), similar to values reported in previous studies (Supplementary Figure 4C) (32, 35). Ferrichrome-Fe^{3+} weakly quenched the fluorescence of cells expressing FpvA T660C (~20%), suggesting that ferrichrome may interact weakly with FpvA. No antagonism was observed between TS and ferrichrome, suggesting that the competition is minimal. No quenching was observed with ferrioxamine B-Fe^{3+}.

The estimated K_d of pyoverdine-Fe^{3+} for FpvB was 200-fold higher than FpvA ($2.1x10^3$ ± $4.2x10^2$ ng/mL or $1.7x10^3$ ± $3.4x10^2$ nM), confirming that FpvA has higher affinity for pyoverdine (Figure 3C). Ferrichrome-Fe^{3+} and ferrioxamine B-Fe^{3+} also quenched the fluorescence of cells expressing FpvB R648C (Figure 3C). The K_d of ferrichrome-Fe^{3+} for FpvB was 11 ± 1.4 ng/mL (15 ± 1.9 nM). Titration of ferrioxamine B-Fe^{3+} yielded a curve with two quenching events, suggesting that it may bind at two sites on FpvB – one of higher affinity than the other. For K_{d1}, the binding constant was $1.0x10^2$ ± 50 ng/mL and K_{d2} was $2.7x10^5$ ± $4.7x10^4$ ng/mL. These results may explain the pattern of antagonism between the siderophores and TS. Ferrichrome, which has the highest affinity for FpvB, also had the greatest impact on TS susceptibility. The K_{d1} of ferrioxamine B is approximately 10-fold greater than ferrichrome, suggesting reduced affinity for FpvB, but was sufficient to antagonize TS susceptibility. However, the K_d of pyoverdine for FpvB is 200 and 20-fold greater than ferrichrome and ferrioxamine B respectively, and it had the least impact on TS susceptibility.

Siderophore uptake by FpvB was monitored by fluorescence recovery at a concentration of ½ K_d. In the case of ferrioxamine B, we chose ½ K_{d2} since the quenching signal was greater.

Cells were equilibrated for 5 min prior to introduction of the siderophores. Fluorescence was recorded every min for 1 h. Carbonyl cyanide m-chlorophenylhydrazone (CCCP) was used as a control to inhibit fluorescence recovery through dissipation of the proton motive force (PMF) (2, 3), which is required for uptake. Full fluorescence recovery was seen with ferrichrome (Figure 3D). For ferrioxamine B, fluorescence recovered to ~50% of the control; however, no recovery was seen with pyoverdine, suggesting that uptake of this siderophore is slow (Figure 3E,F). These results suggest that of the three siderophores, ferrichrome has the greatest affinity for FpvB and is taken up most rapidly, followed by ferrioxamine B.

Molecular determinants of TS, ferrichrome, and ferrioxamine B uptake through FpvB

Our data suggested that because ferrichrome, ferrioxamine B, and pyoverdine all quenched fluorescence, they might induce similar conformational changes in FpvB. Ferrichrome-Fe^{3+} and ferrioxamine B-Fe^{3+} were docked into the model of FpvB using AutoDock VINA to identify possible molecular interactions (33, 36). Docking assumed that the siderophore-Fe^{3+} complexes are in similar orientations in their native transporter and in FpvB. Based on the predictions, ferrichrome, and ferrioxamine B bind in a highly aromatic pocket with several Trp and Tyr residues, between the plug and barrel domains (Figure 4A,B).

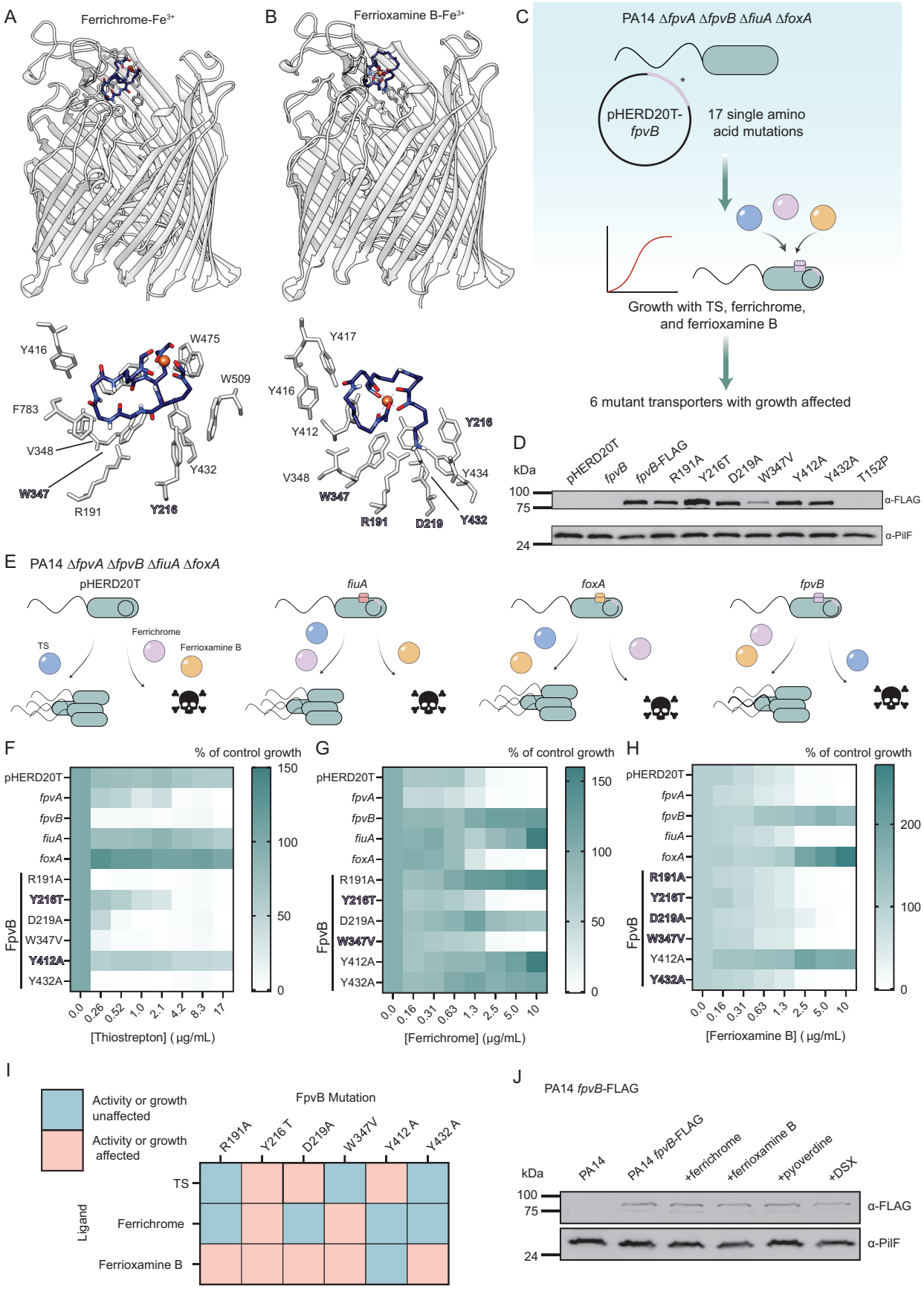
A
Ferrichrome-Fe3+
B
Ferrioxamine B-Fe3+
C
PA14 ΔfpvA ΔfpvB ΔfiuA ΔfoxA
pHERD20T-fpvB
17 single amino acid mutations
Growth with TS, ferrichrome, and ferrioxamine B
6 mutant transporters with growth affected
D
kDa
pHERD20T
fpvB
fpvB-FLAG
R191A
Y216T
D219A
W347V
Y412A
Y432A
T152P
α-FLAG
α-PilF
E
PA14 ΔfpvA ΔfpvB ΔfiuA ΔfoxA
pHERD20T
TS
Ferrichrome
Ferrioxamine B
fiuA
foxA
fpvB
F
% of control growth
[Thiostrepton] (μg/mL)
G
% of control growth
[Ferrichrome] (μg/mL)
H
% of control growth
[Ferrioxamine B] (μg/mL)
FpvB
I
Activity or growth unaffected
Activity or growth affected
FpvB Mutation
Ligand
TS
Ferrichrome
Ferrioxamine B
J
PA14 fpvB-FLAG
kDa
PA14
PA14 fpvB-FLAG
+ferrichrome
+ferrioxamine B
+pyoverdine
+DSX
α-FLAG
α-PilF

Figure 4. Molecular determinants of TS, ferrichrome, and ferrioxamine B uptake through FpvB. Ferrichrome-Fe^{3+} (blue; PDB: 1BY5) was docked into the AlphaFold2 model of FpvB (grey) using Autodock Vina. Predicted molecular interactions are shown below with residues important for uptake highlighted in purple and bolded. (B) Ferrioxamine B-Fe^{3+} (blue; PDB: 6I96) was docked into the AlphaFold2 predicted model of FpvB (grey). Predicted molecular interactions are shown below with residues important for uptake highlighted in purple and bolded. (C) Schematic for validating the docking predictions. (D) Western blot of FLAG-tagged mutant FpvB transporters, with PilF as a loading control. Cells were grown overnight in 10:90 + 2% arabinose. (E) Expected phenotypes for PA14 Δ*fpvA* Δ*fpvB* Δ*foxA* Δ*fiuA* harbouring pHERD20T, pHERD20T-*fpvB*, pHERD20T-*fiuA*, and pHERD20T-*foxA* treated with TS, ferrichrome, and ferrioxamine B. PA14 Δ*fpvA* Δ*fpvB* Δ*foxA* Δ*fiuA* complemented with empty vector, *fpvA*, *fpvB*, *fiuA*, *foxA* and *fpvB* mutants treated with (F) TS, (G) ferrichrome, and (H) ferrioxamine B in 10:90 + 2% arabinose. Growth (green) is expressed as percent of control. Results are averaged from three independent biological replicates. (I) Summary of effects of the mutations on TS susceptibility and growth in the presence of ferrichrome and ferrioxamine B. Teal: growth is affected; coral: growth is unaffected. (J) Western blot for WT PA14 with chromosomally integrated C-terminal FLAG tagged FpvB treated with, 10 μg/mL ferrichrome, 10 μg/mL ferrioxamine B, 10 μg/mL pyoverdine, and 64 μg/mL DSX in 10:90. PilF was used as a loading control for outer membrane proteins.

Site-directed mutagenesis was used to confirm the docking predictions and to define the molecular determinants for ligand uptake through FpvB (Figure 4C). We generated 17 single amino acid substitutions in FpvB and expressed each of them *in trans* in the quadruple Δ*fpvA* Δ*fpvB* Δ*fiuA* Δ*foxA* mutant. Their ability to complement growth of the mutant in the presence of ferrichrome and ferrioxamine B and to restore TS susceptibility was assessed. Of the 17 mutations, six affected TS susceptibility and growth with ferrichrome and ferrioxamine B: R191A (plug domain), Y216T (extracellular loop), D219A (plug domain), W347V (extracellular loop), Y412A (barrel domain), and Y432A (barrel domain). The mutant transporters were tagged with a C-terminal FLAG tag to evaluate expression levels. FLAG-tagged FpvB mutants had WT levels of expression except for Y216T and W347V which were expressed at 140% and 25% of WT respectively. These results suggest that except for W347V, differences in growth are not due to differences in expression (Figure 4D). FpvB-FLAG is functional and restores TS activity, ferrichrome uptake, and ferrioxamine B uptake (Supplementary Figure 5A).

The Δ*fpvA* Δ*fpvB* Δ*fiuA* Δ*foxA* mutant was complemented with WT *fpvA*, *fpvB*, *fiuA*, and *foxA in trans* as controls (Figure 4E). The quadruple mutant with the empty vector is resistant to TS and its growth inhibited by ferrichrome and ferrioxamine B. Complementation with *fpvA* was predicted to restore susceptibility to TS but not growth with ferrichrome or ferrioxamine B, while complementation with *fpvB* was expected to restore susceptibility to TS and growth with ferrichrome and ferrioxamine B. Complementation with *fiuA* was expected to restore growth with ferrichrome but not ferrioxamine B, while cells remain resistant to TS. Finally, complementation with *foxA* was expected to restore growth with ferrioxamine B but not ferrichrome, while cells remain resistant to TS. Several mutations within the binding pocket negatively affected TS susceptibility or growth with ferrichrome and ferrioxamine B (Figure 4F-H). Y216T, D219A, and Y412A reduced TS susceptibility. Y216T and W347V prevented growth in the presence of ferrichrome. All mutations except Y412A prevented growth in the presence of ferrioxamine B. The effects of the mutations on TS susceptibility and growth in the presence of ferrichrome and ferrioxamine B are summarized in Figure 4I. Finally, we tested whether ferrichrome, ferrioxamine B, and pyoverdine could stimulate FpvB expression (Figure 4J). DSX was included as a negative control since it does not bind FpvB. None of the compounds stimulated expression, consistent with previous proteomic and RT-PCR assays (27).

To determine if these mutations affected binding of ferrichrome and ferrioxamine B to FpvB, we introduced R648C to allow fluorescent labeling of the six point mutants; however, only R191A and W347V could be labeled with AlexaFluor 594 (Figure 5A). Quenching assays with the two xenosiderophores were repeated for the quadruple TBDT mutant expressing WT FpvB, FpvB R191A R648C, or W347V R648C. The R191A mutation increased the K_d of ferrichrome-Fe^{3+} by 76-fold to $6.5x10^2 \pm 1.5x10^2$ ng/mL ($8.7x10^2 \pm 2.0x10^2$ nM) while the W347V mutation

increased the K_d >76-fold (Figure 5B). FpvB R191A allowed growth of the quadruple mutant in the presence of ferrichrome whereas W347V did not (Figure 4G,H). These data suggest that certain mutations in FpvB can be tolerated and allow sufficient ferrichrome uptake, potentially because the K_d of ferrichrome for WT FpvB is naturally low.

R191A and W347V also compromised ferrioxamine B uptake, suggesting reduced affinity (Figure 4H,I). This was confirmed with the fluorescence quenching assay using the quadruple transporter mutant expressing FpvB R648C (Figure 5C). The K_{d1} and K_{d2} were $1.0x10^2 \pm 59$ ng/mL ($1.7x10^2 \pm 96$ nM) and $3.7x10^5 \pm 9.5\ x10^4$ ng/mL ($6.0x10^5 \pm 1.5x10^4$ nM), similar to Δ*fpvA* Δ*fpvB* (Figure 3C, Figure 5C). The quenching curves for the R191A and W347V mutants fit a typical one-site model rather than the two-site model observed for the WT with K_d values of $3.0x10^5 \pm 4.3x10^4$ ng/mL ($4.8x10^5 \pm 7.0x10^4$ nM) and $4.9x10^5 \pm 6.8x10^4$ ng/mL ($8.0x10^2 \pm 1.1x10^2$ nM) respectively. Neither mutation affected the K_{d2}. These results suggest that mutating the predicted binding pocket prevents the initial interaction of ferrioxamine B with FpvB and further supports the hypothesis that ferrioxamine B binds at two distinct sites. Additionally, conformational changes that occur from the first binding event appear to be independent from the second since the quenching is still observed in the mutants.

Pyoverdine-Fe^{3+} binding to FpvB single residue mutants was also assessed using the fluorescence quenching assay. The K_ds of pyoverdine for FpvB were similar in the Δ*fpvA* Δ*fpvB* mutant and the quadruple mutant (Figure 3C, Figure 5D). For the R191A and W347V mutants, the K_d could not be determined because saturation was not reached even at the highest concentration tested, indicating that pyoverdine has reduced affinity for the two FpvB mutants. Overall, the R191A and W347V mutations reduced the affinity of FpvB for all three ligands.

Since only a subset of FpvB mutant transporters could be fluorescently labeled, we tested competition between TS and ferrichrome via checkerboard assays. The quadruple transporter mutant complemented with WT FpvB or FpvB single-residue mutants was treated with ferrichrome and TS and assessed for antagonism of TS susceptibility (Supplementary Figure 5B). Ferrioxamine B was not tested because the quadruple mutant expressing 5 of 6 FpvB single residue mutants was unable to grow with that siderophore (Figure 4H,I). Antagonism was observed between ferrichrome and TS when WT FpvB was expressed. Consistent with the data in Figure 4G, the Y216T and W347V mutant FpvB transporters were unable to support growth with ferrichrome. Interestingly, while R191A and D219A supported growth of the quadruple mutant in the presence of ferrichrome, no competition with TS was observed, suggesting that these mutations specifically reduce the affinity of FpvB for ferrichrome. When the Y432A mutant transporter was expressed, ferrichrome antagonised TS activity, although to a lesser extent than observed with the WT. Overall, the mutations diminished the ability of ferrichrome to compete with TS.

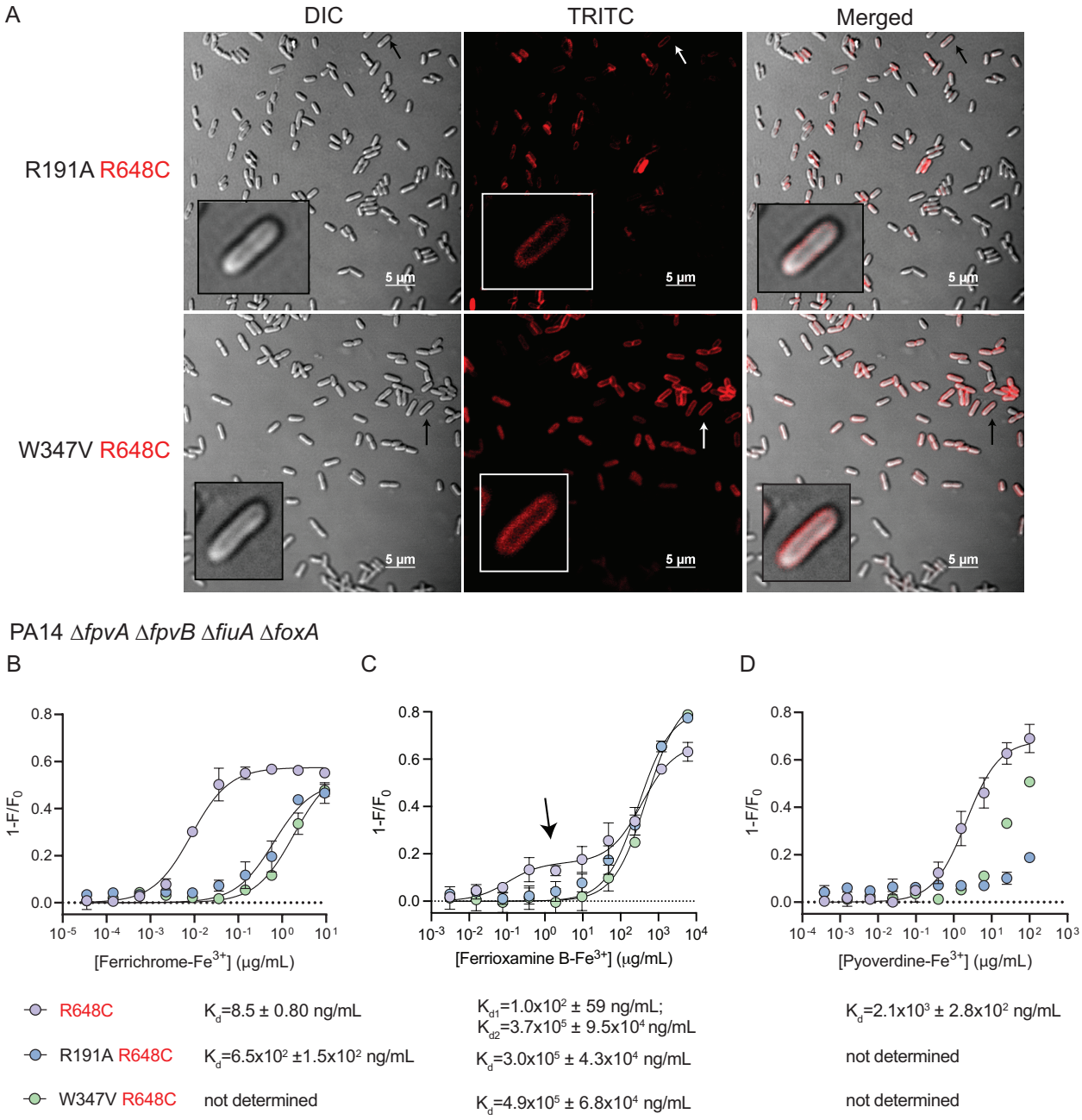

Figure 5. FpvB single residue mutants are stably expressed but have reduced affinity for siderophores. (A) Microscope images of Δ*fpvA* Δ*fpvB* Δ*fiuA* Δ*foxA* expressing FpvB R191A R648C or W347V R648C labeled with AlexaFluor594. Scale bar: 5 µm. Quenching curves of PA14 Δ*fpvA* Δ*fpvB* Δ*fiuA* Δ*foxA* expressing fluorescein-5-maleimide-labeled FpvB R648C (purple), R191A R648C (blue), and W347V R648C (green) titrated with (B) ferrichrome-Fe^{3+}, (C) ferrioxamine B-Fe^{3+}, or (D) pyoverdine-Fe^{3+}. The arrow in panel B highlights the first saturation event observed with FpvB R648C titrated with ferrioxamine B-Fe^{3+}. Results are averaged from three independent biological replicates.

Discussion

This work expands on the discovery of FpvB as an alternative transporter for pyoverdine (18). Ghysels et al. made a *P. aeruginosa* PAO1 mutant unable to produce FpvA, pyoverdine, or pyochelin, which grew in casamino acids (CAA) medium. Supplementing the media with ethylene diamine di(o-hydroxyphenyl)acetic acid (EDDHA), an iron chelator unable to enter cells, inhibited growth, similar to our results with the PA14 Δ*fpvA* mutant and DSX (Supplementary Figure 1A). Supplementing the media with pyoverdine restored growth of the mutant after 24 h but not 12 h, suggesting expression of a TBDT with limited affinity for pyoverdine. Deleting *fpvB* inhibited growth recovery, suggesting that FpvB transports pyoverdine. Another study showed that a PAO1 Δ*fpvA* mutant was unable to grow in media supplemented with EDDHA even if pyoverdine was added, although growth was only monitored for 10 h rather than 24 h (37). Similarly, a PAO1 FpvA-deficient strain was unable to take up iron from pyoverdine-^{59}Fe, regardless of whether pyoverdine from PAO1 or other Pseudomonads was provided, although uptake was measured only for 15 min (38). Together, these results suggest that FpvB is a poor transporter for pyoverdine, which informed our hypothesis that FpvB may transport other siderophores.

In this work, we uncovered additional uptake pathways for the fungal siderophore, ferrichrome, and the bacterial siderophore, ferrioxamine B, in *P. aeruginosa*. Canonically, ferrichrome is taken up via FiuA while ferrioxamine B uses FoxA. Both siderophores can be recognized by FpvB (Figure 6), and ferrichrome binds with greater affinity than ferrioxamine B or pyoverdine, based on fluorescence quenching data (Figure 3C). Unexpectedly, the quenching curve of ferrioxamine B-Fe^{3+} supported a two-site binding model. This result suggests that the binding mode of ferrioxamine B for FpvB is different than those of ferrichrome and pyoverdine, and shows that different ligands can interact in distinct ways with the same TBDT. A two-site

model has been proposed for binding of enterobactin to its transporter PfeA, but ferrioxamine B and E were reported to bind their primary transporter FoxA only at a single site (4, 5, 27). We also used fluorescence recovery as an indicator of ligand uptake. Fluorescence recovery was not observed for pyoverdine even after 1 h (Figure 3F), suggesting that pyoverdine uptake through FpvB is slow. A combination of a high K_d and slow uptake may explain why FpvB is a poor transporter for pyoverdine.

The site-directed mutagenesis data suggest that all three ligands bind a similar hydrophobic pocket in FpvB, but the molecular determinants for uptake depend on the ligand. For example, W347 is important for both ferrichrome and ferrioxamine B but not TS uptake. Y412 is important for TS uptake but not for the two xenosiderophores, and Y216 is essential for uptake of all three ligands. Co-structures of FpvB with each of ligands will be informative. Combining the site-directed mutagenesis data with fluorescence quenching and checkerboard competition assays, we showed that modifying the hydrophobic pocket of FpvB reduced its affinity for the ligands. With ferrioxamine B, the R191A and W347V mutations abolished the initial quenching event observed in WT FpvB (Figure 5C). However, the second quenching event was unaffected, suggesting that the two binding events occur independently, and that conformational changes caused by the first event are not required for the second. Future work will focus on locating the second site, to understand how ferrioxamine B interacts with FpvB. Additionally, this work supports the idea that the binding mechanism of different siderophores can vary even for the same transporter.

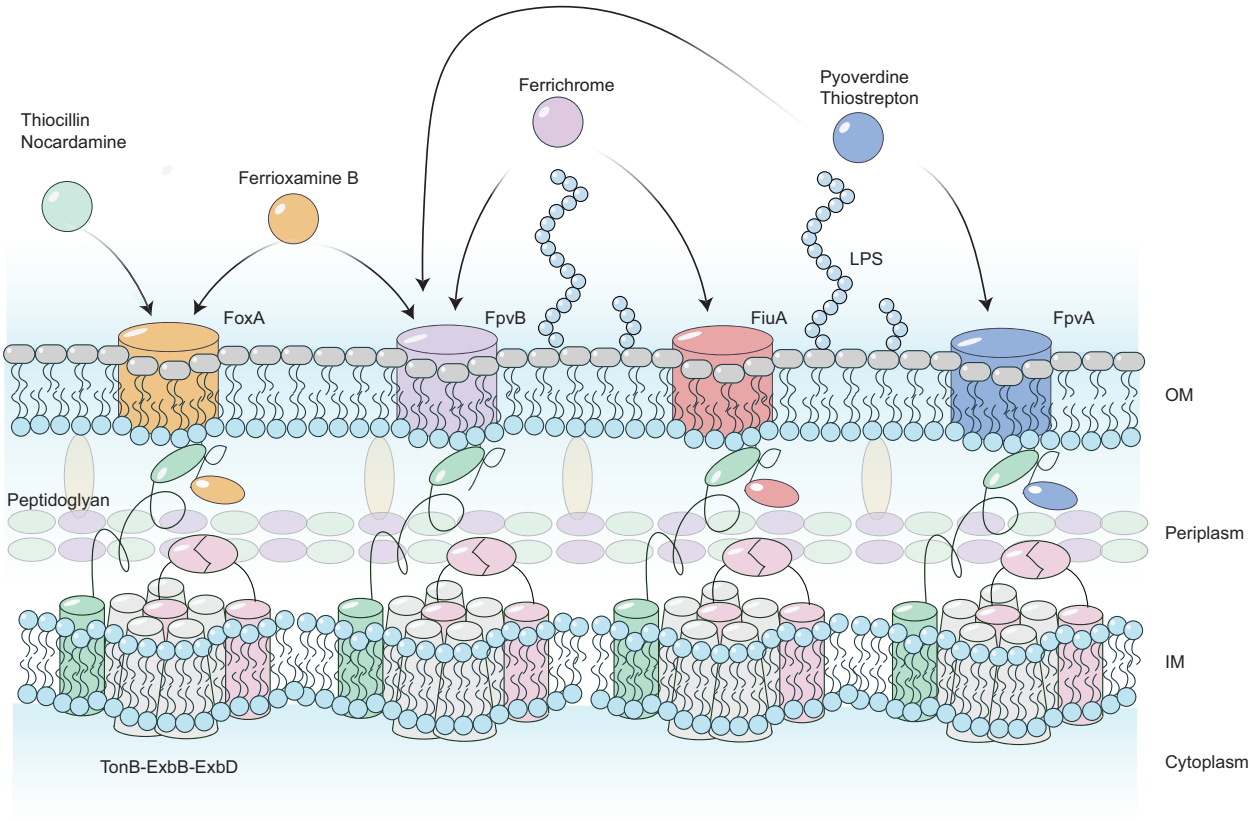

Figure 6. Model for thiopeptide and siderophore uptake through the TBDTs FpvA, FpvB, FoxA, and FiuA in *P. aeruginosa*. OM – outer membrane; IM – inner membrane.

Determining the ligand specificity of TBDTs can be challenging. Traditionally, sequence alignments of transporters with known ligands and transporters with unknown ligands were used to make inferences about the function of the new transporter. This method works well for those that share high sequence similarity. For example, the aerobactin transporter in *P. aeruginosa* was discovered by comparing the sequences of *Escherichia coli* IutA and *P. aeruginosa* ChtA which share 46% identity (63% similarity) (39). FpvB was initially discovered as a secondary ferripyoverdine transporter using this method, as it shares 54% amino acid similarity with FpvA (18). However, alignments do not provide a comprehensive picture of the range of ligands that can be taken up. FpvB shares only 30-40% similarity with FoxA and FiuA, even though our data suggest that it has higher affinity for ferrichrome than pyoverdine.

Proteomic and RT-PCR approaches have also been used to identify the transporters for ferrioxamine E, ferrioxamine B, and ferrichrome in *P. aeruginosa* (27). FoxA expression was upregulated in the presence of ferrioxamine E and ferrioxamine B, while FiuA expression was upregulated by ferrichrome. However, only a subset of TBDTs have N-terminal signalling domains that respond to the presence of ferrisiderophores in a feed-forward regulation loop to increase their expression. Further, many TBDTs have redundant functions and knocking out single transporters may be insufficient to abolish uptake, making it difficult to understand the complete uptake pathway for a ligand. As an alternative, competition between an antimicrobial and siderophore has been used to show that an antimicrobial exploits a particular TBDT for uptake (40, 41). Here, we used competition between TS and various siderophores to show that FpvB recognizes ferrichrome and ferrioxamine B, antagonizing TS susceptibility. This method may be applicable to study the range of ligands that can be recognized by TBDTs in bacteria besides *P. aeruginosa*. The disadvantage of this method is that a antimicrobial known to use the TBDT of interest for uptake is required.

Previous studies established that 93% of *P. aeruginosa* clinical and environmental isolates have *fpvB* (13, 18, 42). It may be advantageous to produce a single transporter that recognizes at least three different siderophores; therefore, the observation that 7% of isolates lack *fpvB* seems paradoxical. Loss of *fpvB* may improve the fitness of *P. aeruginosa* in the lungs of cystic fibrosis patients through genome reduction (43). Supporting this finding, we previously identified a TS-resistant but thiocillin-sensitive clinical isolate, C0379, missing ~800 bp from the 5' region of *fpvB*, suggesting that it may have once produced functional FpvB (13). Δ*fpvB* mutants are also fitter than WT cells when treated with the antibiotic gentamicin (44). Its absence may reduce the metabolic burden on cells living in stressful environments whether due to nutrient limitation or

antibiotic stress. However, the proportion of isolates from environmental or clinical sources lacking *fpvB* is similar, suggesting that there are multiple factors involved (42). For example, while we identified TS + DSX-resistant mutants with a single point mutation in *fpvB* (T152P) that abolished its expression, we also identified resistant *P. aeruginosa* unable to make TonB1. Although not all *P. aeruginosa* clinical isolates produce FpvB, we previously tested 96 clinical isolates and found that 94/96 were susceptible to a combination of TS + DSX, suggesting that majority of the isolates produce FpvB (Chan et al., 2020). Alignment of FpvB sequences from 32 of 96 clinical isolates revealed 99.8% amino acid identity, showing that it is highly conserved (Supplementary Figure 6). These data support the idea that FpvB could be a clinically relevant uptake pathway for siderophore-antibiotic conjugates to treat *P. aeruginosa* infections.

This work has implications for our understanding of how siderophores are taken up by *P. aeruginosa* compared to other bacteria. In *E. coli*, ferrichrome is recognized by FhuA whereas ferrioxamine B weakly binds FhuE, which does not take up ferrioxamine E or ferrichrome (45, 46). In *P. aeruginosa,* ferrichrome is recognized by FiuA and FpvB, ferrioxamine B is recognized by FoxA and FpvB, and ferrioxamine E is exclusively recognized by FoxA. FpvB is unusual in that TBDTs typically take up siderophore-iron complexes that are structurally related to their native siderophores, which suggests that FpvB may have a high degree of promiscuity compared to other TBDTs. These differences in uptake are important considerations in the design of broad-spectrum siderophore-antibiotic conjugates for gram negative pathogens.

There is growing interest in the use of antimicrobials that exploit TBDTs for uptake. For example, conjugating antibiotics to ferrichrome or ferrioxamine B may permit a compound to be taken up by both FpvB and FiuA or FoxA. The benefits of an antibiotic-siderophore conjugate that can use multiple receptors include a reduced chance of developing resistance, as cells would have

to lose multiple TBDTs. In this context, it would be of interest to see how modifications to the siderophore structure affects binding and uptake. For example, one natural variation that prevents ferrioxamine E from using FpvB is that it is cyclic (Figure 1) whereas ferrioxamine B is linear in its apo-form; however, they both adopt similar cyclic conformations when bound to Fe^{3+}. Further, ferrioxamine B has an amine tail predicted to interact with R191 that does not participate in iron chelation; this extension is absent in ferrioxamine E. Structure-activity relationship studies of ferrichrome and ferrioxamine B may further reveal ligand-transporter interactions to allow for the design of better siderophore-drug conjugates.

Methods and Materials

Strains and primers

All strains and primers used in this study are listed in the supplemental materials (**Supplementary Table S1** and **Supplementary Table S2**).

Compounds and media

Ferrichrome, nocardamine, enterobactin, and fluorescein-5-maleimide were purchased from Cayman Chemicals. Ferrioxamine B was purchased from Calbiochem. Pyoverdine and pyoverdine-Fe^{3+} was purchased from Sigma. Arthrobactin was purchased from MolPort. AlexaFluor594 C5 maleimide was purchased from Fisher Scientific. Carbenicillin was purchased from AK Scientific. L-arabinose was purchased from Bioshop. Glucose was purchased from Fisher Scientific. Stock solutions and powders were stored at -20°C. LB was purchased as a premixed powder from Bioshop. 10:90 medium was prepared as previously described (Chan and Burrows, 2021; Ranieri et al., 2019) consisting of 10% LB and 90% PBS (PBS; pH 7.4; 1X PBS was made from a 10X stock (80 g NaCl, 2 g KCl, 26.8 g Na_2HPO_4-$7H_2O$, 2.4 g KH_2PO_4 in 1 L of de-ionized

H_2O)). L-arabinose was prepared as a 20% (wt/v) stock solution in 10:90 and filter sterilized (0.2µm pore size - Fisherbrand).

Molecular biology

Chromosomal mutants were generated by allelic exchange using pEX18Gm (Hoang et al., 1998). Primers flanking the upstream and downstream regions of each gene of interest were amplified from PA14 genomic DNA (Promega Wizard Genomic DNA Purification Kit) and extracted with GeneJet Gel Extraction Kit (ThermoFisher). The upstream and downstream regions were joined by overlap extension PCR or ligation, digested with the indicated enzymes (FastDigest ThermoFisher), and ligated into pEX18Gm to make each deletion construct (T4 DNA ligase, ThermoFisher) (Hoang et al., 1998). The ligation mixtures were transformed into competent *E. coli* DH5α by heat shock with a recovery period of 2-3 h in LB. Cells were plated on LB 1.5% agar containing 15 µg/mL gentamicin supplemented with 5-bromo-4-chloro-3-indolyl-β-D-galactopyranoside (X-gal) for blue-white screening. The plates were incubated at 37°C overnight. Colony PCR was performed on white colonies to check for the correct inserts and those with the insert were grown in LB + 15 µg/mL gentamicin overnight at 37°C with shaking (200 rpm). Plasmids were isolated using GeneJet Plasmid Miniprep Kit (ThermoFisher).

Plasmids with correct inserts were transformed into competent *E. coli* SM10 by heat shock with a recovery period of 2-3 h in LB. The cells were plated on LB 1.5% agar containing 10 µg/mL gentamicin and grown overnight at 37°C. One colony was picked and inoculated in LB + 10 µg/mL gentamicin. The *P. aeruginosa* mutant of interest was also inoculated from a single colony in LB. Both cultures were grown overnight at 37°C with shaking (200 rpm). SM10 with the desired deletion construct was mated with PA14 by mixing equal volumes of each overnight culture in a

1.5mL centrifuge tube. Cells were spun down and the supernatant was removed. Cells were resuspended in 50 µL fresh LB, spotted on LB 1.5% agar, and incubated overnight at 37°C. Cells from the mating spot were streaked onto *Pseudomonas* Isolation Agar (PIA, Difco) supplemented with 100 µg/mL gentamicin and incubated overnight at 37°C. Single colonies were streaked onto LB (no salt) + 15% sucrose (BioShop) and incubated overnight at 37°C. To check for colonies with the correct deletion, 16 colonies were patched onto LB + 15% sucrose and LB + 30 µg/mL gentamicin and incubated overnight at 37°C. Patches that grew on the sucrose plates but not gentamicin plates were checked by colony PCR with primers flanking the deleted gene and internal primers and compared to WT controls. Patches with the desired deletions were streaked onto LB + 15% sucrose to isolate single colonies, incubated overnight at 37°C and checked again by colony PCR. A single colony was inoculated into LB broth and the process was repeated to generate double, triple, and quadruple mutants.

Complemented strains were made using the plasmid pHERD20T, an arabinose-inducible expression vector with the P_{BAD} promoter under control of AraC (Qiu et al., 2008). Primers flanking the gene of interest including the native ribosome binding site were amplified from *P. aeruginosa* PA14 genomic DNA, digested with the desired restriction enzymes, and ligated into pHERD20T digested with the same enzymes. Ligation mixtures were added to chemically competent DH5α, and DNA introduced by heat shock with a recovery period of 1-2 h in LB at 37°C. All the cells were plated on LB 1.5% agar supplemented 100 µg/mL ampicillin, X-gal, and 0.1% arabinose and incubated at 37°C overnight. White colonies were analyzed by colony PCR and colonies with plasmids containing the desired insert size were cultured in LB broth supplemented with 100 µg/mL ampicillin. Plasmids were isolated, inserts validated by restriction digest, and electroporated into the desired *P. aeruginosa* strain or mutant with a recovery of 1-2 h

in LB at 37°C. All the cells were plated on LB 1.5% agar supplemented with 200 µg/mL carbenicillin (AK Scientific). A single colony was picked and grown in LB supplemented with 200 µg/mL carbenicillin overnight at 37°C and used to make glycerol stocks and for subsequent assays. Correct inserts were verified by Sanger sequencing by the McMaster Genomics Facility Mobix Lab.

MIC assays

MIC assays were conducted as previously described (Chan and Burrows, 2021; Ranieri et al., 2019). Overnight cultures were grown in LB from a glycerol stock at 37°C with shaking (200 rpm). Subcultures in 10:90 (1:100 dilution) were cultured for 4 h. Cells were adjusted to an OD_{600} of 0.1/500 in 10:90. All compounds were serially diluted 2-fold in DMSO or H_2O at 75x the final concentration. Plates were sealed to prevent evaporation and incubated at 37°C overnight in a shaking incubator (200 rpm). The next day, the OD_{600} was determined with a plate reader (Thermo Scientific) and normalized to percent of growth of the vehicle control after subtracting the OD_{600} from blank media.

Checkerboard assays

Checkerboards (8 rows x 8 columns) were conducted as previously described in a 96-well plate (Nunc) (Chan and Burrows, 2021; Ranieri et al., 2019). TS at 75x the final concentration dissolved in DMSO was added in columns from bottom to top in increasing concentrations. Siderophores at 75x the final concentration dissolved in DSMO were added from in rows from left to right in increasing concentrations. Four columns were used for vehicle controls (DMSO) and sterile controls. Media with bacteria as described in the MIC assays were added to obtain a final

volume of 150 µL. Plates were sealed to prevent evaporation and incubated at 37°C overnight in a shaking incubator (200 rpm). The next day, the OD_{600} was determined with a plate reader (Thermo Scientific) and normalized to percent of growth of the vehicle control (DMSO) after subtracting the OD_{600} from blank media.

Microscopy, fluorescence quenching, and recovery assay

Cells were cultured overnight in LB with carbenicillin (200 µg/mL) at 37°C with shaking at 200 rpm. Cells were subcultured (1:200 dilution) in 10:90 + 2% arabinose for four hours without carbenicillin at 37°C with shaking at 200 rpm. Cells were harvested by centrifugation for 5 min and 6000 G and resuspended in sterile 1X PBS with 10 µM AlexaFluor594 C_5-maleimide for microscopy or fluorescein-5-maleimide for fluorescence quenching and recovery assays and incubated in the dark at room temperature for 30 min on a shaking incubator at 37°C (200 rpm). Excess dye was quenched with 1 mM dithiothreitol (DTT) (Sigma) to stop the reaction. Cells were washed 3X with PBS. For fluorescence recovery assays, cells were incubated with 1X PBS + 0.4% glucose at 37°C with shaking at 200 rpm. Glucose was prepared as a 20% stock (wt/v) in 1X PBS and filter sterilized. Cells were spun down and washed 3X with 1X PBS and resuspended in 1X PBS for quenching assays and 1X PBS + 0.4% glucose for fluorescence recovery assays.

For microscopy, AlexaFluor594 C_5-maleimide-labeled cells were spotted onto a 1% agarose pad on a microscope slide. The agarose pad was mounted with a glass coverslip directly prior to imaging. Cells were imaged using brightfield and fluorescence microscopy on a Nikon A1 confocal microscope through a Plan Apo 60X (NA=1.40) oil objective. Image acquisition was done using Nikon NIS Elements Advanced Research (Version 5.11.01 64- bit) software.

For fluorescence quenching and recovery assays, cells were diluted to an OD_{600} of 0.1 for both types of assays and 148 µL was added into wells of a 96-well black plate (Corning). Fluorescence was recorded for 5 mins at 1 min intervals at 37°C (BioTek Neo; Ex. 494nm; Em. 520nm). After 5 min, 2 µL of each serial dilution for ferrioxamine-Fe^{3+}, ferrichrome-Fe^{3+}, and pyoverdine-Fe^{3+} or DMSO for vehicle controls was added to each well. Fluorescence was recorded immediately for quenching assays and for 1 h at 1 min interval for fluorescence recovery assays. Background fluorescence was subtracted from all fluorescence readings and $1\text{-}F/F_0$ was used to calculate the degree of quenching where F_0 is the initial fluorescence. K_d was calculated using GraphPad Prism using a one-site specific binding model or a two-site model. For fluorescence recovery assays, background was subtracted from all fluorescence readings and F/F_0 expressed as a percent of control was plotted versus time.

Outer-membrane preparations, SDS PAGE, and Western Blots

The quadruple mutant expressing mutant FpvB transporters was grown overnight in LB with 200µg/mL carbenicillin at 37°C with shaking (200rpm). Cells were subcultured 1:100 into 10:90 for four h then diluted to OD_{600} 0.1/500 in 50mL of fresh 10:90 + 2% arabinose. Cultures were grown overnight at 37°C with shaking (200 rpm). Cells were harvested by centrifugation (5 min, 6000 G) and resuspended in 10 mM Tris pH 8.0.

Cells were lysed by sonication (Misonix Sonicator 3000) on ice (30s pulse, power level 5.0). Cell debris was removed by centrifugation (6000 G, 5 min, 4°C). Proteins were harvested at 21000 G for 30 min at 4°C. The pellet was resuspended in 100 µL de-ionized H_2O and combined with 900 µL 11.1 mM Tris, 1% sarkosyl (Fisher Scientific), pH 7.6 and incubated at room

temperature for 30 min with shaking (200 rpm). Outer membrane pellets were collected by centrifugation at 21000 G for 30 min at 4°C.

Outer membrane preparations were resuspended in 20 µL 1X loading buffer for SDS-PAGE analysis. SDS-PAGE buffer was made from a 10X tris-glycine buffer stock (30.3 g tris, 144 g glycine, and 20 mL 10% SDS). Each lane was loaded with 10 µL of outer membrane prep and proteins separated at 80V for 10 min and 120V for 1.5 h. Proteins were transferred to nitrocellulose membranes (225mA, 1 h, in transfer buffer (20% methanol, 100 mL of a 10X tris-glycine buffer stock without SDS) and blocked with 5% skim milk in PBS overnight at 4°C. Primary antibodies (mouse α-DYKDDDDK (Invitrogen MA1-91878), and rabbit #3198 α-PilF)) were used at 1:1000 dilutions in PBS and incubated with the blot at room temperature for 1 h. Blots were washed 3x 10 min with PBS and incubated with rabbit α-mouse-alkaline phosphatase for 2 h in PBS at 1:2000 dilutions in PBS. Blots were washed with PBS 3x (10 mins per wash) before incubation with alkaline phosphatase buffer (1 mM Tris, 100 mM NaCl, 5 mM $MgCl_2$ pH 9.5) + 5-bromo-4-chloro-3-indoyl phosphate (BCIP) + nitro-blue tetrazolium (NBT) for 15-30 min. Blots were developed in the dark and imaged on an Azure C400 Imaging System. Band densities were quantified using ImageJ (Schneider et al., 2012).

Mutants resistant to TS

PA14 was cultured in 10:90 supplemented with 17 µg/mL TS + 64 µg/mL DSX at 37°C with shaking at 200 rpm (Ranieri et al., 2019). Cells were passaged when turbidity was evident (1:500 dilution) into fresh media with the same concentrations of TS + DSX. This procedure was repeated for 3 weeks until cells grew overnight with TS + DSX. The cells were streaked on to LB deferrated with FEC-1, to remove iron, overnight at 37°C and supplemented with TS + DSX. FEC-

1 was supplied by Chelation Partners Inc. (Fe Pharmaceuticals) (Parquet et al., 2018). Isolates were picked, cultured in LB, and chromosomal DNA was isolated and whole genome sequencing performed by the McMaster Genomics Facility Mobix Lab. Breseq was used to identify mutations associated with TS+DSX resistance (Deatherage and Barrick, 2014).

Structural Comparisons and Docking

Structural models of FpvB were generated using AlphaFold2 (ColabFold) and compared to the crystal structure of FpvA (PDB: 2O5P) (Jumper et al., 2021; Mirdita et al., 2022). Structural comparisons of FpvB and FpvA were visualized using Chimera (Pettersen et al., 2004). Ferrichrome (PDB: 1BY5) and ferrioxamine B (PDB:6I96) were docking into the AlphaFold2 model of FpvB using AutoDock VINA (Trott and Olson, 2010) with a box size of center_x = -7.729, center_y = 34.958, center_z = 113.797, size_x = 114, size_y = 116, size_z = 118. The top pose generated was used for further studies.

Acknowledgements

We thank Dr. David Sychantha for his valuable comments on the quenching curve of ferrioxamine B. This work was supported by a Natural Sciences and Engineering Research Council Discovery Grant RGPIN-2021-04237 to LLB. LLB holds a Tier 1 Canada Research Chair in Microbe-Surface Interactions. DCKC holds a Canadian Institute of Health Research (CIHR) Canada Graduate Scholarship – Doctoral program (CGS-D).

References

1. Stefánsson A. 2007. Iron(III) hydrolysis and solubility at 25°C. Environ Sci Technol 41:6117–6123.
2. Klebba PE, Newton SMC, Six DA, Kumar A, Yang T, Nairn BL, Munger C, Chakravorty S. 2021. Iron Acquisition Systems of Gram-negative Bacterial Pathogens Define TonB-Dependent Pathways to Novel Antibiotics. *Chem Rev* 121:5193–5239.
3. Noinaj N, Guillier M, Barnard TJ, Buchanan SK. 2010. TonB-dependent transporters: Regulation, structure, and function. *Annu Rev Microbiol.*
4. Moynié L, Milenkovic S, Mislin GLA, Gasser V, Malloci G, Baco E, McCaughan RP, Page MGP, Schalk IJ, Ceccarelli M, Naismith JH. 2019. The complex of ferric-enterobactin with its transporter from *Pseudomonas aeruginosa* suggests a two-site model. *Nat Commun* 2019 101 10:1–14.
5. Josts I, Veith K, Tidow H. 2019. Ternary structure of the outer membrane transporter FoxA with resolved signaling domain provides insights into TonB-mediated siderophore uptake. *Elife* 8.
6. Luna B, Trebosc V, Lee B, Bakowski M, Ulhaq A, Yan J, Lu P, Cheng J, Nielsen T, Lim J, Ketphan W, Eoh H, McNamara C, Skandalis N, She R, Kemmer C, Lociuro S, Dale GE, Spellberg B. 2020. A nutrient-limited screen unmasks rifabutin hyperactivity for extensively drug-resistant *Acinetobacter baumannii. Nat Microbiol* 2020 59 5:1134–1143.
7. White P, Joshi A, Rassam P, Housden NG, Kaminska R, Goult JD, Redfield C, McCaughey LC, Walker D, Mohammed S, Kleanthous C. 2017. Exploitation of an iron transporter for bacterial protein antibiotic import. *Proc Natl Acad Sci USA* 114:12051–12056.
8. Luscher A, Moynie L, Auguste P Saint, Bumann D, Mazza L, Pletzer D, Naismith JH, Köhlera T. 2018. TonB-dependent receptor repertoire of *Pseudomonas aeruginosa* for uptake of siderophore-drug conjugates. *Antimicrob Agents Chemother* 62.
9. Rabsch W, Ma L, Wiley G, Najar FZ, Kaserer W, Schuerch DW, Klebba JE, Roe BA, Laverde Gomez JA, Schallmey M, Newton SMC, Klebba PE. 2007. FepA- and TonB-Dependent Bacteriophage H8: Receptor Binding and Genomic Sequence. *J Bacteriol* 189:5658.
10. Salomon RA, Farias RN. 1993. The FhuA protein is involved in microcin 25 uptake. *J Bacteriol* 175:7741–7742.
11. Ferguson AD, Coulton JW, Diederichs K, Welte W, Braun V, Fiedler H-P. 2000. Crystal structure of the antibiotic albomycin in complex with the outer membrane transporter FhuA. *Protein Sci* 9:956–963.
12. Mathavan I, Zirah S, Mehmood S, Choudhury HG, Goulard C, Li Y, Robinson C V., Rebuffat S, Beis K. 2014. Structural basis for hijacking siderophore receptors by antimicrobial lasso peptides. *Nat Chem Biol* 2014 105 10:340–342.
13. Ranieri MRM, Chan DCK, Yaeger LN, Rudolph M, Karabelas-Pittman S, Abdo H, Chee J, Harvey H, Nguyen U, Burrows LL. 2019. Thiostrepton Hijacks Pyoverdine Receptors to Inhibit Growth of *Pseudomonas aeruginosa. Antimicrob Agents Chemother* 63.
14. Chan DCK, Burrows LL. 2021. Thiocillin and micrococcin exploit the ferrioxamine receptor of *Pseudomonas aeruginosa* for uptake. *J Antimicrob Chemother* 76:2029–2039.
15. Hancock REW, Brinkman FSL. 2002. Function of *Pseudomonas* porins in uptake and efflux. *Annu Rev Microbiol*.
16. Ochsner UA, Johnson Z, Vasil ML. 2000. Genetics and regulation of two distinct haem-uptake systems, phu and has, in *Pseudomonas aeruginosa*. *Microbiology* 146:185–198.
17. Llamas MA, Sparrius M, Kloet R, Jiménez CR, Vandenbroucke-Grauls C, Bitter W. 2006.

The Heterologous Siderophores Ferrioxamine B and Ferrichrome Activate Signaling Pathways in *Pseudomonas aeruginosa. J Bacteriol* 188:1882.
18. Ghysels B, Dieu BTM, Beatson SA, Pirnay JP, Ochsner UA, Vasil ML, Cornelis P. 2004. FpvB, an alternative type I ferripyoverdine receptor of *Pseudomonas aeruginosa. Microbiology* 150:1671–1680.
19. Sokol PA. 1987. Tn5 insertion mutants of *Pseudomonas aeruginosa* deficient in surface expression of ferripyochelin-binding protein. *J Bacteriol* 169:3365–3368.
20. Cobessi D, Celia H, Folschweiller N, Schalk IJ, Abdallah MA, Pattus F. 2005. The crystal structure of the pyoverdine outer membrane receptor FpvA from *Pseudomonas aeruginosa* at 3.6 angstroms resolution. *J Mol Biol* 347:121–134.
21. Meyer J-M, Geoffroy VA, Baysse C, Cornelis P, Barelmann I, Taraz K, Budzikiewicz H. 2002. Siderophore-mediated iron uptake in fluorescent *Pseudomonas*: characterization of the pyoverdine-receptor binding site of three cross-reacting pyoverdines. *Arch Biochem Biophys* 397:179–83.
22. Heinrichs DE, Young L, Poole K. 1991. Pyochelin-mediated iron transport in *Pseudomonas aeruginosa*: involvement of a high-molecular-mass outer membrane protein. *Infect Immun* 59:3680–3684.
23. Albrecht-Gary AM, Blanc S, Rochel N, Ocaktan AZ, Abdallah MA. 1994. Bacterial Iron Transport: Coordination Properties of Pyoverdin PaA, a Peptidic Siderophore of *Pseudomonas aeruginosa. Inorg Chem* 33:6391–6402.
24. Braud A, Hannauer M, Mislin GLA, Schalk IJ. 2009. The *Pseudomonas aeruginosa* pyochelin-iron uptake pathway and its metal specificity. *J Bacteriol* 191:3517–3525.
25. Lamont IL, Beare PA, Ochsner U, Vasil AI, Vasil ML. 2002. Siderophore-mediated signaling regulates virulence factor production in *Pseudomonas aeruginosa. Proc Natl Acad Sci USA* 99:7072–7077.
26. Brandel J, Humbert N, Elhabiri M, Schalk IJ, Mislin GLA, Albrecht-Gary AM. 2012. Pyochelin, a siderophore of *Pseudomonas aeruginosa*: Physicochemical characterization of the iron(III), copper(II) and zinc(II) complexes. *Dalt Trans* 41:2820–2834.
27. Normant V, Josts I, Kuhn L, Perraud Q, Fritsch S, Hammann P, Mislin GLA, Tidow H, Schalk IJ. 2020. Nocardamine-Dependent Iron Uptake in *Pseudomonas aeruginosa*: Exclusive Involvement of the FoxA Outer Membrane Transporter. *ACS Chem Biol* 15:2741–2751.
28. Chan DCK, Guo I, Burrows LL. 2020. Forging new antibiotic combinations under iron-limiting conditions. *Antimicrob Agents Chemother* 64.
29. Koo J, Tammam S, Ku SY, Sampaleanu LM, Burrows LL, Howell PL. 2008. PilF is an outer membrane lipoprotein required for multimerization and localization of the *Pseudomonas aeruginosa* type IV pilus secretin. *J Bacteriol* 190:6961–6969.
30. Qiu D, Damron FH, Mima T, Schweizer HP, Yu HD. 2008. PBAD-Based Shuttle Vectors for Functional Analysis of Toxic and Highly Regulated Genes in *Pseudomonas* and *Burkholderia* spp. and Other Bacteria. *Appl Environ Microbiol* 74:7422.
31. Chakravorty S, Shipelskiy Y, Kumar A, Majumdar A, Yang T, Nairn BL, Newton SM, Klebba PE. 2019. Universal fluorescent sensors of high-affinity iron transport, applied to ESKAPE pathogens. *J Biol Chem* 294:4682–4692.
32. Kumar A, Yang T, Chakravorty S, Majumdar A, Nairn BL, Six DA, dos Santos NM, Price SL, Lawrenz MB, Actis LA, Marques M, Russo TA, Newton SM, Klebba PE. 2022. Fluorescent sensors of siderophores produced by bacterial pathogens. *J Biol Chem* 298:101651.
33. Jumper J, Evans R, Pritzel A, Green T, Figurnov M, Ronneberger O, Tunyasuvunakool K,

Bates R, Žídek A, Potapenko A, Bridgland A, Meyer C, Kohl SAA, Ballard AJ, Cowie A, Romera-Paredes B, Nikolov S, Jain R, Adler J, Back T, Petersen S, Reiman D, Clancy E, Zielinski M, Steinegger M, Pacholska M, Berghammer T, Bodenstein S, Silver D, Vinyals O, Senior AW, Kavukcuoglu K, Kohli P, Hassabis D. 2021. Highly accurate protein structure prediction with AlphaFold. *Nat* 2021 5967873 596:583–589.

34. Mirdita M, Schütze K, Moriwaki Y, Heo L, Ovchinnikov S, Steinegger M. 2022. ColabFold: making protein folding accessible to all. *Nat Methods* 2022 196 19:679–682.

35. Greenwald J, Nader M, Celia H, Gruffaz C, Geoffroy V, Meyer JM, Schalk IJ, Pattus F. 2009. FpvA bound to non-cognate pyoverdines: molecular basis of siderophore recognition by an iron transporter. *Mol Microbiol* 72:1246–1259.

36. Trott O, Olson AJ. 2010. AutoDock Vina: improving the speed and accuracy of docking with a new scoring function, efficient optimization and multithreading. *J Comput Chem* 31:455.

37. Shen J, Meldrum A, Poole K. 2002. FpvA receptor involvement in pyoverdine biosynthesis in *Pseudomonas aeruginosa. J Bacteriol* 184:3268–3275.

38. Meyer J-M, Stintzi A, Poole K. 1999. The ferripyoverdine receptor FpvA of *Pseudomonas aeruginosa* PAO1 recognizes the ferripyoverdines of *P. aeruginosa* PAO1 and *P. fluorescens* ATCC 13525. *FEMS Microbiol Lett* 170:145–150.

39. Cuív PÓ, Clarke P, O'Connell M. 2006. Identification and characterization of an iron-regulated gene, chtA, required for the utilization of the xenosiderophores aerobactin, rhizobactin 1021 and schizokinen by *Pseudomonas aeruginosa. Microbiology* 152:945–954.

40. Southwell JW, Black CM, Duhme-Klair AK. 2021. Experimental Methods for Evaluating the Bacterial Uptake of Trojan Horse Antibacterials. *ChemMedChem* 16:1063–1076.

41. Ferguson AD, Ködding J, Walker G, Bös C, Coulton JW, Diederichs K, Braun V, Welte W. 2001. Active transport of an antibiotic rifamycin derivative by the outer-membrane protein FhuA. *Structure* 9:707–716.

42. Bodilis J, Ghysels B, Osayande J, Matthijs S, Pirnay JP, Denayer S, De Vos D, Cornelis P. 2009. Distribution and evolution of ferripyoverdine receptors in *Pseudomonas aeruginosa. Environ Microbiol* 11:2123–2135.

43. Dingemans J, Ye L, Hildebrand F, Tontodonati F, Craggs M, Bilocq F, De Vos D, Crabbé A, Van Houdt R, Malfroot A, Cornelis P. 2014. The deletion of TonB-dependent receptor genes is part of the genome reduction process that occurs during adaptation of *Pseudomonas aeruginosa* to the cystic fibrosis lung. *Pathog Dis* 71:26–38.

44. González J, Salvador M, Özkaya Ö, Spick M, Reid K, Costa C, Bailey MJ, Avignone Rossa C, Kümmerli R, Jiménez JI. 2021. Loss of a pyoverdine secondary receptor in *Pseudomonas aeruginosa* results in a fitter strain suitable for population invasion. *ISME J* 15:1330–1343.

45. Grinter R, Lithgow T. 2019. Determination of the molecular basis for coprogen import by Gram-negative bacteria. *IUCrJ* 6:401–411.

46. Locher KP, Rees B, Koebnik R, Mitschler A, Moulinier L, Rosenbusch JP, Moras D. 1998. Transmembrane Signaling across the Ligand-Gated FhuA Receptor: Crystal Structures of Free and Ferrichrome-Bound States Reveal Allosteric Changes. *Cell* 95:771–778.

47. Hoang TT, Karkhoff-Schweizer RR, Kutchma AJ, Schweizer HP. 1998. A broad-host-range Flp-FRT recombination system for site-specific excision of chromosomally-located DNA sequences: application for isolation of unmarked *Pseudomonas aeruginosa* mutants. *Gene* 212:77–86.

48. Schneider CA, Rasband WS, Eliceiri KW. 2012. NIH Image to ImageJ: 25 years of image analysis. *Nat Methods* 2012 97 9:671–675.

49. Parquet M del C, Savage KA, Allan DS, Davidson RJ, Holbein BE. 2018. Novel iron-chelator DIBI inhibits *Staphylococcus aureus* growth, suppresses experimental MRSA infection in mice and enhances the activities of diverse antibiotics in vitro. *Front Microbiol* 9.
50. Deatherage DE, Barrick JE. 2014. Identification of mutations in laboratory-evolved microbes from next-generation sequencing data using breseq. *Methods Mol Biol* 1151:165–188.
51. Pettersen EF, Goddard TD, Huang CC, Couch GS, Greenblatt DM, Meng EC, Ferrin TE. 2004. UCSF Chimera--a visualization system for exploratory research and analysis. *J Comput Chem* 25:1605–1612.

Supplementary Figures

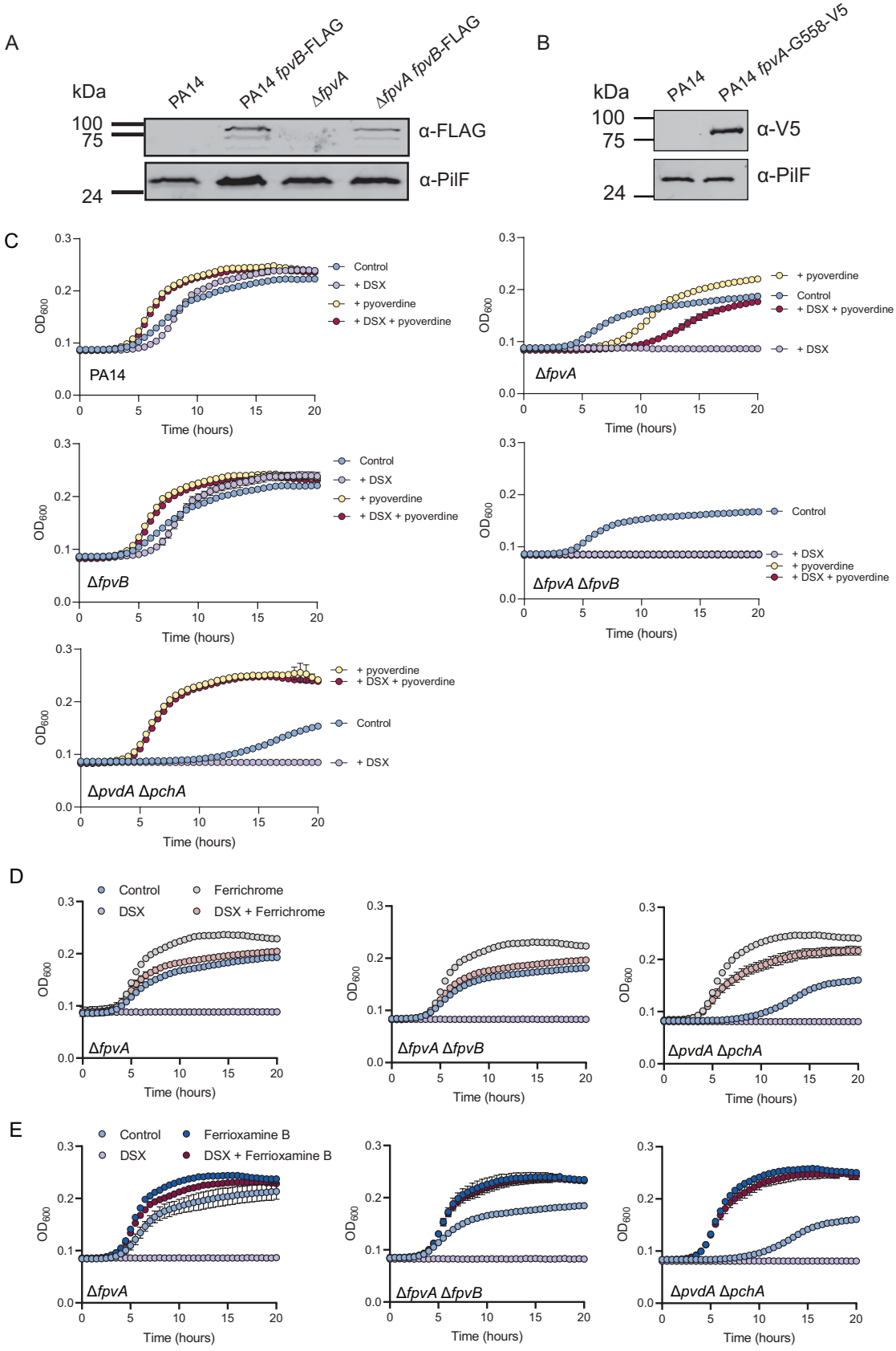

Supplementary Figure 1. **A)** FpvB is expressed in WT PA14 and the Δ*fpvA* mutant grown in 10:90. PilF was used as a loading control for outer membrane proteins. **B)** FpvA is expressed from WT PA14 grown in 10:90. No band was seen for untagged FpvA in WT PA14. PilF was used as a loading control for outer membrane proteins. **C)** Growth curves of PA14 and mutants with DSX and different siderophores in 10:90. PA14, Δ*fpvA,* Δ*fpvB,* Δ*fpvA* Δ*fpvB,* and Δ*pvdA* Δ*pchA* growth. Blue indicates control, purple indicates treatment with 64 µg/mL DSX, yellow indicates treatment with 10 µg/mL pyoverdine (PA14) and red indicates treatment with 64 µg/mL DSX and 10 µg/mL pyoverdine (PA14). **D)** Δ*fpvA,* Δ*fpvA* Δ*fpvB,* and Δ*pvdA* Δ*pchA* growth. Blue indicates control, purple indicates treatment with 64 µg/mL DSX, grey indicates treatment with 10 µg/mL ferrichrome, and red indicates treatment with 64 µg/mL DSX and 10 µg/mL ferrichrome. **E)** Δ*fpvA,* Δ*fpvA* Δ*fpvB,* and Δ*pvdA* Δ*pchA* growth. Blue indicates control, purple indicates treatment with 64 µg/mL DSX, grey indicates treatment with 10 µg/mL ferrioxamine B, and red indicates treatment with 64 µg/mL DSX and 10 µg/mL ferrioxamine B. Results are averaged from three independent biological replicates.

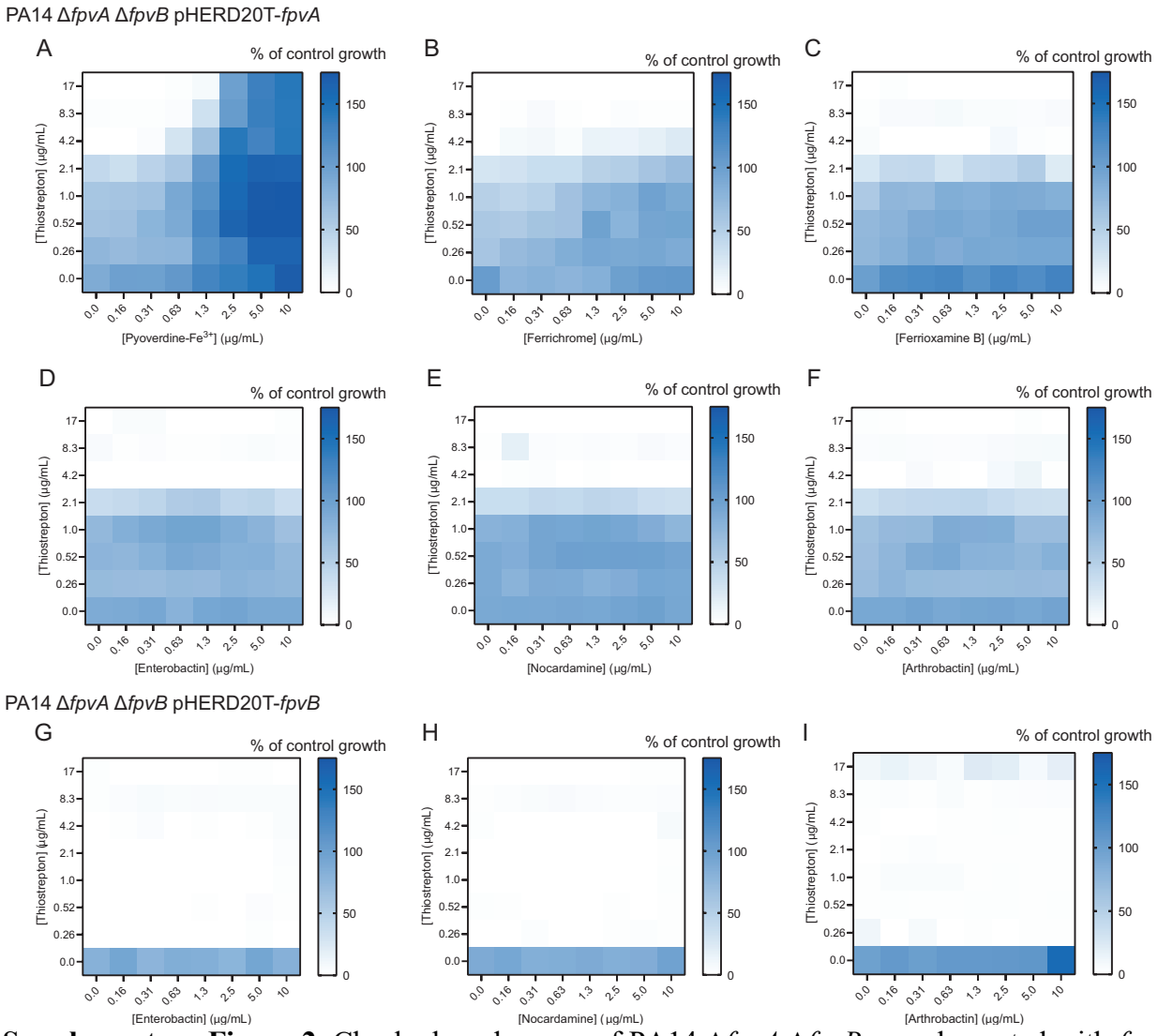

Supplementary Figure 2. Checkerboard assays of PA14 Δ*fpvA* Δ*fpvB* complemented with *fpvA* and *fpvB in trans* with TS and siderophores. Checkerboards of PA14 Δ*fpvA* Δ*fpvB* pHERD20T-

fpvA with TS and **(A)** pyoverdine-Fe^{3+}, **(B)** ferrichrome, **(C)** ferrioxamine B, **(D)** enterobactin, **(E)** ferrioxamine E, and **(F)** arthrobactin. Checkerboards of PA14 Δ*fpvA* Δ*fpvB* pHERD20T-*fpvB* with TS and **(G)** enterobactin, **(H)** ferrioxamine E, and **(I)** arthrobactin. Results are averaged from three independent biological replicates. Cells in the assay were grown in 10:90 + 2% arabinose.

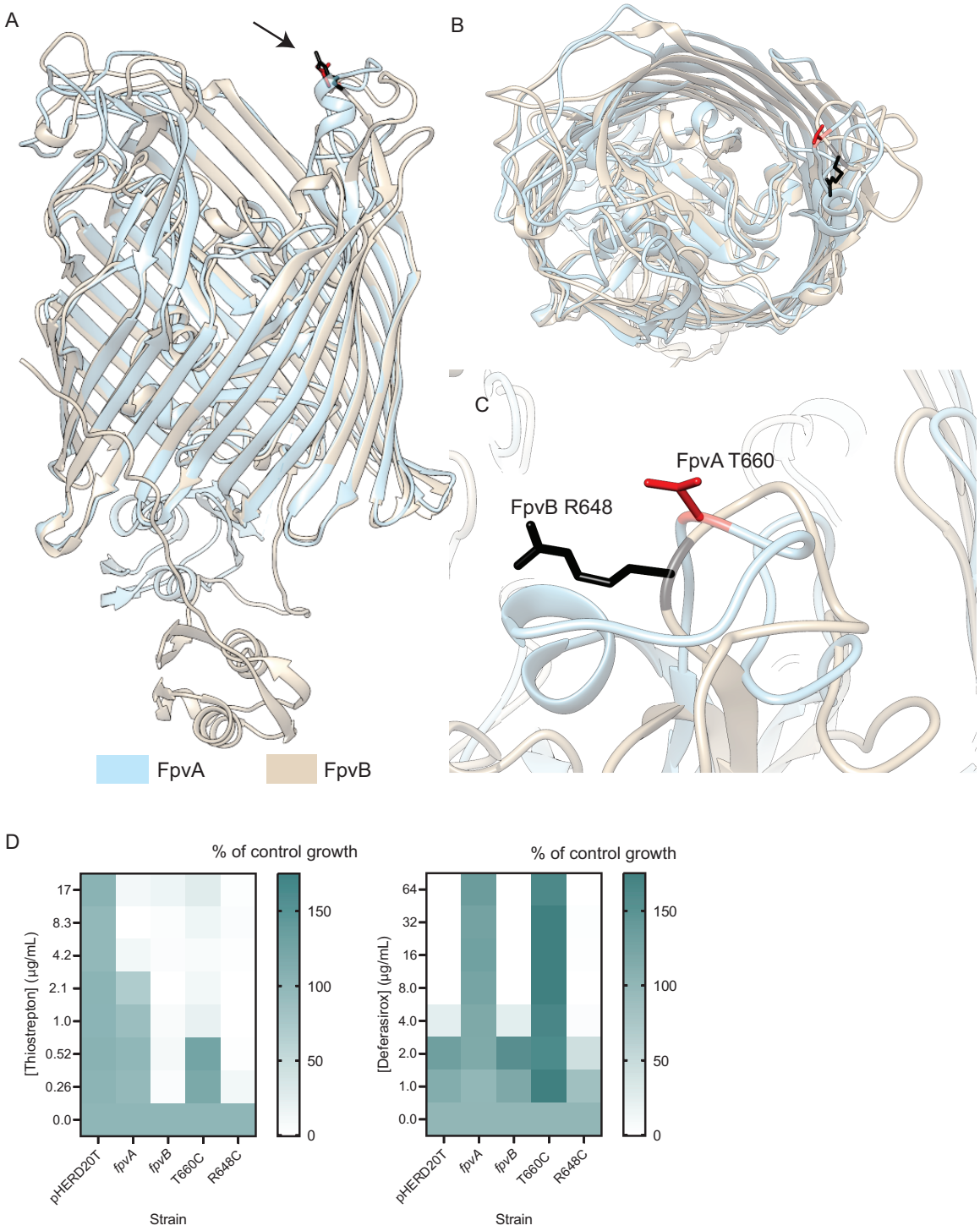

Supplementary Figure 3. Overlay of FpvA and FpvB showing residues mutated to cysteine for labeling with maleimide dyes. FpvA (PDB: 2O5P) was superimposed with the AlphaFold2 model

of FpvB. FpvA is shown in beige and FpvB in blue. **A)** Side view, **B)** top view, and **C)** zoomed in view of the labeled extracellular loop 8. **D)** FpvB R648C growth with TS or DSX is similar to WT. FpvA T660C increases susceptibility to TS by 4-fold and restores growth with DSX. Results are averaged from three independent biological replicates. Assays were conducted in 10:90 +2% arabinose.

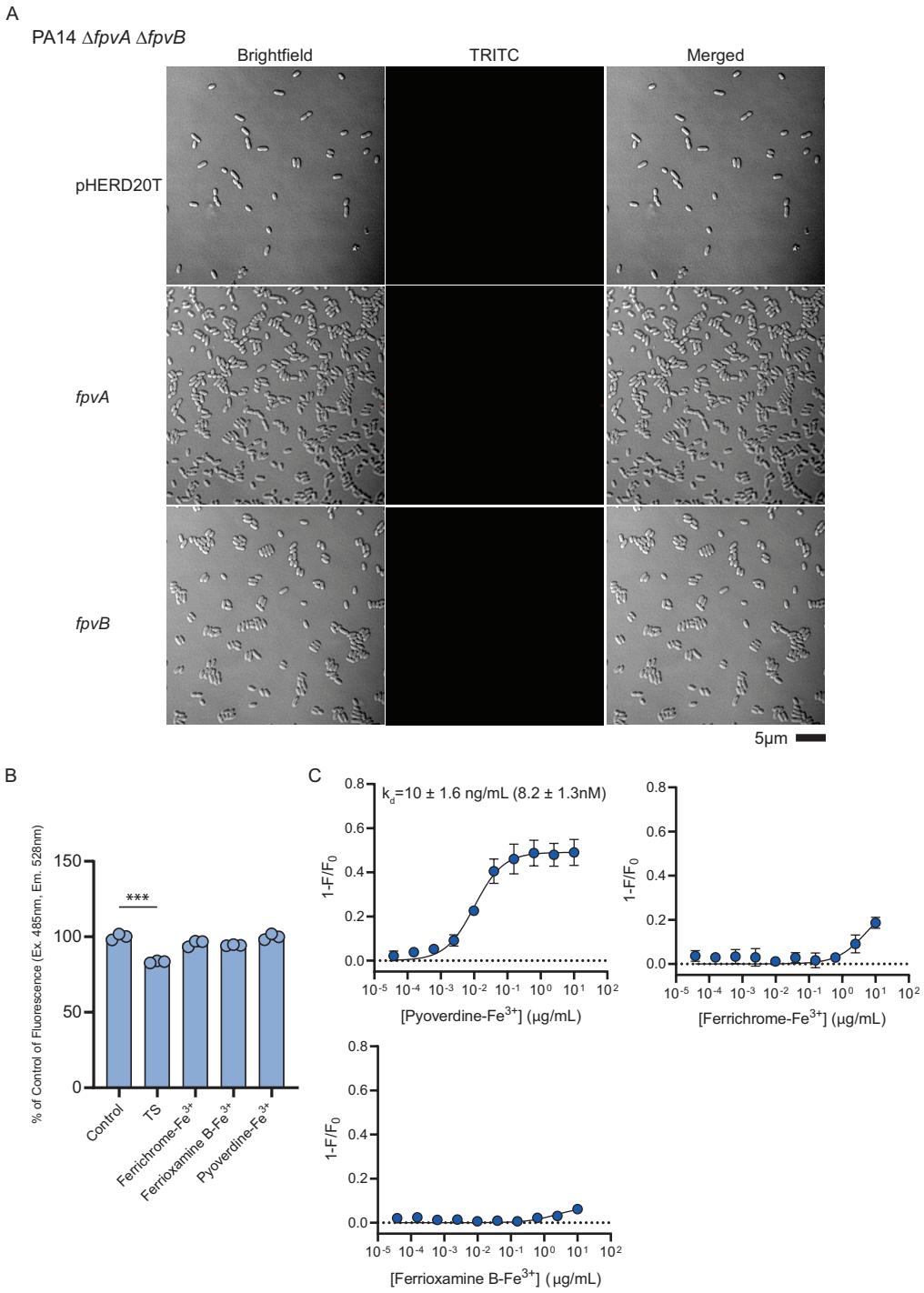

Supplementary Figure 4. A) Microscopy images of PA14 Δ*fpvA* Δ*fpvB* with pHERD20T, pHERD20T-*fpvA*, and pHERD20T-*fpvB* treated with AlexaFluor 594. Representative images are

shown. Scale = 5µm. **B)** TS partly quenches fluorescence of fluorescein-5-maleimide in the absence of cells. Each compound at the highest concentration tested was added to 10µM of fluorescein-5-maleimide in PBS in triplicate. TS reduced fluorescence to about 80% of the control. Excitation: 485nm; emission 528nm). ***, $p<0.001$ (student's t-test). **C)** Pyoverdine-Fe^{3+}, ferrioxamine B-Fe^{3+} and ferrichrome-Fe^{3+} quenching curves with PA14 ΔfpvA ΔfpvB pHERD20T-fpvA T660C. Results are averaged from three independent biological replicates.

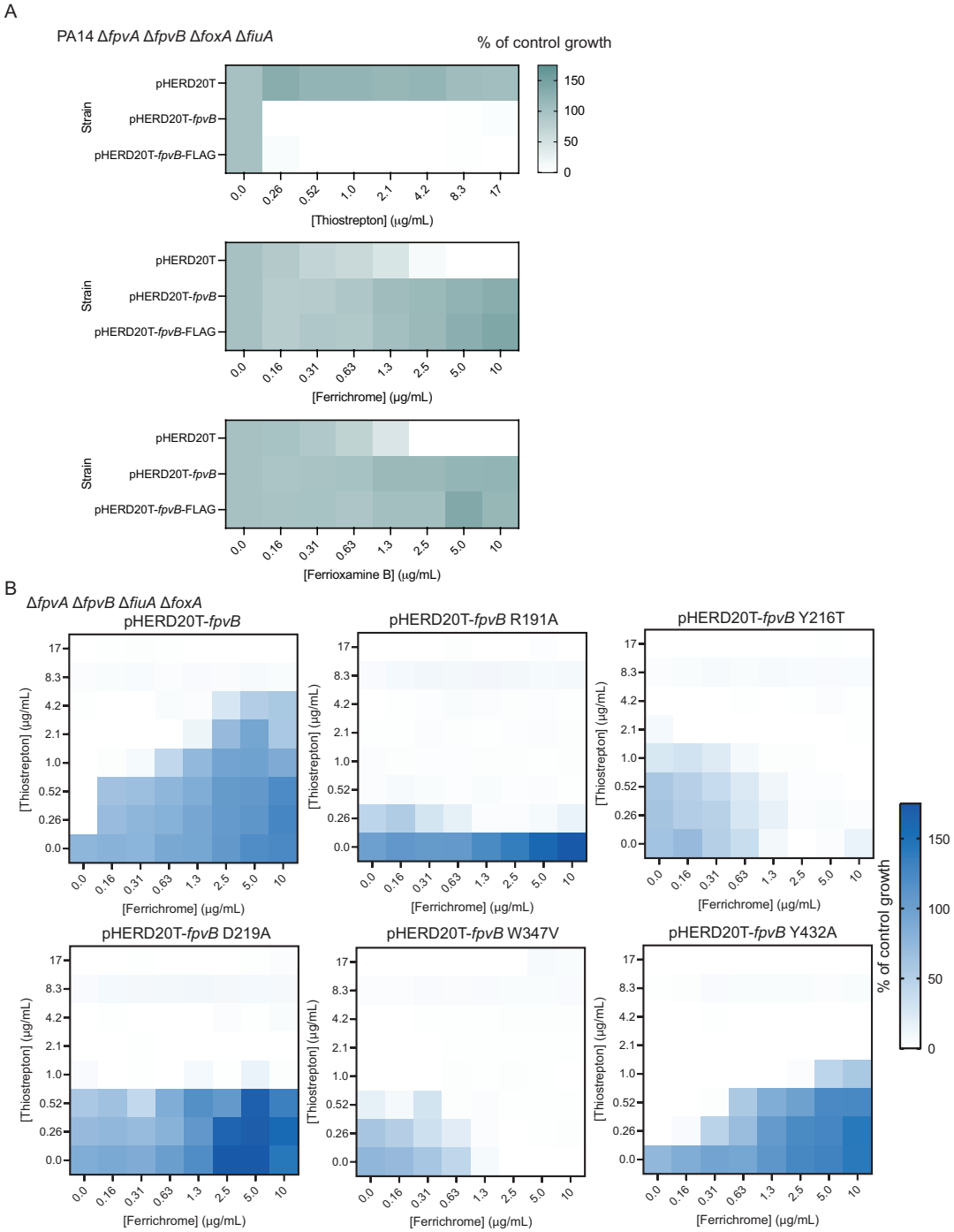

Supplementary Figure 5. **A)** PA14 Δ*fpvA* Δ*fpvB* Δ*fiuA* Δ*foxA* with empty vector (pHERD20T) and complemented with *fpvB* and *fpvB*-FLAG treated with TS, ferrichrome, and ferrioxamine B in

10:90 + 2% arabinose. Heat map depicts growth where green indicates growth and white indicates no growth. Results are averaged from three independent biological replicates. **B)** Checkerboard assays in the quadruple transporter mutant background between TS and ferrichrome. Growth is expressed as percent of control. Checkerboards were conducted in 10:90 + 2% arabinose. Results are averaged from three independent biological replicates.

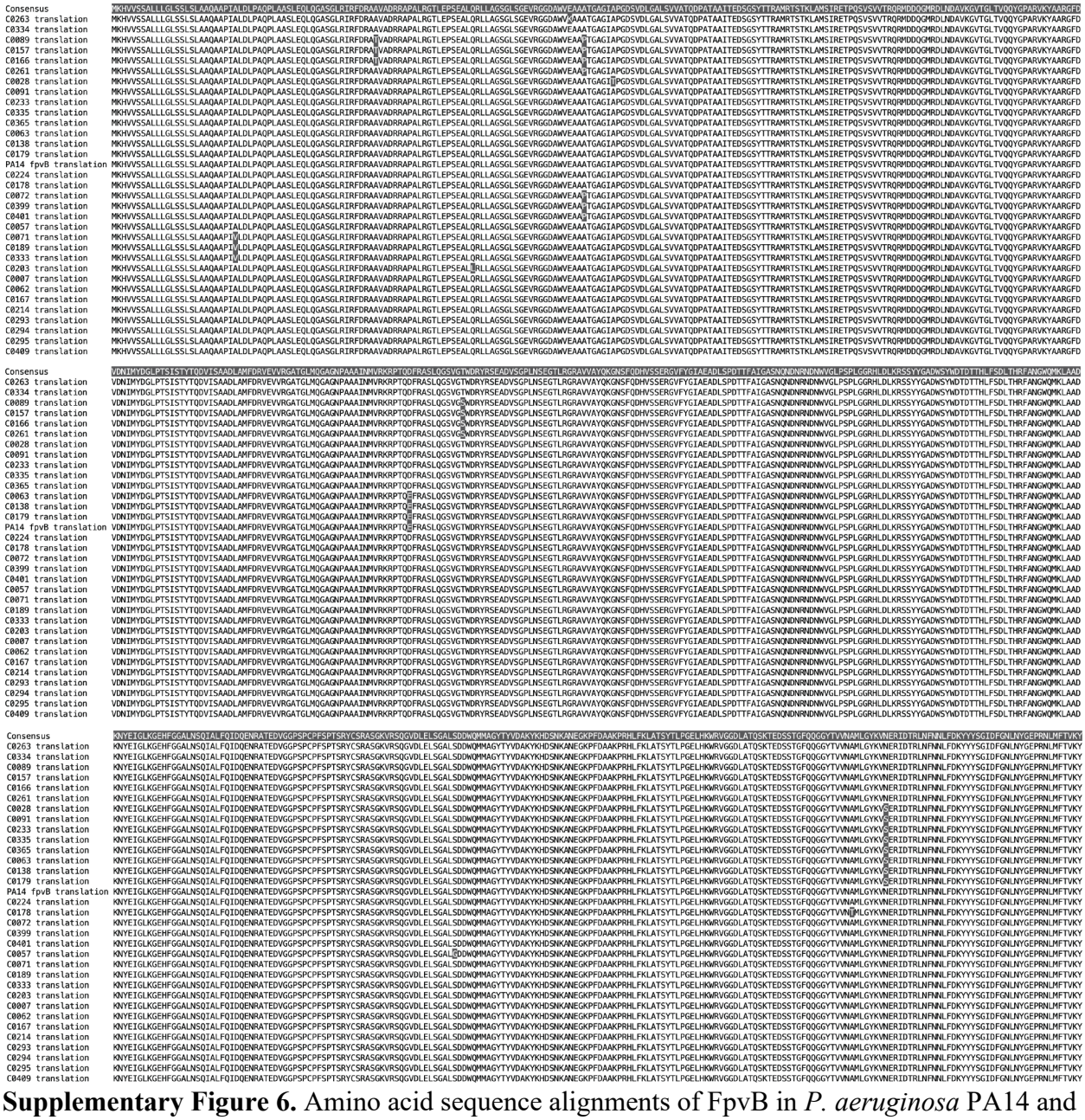

Supplementary Figure 6. Amino acid sequence alignments of FpvB in *P. aeruginosa* PA14 and 32 clinical isolates. Black indicates an identical amino acid position across all 33 sequences. White (grey background) indicates a different amino acid.

Supplementary Tables

Supplementary Table 1. Strains used in this study

Strain	Source
PA14	1
Δ*fpvA*	This study
Δ*fpvB*	This study
Δ*foxA*	This study
Δ*fiuA*	This study
Δ*fpvA*Δ*fpvB*	This study
Δ*pvdA*Δ*pchA*	This study
Δ*fpvA*Δ*fpvB* pHERD20T	This study
Δ*fpvA*Δ*fpvB* pHERD20T-*fpvA*	This study
Δ*fpvA*Δ*fpvB* pHERD20T-*fpvA* T660C	This study
Δ*fpvA*Δ*fpvB* pHERD20T-*fpvB*	This study
Δ*fpvA*Δ*fpvB* pHERD20T-*fpvB* R648C	This study
Δ*fpvA*Δ*foxA*	This study
Δ*fpvA*Δ*fiuA*	This study
Δ*fpvB*Δ*foxA*	This study
Δ*fpvB*Δ*fiuA*	This study
Δ*foxA*Δ*fiuA*	This study
Δ*fpvA*Δ*fpvB*Δ*foxA*	This study
Δ*fpvA*Δ*fpvB*Δ*fiuA*	This study
Δ*fpvA*Δ*foxA*Δ*fiuA*	This study
Δ*fpvB*Δ*foxA*Δ*fiuA*	This study
Δ*fpvA*Δ*fpvB*Δ*foxA*Δ*fiuA*	This study
Δ*fpvA*Δ*fpvB*Δ*foxA*Δ*fiuA* pHERD20T	This study
PA14 *fpvB*-FLAG (C-terminal chromosomal tag)	This study
PA14 Δ*fpvA fpvB*-FLAG (C-terminal chromosomal tag)	This study
Δ*fpvA*Δ*fpvB*Δ*foxA*Δ*fiuA* pHERD20T-*fpvA*	This study
Δ*fpvA*Δ*fpvB*Δ*foxA*Δ*fiuA* pHERD20T-*fpvB*	This study
Δ*fpvA*Δ*fpvB*Δ*foxA*Δ*fiuA* pHERD20T-*fiuA*	This study
Δ*fpvA*Δ*fpvB*Δ*foxA*Δ*fiuA* pHERD20T-*foxA*	This study
Δ*fpvA*Δ*fpvB*Δ*foxA*Δ*fiuA* pHERD20T-*fpvB* R191A	This study
Δ*fpvA*Δ*fpvB*Δ*foxA*Δ*fiuA* pHERD20T-*fpvB* Y216T	This study
Δ*fpvA*Δ*fpvB*Δ*foxA*Δ*fiuA* pHERD20T-*fpvB* D219A	This study
Δ*fpvA*Δ*fpvB*Δ*foxA*Δ*fiuA* pHERD20T-*fpvB* W347V	This study
Δ*fpvA*Δ*fpvB*Δ*foxA*Δ*fiuA* pHERD20T-*fpvB* Y412A	This study
Δ*fpvA*Δ*fpvB*Δ*foxA*Δ*fiuA* pHERD20T-*fpvB* Y432A	This study
Δ*fpvA*Δ*fpvB* pHERD20T-*fpvB* R191A R648C	This study
Δ*fpvA*Δ*fpvB* pHERD20T-*fpvB* W347V R648C	This study

Δ*fpvA*Δ*fpvB*Δ*foxA*Δ*fiuA* pHERD20T-*fpvB*-FLAG	This study
Δ*fpvA*Δ*fpvB*Δ*foxA*Δ*fiuA* pHERD20T-*fpvB*-FLAG R191A	This study
Δ*fpvA*Δ*fpvB*Δ*foxA*Δ*fiuA* pHERD20T-*fpvB*-FLAG Y216T	This study
Δ*fpvA*Δ*fpvB*Δ*foxA*Δ*fiuA* pHERD20T-*fpvB*-FLAG D219A	This study
Δ*fpvA*Δ*fpvB*Δ*foxA*Δ*fiuA* pHERD20T-*fpvB*-FLAG W347V	This study
Δ*fpvA*Δ*fpvB*Δ*foxA*Δ*fiuA* pHERD20T-*fpvB*-FLAG Y412A	This study
Δ*fpvA*Δ*fpvB*Δ*foxA*Δ*fiuA* pHERD20T-*fpvB*-FLAG Y432A	This study
SM10 pEX18Gm-Δ*fpvA*	This study
SM10 pEX18Gm-Δ*fpvB*	This study
SM10 pEX18Gm-Δ*fiuA*	This study
SM10 pEX18Gm-Δ*foxA*	This study
SM10 pEX18Gm-Δ*pvdA*	This study
SM10 pEX18Gm-Δ*pchA*	This study
SM10 pEX18Gm-*fpvB*-FLAG	This study

Supplementary Table 2. Primers used in this study

Deletion primers

Gene	Part		Sequence
fpvA	Upstream	Forward (5' -> 3')	CAATGAATTCTCAGCCGCGCCCAGGTCGCCTTCC
		Reverse (5' -> 3')	GGGCGTTCTTTTTCGCAGCCGGGCGGGTGATTGCT CTTCTTAGGTTGG
	Downstream	Forward (5' -> 3')	CCAACCTAAGAAGAGCAATCACCCGCCCGGCTGCG AAAAAGAACGCCC
		Reverse (5' -> 3')	CGTAAGCTTTTCGGCTCTGTGCACTGTTACAAG
fpvB	Upstream	Forward (5' -> 3')	CATTGGTACCGTTGCTGGCGAGGTTCTCGCGGCG
		Reverse (5' -> 3')	CAATGGATCCCTGCAGTGTCCTGGATGGCGGCGC
	Downstream	Forward (5' -> 3')	CAATGGATCCTGATCCCGGACCGCCGGCGTGCCT
		Reverse (5' -> 3')	CAATAAGCTTGACGGCGGCTTCGGACAGCCACTCG
fiuA	Upstream	Forward (5' -> 3')	CAATGAATTCAGCGCGTTTCTCTATAGCCG
		Reverse (5' -> 3')	TCTGCGGTAGGGCGGATAACCCCTGGATGGAAACG AGTCTCA
	Downstream	Forward (5' -> 3')	TGAGACTCGTTTCCATCCAGGGGTTATCCGCCCTAC CGCAGA
		Reverse (5' -> 3')	CAATAAGCTTGGAGAAATCGAACTGCTCAACAT
foxA	Upstream	Forward (5' -> 3')	CAATGAATTCTGCAACTGAACACCGACAGCGCGG
		Reverse (5' -> 3')	CAATTCTAGAGAACGGAATCCGTTGGAGTCGTT
	Downstream	Forward (5' -> 3')	CAATTCTAGATCCTGGTTCTGCTGCACCGCTAT
		Reverse (5' -> 3')	CAATAAGCTTTACTGCAAGCGGTAGAAACGCTCT
pvdA	Upstream	Forward (5' -> 3')	GCCGAATTCCATTATCGGGAGCTGCTGCGATTC
		Reverse (5' -> 3')	CAATGGATCCTTCCAGTTCCTCTGGATTGGCCCC
	Downstream	Forward (5' -> 3')	CAATGGATCCACGCAGGGCGTTTTCGTTGCATGT
		Reverse (5' -> 3')	CAATAAGCTTGAAGTGGCTGGAGGTATCCACCGT
pchA	Upstream	Forward (5' -> 3')	CAATGAATTCTTCCGTAGCTGGAGCGAACGCCTG
		Reverse (5' -> 3')	CGCCAGACACGGGGTGCCGCATGATTAGAACGGA ATGTCGTCGTCGA
	Downstream	Forward (5' -> 3')	CGCCAGACACGGGGTGCCGCATGATTAGAACGGA ATGTCGTCGTCGA
		Reverse (5' -> 3')	CAATAAGCTTGTGACCAGCATTCGCCTGCCGCTC

Chromosomal integration of FpvB C-terminal FLAG tag and FpvA G558 V5 Tag			
Gene	Part		Sequence
fpvB	Upstream	Forward (5' -> 3')	CGTGAATTCTGTTCAACAAGGACGGCACC
		Reverse (5' -> 3')	TCACTTGTCGTCATCGTCTTTATAATCGAGCGAGTA CTTCACCGTGAACAT
	Downstream	Forward (5' -> 3')	GATTATAAAGACGATGACGACAAGTGAGCCTCAGC AGGGCCGATAG
		Reverse (5' -> 3')	CGTAAGCTTAAGCGGTTGCGTCGCAGTC
fpvA	Upstream	Forward (5' -> 3')	CAATTCTAGACGCAACTTGCCAACCTAAGAAGAG
		Reverse (5' -> 3')	GGTAGAATCGAGACCGAGGAGAGGGTTAGGGATA GGCTTGCCGGTTACCCGGTAGTCGACCACG
	Downstream	Forward (5' -> 3')	AAGCCTATCCCTAACCCTCTCCTCGGTCTCGATTCT ACCCTGAATCCGACCATTCGCGAG
		Reverse (5' -> 3')	CAATCTGCAGGGGCGCTGATCTCAGGTCCGTTCC
Expression primers			
Gene			Reverse (5' -> 3')
fpvA		Forward (5' -> 3')	CAATTCTAGACGCAACTTGCCAACCTAAGAAGAG
		Reverse (5' -> 3')	CAATCTGCAGGGGCGCTGATCTCAGGTCCGTTCC
fpvB		Forward (5' -> 3')	CAATGAATTCTGCGCCGCCATCCAGGACACTGCA
		Reverse (5' -> 3')	CAATAAGCTTCGAGCGAGTTCGAGCGCCGCTATC
foxA		Forward (5' -> 3')	CAATTCTAGATTCAACGACTCCAACGGATTCC
		Reverse (5' -> 3')	CAGTAAGCTTGTAGCCAGACCGACATAGCG
fiuA		Forward (5' -> 3')	AATGAATTCCATCCAGGAGCCCCGCACATG
		Reverse (5' -> 3')	AATAAGCTTTCACCACTTGTAGCTGACGCTG
FpvA and FpvB mutations			
Gene	Mutation		Upstream Reverse (5' -> 3')
fpvA	T660C	Forward (5' -> 3')	CCGCCATCTGTTACGCCTACAAGG
		Reverse (5' -> 3')	CCTTGTAGGCGTAACAGATGGCGG
fpvB	R648C	Forward (5' -> 3')	CACCTCGTGCTATTGCTCGCG
		Reverse (5' -> 3')	CGCGAGCAATAGCACGAGGTG
	C-terminal FLAG tag	Forward (5' -> 3')	same as *fpvB* forward expression primer
		Reverse (5' -> 3')	AGTCAAGCTTTTACTTGTCGTCATCGTCTTTGTAGT CGAGCGAGTACTTCACCGTGAACA
	W347V	Forward (5' -> 3')	CGACAACGTTGTAGGCCTGCCCAG
		Reverse (5' -> 3')	CTGGGCAGGCCTACAACGTTGTCG
	F783L	Forward (5' -> 3')	CGGCATCGACCTAGGCAACCTCAA
		Reverse (5' -> 3')	TTGAGGTTGCCTAGGTCGATGCCG
	Y187V	Forward (5' -> 3')	TCACCGTGCAACACGTGGGGCCGG
		Reverse (5' -> 3')	CCGGCCCCACGTGTTGCACGGTGA
	R191A	Forward (5' -> 3')	TACGGGCCGGCTGCAGTGAAGTAC
		Reverse (5' -> 3')	GTACTTCACTGCAGCCGGCCCGTA
	S214I	Forward (5' -> 3')	CGAGCATTATAACCTATACCCAGG
		Reverse (5' -> 3')	CCTGGGTATAGGTTATAATGCTCG
	T215V	Forward (5' -> 3')	ACGAGCATTTCCGTGTACACCCAG
		Reverse (5' -> 3')	CTGGGTGTACACGGAAATGCTCGT
	Y216L	Forward (5' -> 3')	AGCATTTCCACGTTAACCCAGGAC
		Reverse (5' -> 3')	GTCCTGGGTTAACGTGGAAATGCT
	T217L	Forward (5' -> 3')	AGCATTTCCACCTATCTGCAGGAC
		Reverse (5' -> 3')	GTCCTGCAGATAGGTGGAAATGCT
	Q218V	Forward (5' -> 3')	CCACCTATACCGTCGACGTCATTT
		Reverse (5' -> 3')	AAATGACGTCGACGGTATAGGTGG
	T217Y	Forward (5' -> 3')	CTATTATCATGACGTCATTTCCGCC
		Reverse (5' -> 3')	GGCGGAAATGACGTCATGATAATAG
	Y434A	Forward (5' -> 3')	GACTACAGCGCAACCGACGACCAC
		Reverse (5' -> 3')	GTGGTCGTCGGTTGCGCTGTAGTC

Y432A	Forward (5' -> 3')	GACGCAAGCTACACCGACGACCAC
	Reverse (5' -> 3')	GTGGTCGTCGGTGTAGCTTGCGTC
Y412A	Forward (5' -> 3')	GGCTGGCAAACGACTGCTACTACTC
	Reverse (5' -> 3')	GAGTAGTAGCAGTCGTTTGCCAGCC
Y416A	Forward (5' -> 3')	GGCTGTACAACGACTGCGCATACTC
	Reverse (5' -> 3')	GAGTATGCGCAGTCGTTGTACAGCC
Y417A	Forward (5' -> 3')	GGCTGTACAACGACTGCTACGCATC
	Reverse (5' -> 3')	GATGCGTAGCAGTCGTTGTACAGCC
W509A	Forward (5' -> 3')	CTGGCCGGCATGAAGCTCG
	Reverse (5' -> 3')	CGAGCTTCATGCCGGCCAG
W475A	Forward (5' -> 3')	CGCGGGCAGCCTGTTCAAC
	Reverse (5' -> 3')	GTTGAACAGGCTGCCCGCG
D219A	Forward (5' -> 3')	ATACCCAGGCAGTCATTTCCGCC
	Reverse (5' -> 3')	GGCGGAAATGACTGCCTGGGTAT

Chapter Four: Thiocillin Exploits the Ferrioxamine Transporter for Uptake

Preface

The work presented in the following chapter has been published in:

Chan D. C. K., and Burrows, L. L. (2020). Thiocillin and Micrococcin Exploit the Ferrioxamine Receptor of *Pseudomonas aeruginosa* for uptake. *J. Antimicrob. Chemother.* 76(8), 2029-39. https://doi.org/10.1093/jac/dkab124

D.C. and L.L.B. conceived the study and designed the experiments. D.C.K.C and L.L.B. wrote the manuscript.

Synopsis

Background: Thiopeptides are a class of antibiotics active against Gram-positive bacteria and inhibit translation. They were considered inactive against Gram-negative bacteria due to their inability to cross the outer membrane. However, we discovered previously that a member of this class, thiostrepton (TS), has activity against *Pseudomonas aeruginosa* and *Acinetobacter baumannii* under iron-limiting conditions. TS hijacks the pyoverdine siderophore receptors of *P. aeruginosa* to cross the outer membrane and synergizes with iron chelators.

Objectives: To test other thiopeptides for antimicrobial activity against *P. aeruginosa* and determine their mechanism of uptake, action, and spectrum of activity.

Methods: Eight thiopeptides were screened in checkerboard assays against a mutant of *P. aeruginosa* PA14 lacking both pyoverdine receptors. Thiopeptides that retain activity against a pyoverdine receptor-null mutant may use alternative siderophore receptors for entry. Susceptibility testing against siderophore receptor mutants was used to determine thiopeptide mechanism of uptake.

Results: The thiopeptides thiocillin (TC) and micrococcin (MC) use the ferrioxamine siderophore receptor (FoxA) for uptake and inhibit the growth of *P. aeruginosa* at low micromolar concentrations. The activity of TC required the TonB-ExbBD system used to energize siderophore uptake. TC acted through its canonical mechanism of action of translation inhibition.

Conclusions: Multiple thiopeptides have antimicrobial activity against *P. aeruginosa,* countering the historical assumption that they cannot cross the outer membrane. These results demonstrate the potential for thiopeptides to act as antipseudomonal antibiotics.

Introduction

The number of antibiotics available to treat multidrug-resistant bacteria is dwindling, especially in the case of Gram-negative pathogens. Many large pharmaceutical companies have discontinued their antibiotic research programs due to low return on investment.[1] Consequently, there has been an increased reliance on last-resort antibiotics, which selects for resistant bacteria and further exacerbates the issue. One strategy to replenish the arsenal of antibiotics is to probe previously-approved drugs for unrecognized antimicrobial activity.

Pseudomonas aeruginosa is a Gram-negative opportunistic pathogen that causes serious healthcare-acquired infections. It is intrinsically resistant to many antibiotics due to its low-permeability outer membrane combined with expression of multiple efflux pumps.[2,3] We previously screened a collection of bioactive and off-patent FDA-approved drugs for *P. aeruginosa* biofilm-modulating activity and identified thiostrepton (TS) as having stimulatory effects, a hallmark of sub-inhibitory antibiotic activity.[4,5] Follow-up studies showed that TS hijacks the pyoverdine siderophore receptors FpvA and FvpB to cross the outer membrane under iron-limiting conditions.[4] Deferasirox (DSX), an FDA-approved iron chelator, showed potent synergy with TS to inhibit the growth of multiple clinical isolates, while combinations of TS with other iron chelators were also effective.[6]

TS belongs to the thiopeptide class of antibiotics, which are natural products with potent activity against Gram-positive bacteria, including methicillin-resistant *Staphylococcus aureus*.[7] Thiopeptides inhibit translation through one of two mechanisms, depending on the number of members in the core macrocyclic ring. The 26-membered macrocycles like TS and thiocillin (TC) (**Figure 1**), inhibit elongation factor G binding at the GTPase-associated centre of the ribosome.[8,9] The 35-membered macrocycle thiopeptides like berninamycin act similarly.[10] However, 29-

membered macrocycle thiopeptides like GE2270A inhibit binding of elongation factor Tu.[11] *Streptomyces azureus* produces TS and protects itself from self-intoxication through methylation of the 23S rRNA at A1067, which prevents TS binding.[12] *Bacillus cereus* ATCC 14579 produces TC (**Figure 1**), and is immune to its own antibiotic through the expression of RplK (L11) variants that prevent TC binding to the ribosome.[13,14] RplK is a conserved ribosomal protein involved with elongation during protein synthesis.[9]

Recent studies have focused on the total synthesis of thiopeptides,[15] discovery of new members and structure elucidation,[16,17] identification and characterization of biosynthetic gene clusters,[18,19] and modification of existing thiopeptides to improve solubility and activity.[20–22] While we have learned much about these aspects of thiopeptide biology and chemistry, there is a gap in knowledge regarding their utility against Gram-negative bacteria, stemming from the long-standing assumption that the outer membrane prevents thiopeptide uptake. Our work with TS informed the hypothesis that other thiopeptides could have antipseudomonal activity by hijacking siderophore receptors. Here, we screened eight additional thiopeptides (**Figure 1**) for activity against *P. aeruginosa* PA14 and synergy with DSX, and investigated their mechanisms of uptake and action, and spectrum of activity.

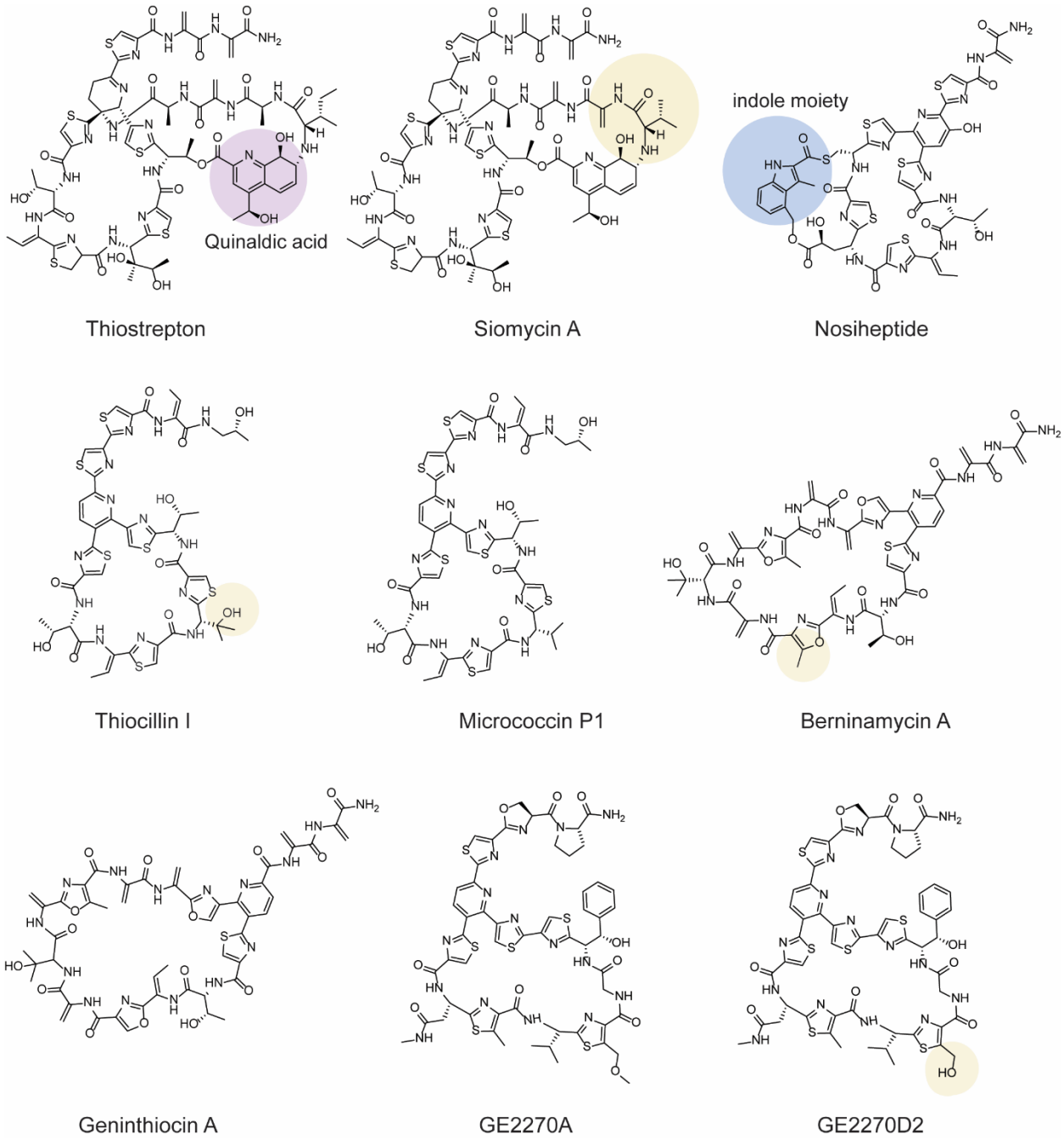

Figure 1. Structures of thiopeptides tested for activity against *P. aeruginosa*. Thiostrepton (TS), siomycin (SM), nosiheptide, thiocillin (TC), and micrococcin (MC) belong to the 26-membered macrocycle thiopeptides. TS and SM are structural analogues with the differences circled in yellow on SM. The quinaldic acid moiety is circled in purple. TC and MC are structural analogues with the differences circled on TC in yellow. No structural analogues of nosiheptide were tested. The unique indole group is circled in blue. Berninamycin and geninthiocin belong to the 35-membered macrocycle thiopeptides and are structural analogues of one another with the difference between the two circled in yellow on berninamycin. GE2270A and GE2270D2 belong to the 29-membered macrocycle thiopeptides and are structural analogues. The difference between the two are circled in yellow on GE2270D2.

Results

Thiocillin activity against *P. aeruginosa* requires the FoxA receptor and the TonB system

The activity of eight thiopeptides (**Figure 1**) in combination with DSX against wild type *P. aeruginosa* PA14 and a pyoverdine receptor-null mutant (Δ*fpvA fpvB*::Mar2xT7) was tested using checkerboard assays (**Figure 2A**). The mutant is resistant to TS and was used to rule out thiopeptides that require the pyoverdine receptors.[4] None of the thiopeptides alone inhibited growth. Synergy with DSX was observed for siomycin (SM), TC, and micrococcin (MC) (**Figure 2B**). Since the MIC of the thiopeptides is greater than their aqueous solubility and the MIC of DSX is greater than 1mg/mL, the fractional inhibitory concentration (FIC) could not be determined. However, the combination of SM, TC, or MC with DSX reduced the MIC of each compound greater than 4-fold, which is equivalent to an individual FIC<0.25, and considered synergistic.

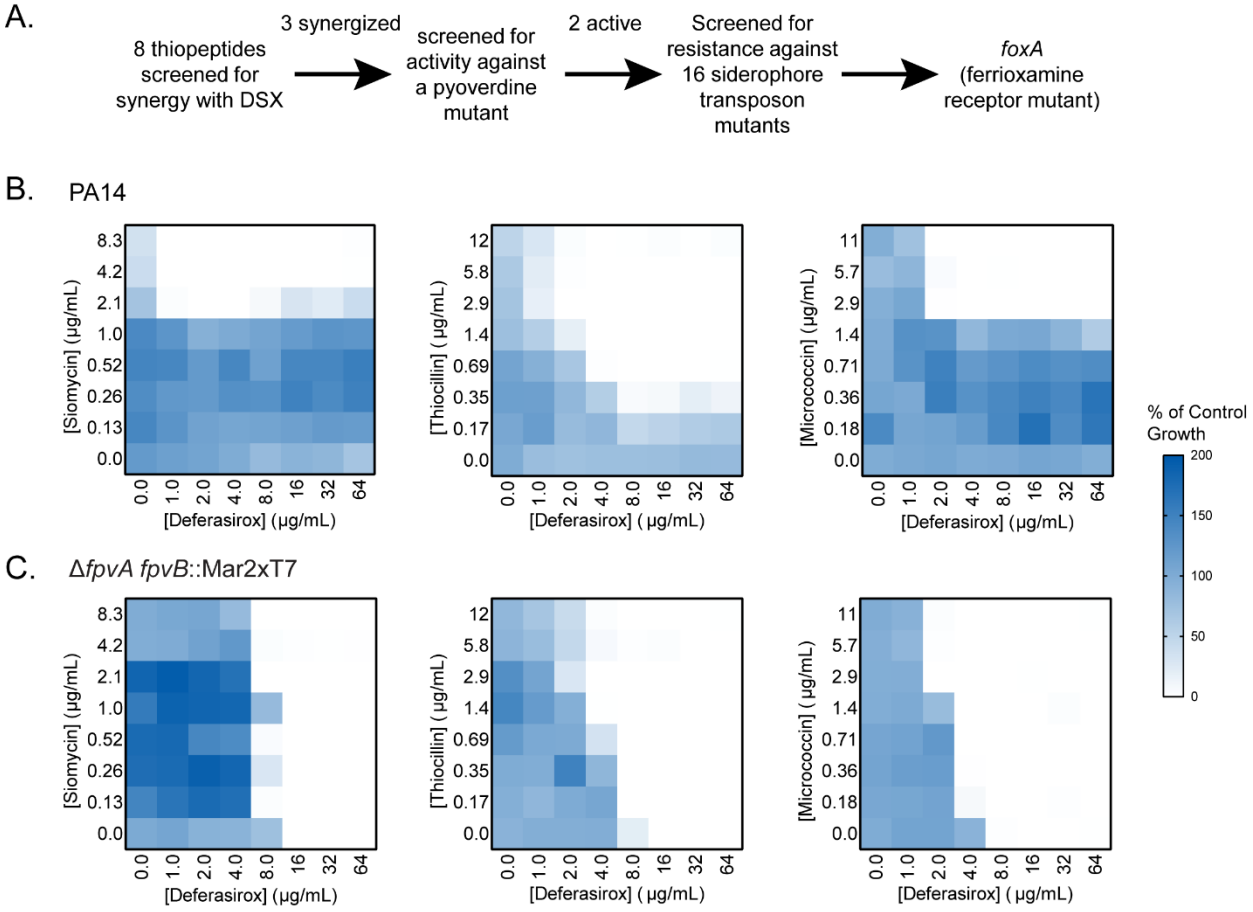

Figure 2. SM, TC, and MC checkerboards with DSX against PA14. **A)** Schematic diagram of the thiopeptide screen. **B)** Checkerboards of thiopeptides active against *P. aeruginosa* PA14. **C)** Checkerboards of thiopeptides against PA14 tested against Δ*fpvA fpvB*::Mar2xT7. Results are averaged from three independent biological replicates.

Thiopeptides that synergized with DSX were tested for activity against a pyoverdine receptor double mutant, Δ*fpvA fpvB*::Mar2xT7 (**Figure 2C**). Compared to the wild type, this strain

is susceptible to DSX, as it is unable to take up pyoverdine in response to iron deprivation. As expected, synergy was lost for the SM+DSX combination, since SM is structurally similar to TS. However, TC+DSX and MC+DSX retained activity, suggesting that those thiopeptides use an alternative receptor. These combinations were tested against 16 different siderophore receptor mutants and only the *foxA* mutant was resistant, with a >4-fold increase in MIC (data for TC is shown; **Figure 3AB, Table S4**). FoxA is a xenosiderophore receptor that scavenges ferrioxamine, a siderophore produced by *Streptomyces* spp. Complementation of the *foxA* mutant *in trans* restored its susceptibility to TC+DSX and TC+DSX (**Figure 3B**).

Iron limitation increases siderophore production and receptor expression.[27] We hypothesized that increasing FoxA levels by expression *in trans* may potentiate TC activity against *P. aeruginosa* even in the absence of DSX-induced iron starvation. Consistent with this idea, susceptibility to TC increased when FoxA was expressed from an arabinose-inducible vector, pHERD20T (**Figure 3C**). As a control, FpvA was expressed *in trans* and the recombinant strain tested for TC susceptibility, while the recombinant FoxA-expression strain was tested for TS susceptibility. No cross-susceptibility was observed, confirming that TS is specific for FpvA and TC is specific for FoxA (**Figure S1**).

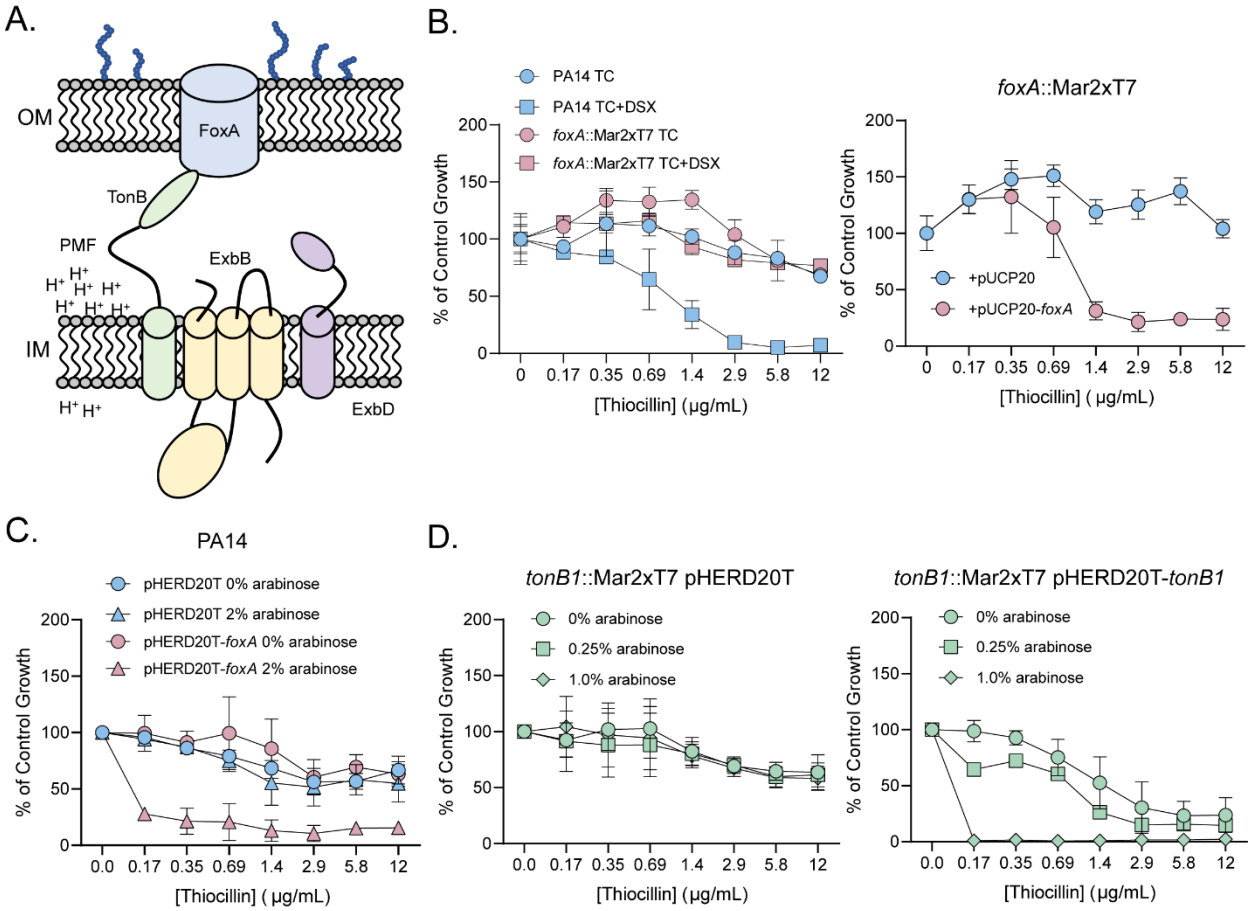

Figure 3. TC activity requires FoxA and the TonB system. **A)** Architecture of TonB-dependent receptors. A ligand-specific receptor in the outer membrane (OM) interacts with TonB, an inner membrane (IM) protein. The TonB-ExbB-ExbD complex couples the energy of the proton motive force to activate transport of recognized ligands. **B)** PA14 (blue) and a *foxA* mutant (red) treated with TC (circles) or TC+DSX (squares) (left). A *foxA* transposon mutant complemented with *foxA in trans* treated with TC (blue) and TC+DSX (red) (right). **C)** Recombinant PA14 with empty vector (blue) or overexpressing FoxA (red) treated with TC only. Expression was induced with arabinose (0% - squares; 2% triangles). **D)** *tonB1* mutant with empty vector treated with TC+DSX and supplemented with different concentrations of arabinose (0% - circles; 0.25% - squares; 1.0% - diamonds) (left). *tonB1* mutant with expressing *tonB1* treated with TC+DSX and supplemented with different concentrations of arabinose (0% - circles; 0.25% - squares; 1.0% - diamonds) (right). Results are averaged from three independent biological replicates. For all graphs, the MIC was defined as <20% of control.[4] For all experiments involving DSX, a concentration of 64µg/mL was used.

Siderophore receptors like FoxA require the TonB-ExbB-ExbD inner membrane complex and the proton motive force for active transport of siderophores (**Figure 3A**).[28,29,30] *P. aeruginosa* encodes two complete sets of TonB-ExbB-ExbD components, plus an orphan TonB homolog,

TonB3, which does not contribute to siderophore uptake.[31–33] TonB1 is the primary component that interfaces with siderophore receptors to act as an energy coupler.[34] Consistent with the role of TonB1 in siderophore uptake, a *tonB1* mutant was less susceptible to TC+DSX (>8-fold increase in MIC) compared to PA14 (**Figure 3D**). Complementation of TonB1 increased susceptibility to TC, but only in the presence of DSX. This result confirms that thiopeptide activity requires an iron-limited environment, and that TonB1 is required for thiopeptide activity. Although the *tonB1* mutant was more resistant to the combination, ~30% growth inhibition occurred at the highest concentration of TC+DSX tested.

Table 1. Summary of MIC values for wild type, mutant, and recombinant PA14 strains challenged with TC or TC+DSX.

		MIC (μg/mL)	
Strain	Arabinose (%)[a]	TC	TC+DSX[b]
PA14	NA	>12	2.9
PA14 *foxA*::Mar2xT7	NA	>12	>12
PA14 *foxA*::Mar2xT7 pUCP20	NA	>12	>12
PA14 *foxA*::Mar2xT7 pUCP20-*foxA*	NA	>12	2.9
PA14 pHERD20T	0.0	>12	NT
PA14 pHERD20T-*foxA*	2.0	0.35	NT
PA14 *tonB1*::Mar2xT7 pHERD20T	0.0	NT[c]	>12
PA14 *tonB1*::Mar2xT7 pHERD20T	0.25	NT	>12
PA14 *tonB1*::Mar2xT7 pHERD20T	1.0	NT	>12
PA14 *tonB1*::Mar2xT7 pHERD20T-*tonB1*	0.0	NT	>12
PA14 *tonB1*::Mar2xT7 pHERD20T-*tonB1*	0.25	NT	2.9
PA14 *tonB1*::Mar2xT7 pHERD20T-*tonB1*	1.0	NT	≤0.17

[a]Arabinose was only supplemented to cultures with the arabinose-inducible vector pHERD20T; NA = not added
[b]DSX concentration of 64μg/mL
[c]NT = not tested

ExbB-ExbD are inner-membrane proteins that form a proton channel (**Figure 3A**) and *P. aeruginosa* encodes two sets.[35] Previous studies showed that single pair *exbB-exbD* deletion mutants of *P. aeruginosa* had wild-type growth in low iron media,[34] suggesting that siderophore uptake continued. The redundancy of these components suggests that *exbB1* and *exbB2* single

mutants have wild-type susceptibility to TC+DSX, which we observed (**Figure S2**). The MICs for wild type, mutant, or recombinant PA14 strains challenged with TC or TC+DSX are summarized in **Table 1**.

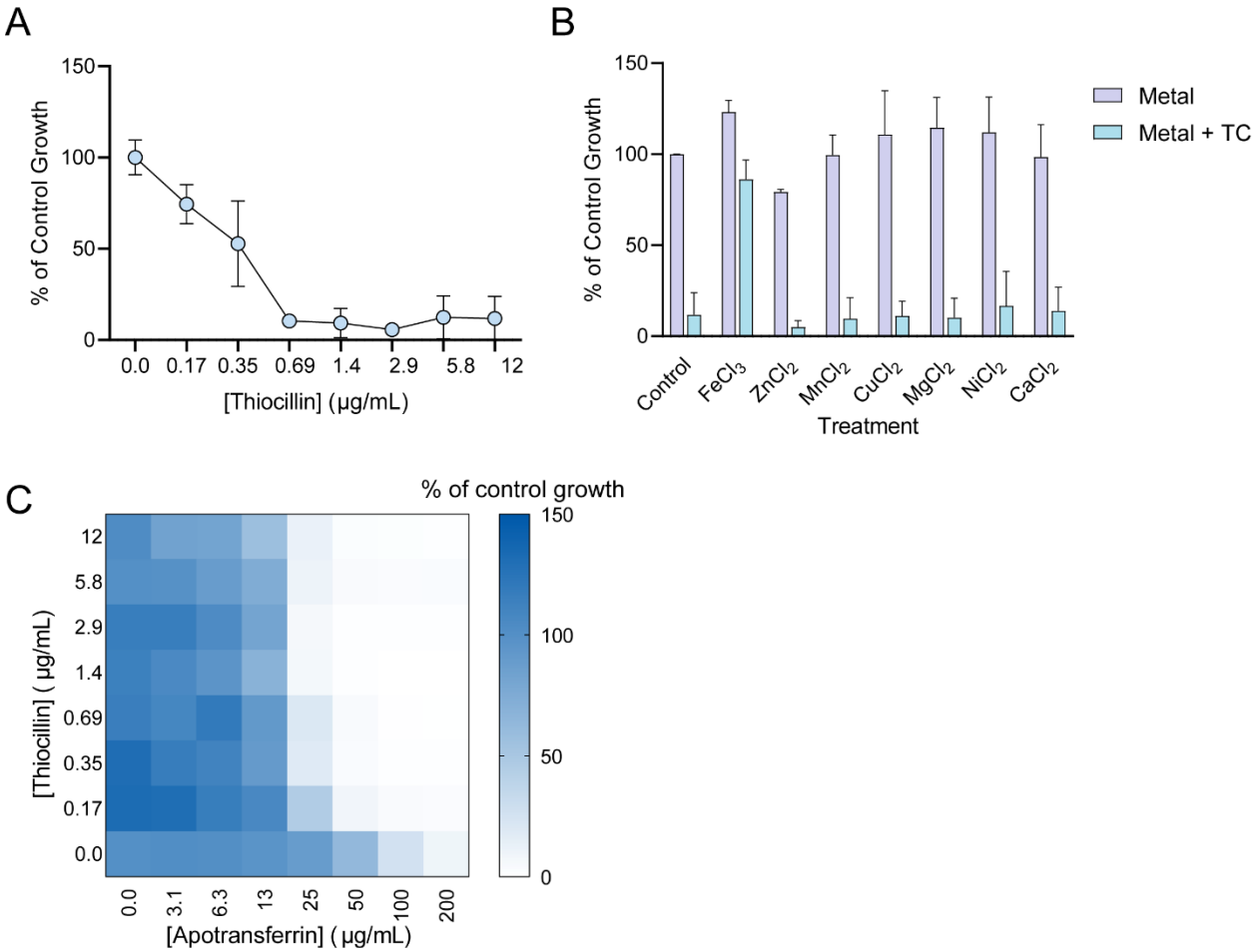

Figure 4. TC is potentiated by human serum through iron restriction. **A)** Activity of TC alone against PA14 in 10% human serum. **B)** Growth of PA14 in 10% human serum without (purple bars) or with (blue bars) supplementation of TC (12 µg/mL) and various chloride salts (12.5µM). **C)** Checkerboard of TC and apotransferrin against PA14. All experiments were repeated three times and averaged results are shown.

In mammalian systems, high-affinity iron chelation by transferrin and lactoferrin contribute to the defensive response against bacteria. We investigated whether serum, which is rich in transferrin, could potentiate TC activity. The addition of 10% heat-inactivated human serum to the growth medium sensitized cells to TC without the addition of DSX, while adding $FeCl_3$

rescued growth (**Figure 4AB**). A lack of growth inhibition in serum-free controls was observed, consistent with the idea that TC cannot enter cells (**Figure S3**). Apotransferrin also potentiated TC activity (**Figure 4C**). Together these data show that the activity of TC against *P. aeruginosa* requires an iron-limited environment, FoxA, and the TonB system. This mechanism is consistent with active uptake through outer membrane transporters.

Thiocillin acts through its canonical mechanism of protein synthesis inhibition

Although thiopeptides inhibit growth of Gram-positive bacteria by targeting protein synthesis, we considered whether TC could act on Gram-negative bacteria through another mechanism. The inhibitory activity of SM, TS, and TC against ribosomes was first confirmed using a coupled *in vitro* transcription/translation system. *E. coli* ribosomes were incubated with thiopeptides or a vehicle control and a template plasmid that encodes dihydrofolate reductase (DHFR). Relative DHFR expression was assessed by measuring enzyme activity through the depletion of NADPH in the presence of dihydrofolate. IC_{50} values were similar for all three thiopeptides (**Table 2**) and agreed with previously published results with the exception of those of Mikolajka et al., who reported a ~10-fold higher IC_{50}.

Table 2. Thiopeptides inhibit protein synthesis in a coupled *in vitro* transcription/translation system using *E. coli* ribosomes

		IC_{50} (μg/mL)		
Thiopeptide	This Study[a]	Lentzen *et al.*, 2003[51]	Walter *et al.*, 2012[54]	Mikolajka *et al.*, 2012[55]
TS	0.41 ± 0.05	0.17 ± 0.01	~0.25	~5.0
SM	0.40 ± 0.07	0.41 ± 0.04	NT	NT
TC	0.70 ± 0.15	NT	NT	NT
MC	NT	0.34 ± 0.01	NT	~3.4

NT: not tested

[a]IC_{50} for TS, SM, and TC are based on residual DHFR activity. Results are averaged from three independent replicates.

Bacillus cereus ATCC 14579 produces TC and its biosynthetic gene cluster has been extensively studied.[19] It encodes TclT and TclQ, identical L11 variants that replace the native L11 to prevent thiopeptide binding to the ribosome, conferring resistance to TC.[13,14] At position 26 (*P. aeruginosa* RplK numbering), TC-resistant variants have a threonine (**Figure 5A**), while susceptible species including *Mycobacterium tuberculosis, Deinococcus radiodurans,* and *Bacillus megaterium* have proline. Mutations at this site confer cross-resistance to TC and its structural analogue, MC.[9,36,37] *P. aeruginosa* L11 has Pro26, suggesting that TC may target the same site.

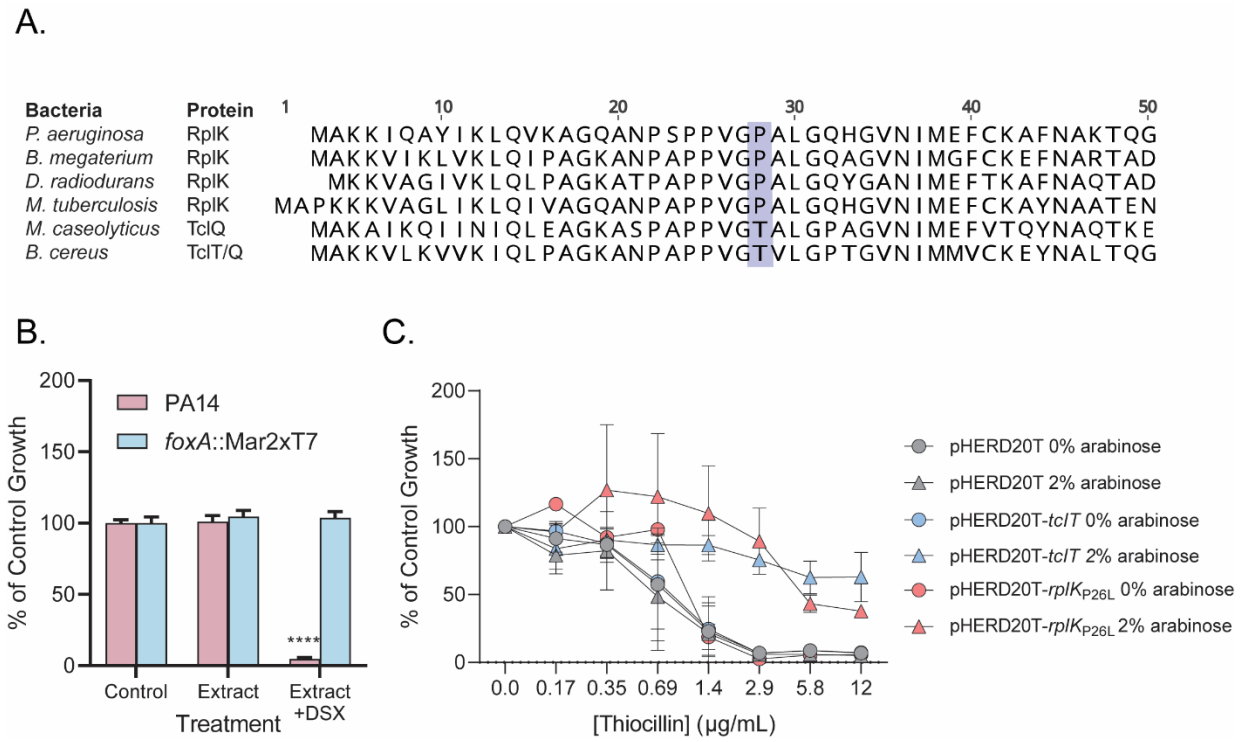

Figure 5. Mutation at P26 of RplK protects *P. aeruginosa* against TC. **A)** Alignments of RplK amino acid sequences from *P. aeruginosa* PAO1, *P. aeruginosa* PA14, *B. megaterium*, *D. radiodurans*, *M. tuberculosis*, TclQ from *Micrococcus caseolyticus*, and TclT/Q from *B. cereus*. TclT/Q are identical homologs. Residue 26 is highlighted in purple showing that TC and MC producing bacteria have a threonine instead of a proline in L11 variants. **B)** The effects of *B. cereus* ATCC 14579 crude extracts against PA14 (red bars) and *foxA*::Mar2xT7 (blue bars) in 10:90. The concentration of TC in crude extracts was determined to be 32.3µg/mL using LC-MS. Statistics were calculated using a two-way ANOVA followed by Dunnett's test. ****, $p<0.0001$. **C)** Dose-response assay of TC+DSX against recombinant PA14 strains expressing TclT (blue) from *B. cereus* and RplK$_{PA14}$ P26L (red). Empty vector controls are in grey. Expression was induced with

0% arabinose (circles) or 2% arabinose (triangles). All results are averaged from three independent experiments. For all experiments involving DSX, a concentration of 64μg/mL was used.

We tested whether expression of a TC-resistant form of L11 sourced from *B. cereus* could protect *P. aeruginosa*. First, crude extracts from *B. cereus* were analyzed using LC-MS to confirm TC production (**Figure S4**). Next, the antibacterial activity of the extracts against *P. aeruginosa* was tested. The extracts alone lacked growth inhibitory activity; however, when combined with DSX, they inhibited the growth of PA14, but not the *foxA* mutant (**Figure 5B**). Previous studies showed that expression of *B. cereus* TclQ in *Bacillus subtilis* conferred resistance to MC.[13] We hypothesized that the identical homolog, TclT, would similarly provide resistance to *P. aeruginosa*. PA14 harbouring pHERD20T-*tclT* was >4-fold more resistant to TC+DSX compared to the empty vector control (**Figure 5C**), while the same strain expressing *P. aeruginosa* L11 was as susceptible to TC as the wild type, showing that expression of TclT – rather than an increase in L11 levels – specifically protected cells (**Figure S5**). We next introduced a P26L mutation into $RplK_{PA14}$ to confirm that proline is necessary for TC activity. Leucine was selected to replace proline based on analyses of MC-resistant *M. tuberculosis* mutants.[36,37] This mutation increased the TC MIC >4-fold in *P. aeruginosa*, confirming that L11 P26 is important for TC activity (**Figure 5C**). Because the wild-type background still produces native L11, expression of TclT or $RplK_{P26L}$ *in trans* conferred only partial TC resistance compared to loss of FoxA.

Thiocillin and Deferasirox Susceptibility is Strain- and Species-Specific

To investigate the breadth of thiopeptide activity, we tested the multidrug resistant *P. aeruginosa* strain PA7 for susceptibility. Its susceptibility profile could be predicted based on similarity of its pyoverdine and ferrioxamine receptors to those of susceptible strains. PA7 lacks FpvB and its FpvA homologue only has 28% similarity to that of PA14; it was resistant to TS+DSX

(**Figure S6**). However, the sequence of $FoxA_{PA7}$ is 96% similar to those of PAO1 and PA14, and PA7 was susceptible to TC+DSX (**Figure 6A**). Similarly, the sequence of FoxA from C0379, a TS-resistant isolate,[4] was nearly identical to PA14, and it was susceptible to TC+DSX (**Figure 6B**).

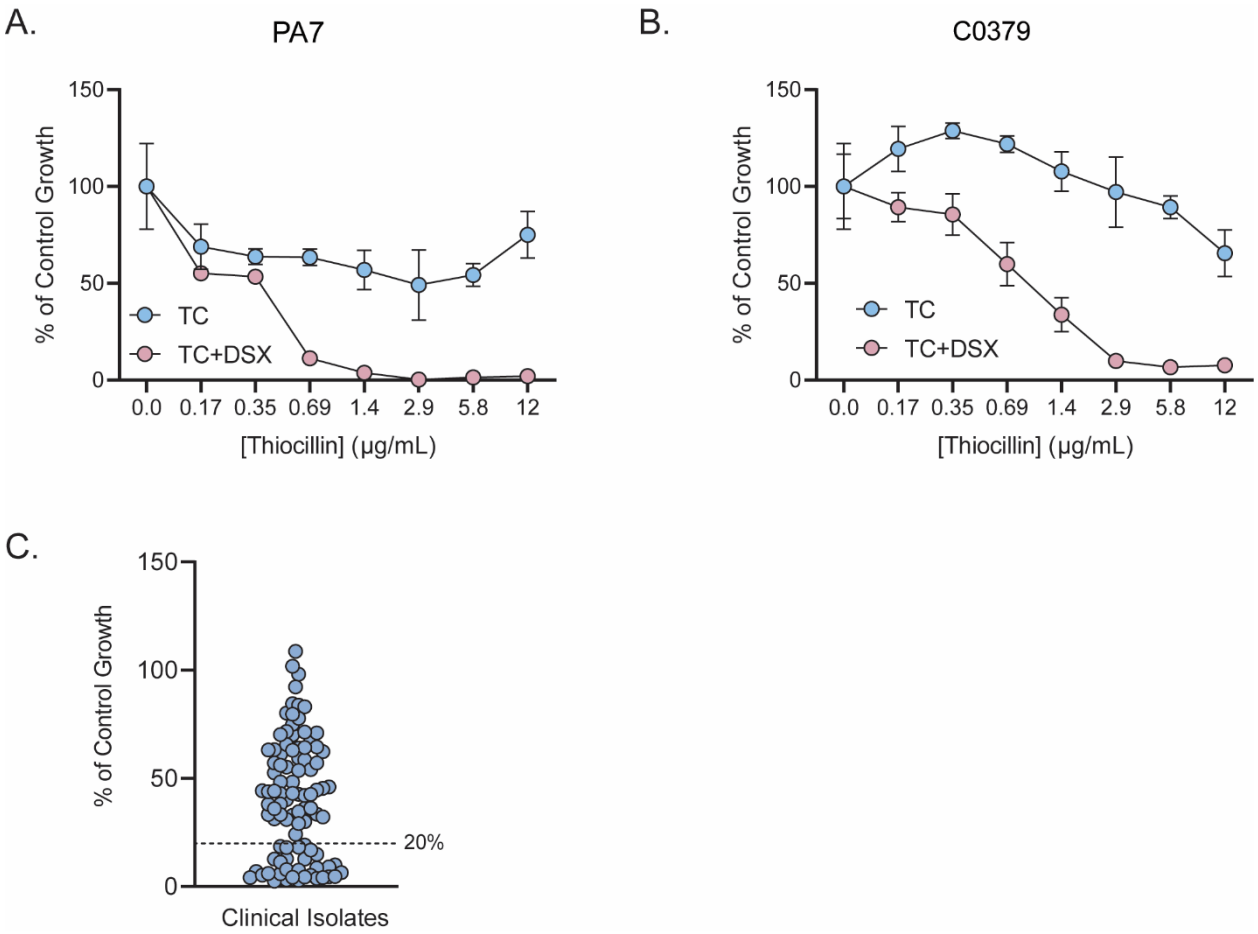

Figure 6. The effects of TC+DSX against *P. aeruginosa* clinical isolates. **A)** Dose-response assay of TC (blue circles) or TC+DSX (red circles) against PA7 in 10:90. **B)** Dose-response assay of TC (blue circles) and TC+DSX (red circles) against C0379 in 10:90. **C)** Growth of an additional 95 *P. aeruginosa* clinical isolates challenged with TC (12 µg/mL) + DSX (64 µg/mL). Growth was grouped into susceptible (<20% of control) or resistant (>20% of control). All results are averaged from three independent experiments. For all experiments involving DSX, a concentration of 64µg/mL was used.

A collection of 95 *P. aeruginosa* clinical isolates was screened for susceptibility to TC+DSX (**Figure 6C**). Thirty-one isolates were susceptible (growth <20% of control) while 64

were resistant (growth >20% of control). However, 56/64 resistant isolates had reduced growth compared to controls, suggesting that higher TC concentrations may further inhibit growth. Strains C0062, C0261, and C0275 were unaffected by TC+DSX, even though they are susceptible to TS+DSX.[4] However, sequence analyses showed that the *foxA, tonB1,* and *rplK* homologues in those strains were similar to those of susceptible strains (data not shown).[38] This result suggests that other features can affect TC susceptibility, or that FoxA expression in those strains was low. Further work is needed to understand the mechanism of resistance in these isolates; however, all isolates tested were susceptible to at least one or both of TS+DSX and TC+DSX.[4]

Other Gram-negative bacteria including *Salmonella enterica* Typhimurium*, Klebsiella pneumoniae*, *A. baumannii* and *E. coli* encode FoxA homologs or other receptors that recognize ferrioxamine.[39–43] However, no growth inhibition was seen when isolates of these species were challenged with TC+DSX (**Table 3**). TS+DSX was also tested to investigate its spectrum of activity against other Pseudomonads. All strains tested were inhibited by TS+DSX or TC+DSX, except for *P. protegens* Pf-5. Overall, the results indicate that TC and TS susceptibility is species-specific, with further strain-dependent differences in susceptibility. Among the factors influencing susceptibility could be differences in receptor protein sequence and/or levels of expression.

Table 3. Thiopeptide combinations are Pseudomonas specific with interstrain and interspecies differences in susceptibility

	TS+DSX	TC+DSX
Pseudomonas aeruginosa PAO1	S[a]	S
Pseudomonas aeruginosa PA14	S	S
Pseudomonas aeruginosa PA7	R[b]	S
Pseudomonas aeruginosa C0379	R	S
Pseudomonas protegens Pf-5	R	R
Pseudomonas putida KT2440	R	S
Pseudomonas putida PP578	R	S
Pseudomonas fluorescens WCS374R	S	S
Pseudomonas fluorescens PV5	S	R[c]
Pseudomonas marginalis CVCOB 1152	R[c]	R[c]
Escherichia coli K12 BW25113	R	R
Salmonella enterica serovar Typhimurium ATCC SL1344	R	R
Klebsiella pneumoniae	R	R
Acinetobacter baumannii ATCC 17978	R	R

[a]Susceptible (S), growth <20% of control
[b]Resistant (R), growth >20% of control
[c]A decrease in culture turbidity was observed compared to the vehicle control although growth was >20% of control

Discussion

The specificity of natural siderophore antibiotics for a particular receptor is a common theme – microcin J25 is one example.[44] Microcin J25 is a lasso peptide produced by *E. coli* AY25 that belongs to the same family of natural products as the thiopeptides.[44,45] It uses the ferrichrome receptor FhuA for uptake.[45] Although FhuA homologs are expressed by other Gram-negative bacteria, the spectrum of activity of microcin J25 is limited to a few bacterial species and strains, similar to TC+DSX. Of note, uptake of microcin J25 requires the TonB system, consistent with our findings.[44,46,47] Some microcins use the SbmA[47] and YejABEF[48] transporters to cross the inner membrane of *E. coli*; however, an inner membrane transporter for thiopeptides have yet to be identified in *P. aeruginosa*.

Overall, TS+DSX is more potent than TC+DSX against *P. aeruginosa* even though a greater number of Pseudomonad species were susceptible to TC+DSX. TS was potentiated by 1μg/mL DSX, whereas TC required 64μg/mL DSX to exert a similar inhibitory effect. The weaker activity of TC could be an uptake issue. There is a single FoxA receptor, compared to two pyoverdine receptors, and FoxA expression is lower.[27] However, deferoxamine induces chromosomal *foxA* expression and may potentiate TC activity.[28] Our results with clinical isolates indicate that use of thiopeptide cocktails may offer an advantage over single thiopeptide treatments by targeting multiple siderophore receptors and reducing the likelihood of resistance through loss of uptake. This work also suggests links between thiopeptide structure and activity. The core macrocycles of TC and TS are nearly identical. However, TS has a second macrocyclic ring with a structurally-distinct quinaldic acid moiety (**Figure 1**). It is likely that this second ring is involved in the specificity of TS for the pyoverdine receptors compared to TC for FoxA.

Thiopeptides have been tested in human clinical trials orally and topically with few adverse effects.[49,50] The crystal structures of TS and MC with prokaryotic ribosomes show that interacting residues are different than those in eukaryotic systems.[9] Complementing this observation, previous studies found that thiopeptides lack inhibitory effects against rabbit reticulocytes with an IC_{50} >100-200μM.[51] Moreover, TS is a component in a commercially-available veterinary ointment (Animax) intended to treat Gram-positive infections. These data support the claim that thiopeptides are safe in mammalian systems and provide encouragement to move this class forward for use in humans.

SM – a thiopeptide structurally similar to TS – also requires the pyoverdine receptors to inhibit *P. aeruginosa* growth (**Figure 2BC**). More importantly, we discovered that TC and MC use the FoxA receptor to enter the cell. To our knowledge, this is the first example of an

antimicrobial that exploits FoxA. Thiopeptides were presumed to have little or no activity against Gram-negative pathogens due to their inability to cross the outer membrane. However, thiopeptide producers are mainly marine and soil bacteria, which inhabit environments shared by Pseudomonads. We propose that thiopeptide structures may have evolved to target the siderophore receptors of co-habiting Gram-negatives. This idea is not unprecedented, as many other natural products can use such receptors to cross the outer membrane. For example, *P. aeruginosa* produces pyocins that target the pyoverdine and pyochelin receptors of competing strains.[52,53]

While thiopeptides been overlooked for use in the clinic, we show the potential for these antibiotics to be developed as selective Gram-negative antimicrobials that target critical-priority pathogens such as *P. aeruginosa*. Thiopeptides are an underutilized class of antibiotics with potential for development as clinically useful drugs – especially because many sites of infection are iron-limited.

Methods and Materials

Bacterial Strains and Culture Conditions

Bacterial strains are listed in Table S1. Bacteria were inoculated from -80ºC glycerol stocks and grown overnight in lysogeny broth (LB) (Bioshop) at 37°C with shaking (200 rpm) and subcultured (1:500) into fresh 10:90 (10% lysogeny broth and 90% 1X phosphate-buffered saline) media or 10:90 + 10% human serum (Sigma) prepared as previously described.[4] At 4h, the OD_{600} was standardized to 0.1 and diluted 1/500 in 10:90 for susceptibility assays. L-arabinose (Bioshop) was prepared as a 20% solution (wt/vol) in 10:90 and sterilized using 0.2µm filters (Fisher Scientific). Clinical isolates were cultured as previously described.[4] *Pseudomonas fluorescens, Pseudomonas putida, Pseudomonas protegens,* and *Pseudomonas marginalis* were grown at 25°C. Serum experiments were conducted as previously described.[4]

Chemicals and Compounds

Thiopeptides were purchased from Cayman Chemicals and AdipoGen. Deferasirox was purchased from AK Scientific. Metal salts and apotransferrin were purchased from Sigma. Antibiotics used for plasmid selection were purchased from Bioshop.

Cloning and Transformation Procedures

Genomic DNA from PA14 or *Bacillus cereus* ATCC 14579 was used for all PCR reactions (Promega Wizard Genomic DNA Isolation Kit). Primers are listed in Table S2. PCR products were separated on a 1% agarose gel, purified (Thermo Scientific GeneJET DNA Extraction Kit), digested (Thermo Scientific Fast Digest), and ligated in the appropriate vector using T4 DNA Ligase (Thermo Scientific). Ligation mixtures were used to transform competent *Escherichia coli* DH5α by heat shock. Transformants were selected on LB supplemented with antibiotics (pHERD20T and pUCP20: 100μg/mL ampicillin). pHERD20T is a pUCP20T-based broad host range expression vector with an L-arabinose-inducible P_{BAD} promoter.[23] Individual constructs were purified and verified by restriction digest (Thermo Fisher GeneJET Plasmid Miniprep Kit). For transformation into *P. aeruginosa*, 1mL of an overnight culture was washed 2x and resuspended in 500μL sterile water. One hundred ng of construct was added to 100μL of resuspended cells and electroporated (2.50V). After 2-4h of recovery at 37°C, cells were plated on LB agar with antibiotic (pUCP20 and pHERD20T: 200μg/mL carbenicillin). The *rplK*$_{P26L}$ point mutation was generated by overlap extension PCR[24] and confirmed through restriction digest at a newly introduced BfaI site. Accession numbers for *fpvA, foxA,* and *rplK* are listed in Table S3. The Δ*exbB2* mutant was generated by allelic exchange as previously described.[25]

Dose Response and Checkerboard Assays

Compounds (2-fold serial dilutions) or vehicle were added to wells of a 96-well plate (Nunc) at 75x final concentration. Wells were filled with a bacterial suspension standardized to an OD_{600} of 0.1/500 in 10:90 to a final volume of 150µL in triplicate. Sterility controls were included to allow for subtraction of background. After overnight incubation at 37°C and shaking at 200rpm, the OD_{600} was determined using a plate reader (Thermo Scientific Multiskan Go). As previously described, the minimal inhibitory concentration (MIC; defined as the concentration at which growth is no longer visible) in this medium is equivalent to <20% of control.[4]

Checkerboard assays were set up in 96-well plates (Nunc) in an 8x8-well format with vehicle and sterility controls. Serial dilutions of each thiopeptide were added along the ordinate of the checkerboard (increasing concentrations from bottom to top) while serial dilutions of DSX or apotransferrin were added along the abscissa (increasing concentrations from left to right). Plates were incubated as described above and the final OD_{600} was determined as described.

IC_{50} Measurements

An *in vitro* transcription/translation kit (NEB PURExpress)[26] was used to compare expression of dihydrofolate reductase (DHFR) in the absence and presence of thiopeptide. Reactions were scaled down to 10µL. Solution B (3µL) was added to solution A (4µL) (NEB PURExpress) followed by 1µL of thiopeptide (10x the final concentration) or vehicle control (nuclease free H_2O), 1.5µL of nuclease free H_2O (Qiagen), and 0.5µL of 250ng/mL plasmid (PURExpress DHFR template). Reactions were incubated at 37°C for 2h. DHFR activity was measured using a spectrophotometric assay kit (Sigma). Reactions were scaled down to 200µL from 1mL. Five µL of NEB PURExpress reaction was added to 1X assay buffer, followed by 1.2µL of 10mM NADPH. Reactions were initiated upon the addition of 1.0µL of 10mM

dihydrofolic acid. Abs_{340} was read immediately, then every 15s for 2.5min and normalized to the control. IC_{50} values were calculated using the four-parameter Hill equation.

Isolation of Crude *B. cereus* Extracts

Extracts from *B. cereus* were isolated as described previously with modifications.[19] One hundred mL of LB broth was separated into x20 5mL tubes and each tube was inoculated with 10µL of an overnight culture of *B. cereus* grown at 30°C with shaking (200 rpm). The tubes were incubated for 68h, pooled, centrifuged to collect the cells, and the supernatant was discarded. The cells were resuspended in 7mL of HPLC grade methanol (Honeywell) and cell debris removed by filtration using Whatman filter paper. The methanol was evaporated under nitrogen and the extract was resuspended in 0.5mL DMSO.

Mass Spectrometry

LC-MS with an XDB-C18 column, 2.1 x 100mm, 3.5µm on an Agilent 1290 LC system coupled with an Orbitrap LTQ mass spectrophotometer was used for identification of TC in *B. cereus* extracts. The mobile phase consisted of solvent A (water + 0.1% formic acid) and solvent B (acetonitrile + 0.1% formic acid). TC was detected in an isocratic run with a flow rate of 0.4mL/min based on its mass-retention time and compared to an internal standard. The concentration of TC in the crude extract as determined by comparison to a standard curve was 32.3µg/mL. The extracts were diluted 75x in 10:90 (2µl extract in 150µl total, final concentration of TC of ~0.4µg/ml) for susceptibility assays.

Acknowledgements

We thank Kara Tsang for her assistance with breseq and Nicola Henriquez for assistance with the LC-MS analyses. We thank Drs. Gerry Wright, David Guttman, Eric Brown, Brian Coombes, Paul Roy, and John Whitney for the strains listed in the supplementary information.

References

1. Årdal C, Balasegaram M, Laxminarayan R, *et al.* Antibiotic development — economic, regulatory and societal challenges. *Nat Rev Microbiol* 2020; **18**: 267–74.
2. Hancock REW. Resistance mechanisms in *Pseudomonas aeruginosa* and other nonfermentative gram-negative bacteria. *Clin Infect Dis* 1998; **27**: SUPPL.1:S93-9.
3. De Kievit TR, Parkins MD, Gillis RJ, *et al.* Multidrug efflux pumps: Expression patterns and contribution to antibiotic resistance in *Pseudomonas aeruginosa* biofilms. *Antimicrob Agents Chemother* 2001; **45**: 1761–70.
4. Ranieri MRM, Chan DCK, Yaeger LN, *et al.* Thiostrepton Hijacks Pyoverdine Receptors to Inhibit Growth of *Pseudomonas aeruginosa*. *Antimicrob Agents Chemother* 2019; **63**: e00472-19.
5. Hoffman LR, Jones RA, Zhang Z, *et al*. Aminoglycoside antibiotics induce bacterial biofilm formation. *Nature* 2005; **436**: 1171–5.
6. Chan DCK, Guo I, Burrows LL. Forging new antibiotic combinations under iron-limiting conditions. *Antimicrob Agents Chemother* 2020; **64**: e01909-19.
7. Haste NM, Thienphrapa W, Tran DN, *et al.* Activity of the thiopeptide antibiotic nosiheptide against contemporary strains of methicillin-resistant *Staphylococcus aureus. J Antibiot (Tokyo)* 2012; **65**: 593–8.
8. Baumann S, Schoof S, Bolten M, *et al.* Molecular determinants of microbial resistance to thiopeptide antibiotics. *J Am Chem Soc* 2010; **132**: 6973–81.
9. Harms JM, Wilson DN, Schluenzen F, *et al.* Translational Regulation via L11: Molecular Switches on the Ribosome Turned On and Off by Thiostrepton and Micrococcin. *Mol Cell* 2008; **30**: 26–38.
10. Thompson J, Cundliffe E, Stark MJR. The mode of action of berninamycin and the mechanism of resistance in the producing organism, *Streptomyces bernensis*. *J Gen Microbiol* 1982; **128**: 875–84.
11. Heffron SE, Jurnak F. Structure of an EF-Tu complex with a thiazolyl peptide antibiotic determined at 2.35 Å resolution: Atomic basis for GE2270A inhibition of EF- Tu. *Biochemistry* 2000; **39**: 37–45.
12. Cundliffe E. Mechanism of resistance to thiostrepton in the producing-organism *Streptomyces azureus*. *Nature* 1978; **272**: 792–5.
13. Bennallack PR, Bewley KD, Burlingame MA, *et al*. Reconstitution and minimization of a micrococcin biosynthetic pathway in *Bacillus subtilis*. *J Bacteriol* 2016; **198**: 2431–8.
14. Bennallack PR, Burt SR, Heder MJ, *et al.* Characterization of a novel plasmid-borne thiopeptide gene cluster in *Staphylococcus epidermidis* strain 115. *J Bacteriol* 2014; **196**: 4344–50.
15. Akasapu S, Hinds AB, Powell WC, *et al*. Total synthesis of micrococcin P1 and thiocillin I enabled by Mo(vi) catalyst. *Chem Sci* 2019; **10**: 1971–5.
16. Schwalen CJ, Hudson GA, Kille B, *et al*. Bioinformatic Expansion and Discovery of Thiopeptide Antibiotics. *J Am Chem Soc* 2018; **140**: 9494–501.
17. Stella S, Montanini N, Le Monnier F, *et al.* Antibiotic GE37468 A: A New Inhibitor of Bacterial Protein Synthesis: I. Isolation and Characterization. *J Antibiot (Tokyo)* 1995; **48**: 780–6.
18. Liao R, Duan L, Lei C, *et al.* Thiopeptide Biosynthesis Featuring Ribosomally Synthesized Precursor Peptides and Conserved Posttranslational Modifications. *Chem Biol* 2009; **16**: 141–7.

19. Brown LCW, Acker MG, Clardy J, *et al*. Thirteen posttranslational modifications convert a 14-residue peptide into the antibiotic thiocillin. *Proc Natl Acad Sci U S A* 2009; **106**: 2549–53.
20. Luo X, Zambaldo C, Liu T, *et al.* Recombinant thiopeptides containing noncanonical amino acids. *Proc Natl Acad Sci U S A* 2016; **113**: 3615–20.
21. Wang J, Lin Z, Bai X, *et al*. Optimal design of thiostrepton-derived thiopeptide antibiotics and their potential application against oral pathogens. *Org Chem Front* 2019; **6**: 1194–9.
22. LaMarche MJ, Leeds JA, Brewer J, *et al.* Antibacterial and Solubility Optimization of Thiomuracin A. *J Med Chem* 2016; **59**: 6920–8.
23. Qiu D, Damron FH, Mima T, *et al*. PBAD-based shuttle vectors for functional analysis of toxic and highly regulated genes in *Pseudomonas* and *Burkholderia* spp. and other bacteria. *Appl Environ Microbiol* 2008; **74**: 7422–6.
24. Ho SN, Hunt HD, Horton RM, *et al*. Site-directed mutagenesis by overlap extension using the polymerase chain reaction. *Gene* 1989; **77**: 51–9.
25. Hoang TT, Karkhoff-Schweizer RR, Kutchma AJ, *et al*. A broad-host-range F1p-FRT recombination system for site-specific excision of chromosomally-located DNA sequences: Application for isolation of unmarked *Pseudomonas aeruginosa* mutants. *Gene* 1998; **212**: 77–86.
26. New England Biosciences. *Protein Synthesis Reaction using PURExpress.* https://www.neb.ca/neb_protocols.php?p=protocols/0001/01/01/protein-synthesis-reaction-using-purexpress-e6800.
27. Luscher A, Moynie L, Auguste P Saint, *et al.* TonB-dependent receptor repertoire of *Pseudomonas aeruginosa* for uptake of siderophore-drug conjugates. *Antimicrob Agents Chemother* 2018; **62**: e00097-18.
28. Llamas MA, Sparrius M, Kloet R, *et al*. The heterologous siderophores ferrioxamine B and ferrichrome activate signaling pathways in *Pseudomonas aeruginosa*. *J Bacteriol* 2006; **188**: 1882–91.
29. Schalk IJ, Mislin GLA, Brillet K. Structure, Function and Binding Selectivity and Stereoselectivity of Siderophore-Iron Outer Membrane Transporters. *Curr Top Membr* 2012; **69**: 37–66.
30. Noinaj N, Guillier M, Barnard TJ, *et al.* TonB-dependent transporters: Regulation, structure, and function. *Annu Rev Microbiol* 2010; **64**: 43–60.
31. Cowles KN, Moser TS, Siryaporn A, *et al.* The putative Poc complex controls two distinct *Pseudomonas aeruginosa* polar motility mechanisms. *Mol Microbiol* 2013; **90**: 923–38.
32. Huang B, Ru K, Yuan Z, *et al*. tonB3 is required for normal twitching motility and extracellular assembly of type IV pili. *J Bacteriol* 2004; **186**: 4387–9.
33. Shirley M, Lamont IL. Role of TonB1 in pyoverdine-mediated signaling in *Pseudomonas aeruginosa*. *J Bacteriol* 2009; **191**: 5634–40.
34. Zhao Q, Poole K. A second tonB gene in *Pseudomonas aeruginosa* is linked to the exbB and exbD genes. *FEMS Microbiol Lett* 2000; **184**: 127–32.
35. Celia H, Botos I, Ni X, *et al.* Cryo-EM structure of the bacterial Ton motor subcomplex ExbB–ExbD provides information on structure and stoichiometry. *Commun Biol* 2019; **2**: 1–6.
36. Porse BT, Cundliffe E, Garrett RA. The antibiotic micrococcin acts on protein L11 at the ribosomal GTPase centre. *J Mol Biol* 1999; **287**: 33–45.
37. Degiacomi G, Personne Y, Mondésert G, *et al.* Micrococcin P1 – A bactericidal thiopeptide active against *Mycobacterium tuberculosis*. *Tuberculosis* 2016; **100**: 95–101.
38. Deatherage DE, Barrick JE. Identification of mutations in laboratory-evolved microbes from

next-generation sequencing data using breseq. *Methods Mol Biol* 2014; **1151**: 165–88.
39. Báumler AJ, Hantke K. Ferrioxamine uptake in *Yersinia enterocolitica*: characterization of the receptor protein FoxA. *Mol Microbiol* 1992; **6**: 1309–21.
40. Kingsley RA, Reissbrodt R, Rabsch W, *et al.* Ferrioxamine-mediated iron(III) utilization by *Salmonella enterica*. *Appl Environ Microbiol* 1999; **65**: 1610–8.
41. Nelson M, Carrano CJ, Szaniszlo PJ. Identification of the ferrioxamine B receptor, FoxB, in *Escherichia coli* K12. *Biometals* 1992; **5**: 37–46.
42. Holden VI, Wright MS, Houle S, *et al.* Iron Acquisition and Siderophore Release by Carbapenem-Resistant Sequence Type 258 *Klebsiella pneumoniae*. *mSphere* 2018; **3**: e00125-18.
43. Funahashi T, Tanabe T, Mihara K, *et al*. Identification and characterization of an outer membrane receptor gene in *Acinetobacter baumannii* required for utilization of desferricoprogen, rhodotorulic acid, and desferrioxamine B as xenosiderophores. *Biol Pharm Bull* 2012; **35**: 753–60.
44. Destoumieux-Garzón D, Duquesne S, Peduzzi J, *et al.* The iron-siderophore transporter FhuA is the receptor for the antimicrobial peptide microcin J25: Role of the microcin Val11-Pro16 β-hairpin region in the recognition mechanism. *Biochem J* 2005; **389**: 869–76.
45. Mathavan I, Zirah S, Mehmood S, *et al.* Structural basis for hijacking siderophore receptors by antimicrobial lasso peptides. *Nat Chem Biol* 2014; **10**: 340–2.
46. Salomon RA, Farias RN. The fhuA protein is involved in microcin 25 uptake. *J Bacteriol* 1993; **175**: 7741–2.
47. Salomon RA, Farias RN. The peptide antibiotic microcin 25 is imported through the tonB pathway and the SbmA protein. *J Bacteriol* 1995; **177**: 3323–5.
48. Novikova M, Metlitskaya A, Datsenko K, *et al.* The *Escherichia coli* Yej Transporter Is Required for the Uptake of Translation Inhibitor Microcin C. *J Bacteriol* 2007; **189**: 8361–5.
49. Mullane K, Lee C, Bressler A, *et al.* Multicenter, randomized clinical trial to compare the safety and efficacy of lff571 and vancomycin for *Clostridium difficile* infections. *Antimicrob Agents Chemother* 2015; **59**: 1435–40.
50. EU Clinical Trials Register. *Clinical efficacy and safety of NAI-Acne gel 3% applied twice-a-day to patients with facial acne vulgaris*. https://www.clinicaltrialsregister.eu/ctr-search/trial/2014-001491-62/SK.
51. Lentzen G, Klinck R, Matassova N, *et al*. Structural basis for contrasting activities of ribosome binding thiazole antibiotics. *Chem Biol* 2003; **10**: 769–78.
52. White P, Joshi A, Rassam P, *et al.* Exploitation of an iron transporter for bacterial protein antibiotic import. *Proc Natl Acad Sci U S A* 2017; **114**: 12051–6.
53. Elfarash A, Dingemans J, Ye L, *et al.* Pore-forming pyocin S5 utilizes the FptA ferripyochelin receptor to kill *Pseudomonas aeruginosa*. *Microbiol (United Kingdom)* 2014; **160**: 261–9.
54. Walter JD, Hunter M, Cobb M, *et al*. Thiostrepton inhibits stable 70S ribosome binding and ribosome-dependent GTPase activation of elongation factor G and elongation factor 4. *Nucleic Acids Res* 2012; **40**: 360–70.
55. Mikolajka A, Liu H, Chen Y, *et al.* Differential effects of thiopeptide and orthosomycin antibiotics on translational GTPases. *Chem Biol* 2011; **18**: 589–600.

Supplementary Figures

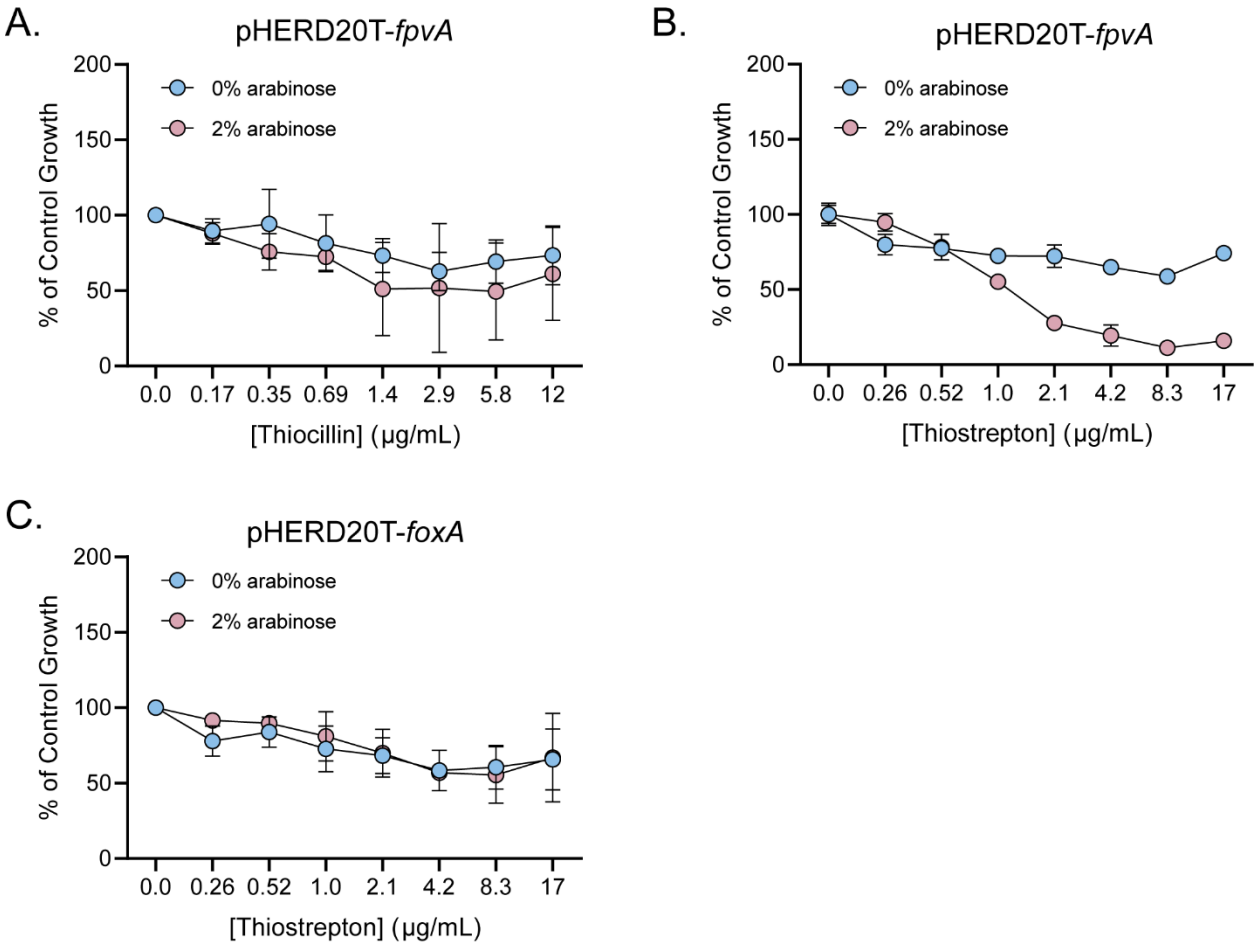

Supplementary Figure 1. FoxA is specific for TC and FpvA is specific for TS. DSX was not supplemented for these experiments. **A)** Overexpression of FpvA in PA14 in trans (pHERD20T-fpvA) does not increase susceptibility to TC. **B)** Overexpression of FpvA increases susceptibility to TS without DSX. **C)** Overexpression of FoxA in PA14 in trans (pHERD20T-foxA) does not increase susceptibility to TS. Results are averaged from three independent biological replicates.

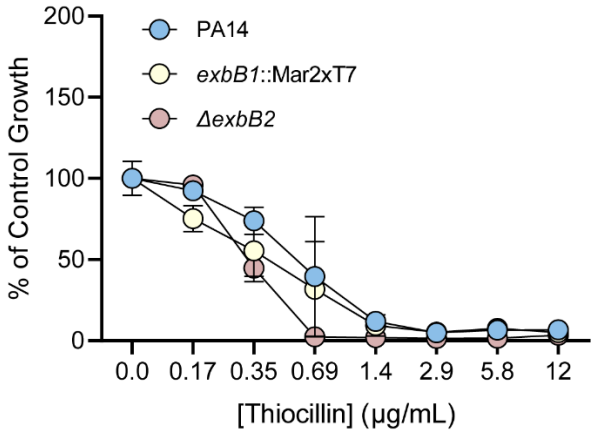

Supplementary Figure 2. PA14, *exbB1*, and *exbB2* mutants challenged with TC+DSX. DSX was supplemented at a constant concentration of 64μg/mL. Results are averaged from three independent biological replicates.

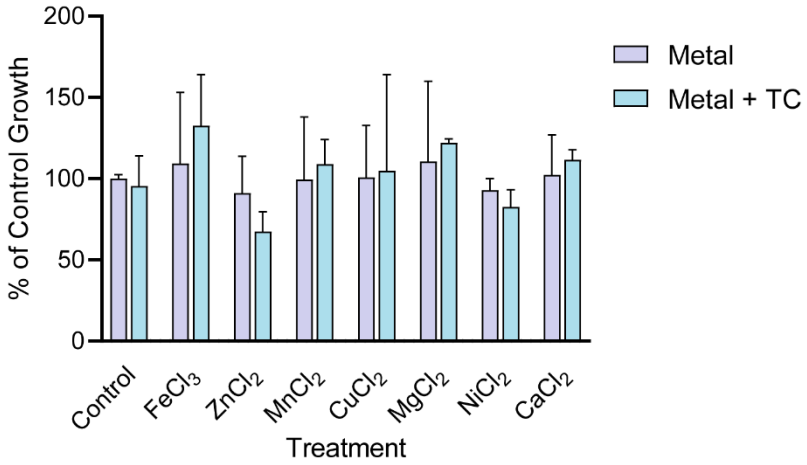

Supplementary Figure 3. Serum-free controls. PA14 challenged with 12μg/mL of TC in 10:90 and supplemented with 12.5μM of different metal salts. Results are averaged from three independent biological replicates.

Supplementary Tables

Supplementary Table 1. Strains used in this study.

Strain	Reference
P. aeruginosa PA14	[1]
P. aeruginosa PAO1	[2]
P. aeruginosa PA14 pHERD20T	This study
P. aeruginosa PA14 pHERD20T-*foxA*	This study
P. aeruginosa PA14 pHERD20T-*fpvA*	This study
P. aeruginosa PA14 *foxA*::Mar2xT7	[1]
P. aeruginosa PA14 *foxA*::Mar2xT7 pUCP20	This study
P. aeruginosa PA14 *foxA*::Mar2xT7 pUCP20-*foxA*	This study
P. aeruginosa PA14 *tonB1*::Mar2xT7	[1]
P. aeruginosa PA14 *tonB1*::Mar2xT7 pHERD20T	This study
P. aeruginosa PA14 *tonB1*::Mar2xT7 pHERD20T-*tonB1*	This study
P. aeruginosa PA14 *exbB1*::Mar2xT7	[1]
P. aeruginosa PA14 Δ*exbB2*	This study
P. aeruginosa PA14 pHERD20T-*tclT*	This study
P. aeruginosa PA14 pHERD20T-*rplK*	This study
P. aeruginosa PA14 pHERD20T-$rplK_{P26L}$	This study
P. aeruginosa PA14 Δ*fpvA fpvB*::Mar2xT7	[2]
P. aeruginosa C0379	[2]
P. aeruginosa PA7	Roy Lab
95 *P. aeruginosa* clinical isolates	[2]
Pseudomonas protegens Pf-5	Whitney Lab
Pseudomonas putida KT2440	Whitney Lab
Pseudomonas putida PP578	Whitney Lab
Pseudomonas fluorescens WCS374R	Whitney Lab
Pseudomonas fluorescens PV5	Whitney Lab
Pseudomonas marginalis CVCOB 1152	Whitney Lab
Bacillus cereus ATCC 14579	Whitney Lab
Klebsiella pneumoniae	Brown Lab
Escherichia coli K12 BW25113	[3]
Acinetobacter baumannii ATCC 17978	[2]
E. coli DH5α	This study
Salmonella enterica serovar Typhimurium SL1344	Coombes Lab

Supplementary Table 2. Primers used in this study. Restriction sites are underlined. Mutations are bolded.

Description	Primers 5' → 3'
tonB1 FWD	CAATGAATTCCTTACCTTTCACTTCTCCGCAGGT
tonB1 REV	CAATAAGCTTGGGAATAAAAAAACCGCGCTCGAA
exbB2 UP FWD	CAATTCTAGACCGGTGGAGTTGCGCGAGGAAGTG
exbB2 UP REV	CAATGCATGCGTCAGCGTCAGAAGCTCGCCTGC
exbB2 DOWN FWD	CAATGCATGCCGTTGCCGGCCTGAGGAGAACGCC
exbB2 DOWN REV	TTTAAGCTTCTGCAGGCGGAACGCCAGGTTGCG
tclT FWD	CCCTGAATTCATAAAAATTAAAGGGGATTTATAT

tclT REV	CCCTAAGCTTCCTTTAAAGAATCAAACTACTTTT
foxA FWD pUCP20	GAAGGAGCTCGTGGACGCTTGCTTTCGT
foxA REV pUCP20	GCGTTCTAGAGACGCCGGCGAATGCCC
foxA FWD pHERD20T	GAAGTCTAGAGTGGACGCTTGCTTTCGT
foxA REV pHERD20T	AATAAGCTTTCAGAACTGGTAGTTCACCGTC
fpvA FWD	AACCCGGGTAAGAAGAGCAATCACCC
fpvA REV	ACAAGCTTCAGAAGTCCCAGCGAGTGA
rplK FWD	CAATTCTAGAGGCGCTTGTACCCGAATTTGGAGT
rplK REV	CAATAAGCTTGGTCAGCTTAGCCATTACACA
$rplK_{P26L}$ FWD	GCCGGTCGGCC**TA**GCCCTG
$rplK_{P26L}$ REV	CAGGGC**TA**GGCCGACCGGC

Supplementary Table 3. Accession numbers for *rplK, fpvA, foxA,* and *tonB1*

Gene	Species	Accession number
rplK	*P. aeruginosa* PAO1	NP_252964.1
	P. aeruginosa PA14	YP_788845.1
	B. megaterium	KNH18684.1
	D. radiodurans	WP_010888678.1
	M. tuberculosis	CCP43383.1
	M. caseolyticus	AIU53943.1
	B. cereus	WP_001085924.1
fpvA	*P. aeruginosa* PA7	WP_012075666.1
	P. aeruginosa PAO1	NP_251088.1
	P. aeruginosa PA14	WP_003139291.1
foxA	*P. aeruginosa* PA7	WP_012075589.1
	P. aeruginosa PAO1	NP_251156.1
	P. aeruginosa PA14	WP_003116885.1
	P. aeruginosa PAO1	NP_254218.1

Supplementary Table 4. Panel of Transposon Mutants Used to Screen for TC and MC resistance. The *foxA* transposon mutant is highlighted.

Strain/mutant	Gene(s)	Function
fpvA::Mar2xT7	PA2398	Type 1 ferripyoverdine receptor
fpvB::Mar2xT7	PA4168	Alternate Type 1 ferripyoverdine receptor
Δ*fpvA fpvB*::Mar2xT7	PA2398, PA4168	Type I ferripyoverdine receptor, Alternate type I ferripyoverdine receptor
fptA::Mar2xT7	PA4221	Pyochelin receptor
PA1322::Mar2xT7	PA1322	Probable TonB-dependent receptor
PA4837::Mar2xT7	PA4837	Probable outer membrane protein precursor
***foxA*::Mar2xT7**	**PA2466**	**Ferrioxamine receptor FoxA**
fiuA::Mar2xT7	PA0470	Ferrichrome receptor FiuA
pirA::Mar2xT7	PA0931	Alternate enterobactin receptor
pfeA::Mar2xT7	PA2688	Enterobactin receptor
hasR::Mar2xT7	PA3408	Heme uptake outer membrane receptor
fvbA::Mar2xT7	PA4516	Vibriobactin receptor
piuA::Mar2xT7	PA4514	Hydroxamate-type ferrisiderophore receptor
PA0151::Mar2xT7	PA0151	Probable TonB-dependent receptor
chtA::Mar2xT7	PA4675	Aerobactin, Rhizobactin 1021, Schizokinen receptor
phuR::Mar2xT7	PA4710	Heme/Hemoglobin uptake receptor precursor

Chapter Five: Interactions of TonB-dependent Transporter FoxA with Siderophores and Antibiotics that Affect Binding, Uptake, and Signal Transduction

Preface

The work presented in the following chapter has been published in the *Proceedings of the National Academy of Sciences* (PNAS):

Chan D. C. K., Josts, I., Koteva, K., Wright, G. D., Tidow, H., and Burrows, L. L. (2023). Interactions of TonB-dependent Transporter FoxA with Siderophores and Antibiotics that Affect Binding, Uptake, and Signal Transduction. 120 (16) e2221253120. https://doi.org/10.1073/pnas.2221253120

D.C.K.C. and L.L.B. designed the experiments and wrote the draft manuscript. K.K. and G.D.W. helped with method development for the thiocillin uptake study and K.K. performed mass spectrometry on initial samples. I.J. isolated and purified FoxA for crystallization with bisucaberin and determined the structure. D.C.K.C. and L.L.B. wrote the manuscript and all authors provided editorial input on the final manuscript.

Abstract

The outer membrane of Gram-negative bacteria prevents many antibiotics from reaching intracellular targets. However, some antimicrobials can take advantage of iron import transporters to cross this barrier. We showed previously that the thiopeptide antibiotic thiocillin exploits the nocardamine xenosiderophore transporter, FoxA, of the opportunistic pathogen *Pseudomonas aeruginosa* for uptake. Here we show that FoxA also transports the xenosiderophore bisucaberin and describe at 2.5 Å resolution the first crystal structure of bisucaberin bound to FoxA. Bisucaberin is distinct from other siderophores because it forms a 3:2 rather than 1:1 siderophore-iron complex. Mutations in a single extracellular loop of FoxA differentially affected nocardamine, thiocillin, and bisucaberin binding, uptake, and signal transduction. These results show that in addition to modulating ligand binding, the extracellular loops of siderophore transporters are of fundamental importance for controlling ligand uptake and its regulatory consequences, which has implications for the development of siderophore-antibiotic conjugates to treat difficult infections.

Significance

Iron is an essential nutrient for bacteria but has poor bioavailability in the environment and in host organisms due to its sequestration and low solubility. To overcome this challenge, bacteria synthesize high-affinity iron-binding molecules called siderophores, which are recognized by specific transporters on the cell surface. Trojan horse antibiotics have evolved to hijack these transporters for uptake across the outer membrane. Here, we report the first structure of the *P. aeruginosa* nocardamine transporter FoxA bound to the xenosiderophore, bisucaberin. The interactions revealed by this co-structure help to explain how the thiopeptide antibiotic thiocillin may bind FoxA. We identify distinct residues important for ligand discrimination and recognition,

uptake, and signaling, and show that a conserved extracellular loop controls access to FoxA, allowing thiocillin to breach the outer membrane barrier.

Introduction

Iron is an essential micronutrient for bacteria, involved in biofilm formation (1), virulence factor production (2), and colonization and infection (3). Bacteria have evolved ways to survive in iron-limited conditions such as those encountered at sites of infection (4, 5). One common strategy includes the production and release of siderophores into the environment. Siderophores are natural products with high affinity for iron, and ferri-siderophore complexes are taken up via specific transporters in the outer membrane (OM) (6–9). The opportunistic human pathogen, *P. aeruginosa,* makes two main siderophores, pyoverdine and pyochelin (10–12) and mutants deficient in production of those siderophores are unable to grow in iron-limited conditions (6). Transport of siderophores into the cell is an energy-dependent process (7). The inner membrane TonB-ExbD-ExbD complex (**Fig. 1A**) couples the proton motive force (PMF) to TonB-dependent transporters (TBDTs) (14, 15), 22-stranded β-barrel proteins normally occluded by a central plug domain that prevents nonspecific diffusion. *P. aeruginosa* encodes dozens of predicted TBDTs that recognize native siderophores and xenosiderophores produced by other microorganisms.

Extracellular loops connecting the β-strands of TBDTs are involved in ferri-siderophore recognition (7). Upon ligand binding, the transporter undergoes conformational changes, including the inward movement of an extracellular loop (13, 16) and exposure of a TonB-box motif on the periplasmic face of the plug that interacts with TonB (13). Some transporters also have an extended periplasmic N-terminus containing a signaling domain (17–19). In a feed-forward loop, ligand uptake via the transporter triggers the release of a σ/anti-σ pair that recruits RNA polymerase to the promoter of the relevant TBDT (20) to increase expression.

Some bacteriophages (21), bacteriocins (22, 23), lassopeptides (24, 25), and antibiotics (26, 27) use TBDTs to cross the OM, although the details of uptake remain unclear. The ability of TBDT-dependent antimicrobials to bypass the OM barrier, coupled with their narrow-spectrum activity, makes them interesting candidates for human use. Previously, we showed that the thiopeptide antibiotic thiocillin requires the FoxA transporter to inhibit growth of *P. aeruginosa* (28) (**Fig. 1A**). Thiocillin is a cyclic thiazole-containing antibiotic (**Fig. 1B**) that binds the ribosome at the interface of the L11 protein and elongation factor G to inhibit protein synthesis (29). FoxA is the TBDT for the siderophores ferrioxamine B and nocardamine (ferrioxamine E) (6, 13, 20) (**Fig. 1B**), which prior to our work were its only known ligands. This work focuses on nocardamine as it exclusively uses FoxA for uptake (6) whereas ferrioxamine B uses both FoxA and FpvB (30). *P. aeruginosa* FoxA has an extended N-terminus containing a signaling domain (19, 20) involved in upregulating FoxA expression in response to ligand binding through release of anti-σ/σ factor pair FoxI/FoxR (18, 20). However, the way in which thiocillin interacts with FoxA and whether it triggers conformational changes and signaling events similar to those induced by nocardamine are unknown.

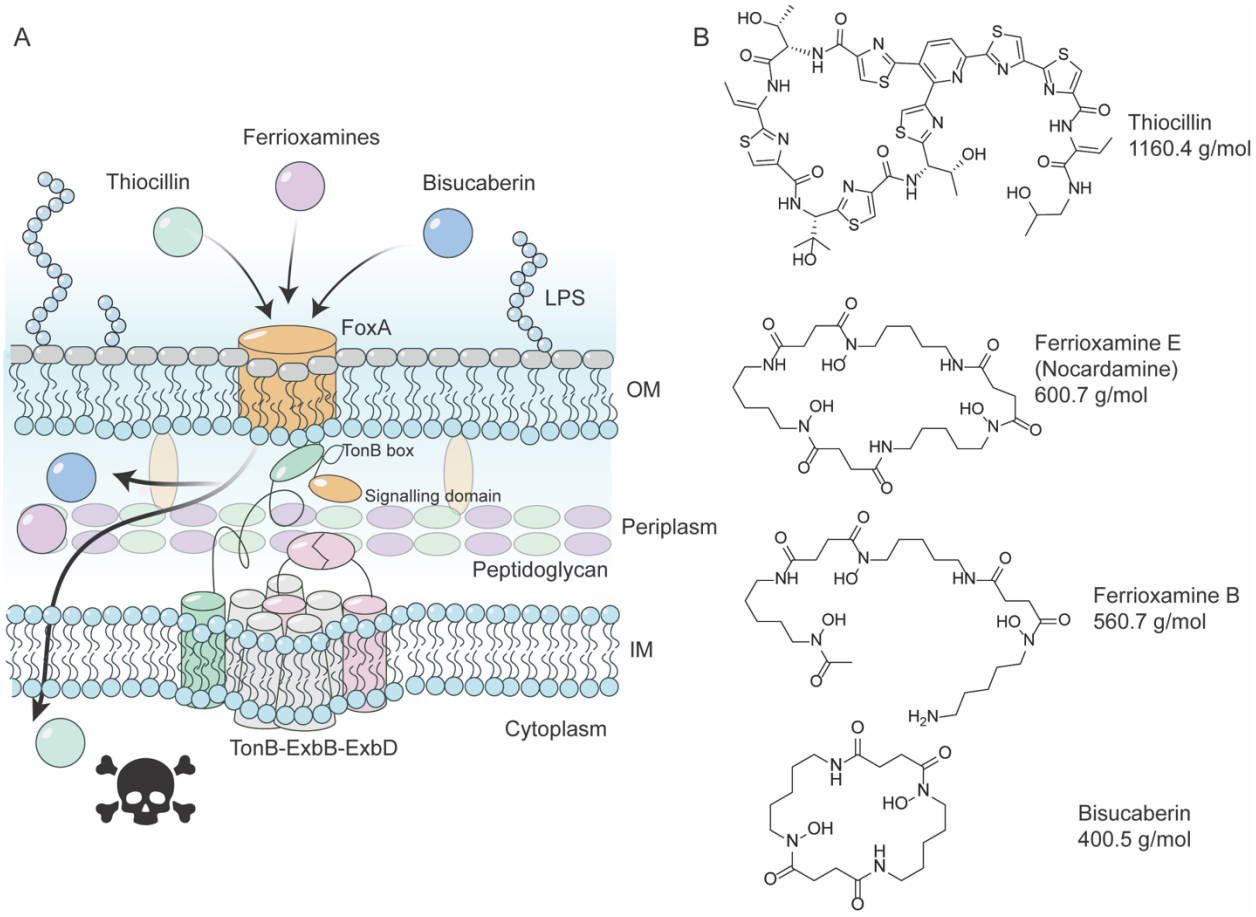

Figure 1. Thiocillin and siderophores use FoxA to cross the outer membrane. (**A**) Model of thiocillin and siderophore uptake. OM = outer membrane. IM = inner membrane. LPS = lipopolysaccharide. (**B**) Structures of thiocillin, nocardamine, ferrioxamine B, and bisucaberin. Siderophores are shown in their apo states.

Here we show that binding, uptake, and signaling through FoxA depends on the nature of the ligand and is controlled by a mobile extracellular loop. Besides thiocillin and nocardamine, FoxA also acts as a low-affinity transporter for the nocardamine-like hydroxamate siderophore, bisucaberin (**Fig. 1B**). The co-crystal structure of a 3:2 bisucaberin-iron complex with FoxA was determined at 2.5 Å resolution (31), showing that bisucaberin mimics the binding conformation of nocardamine but interacts with unique residues, similar to thiocillin. Despite these differences, we show that extracellular loop 8 (L8) of FoxA modulates uptake and signaling for all three ligands.

The conservation of this loop configuration among TBDTs suggests that it may play a similar role in other transporters.

Results

Bisucaberin exclusively uses the FoxA receptor for uptake

Our previous discovery that thiocillin could use FoxA to cross the outer membrane of *P. aeruginosa* (28) suggested that the transporter could recognize multiple ligands. To better understand the scope of FoxA ligand recognition, we next tested if siderophores other than the ferrioxamines were taken up. This search led us to bisucaberin, which belongs to a family of dihydroxamate siderophores. Unlike the 1:1 nocardamine:iron complex, bisucaberin forms a 3:2 complex at physiological pH (31) which might impact its recognition by FoxA (**Fig. 2A**). To determine if bisucaberin could be used by *P. aeruginosa*, we generated a mutant unable to make native siderophores pyoverdine and pyochelin, Δ*pvdA* Δ*pchA.* This mutant requires exogenously-supplemented siderophores to grow in iron-limited media (30). Δ*pvdA* Δ*pchA* grew in iron-limited casamino acids (CAA) media when provided with bisucaberin, suggesting that the siderophore was taken up (**Fig. 2B**). Next, we wanted to identify the transporter for bisucaberin. A previous study suggested that alcaligin, a similar dihydroxamate siderophore to bisucaberin, may be taken up via the uncharacterized transporter PA14_46640 (32). To identify the transporter for bisucaberin, we deleted *PA14_46640* or *foxA* in the Δ*pvdA* Δ*pchA* background and grew the mutants with bisucaberin (**Fig. 2B**). The Δ*pvdA* Δ*pchA* Δ*PA14_46640* triple mutant grew similarly to Δ*pvdA* Δ*pchA* when provided with bisucaberin; however, loss of *foxA* prevented growth, suggesting that bisucaberin uses FoxA exclusively for uptake in the absence of pyoverdine and pyochelin.

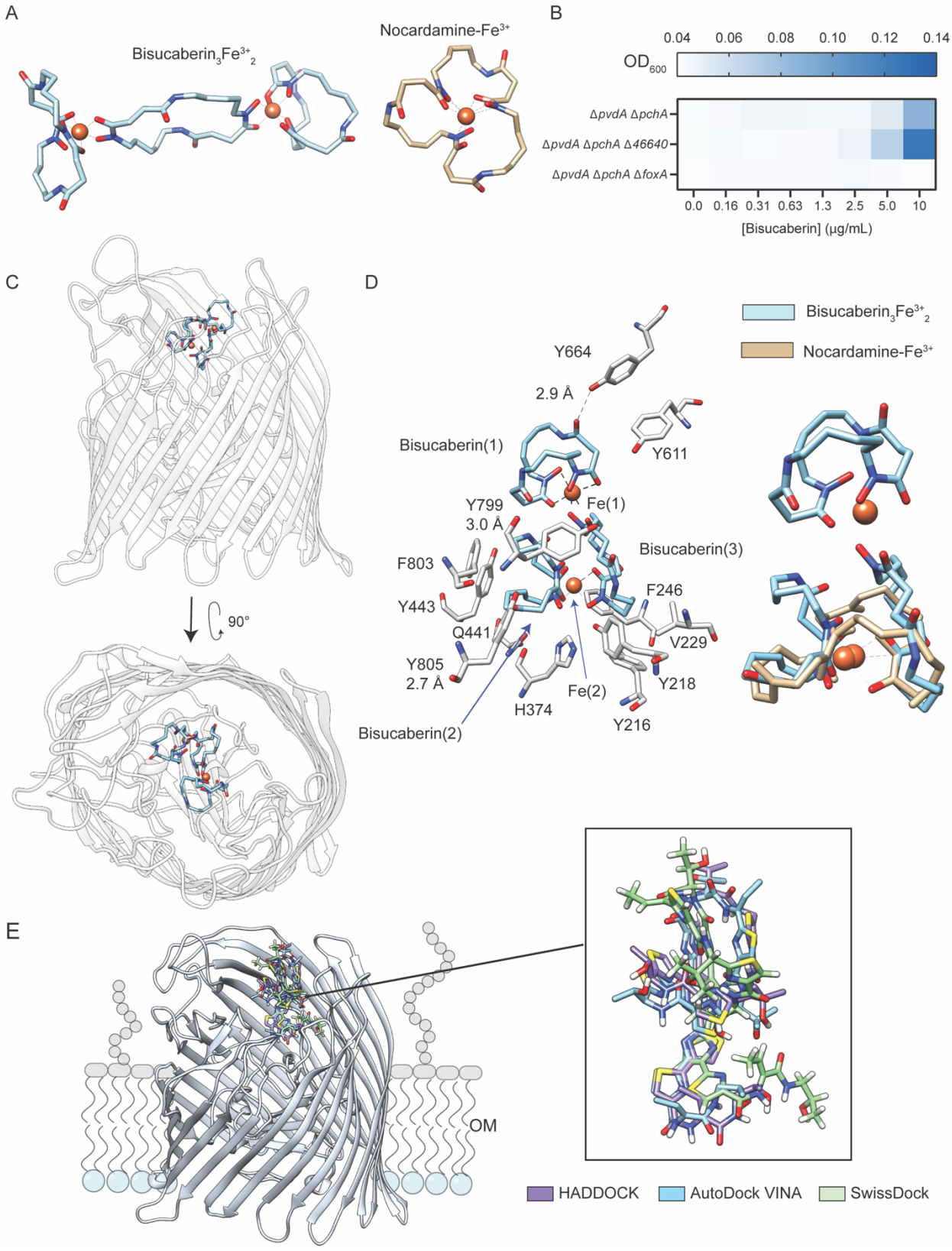

Figure 2. Bisucaberin is taken up through FoxA. (**A**) Structures of bisucaberin (left) and nocardamine (right) iron complexes modeled based on the mono-bridged complex of ferri-

bisucaberin and PDB: 6Z8A with FoxA removed respectively. Heteroatoms are in different colours: blue: nitrogen, red: oxygen, and Fe^{3+} is depicted as an orange sphere. (**B**) Growth recovery of PA14 Δ*pvdA* Δ*pchA,* Δ*pvdA* Δ*pchA* Δ*PA14_46640*, and Δ*pvdA* Δ*pchA* Δ*foxA* treated with bisucaberin in CAA supplemented with increasing concentrations of bisucaberin. Legend shows OD_{600} where blue indicates growth and white indicates no growth. (**C**) Structure of bisucaberin$_3$-Fe^{3+}_2 bound to FoxA. Side view (top) and bird's-eye view (bottom) are shown. (**D**) Binding pocket interactions of bisucaberin$_3$-Fe^{3+}_2 (orange) with FoxA (left) and overlay with FoxA-bound nocardamine-Fe^{3+} (orange; right) are shown. Nocardamine-Fe^{3+} structure from PDB:6Z8A was used for this comparison. Distances for H-bonding residues are shown. (**E**) Superimposed docking predictions of thiocillin with apo-FoxA (PDB 6I97). Stick models of thiocillin docked into FoxA (ribbon) using different docking algorithms are shown in purple (HADDOCK), blue (AutoDock VINA), and green (SwissDock). All three docking simulations converge at a similar binding site. Heteroatoms are depicted as different colours.

To determine if molecular interactions of bisucaberin with FoxA resembled those of nocardamine, we determined, at 2.5Å resolution, the crystal structure of bisucaberin bound to FoxA (PDB: 8B43) (**Fig. 2C**, **SI Appendix Fig. S1, SI Appendix Table S1**). Bisucaberin$_3$-Fe^{3+}_2 binds FoxA in a C-shape, unlike its linear configuration in the unbound form (**Fig. 2D**). Like nocardamine and ferrioxamine B, bisucaberin$_3$-Fe^{3+}_2 forms a H-bond with Y805. Rings 2 and 3 of the bisucaberin complex contact the plug and barrel domains whereas ring 1 protrudes outwards and forms a second H-bond with Y664 (Loop 8). A third H-bond is formed between ring 3 and Y799. Nocardamine-Fe^{3+} from PDB:6Z8A was then overlaid with bisucaberin$_3$-Fe^{3+}_2 to highlight any differences in their orientation with respect to FoxA (**Fig. 2D**). Interestingly, rings 2 and 3 of bisucaberin closely mimic the position of nocardamine, with the iron atoms superimposing one another. The hydroxamate moieties involved in chelation are also in similar orientations. Overall, the bisucaberin$_3$-Fe^{3+}_2 complex binds FoxA in a similar position as nocardamine-Fe^{3+}; but forms different H-bonds, and ring 1 interacts with L8, which is not seen with nocardamine.

At least five residues in FoxA are essential for thiocillin susceptibility

We previously showed that thiocillin used FoxA to cross the outer membrane and inhibit growth of *P. aeruginosa*, which prompted us to try co-crystallization. After only apo-FoxA was recovered, we switched to a molecular docking approach to probe the potential interactions between thiocillin and FoxA. Docking simulations using AutoDock VINA (33, 34), SwissDock (35), and HADDOCK (36) were compared (**Fig. 2E**). All three algorithms predicted that thiocillin binds in the same region of FoxA as nocardamine and bisucaberin, with AutoDock VINA and HADDOCK predicting similar poses. Therefore, subsequent experiments to verify predicted interactions by site-directed mutagenesis were based on those results (**Fig. 3A**). Using a low copy number arabinose-inducible expression vector, pHERD20T (37), 83 single residue mutant FoxA transporters were generated based on the predictions, expressed in a *P. aeruginosa* PA14 Δ*foxA* background, and screened for a) restoration of thiocillin susceptibility in 10:90 medium, and b) the ability to grow in iron-limited casamino acids (CAA) medium supplemented with nocardamine. Mutants unable to make FoxA are resistant to thiocillin (28) and growth is inhibited by nocardamine through iron restriction since they cannot take up the siderophore. Complementation with wild-type (WT) FoxA restores thiocillin susceptibility and growth with nocardamine. The mutant FoxA transporters were also expressed in Δ*pvdA* Δ*pchA* Δ*foxA* to look for growth restoration with bisucaberin.

Y664A, P659L, K657A (L8), W503S (barrel), and H374Y (loop 3) mutants failed to restore thiocillin susceptibility (**Fig. 3B**), allowed growth with nocardamine (**Fig. 3C**), and either prevented growth recovery or required higher bisucaberin concentrations for growth (**Fig. 3D**). The data were consistent with the docking predictions, where W503 interacts with the pyridine ring of thiocillin through π-stacking (**Fig. 3E**). Unexpectedly, truncation of $L8_{K657\text{-}T665}$ was permissive for thiocillin uptake but prevented growth with nocardamine and bisucaberin (**Fig. 3B-**

D). The site-directed mutagenesis data were consistent with the bisucaberin structural data. FoxA Y664A prevented growth with bisucaberin, supported by the observation that ring 1 forms a H-bond with this residue. H374, which forms a H-bond with nocardamine-Fe^{3+} is in the same binding pocket as the bisucaberin complex. H374Y may displace bisucaberin$_3$-$Fe^{3+}{}_2$ in the pocket, reducing its interactions with other side chains. Compared to the strain expressing WT FoxA, those expressing P659L or W503S required at least a 4-fold increase in bisucaberin to restore growth. These results further highlight the differences in ligand recognition, although there may be some overlap between the molecular determinants for thiocillin and bisucaberin uptake.

To verify stability of the mutant transporters, WT FoxA was tagged with V5 or FLAG epitope tags at one of 32 different locations to identify functionally permissive sites, and each variant tested in the Δ*foxA* background for restoration of WT levels of thiocillin susceptibility and growth with nocardamine (**SI Appendix Fig. S2**). Then, each point mutant transporter was similarly tagged to monitor expression levels. T755-V5 and D570-FLAG variants were selected for monitoring because the tags were in loops distinct from those containing residues important for thiocillin uptake. Outer-membrane fractions were isolated and the levels of WT and mutant transporters assessed by Western blot (**Fig. 3F-G**). PilF, an outer membrane lipoprotein necessary for type IV pilus secretin localization and multimerization (38) was used as a loading control. Although Y664A T755-V5, and P659L D570-FLAG could not be detected, the alternately tagged Y664A D570-FLAG and P659L T755-V5 were detectable, confirming that they are expressed. All other receptors were expressed at levels similar to the tagged WT.

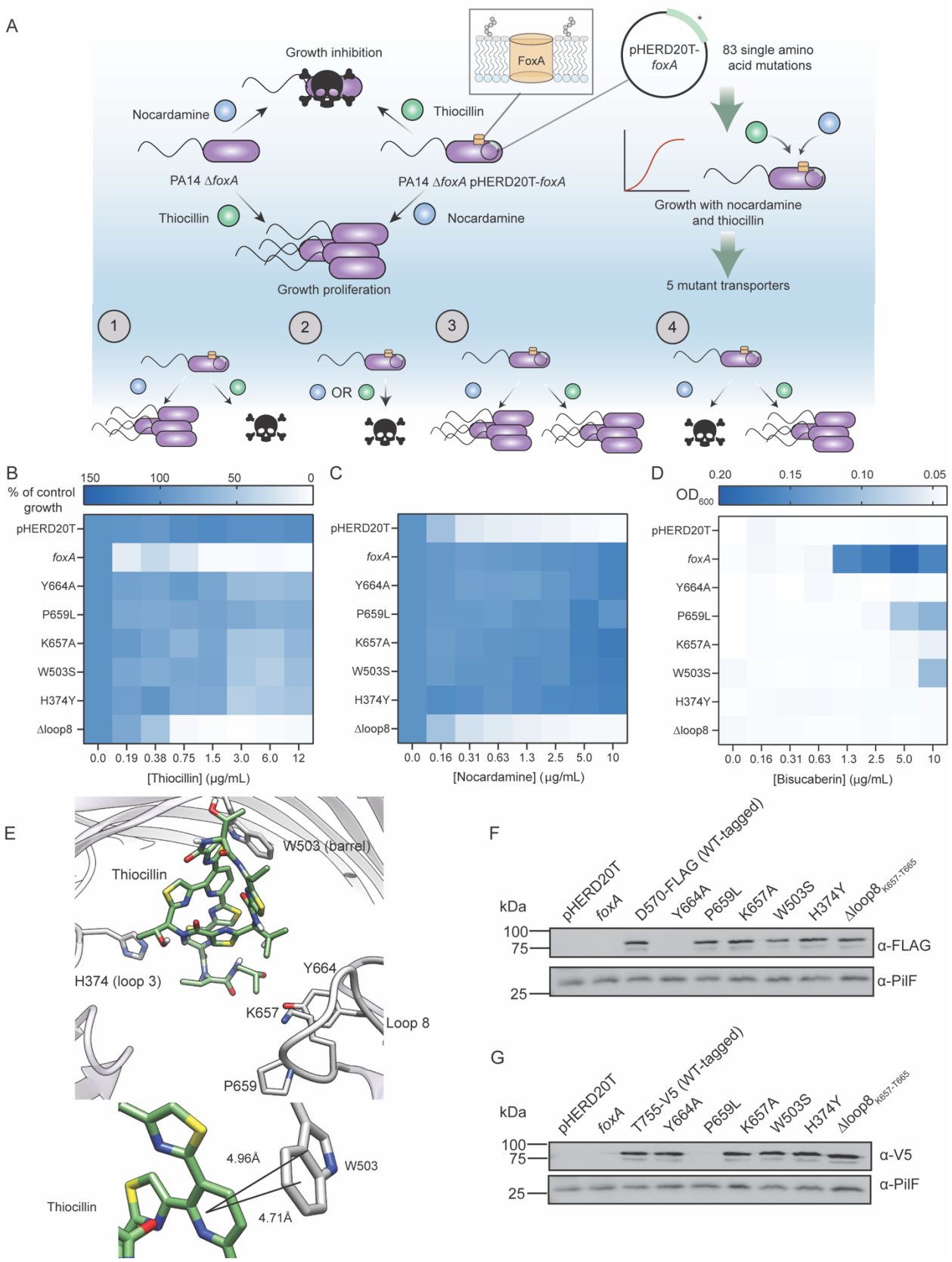
A
Growth inhibition
Nocardamine
Thiocillin
FoxA
pHERD20T-foxA
83 single amino acid mutations
PA14 ΔfoxA
PA14 ΔfoxA pHERD20T-foxA
Thiocillin
Nocardamine
Growth with nocardamine and thiocillin
Growth proliferation
5 mutant transporters
1
2
3
4
OR
B
% of control growth
150 100 50 0
pHERD20T
foxA
Y664A
P659L
K657A
W503S
H374Y
Δloop8
0.0 0.19 0.38 0.75 1.5 3.0 6.0 12
[Thiocillin] (μg/mL)
C
0.0 0.16 0.31 0.63 1.3 2.5 5.0 10
[Nocardamine] (μg/mL)
D
OD600
0.20 0.15 0.10 0.05
0.0 0.16 0.31 0.63 1.3 2.5 5.0 10
[Bisucaberin] (μg/mL)
E
W503 (barrel)
Thiocillin
H374 (loop 3)
Y664
K657
Loop 8
P659
4.96Å
W503
Thiocillin
4.71Å
F
kDa
pHERD20T
foxA
D570-FLAG (WT-tagged)
Y664A
P659L
K657A
W503S
H374Y
Δloop8K657-T665
100
75
25
α-FLAG
α-PilF
G
kDa
pHERD20T
foxA
T755-V5 (WT-tagged)
Y664A
P659L
K657A
W503S
H374Y
Δloop8K657-T665
100
75
25
α-V5
α-PilF

Figure 3. Identifying FoxA residues important for thiocillin, nocardamine, and bisucaberin uptake. (**A**) Schematic depicting dual growth phenotype screening for the identification of single residues important for nocardamine and thiocillin uptake through FoxA. In iron-limited media, *P. aeruginosa* Δ*foxA* is susceptible to growth inhibition by nocardamine but resistant to thiocillin. Complementation of the mutant in trans with a WT copy of foxA restores growth with nocardamine and susceptibility to thiocillin. Based on the docking simulations, 83 single amino acid mutations hypothesized to be important for ligand interaction were made and expressed in trans for screening. Of these mutant transporters, five failed to restore thiocillin susceptibility but supported growth with nocardamine. From the screen, four categories of mutant were observed. Category 1: the transporter permits uptake of both ligands similar to WT. Category 2: the transporter restores thiocillin susceptibility but does not support growth with nocardamine. Category 3: the transporter does not restore thiocillin susceptibility but supports growth with nocardamine. Category 4: the transporter is either not expressed or non-functional. (**B**) Thiocillin MIC assays with ΔfoxA expressing WT or mutant FoxA transporters and (**C**) nocardamine growth assays. (**D**) Growth recovery of Δ*pvdA* Δ*pchA* Δ*foxA* overexpressing different FoxA mutant transporters treated with bisucaberin. A darker shade of blue indicates more growth and a lighter shade, less growth. White indicates no growth. Growth is expressed as percent of control of the vehicle control (DMSO). Results are an average of three biological replicates. (**E**) (Top) Stick model of thiocillin docked into FoxA (ribbon model) with residues identified as important for thiocillin activity shown. (Bottom) A zoomed-in view of the predicted interaction between the central pyridine ring of thiocillin and FoxA W503 with distances shown. (**F and G**) Blots of WT and mutant FoxA expression in trans. Empty vector and unlabeled WT-FoxA were included as negative controls. Internal FLAG (D570FLAG) and V5 (T755V5) tagged WT and mutant FoxA receptors are expressed at similar levels. PilF was used as a loading control for outer membrane proteins.

Siderophores compete with thiocillin for binding and uptake

Thiocillin is predicted to bind in the same pocket as nocardamine and bisucaberin (**Fig. 4A-C**), suggesting that ligands could compete for the transporter. Consistent with this prediction, antagonism was observed in checkerboard assays with thiocillin and nocardamine-Fe^{3+} against Δ*foxA* complemented with WT FoxA *in trans* (**Fig. 4B**) and with thiocillin and bisucaberin-Fe^{3+} against Δ*pvdA* Δ*pchA* Δ*foxA* complemented with WT FoxA *in trans* (**Fig. 4C**). Apo-nocardamine also antagonized thiocillin uptake, although >100-fold higher concentrations were required compared to the iron-bound form (**SI Appendix Fig. S3A**). Thiocillin antagonism was observed only with nocardamine and bisucaberin, not other siderophores, supporting the model of competition for similar binding sites (**SI Appendix Fig. S3B-D**).

A FoxA whole-cell fluorescent sensor was developed to detect nocardamine-Fe^{3+} binding and uptake. Previous studies used site-specific cysteine labeling to incorporate fluorescein-5-maleimide at extracellular loops to detect ligand binding (39, 40). The fluorescence of the labeled TBDT can be quenched with increasing concentrations of siderophore-Fe^{3+} due to conformational changes that alter the environment surrounding the fluorophore. Comparison of apo- and ferrioxamine B-bound FoxA structures showed that loop 7 (L7) and L8 fold downwards toward the ligand upon binding (**Fig. 4D**, **SI Appendix Fig. S4A**) (13); therefore, 19 amino acid residues in those loops were individually mutated to Cys and screened for those that could be labeled for detection (**SI Appendix Fig. S4A**). The Cys-substituted transporters were expressed in the Δ*foxA* background and screened for functionality based on their ability to complement thiocillin susceptibility and growth with nocardamine (**SI Appendix Fig. S4B-C**). Of 17 functional Cys point mutants, we observed fluorescence quenching by nocardamine-Fe^{3+} for Q660C (L8) and A614C (L7) (**SI Appendix Fig. S4D**). Fluorescence of labeled A614C and Q660C FoxA was significantly greater than WT FoxA and labeling did not affect thiocillin susceptibility (**SI Appendix Fig. S4E-F**). A614C was selected for further experiments to avoid potential steric interactions with residues important for thiocillin uptake. Interestingly, no fluorescence quenching was observed for thiocillin or apo-nocardamine even at 12µg/mL (10µM) and 200µg/mL respectively, suggesting that the two ligands induce conformational changes different from those caused by nocardamine-Fe^{3+} (**SI Appendix Fig. S4G-H**). A614C-labeling was specific, as fluorescence was localized to the periphery of cells (**Fig. 4E**). A614C was then introduced into the FoxA binding pocket mutants and expressed in Δ*foxA* to confirm that the Cys mutation had no impact on their profile of thiocillin susceptibility and growth with nocardamine (**SI Appendix Fig. S5A-B**).

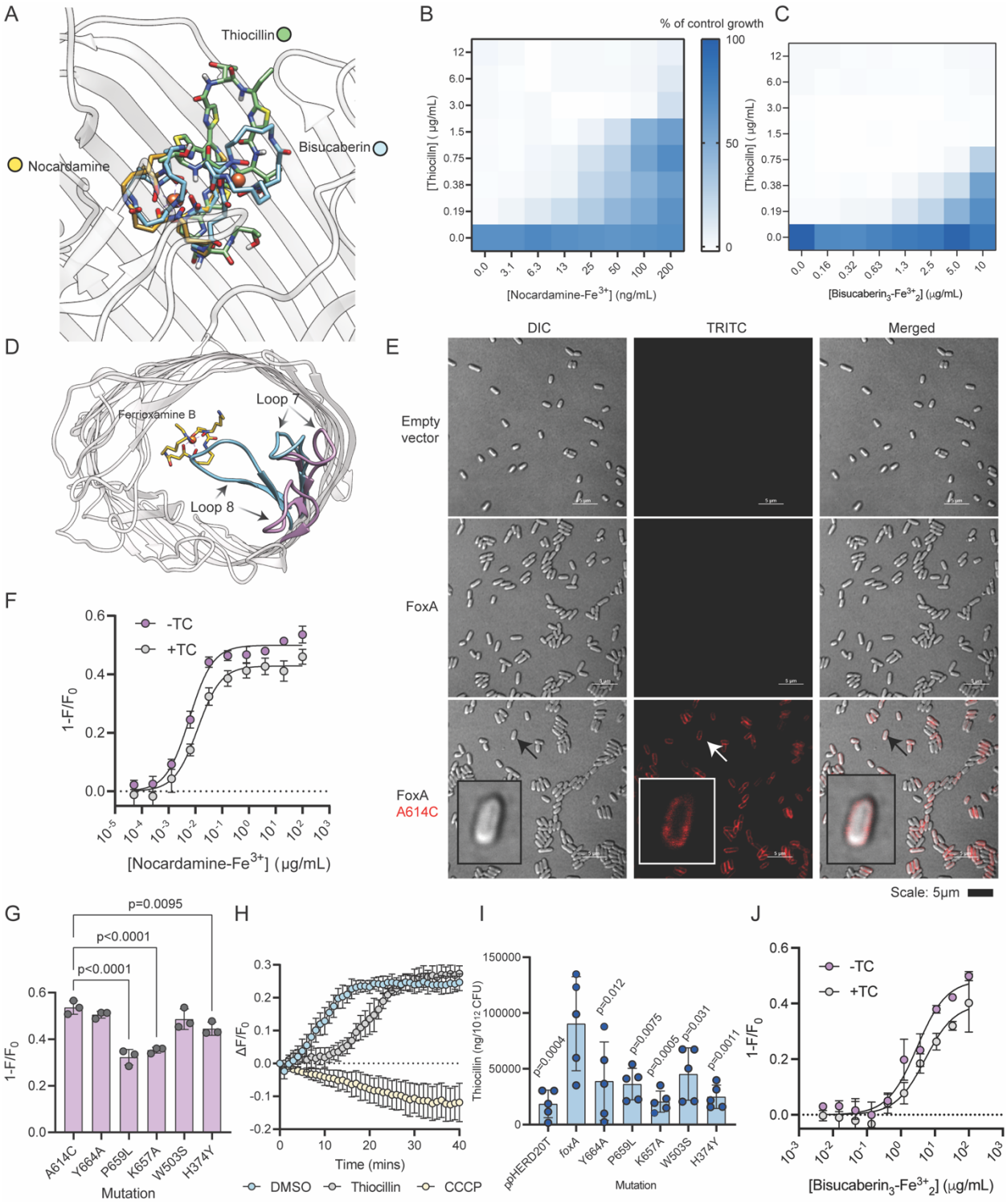

Figure 4. Thiocillin competes with nocardamine-Fe^{3+} for FoxA. (**A**) Superimposed structures of nocardamine-Fe^{3+} (PDB:6Z8A), bisucaberin, and thiocillin (AutoDock Vina) in FoxA. All compounds are shown as stick models, with nocardamine in yellow, bisucaberin in blue, and thiocillin in green. (**B**) Checkerboard assay of PA14 ΔfoxA pHERD20T-foxA treated with thiocillin and nocardamine-Fe^{3+}. (**C**) Checkerboard assay with PA14 Δ*pvdA* Δ*pchA* Δ*foxA* pHERD20T-*foxA* treated with thiocillin and bisucaberin-Fe^{3+} in 10:90 + 1% arabinose. Results are

averaged from three independent biological replicates. (**D**) L7 and L8 movement upon ferrioxamine B-Fe^{3+} binding (PDB 6I96 and 6I97). Purple loops indicate the orientation prior to ferri-siderophore binding while blue loops indicate the orientation after binding. (**E**) Fluorescence microscopy images of PA14 Δ*foxA* with pHERD20T, foxA, or foxA A614C labeled with AlexaFluor 594. Inset: zoomed-in view of a single labeled cell. Scale bar is 5μm. (**F**) Fluorescence quenching of A614C-labeled FoxA after the addition of nocardamine-Fe^{3+} without thiocillin pre-treatment (purple) or with thiocillin pre-treatment (grey). Results are averaged from three independent biological replicates. K_d was calculated in GraphPad Prism with a one-site binding model. A614C is highlighted in red to indicate the labeled residue. (**G**) Fluorescence quenching of A614C-labeled FoxA at 100 μg/mL nocardamine-Fe^{3+} in the absence of thiocillin pre-treatment. Statistics were calculated with GraphPad Prism using one-way ANOVA followed by Dunnett's test; p values are shown. Results from three independent biological replicates are shown. (**H**) Fluorescence recovery of PA14 Δ*foxA* pHERD20T-*foxA* A614C labeled with fluorescein-5-maleimide treated with 6.4 ng/mL nocardamine-Fe^{3+} with DMSO (blue), 12 μg/mL (10 μM) thiocillin (grey), and 100 μM CCCP. Results are averaged from three independent biological replicates. (**I**) Uptake of thiocillin through FoxA or its single amino acid mutants. Thiocillin concentrations are normalized to ng of thiocillin per 10^{12} CFU. Results were averaged from five independent biological replicates. Statistics were calculated with GraphPad Prism using one-way ANOVA followed by Dunnett's test; p-values are shown. (**J**) Fluorescence quenching of PA14 Δ*pvdA* Δ*pchA* Δ*foxA* pHERD20T-*foxA* A614C with bisucaberin-Fe^{3+} in the absence (purple) and presence (grey) of thiocillin.

In the absence of thiocillin, the K_d of nocardamine-Fe^{3+} was 6.0 ± 0.62 ng/mL (**Fig. 4F**, **SI Appendix Table S2**). Since thiocillin failed to quench fluorescence, we could isolate its impact on the binding affinity of nocardamine-Fe^{3+}. Pre-treating cells with 12μg/mL thiocillin for 5 min increased the K_d to 12 ± 1.8 ng/mL, indicating weak competition, consistent with the results of checkerboard assays that demonstrated antagonism between the two ligands. As a control, 11 μg/mL (10 μM) of geninthiocin A, a thiopeptide that lacks activity against *P. aeruginosa,* was tested; the K_d was similar to that of nocardamine-Fe^{3+} alone (**SI Appendix Fig. S5C**).

The effects on K_d of the single residue mutations and the L8 deletion were also determined using A614C labeled transporters (**SI Appendix Fig. S5D-I, SI Appendix Table S2, SI Appendix Fig. S6**). The K_d of nocardamine-Fe^{3+} for Y664A, P659L, K657A, and W503S was similar to WT in the absence of thiocillin (**SI Appendix Fig. S5D-H, SI Appendix Table S2**); however, H374Y increased the K_d 26-fold. This increase was expected because H374 forms a H-bond with the hydroxamate side chain of nocardamine (6, 13). Thiocillin pre-treatment increased the K_d of

nocardamine-Fe^{3+} for all the single residue mutants. P659L and K657A had 14- and 8-fold increases with thiocillin treatment, respectively, compared to WT (**SI Appendix Table S2**). Unexpectedly, P659L and K657A also showed significantly reduced quenching, possibly due to reduced loop movement since the K_ds are similar to the WT (**Fig. 4G**, **SI Appendix Table S2**). $FoxA_{\Delta K657\text{-}T665}$ could still bind nocardamine-Fe^{3+} with a 14-fold increase in K_d even though uptake of the ferri-siderophore was compromised (**Fig. 3C, SI Appendix Fig. S5I, SI Appendix Table S2**).

Thiocillin competed with nocardamine for uptake as well as binding. Fluorescence recovery was used as an indicator of uptake (40) as the protein reverts to the apo-state once the siderophore is released into the periplasm. As a control, cells were also incubated with 100 μM carbonyl cyanide-m-chlorophenyl hydrazone (CCCP), a PMF uncoupler, to prevent uptake. The sensor strain treated with 6.4 ng/mL of nocardamine-Fe^{3+} recovered 50% of baseline fluorescence after 8.9 min (**Fig. 4H**). Cells pretreated with thiocillin took 20 min to recover 50% fluorescence, more than twice as long. CCCP treatment inhibited fluorescence recovery and continuous quenching was observed, suggesting that once bound, the ligand must be taken up to allow the transporter to return to its apo confirmation.

Since thiocillin increased the K_d for nocardamine in WT FoxA and the mutants, we inferred that the thiopeptide could bind the mutant transporters. This result suggested that the reduced susceptibility to thiocillin is due to reduced uptake rather than binding. A mass spectrometry approach was used to test this idea, measuring intracellular thiocillin accumulation after treating with 12 μg/mL thiocillin for 1 h. Thiocillin concentrations in Δ*foxA* complemented with WT FoxA were significantly greater than the vector control or when Δ*foxA* was complemented with the mutant transporters, supporting the hypothesis that the mutations reduce thiocillin uptake (**Fig. 4I**).

We also investigated the effects of the single amino acid mutations on binding of bisucaberin to FoxA (**Fig. 4J**). Saturation was not obtained even with 100 μg/mL of bisucaberin$_3$-$Fe^{3+}{}_2$, suggesting that it has a lower affinity for FoxA than nocardamine. Thiocillin pre-treatment reduced quenching, similar to nocardamine. When this assay was repeated for the FoxA point mutants, bisucaberin$_3$-$Fe^{3+}{}_2$ could still quench fluorescence of all the mutant transporters, suggesting that although it binds to FoxA, its inability to support growth of specific mutants may be due to reduced uptake (**SI Appendix Fig. S7**).

Residues that impact thiocillin uptake are important for stimulation of FoxA expression by nocardamine

Since mutations that affected thiocillin uptake also reduced nocardamine-Fe^{3+} binding, they could potentially impact signaling (**Fig. 5A**). Binding of nocardamine to FoxA induces conformational changes that lead to the degradation and release of an anti-σ/σ factor pair (FoxI/FoxR). FoxR then guides RNA polymerase to the promoter of *foxA* to upregulate its transcription. The exact mechanism of signal transduction is unknown, but we hypothesized that the residues we identified may be important. We tested signalling using a promoter assay where GFP expression is under control of P_{foxA}. Chromosomal knock-in mutants encoding FoxA Y664A, P659L, K657A, W503S, or H374Y were generated so the transporters were expressed from their native promoter. P_{foxA}-*gfp* and a promoterless control (P_x-*gfp*) were introduced into the WT and each mutant. The strains were treated with increasing concentrations of thiocillin (**Fig. 5B-C**) or nocardamine (**Fig. 5D-E**). Thiocillin did not induce GFP expression. When treated with nocardamine, W503S and Y664A had reduced GFP expression compared to the WT, while GFP production from P659L, K657A, and H374Y was abolished, resembling the negative control. GFP

expression in all the mutants was significantly lower than WT at the highest concentration of nocardamine tested (**Fig. 5F**). These results suggest that the mutated residues are important in the signaling response.

Changes in GFP expression were also monitored in Δ*pvdA* Δ*pchA* with P_x-*gfp* and P_{foxA}-*gfp* treated with bisucaberin (**Fig. 5G**). Bisucaberin stimulated expression from P_{foxA} in Δ*pvdA* Δ*pchA,* suggesting that it triggers the same signaling cascade as nocardamine despite their structural differences (**Fig. 5G**). Overall, the differences in signaling between thiocillin, nocardamine, and bisucaberin further indicates that the protein conformations that result from binding of these ligands are different, consistent with the results of mutational analyses and fluorescence quenching assays.

We next looked at FoxA protein expression. FoxA T755-V5 was chromosomally integrated to allow for detection of expression by Western blot and the tagged strain was treated with 5.0 μg/mL each of thiocillin, bisucaberin , or nocardamine (**Fig. 5H**). Surprisingly, only nocardamine stimulated FoxA expression even though bisucaberin also uses FoxA; however, this may be due to the presence of pyoverdine and pyochelin from the WT. The tagged point mutants were also chromosomally integrated (except for P659L T775-V5 since it was not detectable when expressed *in trans*; **Fig. 3G**) and treated with 5.0 μg/mL nocardamine to examine effects on signaling. WT, Y664A, and W503S variants had detectable expression, consistent with the promoter reporter assays (**Fig. 5E,I**). To confirm the bisucaberin promoter-GFP expression data, V5-tagged WT FoxA and W503S were expressed from the chromosome in Δ*pvdA* Δ*pchA* (**Fig. 5J**). The mutants were treated with 5.0 μg/mL bisucaberin and examined for changes in FoxA expression. P659L T755V5 was excluded since it was not detectable and the other mutants were excluded because they compromised uptake and inhibited growth recovery (**Fig. 3D**). Both WT and W503S

responded to bisucaberin treatment with increased FoxA expression (**Fig. 5I**). These data show there is overlap between residues important for thiocillin uptake and signaling by the siderophores (**SI Appendix Fig. S8**).

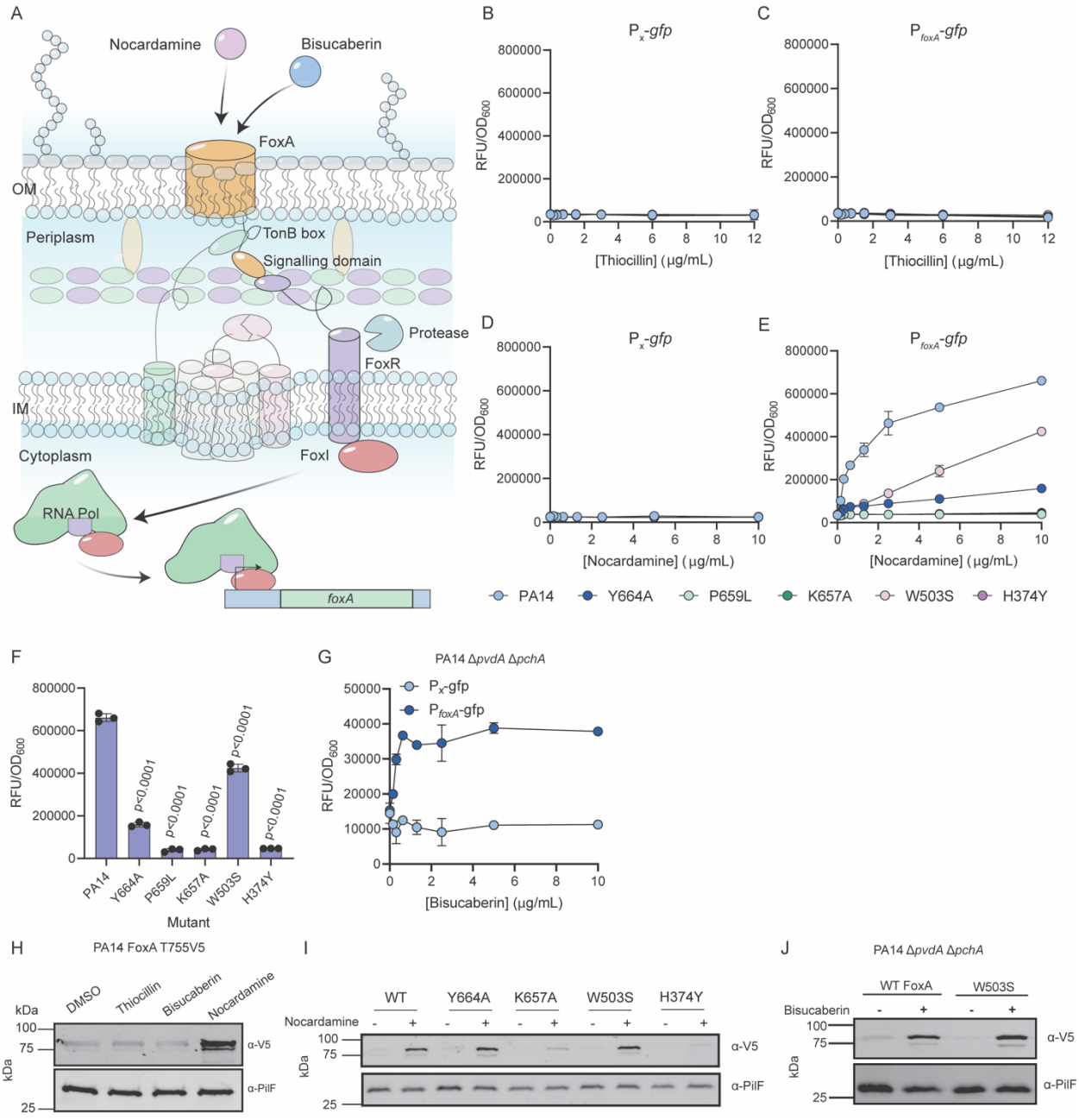

Figure 5. FoxA single-residue mutants are defective in nocardamine signaling. (**A**) Diagram depicting nocardamine and bisucaberin-induced expression of FoxA by the FoxI/FoxR σ/anti-σ factors. Binding and uptake of nocardamine and bisucaberin triggers conformational changes in

FoxA, including exposure of the TonB box motif and signalling domain to the FoxR anti-sigma factor. Proteolytic cleavage of FoxR in the periplasm leads to the release of FoxI into the cytoplasm, which directs RNA polymerase to P_{foxA}. (**B**) WT PA14 and chromosomal FoxA mutants harbouring a promoterless GFP plasmid and (**C**) P_{foxA} treated with increasing concentrations of thiocillin in 10:90. Results are averaged from three independent biological replicates. WT PA14 and chromosomal FoxA mutants harbouring (**D**) a promoterless GFP plasmid and (**E**) P_{foxA} treated with increasing concentrations of nocardamine in CAA. Results are averaged from three independent biological replicates. (**F**) RFU/OD_{600} values for WT PA14 and FoxA chromosomal mutants treated with 10 µg/mL nocardamine in CAA. Statistical significance was calculated using one-way ANOVA followed by Dunnett's test. P values are shown. (**G**) Promoter assays with ΔpvdA ΔpchA P_x-gfp (light blue) and P_{foxA}-gfp (dark blue) treated with bisucaberin in 10:90 medium supplemented with bisucaberin. Raw fluorescence values are normalized to OD_{600}. Growth, fluorescence quenching, and promoter assays were averaged from three independent biological replicates. (**H**) PA14 FoxA T775-V5 treated with 5 µg/mL thiocillin, bisucaberin, or nocardamine in CAA. (**I**) PA14 FoxA V5-tagged chromosomal single amino acid mutants were treated with 5 µg/mL nocardamine in CAA overnight. (**J**) FoxA expression of chromosomally tagged FoxA and FoxA mutants treated with DMSO (-) or with 5.0 µg/mL bisucaberin (+). PilF was used as the loading control. A representative blot is shown. Outer membranes were isolated and probed with an α-V5 antibody and α-PilF was used as a loading control.

Sequence conservation of L8 is low and the loop is important for ligand uptake

Previously we tested a panel of Gram-negative bacteria capable of taking up nocardamine for their potential susceptibility to thiocillin. However, thiocillin showed only narrow spectrum activity against *P. aeruginosa* and some related Pseudomonads (28). Since the data presented here show that single point mutations in FoxA are sufficient to confer thiocillin resistance, a phylogeny approach was used to determine whether the identity of key residues identified by the mutagenesis screen might explain resistance in other Gram-negatives. We constructed a phylogenetic tree for FoxA using shoot.bio (41, 42) in 606 bacterial species (**Fig. 6A**) and identified 16 orthologs (41). Their sequences were aligned and residues of interest were examined for similarity to $FoxA_{PA14}$ (**Fig. 6B**). Y374 was present in 6/16 orthologs while another 6 had H374, which we showed reduces nocardamine-Fe^{3+} binding and prevents thiocillin uptake (**Fig. 2C-D**). There was greater variation at positions corresponding to W503, K657, and Y664; however, some orthologs had S503, A657, and A664, which we showed compromise thiocillin binding and uptake (**Fig. 2C-D**).

Additional substitutions at key residues were tested, and all mutations reduced thiocillin susceptibility without compromising nocardamine uptake (**Fig. 6C-D**).

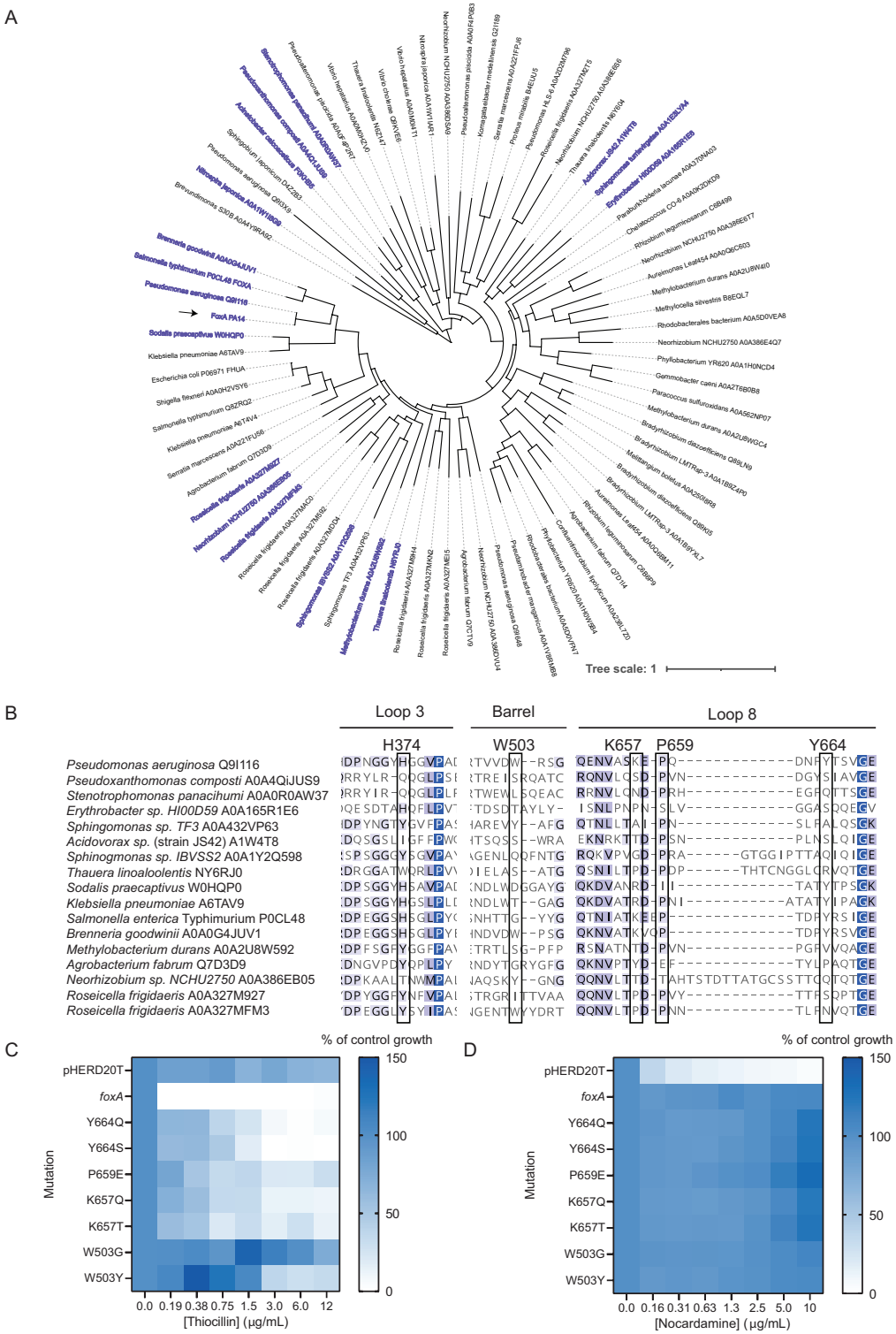

Figure 6. Conservation of amino acid sequences of FoxA orthologs at residues important for thiocillin susceptibility. (**A**) Phylogenetic tree based on the PA14 FoxA amino acid sequence

submitted to shoot.bio. $FoxA_{PA14}$ is indicated by the arrow and orthologs are highlighted in purple. (**B**) Alignment of FoxA orthologs with $FoxA_{PA14}$. Residues important for thiocillin uptake are boxed with the residue number corresponding to $FoxA_{PA14}$ above. The intensity of purple indicates the degree of conservation of a particular amino acid residue with all orthologs where a darker shade indicates that most or all orthologs have a similar residue whereas white indicates that all or most orthologs have a different amino acid at the particular residue. (**C and D**) PA14 ΔfoxA expressing mutant FoxA from pHERD20T in 10:90 medium + 1% arabinose with increasing concentrations of thiocillin or (D) CAA + 1% arabinose with increasing concentrations of nocardamine.

Discussion

In this study, we used X-ray co-crystallography to show how bisucaberin interacts with FoxA, and molecular docking, and site-directed mutagenesis to identify residues in FoxA necessary for thiocillin and siderophore uptake. The results revealed that thiocillin, bisucaberin, and nocardamine interact differently with the TBDT despite occupying the same binding pocket. The molecular details of bisucaberin-FoxA interactions, showing the outward protrusion of ring 1, help to reveal how thiocillin may be accommodated in the transporter.

We focused on the role of L8, an extracellular loop that folds inwards when nocardamine binds (13), because mutations in this loop reduced thiocillin uptake. Similar loop rearrangements are observed with other transporters, suggesting that this is a common feature of TBDTs (24). Paradoxically, L8 was dispensable for thiocillin uptake – as seen with $FoxA_{\Delta K657\text{-}T665}$ – but essential for nocardamine uptake. These data expand on previous studies of the effects of loop deletions in FepA, where deletion of L2 was detrimental for both enterobactin uptake and colicin susceptibility (43). Our data show that molecules do not need to mimic the native ligand in terms of structure or binding to use the same TBDT (30), supported by the lack of fluorescence quenching by thiocillin versus nocardamine. In contrast, other studies showed that the bacteriocin pyocin S2 mimics binding of pyoverdine (22), with similar findings for the rifamycin derivative CGP 4832 and FhuA (44), and the lasso peptide microcin J25 and FhuA (24). Based on the

thiocillin-FoxA docking predictions, L8 may be unable to fold because thiocillin sterically hinders this conformational change. The promiscuity of TBDTs is advantageous for uptake of a range of siderophores produced by diverse microorganisms in iron-limited and competitive environments; however, this promiscuity can also be exploited by antimicrobials. A secondary function of L8 may be to prevent uptake of toxic molecules that can bind the transporter at the plug and barrel regions, which are more conserved than the extracellular loops (17). This gatekeeper role may underlie evolution of variation in L8 of FoxA orthologs and the selectivity of thiocillin towards some Pseudomonads, as single residue differences are sufficient to confer resistance without loss of siderophore uptake. Loss of L8 in $FoxA_{\Delta K657\text{-}T665}$ allowed for thiocillin entry even though single amino acid mutations in the plug prevented its uptake. Our findings with L8 may apply to the extracellular loops of other TBDTS.

GFP-promoter and protein expression assays showed that L8 also contributes to signal transduction in a ligand-dependent manner, as nocardamine and bisucaberin stimulated FoxA expression while thiocillin did not. Although nocardamine uptake was supported by all mutant transporters tested, K657A and H374Y compromised signaling. This result is consistent with prior studies showing that uptake of pyoverdine by FpvA and signalling could be separated (45), suggesting they are independent processes. However, we found overlap between FoxA residues important for thiocillin and bisucaberin uptake and signal transduction by nocardamine, suggesting a series of conformational rearrangements not yet fully understood. Such connectivity may explain how thiocillin can be taken up through FoxA despite its structural differences from the native ligand. Similarly, bisucaberin uptake relied on residues similar to those required by thiocillin (**Fig. 5D**).

Overall, this work demonstrated that there are at least three molecules recognized by FoxA that interact with the TBDT in unique ways that yield different outcomes (**SI Appendix Fig. S6**). These results highlight our as-yet incomplete understanding of the repertoire of ligands potentially recognized by different TBDTs; we suspect that many more molecules can use these transporters to cross the outer membrane. The structural complexity of natural product antimicrobials may relate to their evolution for uptake in addition to target recognition. Discovery of such molecules, improved understanding of how they interact with the transporters, and the consequences of those interactions are all important for guiding drug discovery and design. If an antimicrobial induces expression of the transporter it uses to enter cells, it would potentiate its own uptake, an important consideration for drug development.

Material and Methods

A complete list of strains used in this study are available in SI Appendix Table S3. Bacterial strains were grown overnight at 37°C in lysogeny broth (LB) (Bioshop) at 200 rpm from glycerol stocks stored at -80°C. Bacteria were subcultured into media (1:500 dilution) for 3-4 hours to standardize growth before use in MIC assays. Minimal media used in this study was either 10:90 (27, 28) or CAA (6). 10:90 is composed of 10% LB and 90% 1X PBS. A 1X PBS working buffer was prepared from a 10X stock (80g NaCl, 2g KCl, 26.8g Na_2HPO_4-$7H_2O$, 2.4g KH_2PO_4 in 1L of de-ionized H_2O, pH 7.4). CAA was prepared with 5g/L casamino acids, 1.46g/L K_2HPO_4 $3H_2O$ and 0.25g/L $MgSO_4$ $7H_2O$. Subcultures were further diluted into fresh minimal media (optical density of OD_{600} 0.005) before use. When applicable, antibiotics and supplements were added at the following concentrations: ampicillin 100μg/mL, carbenicillin 200μg/mL, gentamicin μg/mL, arabinose 1-2%. Arabinose was prepared as a 20% solution in either 10:90 or CAA and sterilized by filtration through 0.2μm membranes (Fisherbrand). Bacterial growth was measured as the

OD_{600} with a plate reader (Thermo Scientific MultiSkan Go). Thiocillin, apo-nocardamine, nocardamine-Fe^{3+}, bisucaberin, enterobactin, ferrichrome, and fluorescein-5-maleimide were purchased from Cayman Chemicals. Deferasirox was purchased from AK Scientific. Arthrobactin was purchased from MolPort. AlexaFluor 594 C5-maleimide was purchased from ThermoFisher Scientific. All compounds were dissolved in dimethyl sulfoxide and stored at -20°C.

MIC assays

MIC assays were conducted as previously described (27, 28). Overnight cultures were grown in LB from a glycerol stock at 37°C with shaking (200rpm). Overnights were diluted (1:100) in fresh 10:90 or CAA (1:100 dilution) and subcultures were grown for four hours. Subcultures were diluted to a final OD_{600} of 0.1/500 in fresh media. Compounds dissolved in dimethylsulfoxide (DMSO) or deionized (DI) H_2O were added at 75x the final concentration in 96-well plates (Nunc) for a final volume of 150µL. Plates were sealed to prevent evaporation and incubated at the same conditions and rpm. The percent of control was calculated by subtracting the OD_{600} of sterile media controls from raw OD_{600} values and normalized to the OD_{600} of the vehicle controls. OD_{600} was determined with a plate reader (Thermo Scientific).

Docking of ligands into FoxA

SwissDock (http://www.swissdock.ch/) (35), AutoDock VINA (33, 34), and HADDOCK (https://wenmr.science.uu.nl/haddock2.4/) (36) were used to dock thiocillin into FoxA. A 3D structure of thiocillin was generated using Chem3D after energy minimization. Docking by SwissDock was conducted using the web server where the target (FoxA) and the ligand (thiocillin) were submitted as PDB and mol2 files respectively. Two hundred and thirteen poses were

generated and the pose with the lowest ΔG value (-10.9 kcal/mol) was selected to model binding. For AutoDock VINA, thiocillin was drawn in Chemdraw and transferred to Chem3D for energy minimization prior to docking. Docking was conducted with the following grid parameters that encompasses the expected binding site and the surface of the plug: center_x = -9.628, center_y = 33.621, center_z = 5.268, size_x = 48, size_y = 42, size_z = 120. The pose with the lowest RMSD (0.000) and highest affinity (-10.5 kcal/mol) was selected to model binding. For HADDOCK, thiocillin (ligand) and FoxA (protein) were submitted as PDB files with the protein-ligand option selected and thiocillin indicated as a cyclic peptide. 191 structures were generated and grouped into three clusters. The largest cluster contained 177 structures and the structure with the best score was used for modeling.

Checkerboard assays

Checkerboards were conducted as previously described (27, 28). Thiocillin was added from bottom to top in increasing concentration whereas siderophores were added from left to right in increasing concentrations. Incubation conditions and growth calculations were the same as for the MIC assays.

Molecular Biology

All primers are listed in SI Appendix Table 4. Chromosomal mutants were generated by allelic exchange using *P. aeruginosa* PA14 (46) as previously described (30). The upstream (~1000 bp) and downstream (~750 bp) regions of each gene of interest were amplified from purified PA14 genomic DNA (Promega Wizard Genomic DNA Purification Kit) with overlapping 3' and 5' regions respectively and extracted with GeneJet Gel Extraction Kit (ThermoFisher).

Overlap extension PCR was used to connect the two pieces (47), digested with the appropriate restriction enzymes (FastDigest ThermoFisher), and ligated into pEX18Gm (T4 DNA ligase, ThermoFisher). Ligation mixtures were transformed by heat shock into *E. coli* DH5α and allowed to recover for 2-3 h in LB. Cells were collected and plated onto LB 1.5% agar plates supplemented with 15μg/mL gentamicin supplemented and X-gal for blue-white screening. After overnight incubation at 37°C, white colonies were selected and cultured overnight in LB + 15μg/mL gentamicin. Plasmids were isolated using GeneJet Plasmid Miniprep Kit (ThermoFisher) and checked for the presence of a correctly sized insert.

The plasmids were transformed by heat shock into competent *E. coli* SM10 as above and plated on LB 1.5% agar plates + 15μg/mL gentamicin. After overnight incubation at 37°C, a single colony was cultured in LB + 15μg/mL gentamicin overnight. The two cultures were mixed in a 1.5mL centrifuge tube (500μL of each), spun down, and spotted on LB 1.5% agar, and incubated at 37°C overnight. The mating spot was streaking onto *Pseudomonas* Isolation Agar (PIA, Difco) + 100μg/mL gentamicin and incubated. The next day, single colonies were streaked onto LB 1.5% agar + 15% sucrose (Bioshop) and incubated at 30°C. We then patched 16 colonies onto LB 1.5% agar + 15% sucrose and LB + 15μg/mL gentamicin and grew both plates at 37°C overnight. Patches that grew on sucrose but not gentamicin were picked for colony PCR using the upstream forward and downstream reverse primers. Patches with confirmed deletions were streaked for single colonies on LB 1.5% agar + 15% sucrose and checked again by colony PCR. A single colony was inoculated into LB broth to make a glycerol stock or used to generate double and triple mutants. A similar process was used to generate chromosomal insertions.

To complement or overexpress a gene of interest, we used the plasmid pHERD20T. pHERD20T is an arabinose-inducible expression vector with the P_{BAD} promoter under control of

AraC. Primers flanking the gene of interest including the ribosome binding site were amplified from purified genomic DNA, digested with the appropriate restriction enzymes, and ligated into pHERD20T. Transformations were as above except cells were plated on LB 1.5% agar supplemented 100µg/mL ampicillin, X-gal, and arabinose and incubated at 37°C overnight for blue-white screening. Plasmids were verified by colony PCR as above and colonies were inoculated into LB supplemented with 100µg/mL ampicillin. Plasmids were isolated and inserts verified by Sanger sequencing by the McMaster Genomics Facility Mobix Lab. Plasmids were transformed into PA14 by electroporation with an 1-2h recovery period in LB. Cells were plated on LB 1.5% agar supplemented with 200µg/mL carbenicillin (AK Scientific). A single colony was picked and grown in LB broth supplemented with 200µg/mL carbenicillin overnight at 37°C and used to make glycerol stocks.

Cysteine labeling, fluorescence quenching, and recovery assays

PA14 Δ*foxA* pHERD20T-*foxA* cysteine mutants were subcultured 1:100 from LB overnight cultures into 10:90 + 2% arabinose. Cultures were grown for 4h at 37°C with shaking (200 rpm). Cells were harvested by centrifugation (6000 x g, 5 min) and resuspended in 1mL of PBS (or PBS + 0.4% glucose for uptake studies) + 10µM fluorescein-5-maleimide (Cayman Chemicals) or AlexaFluor 594 C5 maleimide (ThermoFisher) for microscopy. Cells were labeled at 37°C with shaking (200rpm) for 30 min in the dark. Excess dye was quenched with 1 mM dithiothreitol (DTT; Sigma) to stop the reaction. Cells were washed 3X with 1X PBS. For fluorescence recovery assays, cells were incubated with 1X PBS + 0.4% glucose (from a 20% glucose stock in PBS) at 37°C with shaking at 200 rpm rather than 1X PBS. Cells were distributed into black 96-well plates (Corning) with 146 µL of OD_{600} 0.1 cells per well. For pre-treatment with and without thiocillin,

2µL of thiocillin (final concentration of 12µg/mL – equivalent to 10µM) or DMSO was added to the cells and Incubated at room temperature for 5 min before 2 µL of nocardamine-Fe^{3+} or bisucaberin-Fe^{3+} was added. Fluorescence of fluorescein-5-maleimide (ex. 494nm em. 520nm) was read during the thiocillin pre-treatment period and immediately after nocardamine-Fe^{3+} or bisucaberin-Fe^{3+} was added (BioTek Neo). Fluorescence recovery assays were conducted as above but plates were incubated at 37°C and fluorescence was recorded every minute for 1h. Since thiocillin reduced quenching compared to nocardamine-Fe^{3+} alone, differences in baseline quenching were normalized by subtracting F/F_0 at t = 5 min, the time at which nocardamine-Fe^{3+} was added, from F/F_0 at each timepoint to obtain $\Delta F/F_0$.

Microscopy

Cells were imaged as previously described (30). Cells of interest were spotted (5µL) onto a microscope slide with a 1% agarose pad, which was then mounted with a glass coverslip. A Nikon A1 confocal microscope was used to image cells using brightfield and fluorescence microscopy through a Plan Apo 60X (NA=1.40) oil objective. Nikon NIS Elements Advanced Research (Version 5.11.01 64-bit) software was used for image acquisition.

Promoter assays

P_{cdrA}-*gfp* (48) was purchased from Addgene. P_{cdrA} was removed by digestion with XbaI and SacI followed by ligation of P_{foxA} with the same synthetic ribosome binding site into the vector. The plasmid was introduced into PA14, PA14 Δ*pvdA* Δ*pchA*, and PA14 FoxA mutants by electroporation. Siderophores (apo-nocardamine, apo-bisucaberin) and thiocillin were added to cells in the same way as MIC assays in Corning black 96-well plates with clear bottoms. After

incubation overnight at 37°C with shaking (200rpm), GFP production (excitation: 494nm and emission: 515nm)(48) and OD_{600} were determined (BioTek Neo).

Outer membrane preparations

Outer membranes were isolated as previously described (30). PA14 mutants and strains were grown overnight in LB with 200µg/mL carbenicillin (for pHERD20T strains) or without (for chromosomal mutants) at 37°C with shaking (200 rpm). Cells were subcultured in 10:90 or CAA as described in MIC assays into fresh media for 4 h then diluted to OD_{600} 0.1/500 in 50mL of fresh 10:90 (with or without arabinose for plasmid-carrying strains and chromosomal mutants) or CAA (for chromosomal mutants). Cultures were grown overnight at 37°C with shaking (200 rpm). Cells were harvested and resuspended in 6mL 10 mM Tris pH 8.0.

Cells were lysed using a Misonix Sonicator 3000 on ice (30 s pulse, 30 s rest, 3 min, power level 5.0) and debris was removed by centrifugation (6000 x g, 5 min, 4°C). A second centrifugation step (21000 x g, 30 mins, 4°C) was used to harvest membrane proteins. After decanting the supernatant, the pellet was resuspended with 100 µL DI H_2O and 900µL 11.1mM Tris 3% sarkosyl pH 7.6. The mixture was incubated at room temperature with shaking (200 rpm) for 30 min. A final centrifugation step was used to collect insoluble proteins (21000 x g, 30 min, 4°C).

SDS-PAGE and Western Blots

SDS-PAGE and Western Blots were conducted as previously described (30). The outer membrane preparations were solubilized in 20 µL 1X loading buffer and boiled for 10 min before loading 10 µL into a 12.5% polyacrylamide gel. Proteins were separated at 80 V (15 min) and 120

V for 1-1.5 h then transferred to a nitrocellulose membrane (225 mA, 1 h) followed by blocking overnight at 4°C with 5% skim milk in PBS. The next day blots were rinsed briefly with DI H_2O and primary antibodies were added at 1:1000 dilutions in PBS for 1 h at room temperature (rabbit α-V5 (Sigma 21160752), mouse α-DYKDDDDK (Invitrogen MA1-91878), and rabbit #3198 α-PilF). After three washes with PBS, the secondary antibody, goat α-rabbit-alkaline phosphatase (AP) or rabbit α-mouse-AP, was added at 1:2000 dilution and incubated for 2 h in PBS. Blots were washed 3X with PBS and developed in the dark for 15-30 mins. Developing solution consisted of AP buffer (1mM Tris, 100mM NaCl, 5mM $MgCl_2$ pH 9.5) + 5-bromo-4-chloro- 3-indoyl phosphate (BCIP) + nitro-blue tetrazolium (NBT) and blots were imaged on an Azure C400 Imaging System. Raw and labeled gels are available (SI Appendix Fig. S9).

Thiocillin uptake assays, HPLC, and mass spectrometry

PA14 strains were grown overnight in LB with 200μg/mL carbenicillin at 37°C with shaking (200 rpm). Cells were subcultured 1:100 into 10:90 + 2% arabinose for 4 h and collected by centrifugation. Cells were washed 3X in 10:90 and resuspended in fresh 10:90 + 12μg/mL (10μM) thiocillin to an OD_{600} of 1.0. Cells were aliquoted into 1.5mL centrifuge tubes and incubated at 37°C with shaking (200rpm) for 1h then collected by centrifugation. Cells were washed 3x with PBS then resuspended in 100 μL H_2O. Cultures were subjected to three cycles of freeze-thaw at -80°C and 60°C for 5 min per freeze-thaw. Lysed cells were collected by centrifugation for 10 min at 21000 x g at room temperature and the supernatant was collected in a clean centrifuge tube. Methanol (100 μL) was added to the cell pellet and mixed to collect residual thiocillin and centrifuged for 10 min at 21000 x g. The methanol layer was combined with the previous supernatant and mixed.

LC-MS was used to analyze the concentration of thiocillin in the samples (Eclipse Plus C18 column, 2.1 x 100mm, 1.8µm; solvent A: water + 0.1% formic acid; solvent B: acetonitrile + 0.1% formic acid; flow rate 0.3mL/min; gradient 95:5 A:B; total run time = 10 min; injection volume = 5 µL; MS method: QQQ; mode: positive). Matrix effects were accounted for by preparing thiocillin standards in blank samples from PA14 Δ*foxA* pHERD20T. Thiocillin concentrations were normalized based on the CFUs from each sample.

Bisucaberin-FoxA co-crystallization and data collection

FoxA was overexpressed in *Escherichia coli* Lemo21 DE3 cells as previously described(13). Cells were grown in 2xYT media supplemented with 0. 5 mM L-rhamnose at 37 °C to an OD_{600} of 0.8-1 and induced with 0.1 mM isopropyl β-D-1-thiogalactopyranoside. Cells were grown at 19°C for 16-18 h and lysed using high-pressure homogenizer (EmulsiFlex-C3, Avestin). Cell debris was removed by centrifugation at 22,000 g for 30 min, and the supernatant was incubated with 1% Triton X-100 for 1 hr. The outer membrane fraction was isolated by centrifugation at 150,000 g for 1 h and solubilized using 1% octyl-β-glucoside and 1% C8E4 in TBS buffer (20 mM Tris-HCl pH 7.5, 200 mM NaCl). Solubilised outer membranes were cleared by another round of centrifugation at 150,000 g for 20 min and loaded onto Ni^{2+}-NTA beads for 1 h. The beads were washed with TBS buffer supplemented with 30 mM imidazole and 0.6% C8E4 and eluted with 300 mM imidazole in the same buffer. Fractions containing the protein were pooled and tobacco etch virus protease (TEV, 10:1 w/w) was added overnight to cleave the His_6-tag from FoxA. Next day, the eluate was passed through the Ni-NTA beads to remove TEV and any impurities, the flow-through concentrated to 500 µl and loaded onto a Superdex S200 10/300 size-

exclusion column. Peak fractions were concentrated to 6-8 mg/ml and used for crystallization or stored at -80 °C.

Purified FoxA in C8E4 detergent was mixed with 10-fold excess Fe-bisucaberin, incubated on ice for 30 min and used for crystallization. Crystallisation conditions were 1.8 M ammonium sulfate, 0.1 M MES pH 6.5, 0.8% OG. Crystals typically appeared within 1-2 weeks at 19 °C.

All X-ray diffraction data were collected at PETRA III/EMBL P13 beamline, dataset processed with XDS (49), merged with AIMLESS (50), anisotropy correction was performed with STARANISO server. The structure was determined using molecular replacement with PHENIX Phaser using apo FoxA as a starting model (PDB:6I98) and refined using phenix.refine (51). Structural coordinates have been deposited in the RCSB Protein Data Bank under the accession number 8B43. Data collection and refinement statistics are found in SI Appendix Table 1. Structures were visualized using UCSF Chimera (52).

Phylogenetic Tree, ortholog identification, and sequence alignments

The FoxA phylogenetic tree and ortholog identification was conducted using SHOOT (41) (shoot.bio). The tree was visualized with iTOL (42) (https://itol.embl.de/). Ortholog sequences were imported from Uniprot(53) and sequences were aligned in Geneious Prime by MUSCLE alignment (54). Accession numbers for the orthologs are as follows: *Pseudomonas aeruginosa* Q9I116, *Pseudoxanthomonas composti* A0A4QiJUS9, *Stenotrophomonas panacihumi* A0A0R0AW37, *Erythrobacter sp. HI00D59* A0A165R1E6, *Sphingomonas sp. TF3* A0A432VP63, *Acidovorax sp.* (strain JS42) A1W4T8, *Sphinogmonas sp. IBVSS2* A0A1Y2Q598, *Thauera linoaloolentis* NY6RJ0, *Sodalis praecaptivus* W0HQP0, *Klebsiella pneumoniae* A6TAV9, *Salmonella enterica* Typhimurium P0CL48, *Brenneria goodwinii* A0A0G4JUV1,

Methylobacterium durans A0A2U8W592, *Agrobacterium fabrum* Q7D3D9, *Neorhizobium sp. NCHU2750* A0A386EB05, *Roseicella frigidaeris* A0A327M927, *Roseicella frigidaeris* A0A327MFM3.

Acknowledgements

We thank Nikki Henriquez from the Centre for Microbial Chemical Biology (CMCB) at the Institute for Infectious Diseases Research (IIDR) for assistance with experiments to measure intracellular concentrations of thiocillin. We are grateful to the staff at beamlines P13 and P14 (EMBL, Hamburg) and acknowledge access to the Sample Preparation and Characterization (SPC) Facility of EMBL, Hamburg. This work was supported by a Natural Sciences and Engineering Research Council Discovery Grant RGPIN-2021-04237 to LLB, a Canadian Institutes of Health Research grant (FRN-148463) to GDW, and the excellence cluster 'The Hamburg Centre for Ultrafast Imaging – Structure, Dynamics and Control of Matter at the Atomic Scale' of the Deutsche Forschungsgemeinschaft (DFG EXC 1074) to IJ and HT. LLB and GDW hold Tier 1 Canada Research Chairs in Microbe-Surface Interactions and Antimicrobial Biochemistry, respectively. DCKC holds a Canadian Institute of Health Research (CIHR) Canada Graduate Scholarship – Doctoral program (CGS-D).

References

1. E. Banin, M. L. Vasil, E. P. Greenberg, Iron and *Pseudomonas aeruginosa* biofilm formation. *Proc. Natl. Acad. Sci. U. S. A.* **102**, 11076–11081 (2005).
2. I. L. Lamont, P. A. Beare, U. Ochsner, A. I. Vasil, M. L. Vasil, Siderophore-mediated signaling regulates virulence factor production in *Pseudomonas aeruginosa*. *Proc. Natl. Acad. Sci. U. S. A.* **99**, 7072–7077 (2002).
3. H. Takase, H. Nitanai, K. Hoshino, T. Otani, Requirement of the *Pseudomonas aeruginosa tonB* gene for high-affinity iron acquisition and infection. *Infect. Immun.* **68**, 4498–4504 (2000).
4. J. E. Cassat, E. P. Skaar, Iron in infection and immunity. *Cell Host Microbe* **13**, 509–519 (2013).
5. M. Nairz, *et al.*, The co-ordinated regulation of iron homeostasis in murine macrophages limits the availability of iron for intracellular *Salmonella* typhimurium. *Cell. Microbiol.* **9**, 2126–2140 (2007).
6. V. Normant, *et al.*, Nocardamine-Dependent Iron Uptake in *Pseudomonas aeruginosa*: Exclusive Involvement of the FoxA Outer Membrane Transporter. *ACS Chem. Biol.* **15**, 2741–2751 (2020).
7. L. Moynié, *et al.*, The complex of ferric-enterobactin with its transporter from *Pseudomonas aeruginosa* suggests a two-site model. *Nat. Commun. 2019 101* **10**, 1–14 (2019).
8. P. Ó. Cuív, P. Clarke, M. O'Connell, Identification and characterization of an iron-regulated gene, *chtA*, required for the utilization of the xenosiderophores aerobactin, rhizobactin 1021 and schizokinen by *Pseudomonas aeruginosa*. *Microbiology* **152**, 945–954 (2006).
9. P. E. Klebba, *et al.*, Iron Acquisition Systems of Gram-negative Bacterial Pathogens Define TonB-Dependent Pathways to Novel Antibiotics. *Chem. Rev* **121**, 5193–5239 (2021).
10. J. Brandel, *et al.*, Pyochelin, a siderophore of *Pseudomonas aeruginosa*: Physicochemical characterization of the iron(III), copper(II) and zinc(II) complexes. *Dalt. Trans.* **41**, 2820–2834 (2012).
11. A. M. Albrecht-Gary, S. Blanc, N. Rochel, A. Z. Ocaktan, M. A. Abdallah, Bacterial Iron Transport: Coordination Properties of Pyoverdin PaA, a Peptidic Siderophore of *Pseudomonas aeruginosa*. *Inorg. Chem.* **33**, 6391–6402 (1994).
12. J. M. Meyer, M. A. Abdallah, The fluorescent pigment of *Pseudomonas fluorescens*: Biosynthesis, purification and physicochemical properties. *J. Gen. Microbiol.* **107**, 319–328 (1978).
13. I. Josts, K. Veith, H. Tidow, Ternary structure of the outer membrane transporter FoxA with resolved signaling domain provides insights into TonB-mediated siderophore uptake. *Elife* **8** (2019).
14. H. Celia, *et al.*, Structural insight into the role of the Ton complex in energy transduction. *Nature* **538**, 60–65 (2016).
15. C. Bradbeer, The proton motive force drives the outer membrane transport of cobalamin in *Escherichia coli*. *J. Bacteriol.* **175**, 3146 (1993).
16. A. D. Ferguson, *et al.*, Structural basis of gating by the outer membrane transporter FecA. *Science (80-.).* **295**, 1715–1719 (2002).
17. N. Noinaj, M. Guillier, T. J. Barnard, S. K. Buchanan, TonB-dependent transporters: Regulation, structure, and function. *Annu. Rev. Microbiol.* **64**, 43–60 (2010).
18. K. C. Bastiaansen, P. Van Ulsen, M. Wijtmans, W. Bitter, M. A. Llamas, Self-cleavage of

the *Pseudomonas aeruginosa* cell-surface signaling anti-sigma factor FoxR occurs through an N-O acyl rearrangement. *J. Biol. Chem.* **290**, 12237–12246 (2015).
19. A. D. Ferguson, *et al.*, Signal transduction pathway of TonB-dependent transporters. *Proc. Natl. Acad. Sci. U. S. A.* **104**, 513–518 (2007).
20. M. A. Llamas, *et al.*, The Heterologous Siderophores Ferrioxamine B and Ferrichrome Activate Signaling Pathways in *Pseudomonas aeruginosa*. *J. Bacteriol.* **188**, 1882 (2006).
21. W. Rabsch, *et al.*, FepA-and TonB-Dependent Bacteriophage H8: Receptor Binding and Genomic Sequence. *J. Bacteriol.* **189**, 5658–5674 (2007).
22. P. White, *et al.*, Exploitation of an iron transporter for bacterial protein antibiotic import. *Proc. Natl. Acad. Sci. U. S. A.* **114**, 12051–12056 (2017).
23. I. Atanaskovic, *et al.*, Targeted Killing of *Pseudomonas aeruginosa* by Pyocin G Occurs via the Hemin Transporter Hur. *J. Mol. Biol.* **432**, 3869–3880 (2020).
24. I. Mathavan, *et al.*, Structural basis for hijacking siderophore receptors by antimicrobial lasso peptides. *Nat. Chem. Biol. 2014 105* **10**, 340–342 (2014).
25. R. A. Salomon, R. N. Farias, The FhuA protein is involved in microcin 25 uptake. *J. Bacteriol.* **175**, 7741–7742 (1993).
26. B. Luna, *et al.*, A nutrient-limited screen unmasks rifabutin hyperactivity for extensively drug-resistant *Acinetobacter baumannii*. *Nat. Microbiol. 2020 59* **5**, 1134–1143 (2020).
27. M. R. M. Ranieri, *et al.*, Thiostrepton Hijacks Pyoverdine Receptors to Inhibit Growth of *Pseudomonas aeruginosa*. *Antimicrob. Agents Chemother.* **63** (2019).
28. D. C. K. Chan, L. L. Burrows, Thiocillin and micrococcin exploit the ferrioxamine receptor of *Pseudomonas aeruginosa* for uptake. *J. Antimicrob. Chemother.* **76**, 2029–2039 (2021).
29. D. C. K. Chan, L. L. Burrows, Thiopeptides: antibiotics with unique chemical structures and diverse biological activities. *J. Antibiot. 2020 743* **74**, 161–175 (2020).
30. D. C. K. Chan, L. L. Burrows, *Pseudomonas aeruginosa* FpvB Is a High-Affinity Transporter for Xenosiderophores Ferrichrome and Ferrioxamine B. *MBio* (2022) https:/doi.org/10.1128/MBIO.03149-22.
31. Z. Hou, K. N. Raymond, B. O'Sullivan, T. W. Esker, T. Nishio, A Preorganized Siderophore: Thermodynamic and Structural Characterization of Alcaligin and Bisucaberin, Microbial Macrocyclic Dihydroxamate Chelating Agents. *Inorg. Chem.* **37**, 6630–6637 (1998).
32. R. E. W. Hancock, F. S. L. Brinkman, Function of *Pseudomonas* porins in uptake and efflux. *Annu. Rev. Microbiol.* **56**, 17–38 (2002).
33. O. Trott, A. J. Olson, AutoDock Vina: Improving the speed and accuracy of docking with a new scoring function, efficient optimization, and multithreading. *J. Comput. Chem.* **31**, 455–461 (2010).
34. J. Eberhardt, D. Santos-Martins, A. F. Tillack, S. Forli, AutoDock Vina 1.2.0: New Docking Methods, Expanded Force Field, and Python Bindings. *J. Chem. Inf. Model.* **61**, 3891–3898 (2021).
35. A. Grosdidier, V. Zoete, O. Michielin, SwissDock, a protein-small molecule docking web service based on EADock DSS. *Nucleic Acids Res.* **39**, W270 (2011).
36. C. Dominguez, R. Boelens, A. M. J. J. Bonvin, HADDOCK: A protein-protein docking approach based on biochemical or biophysical information. *J. Am. Chem. Soc.* **125**, 1731–1737 (2003).
37. D. Qiu, F. H. Damron, T. Mima, H. P. Schweizer, H. D. Yu, PBAD-Based Shuttle Vectors for Functional Analysis of Toxic and Highly Regulated Genes in *Pseudomonas* and

Burkholderia spp. and Other Bacteria. *Appl. Environ. Microbiol.* **74**, 7422 (2008).
38. J. Koo, *et al.*, PilF is an outer membrane lipoprotein required for multimerization and localization of the *Pseudomonas aeruginosa* type IV pilus secretin. *J. Bacteriol.* **190**, 6961–6969 (2008).
39. A. Kumar, *et al.*, Fluorescent sensors of siderophores produced by bacterial pathogens. *J. Biol. Chem.* **298** (2022).
40. Z. Cao, P. Warfel, S. M. C. Newton, P. E. Klebba, Spectroscopic observations of ferric enterobactin transport. *J. Biol. Chem.* **278**, 1022–1028 (2003).
41. D. M. Emms, S. Kelly, SHOOT: phylogenetic gene search and ortholog inference. *Genome Biol. 2022 231* **23**, 1–13 (2022).
42. I. Letunic, P. Bork, Interactive Tree Of Life (iTOL) v5: an online tool for phylogenetic tree display and annotation. *Nucleic Acids Res.* **49**, W293–W296 (2021).
43. S. M. C. Newton, J. D. Igo, D. C. Scott, P. E. Klebba, Effect of loop deletions on the binding and transport of ferric enterobactin by FepA. *Mol. Microbiol.* **32**, 1153–1165 (1999).
44. A. D. Ferguson, *et al.*, Active transport of an antibiotic rifamycin derivative by the outer-membrane protein FhuA. *Structure* **9**, 707–716 (2001).
45. H. E. James, P. A. Beare, L. W. Martin, I. L. Lamont, Mutational analysis of a bifunctional ferrisiderophore receptor and signal-transducing protein from *Pseudomonas aeruginosa*. *J. Bacteriol.* **187**, 4514–4520 (2005).
46. T. T. Hoang, R. R. Karkhoff-Schweizer, A. J. Kutchma, H. P. Schweizer, A broad-host-range Flp-FRT recombination system for site-specific excision of chromosomally-located DNA sequences: application for isolation of unmarked *Pseudomonas aeruginosa* mutants. *Gene* **212**, 77–86 (1998).
47. S. N. Ho, H. D. Hunt, R. M. Horton, J. K. Pullen, L. R. Pease, Site-directed mutagenesis by overlap extension using the polymerase chain reaction. *Gene* **77**, 51–59 (1989).
48. M. T. Rybtke, *et al.*, Fluorescence-Based Reporter for Gauging Cyclic Di-GMP Levels in Pseudomonas aeruginosa. *Appl. Environ. Microbiol.* **78**, 5060 (2012).
49. W. Kabsch, XDS. *urn:issn:0907-4449* **66**, 125–132 (2010).
50. P. R. Evans, An introduction to data reduction: Space-group determination, scaling and intensity statistics. *Acta Crystallogr. Sect. D Biol. Crystallogr.* **67**, 282–292 (2011).
51. P. V. Afonine, *et al.*, Towards automated crystallographic structure refinement with phenix.refine. *Acta Crystallogr. Sect. D Biol. Crystallogr.* **68**, 352–367 (2012).
52. E. F. Pettersen, *et al.*, UCSF Chimera—A visualization system for exploratory research and analysis. *J. Comput. Chem.* **25**, 1605–1612 (2004).
53. R. Apweiler, *et al.*, UniProt: The universal protein knowledgebase. *Nucleic Acids Res.* **32**, 13–14 (2004).
54. R. C. Edgar, MUSCLE: A multiple sequence alignment method with reduced time and space complexity. *BMC Bioinformatics* **5**, 1–19 (2004).

Supporting Information

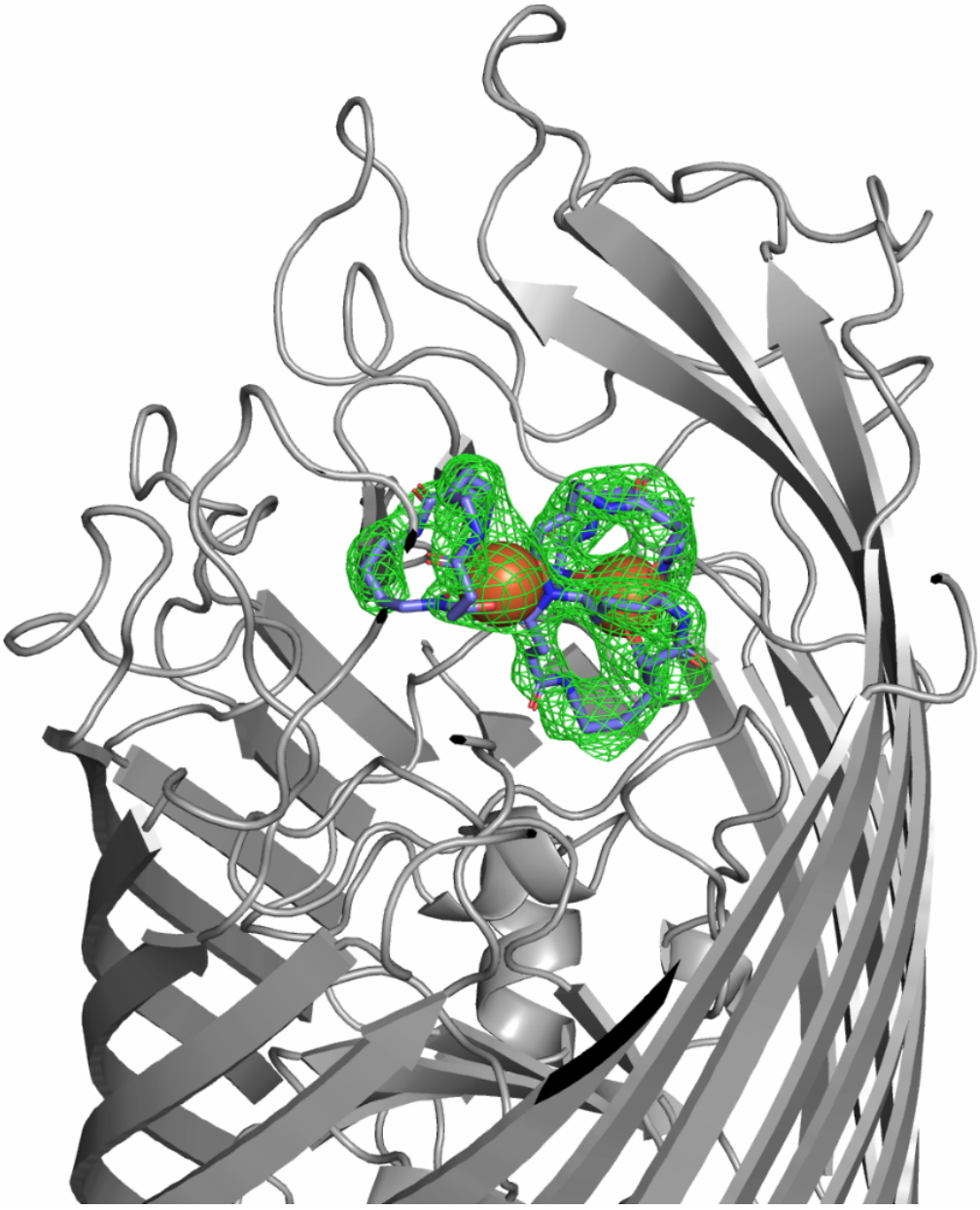

Supplementary Figure 1. OMIT electron density map for bisucaberin$_3$(blue)-$Fe^{3+}{}_2$ (orange)-FoxA (grey).

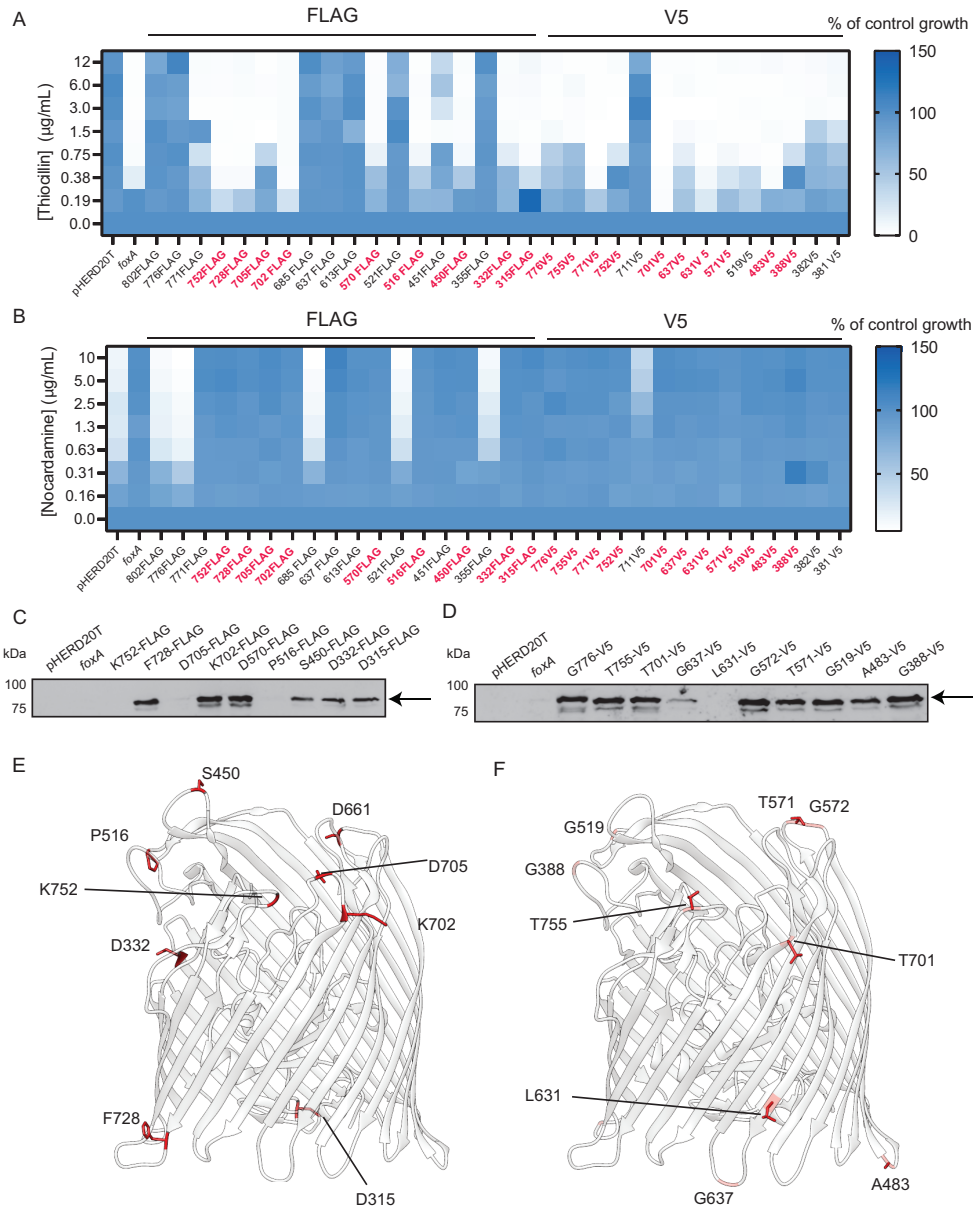

Supplementary Figure 2. Screening for permissive locations on FoxA for insertion of FLAG or V5 epitopes. Epitope tags were introduced into foxA by overlap extension PCR and the resulting proteins expressed in trans. (A) Thiocillin MIC assay with PA14 Δ*foxA* harbouring tagged foxA in pHERD20T tested in 10:90 + 1% arabinose. Transporters that resensitized Δ*foxA* to thiocillin are bolded in red. (B) Nocardamine growth assay with PA14 Δ*foxA* harbouring tagged *foxA* in pHERD20T in 10:90 + 1% arabinose. Transporters that complemented Δ*foxA* growth with nocardamine are bolded and highlighted in red. (C) Detection of selected FLAG tags in strains with WT susceptibility to thiocillin and that grow in the presence of nocardamine. Empty vector and WT FoxA were used as negative controls. (D) Detection of selected V5 tags in strains that had WT susceptibility to thiocillin and that grow in the presence of nocardamine. Empty vector and WT FoxA were used as negative controls. (E and F) Locations of inserted FLAG and V5 epitope tags respectively (PDB:6I98).

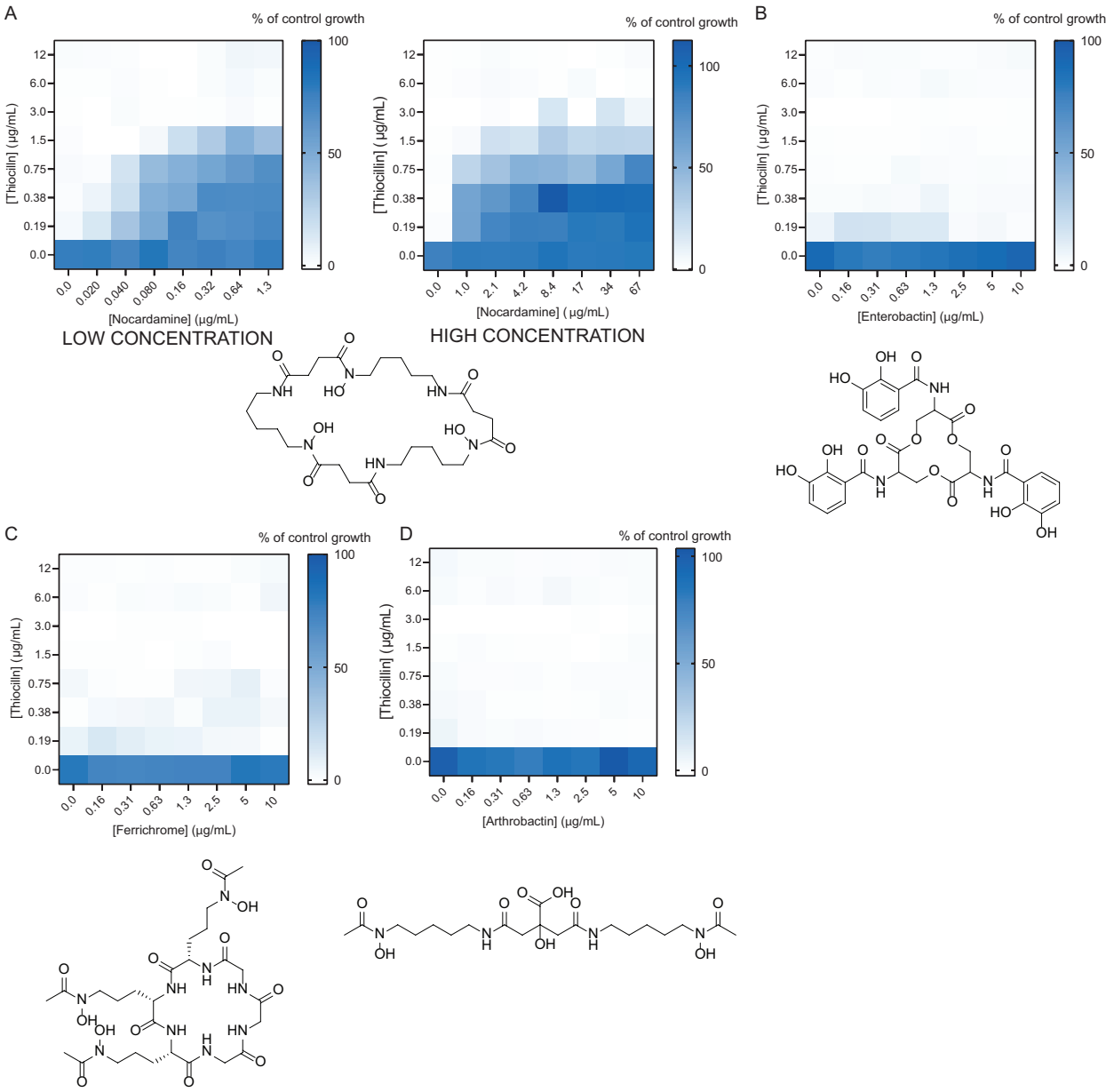

Supplementary Figure 3. Only nocardamine antagonizes thiocillin uptake. Checkerboard assays of PA14 Δ*foxA* pHERD20T-*foxA* grown with thiocillin and different siderophores. (A) Nocardamine (highest concentration tested at 1.3 µg/mL and 67 µg/mL), (B), enterobactin, (C) ferrichrome, and (D) arthrobactin in 10:90 + 1% arabinose. Structures of the siderophores are shown. Growth is expressed as percent of vehicle control where blue indicates growth and white indicates no growth. All checkerboards are averages of three independent biological replicates.

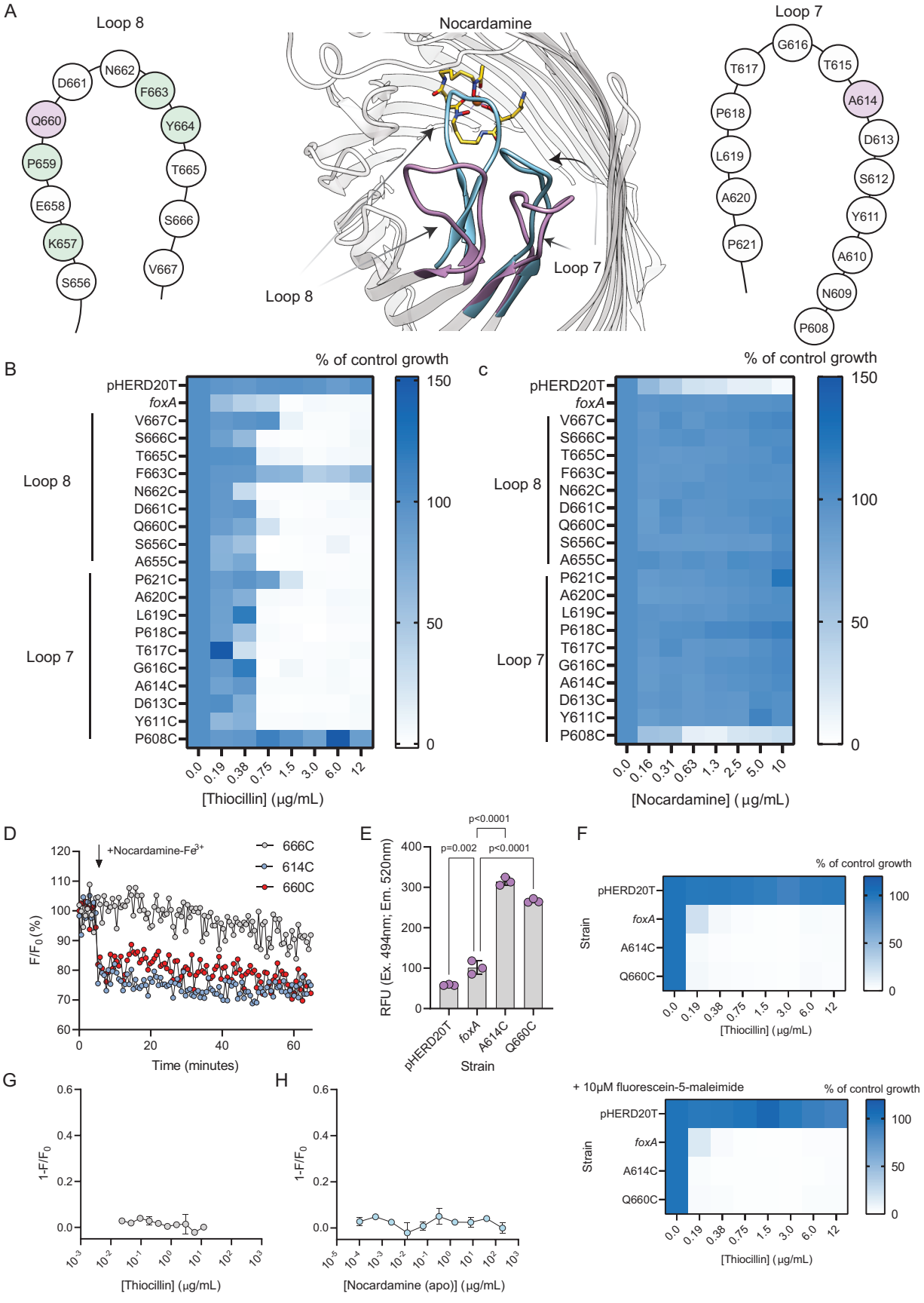
A
Loop 8
N662
D661
F663
Q660
Y664
P659
T665
E658
S666
K657
V667
S656
Nocardamine
Loop 8
Loop 7
Loop 7
G616
T617
T615
P618
A614
D613
L619
S612
A620
Y611
P621
A610
N609
P608
B
% of control growth
pHERD20T
foxA
V667C
S666C
T665C
F663C
N662C
D661C
Q660C
S656C
A655C
P621C
A620C
L619C
P618C
T617C
G616C
A614C
D613C
Y611C
P608C
Loop 8
Loop 7
150
100
50
0
0.0
0.19
0.38
0.75
1.5
3.0
6.0
12
[Thiocillin] (µg/mL)
c
% of control growth
pHERD20T
foxA
V667C
S666C
T665C
F663C
N662C
D661C
Q660C
S656C
A655C
P621C
A620C
L619C
P618C
T617C
G616C
A614C
D613C
Y611C
P608C
Loop 8
Loop 7
150
100
50
0
0.0
0.16
0.31
0.63
1.3
2.5
5.0
10
[Nocardamine] (µg/mL)
D
+Nocardamine-Fe3+
666C
614C
660C
F/F0 (%)
120
110
100
90
80
70
60
0
20
40
60
Time (minutes)
E
p<0.0001
p=0.002
p<0.0001
RFU (Ex. 494nm; Em. 520nm)
400
300
200
100
0
pHERD20T
foxA
A614C
Q660C
Strain
F
% of control growth
pHERD20T
foxA
A614C
Q660C
Strain
100
50
0
0.0
0.19
0.38
0.75
1.5
3.0
6.0
12
[Thiocillin] (µg/mL)
G
1-F/F0
0.6
0.4
0.2
0.0
10-3
10-2
10-1
100
101
102
103
[Thiocillin] (µg/mL)
H
1-F/F0
0.6
0.4
0.2
0.0
10-5
10-4
10-3
10-2
10-1
100
101
102
103
[Nocardamine (apo)] (µg/mL)
+ 10µM fluorescein-5-maleimide
% of control growth
pHERD20T
foxA
A614C
Q660C
Strain
100
50
0
0.0
0.19
0.38
0.75
1.5
3.0
6.0
12
[Thiocillin] (µg/mL)

Supplementary Figure 4. Screening for permissive cysteine-labeling sites for FoxA that allow WT responses to nocardamine. Cysteine mutagenesis of L7 and L8 was conducted to find residues that could be used for detecting nocardamine-Fe^{3+} binding. (A) Depiction of FoxA L7 and L8 movement upon siderophore binding generated from PBD 6I96 and 6I97, respectively. Loop orientation before and after siderophore binding is shown in purple and blue, respectively. Ferrioxamine B-Fe^{3+} is shown in orange. L8 (left) and L7 (right) amino acid compositions are shown with residues important for thiocillin susceptibility highlighted in green. Residues that can be used for detection are highlighted in purple. PA14 Δ*foxA* expressing L7 and L8 cysteine mutants in trans were tested for susceptibility to (B) thiocillin and (C) ability to grow with nocardamine. Thiocillin tests were conducted in 10:90 + 1% arabinose while apo-nocardamine tests were conducted in iron-limited CAA + 1% arabinose. (D) Screening of fluorescein-5-maleimide labeled FoxA cysteine mutants for fluorescence quenching upon addition of nocardamine-Fe^{3+}. Fluorescence was measured for 5 min initially (Ex. 494nm Em. 518nm) and nocardamine-Fe^{3+} was added where indicated by the arrow. All cysteine mutants were screened with 0.050 µg/mL nocardamine-Fe^{3+}. Fluorescence of labeled A614C and Q660C was quenched. S666C is shown as an example of the remaining transporters that did not respond to addition of nocardamine-Fe^{3+}. (E) Labeling by fluorescein-5-maleimide of A614C and Q660C compared to WT FoxA and empty vector controls. Three independent biological replicates are shown. One-way ANOVA followed by Dunnett's test was used for statistical determinations. (F) Thiocillin activity in the absence (top) and presence of 10µM fluorescein-5-maleimide. Three independent biological replicates were conducted with the averaged result shown. (G) Quenching by thiocillin and (H) apo-nocardamine using the A614C sensor strain. Results shown are averaged from two independent biological replicates.

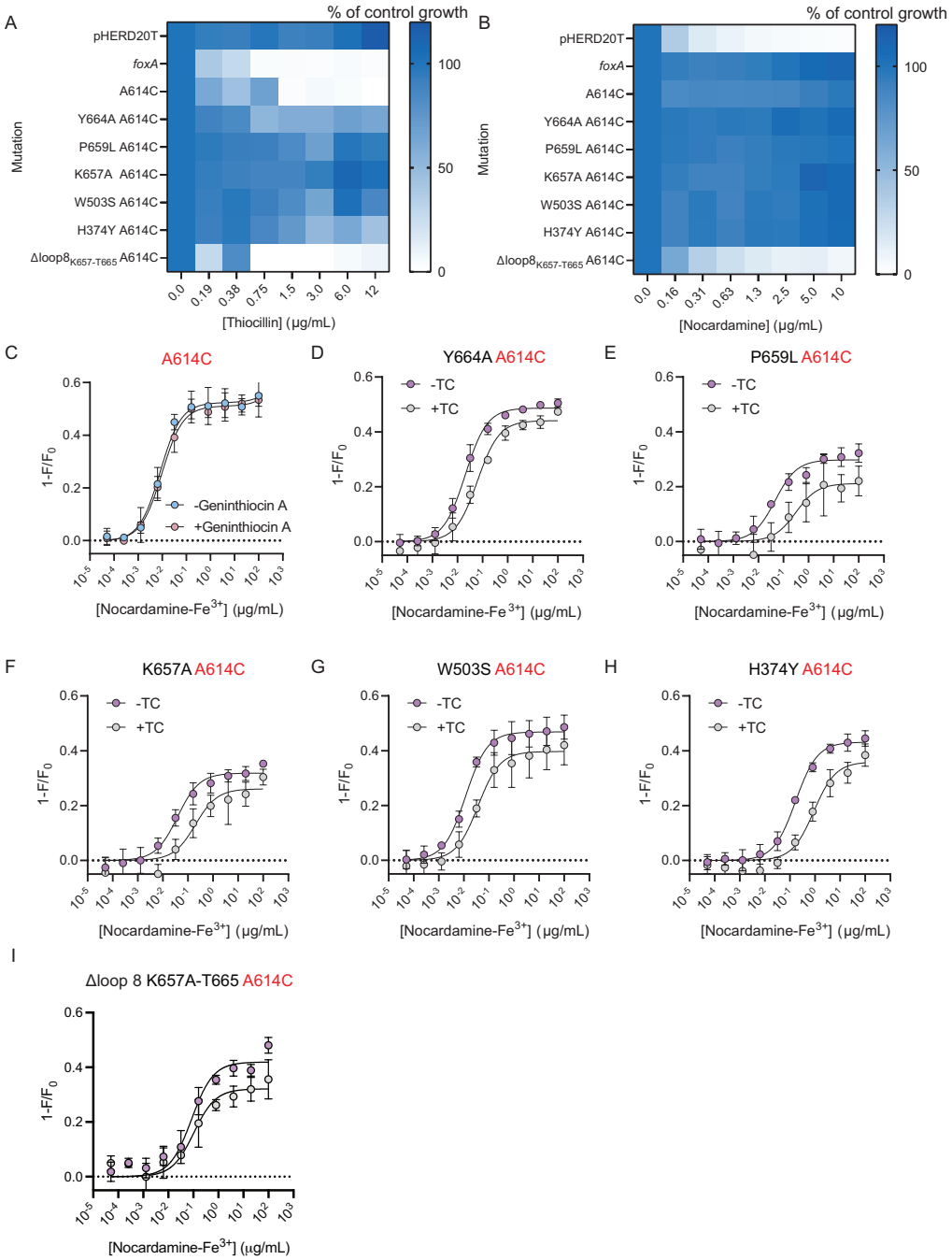

Supplementary Figure 5. Labeled single residue mutants have reduced affinity for nocardamine-Fe^{3+} and addition of thiocillin further reduces the K_d. (A) MIC assays with PA14 Δ*foxA* expressing labeled single amino acid mutants treated with thiocillin. (B) MIC assays with PA14 ΔfoxA expressing labeled single amino acid mutants treated with apo-nocardamine. (C) Fluorescence quenching of FoxA A614C labeled with fluorescein-5-maleimide. Cells were treated without (blue circles) or with 11 μg/mL (10 μM) geninthiocin A (red circles) for 5 mins prior to nocardamine-Fe^{3+} addition. (D-I) Fluorescence quenching of fluorescein-5-maleimide-labeled FoxA mutants. Results are averaged from three independent biological replicates with standard deviations shown. Purple circles indicate quenching in the absence of thiocillin pre-treatment whereas grey circles indicate quenching after thiocillin pre-treatment.

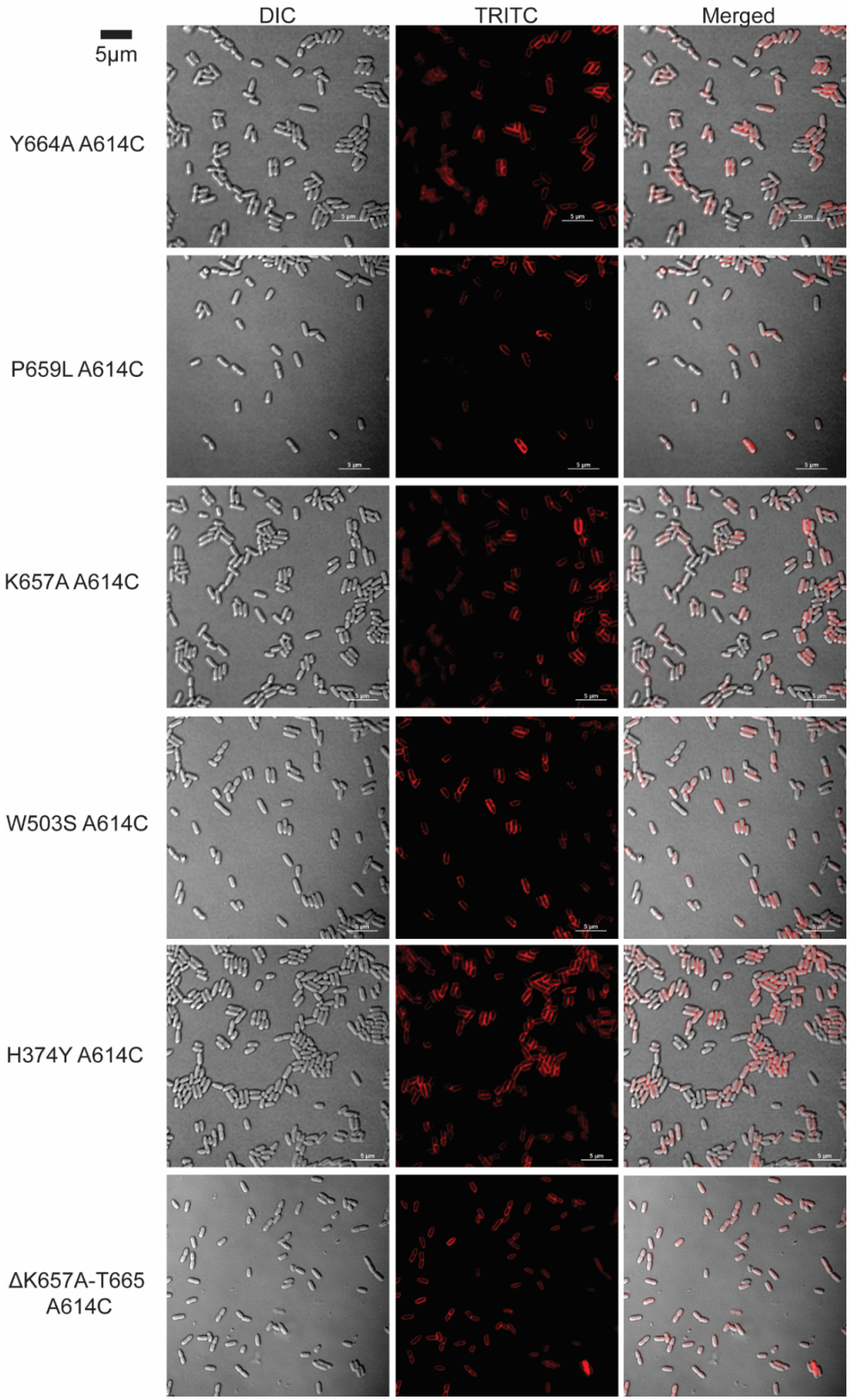

Supplementary Figure 6. Confocal microscopy images of AlexaFluor 594 labeled FoxA A614C with amino acid mutations. Representative images for each strain are shown. Scale bar = 5µm.

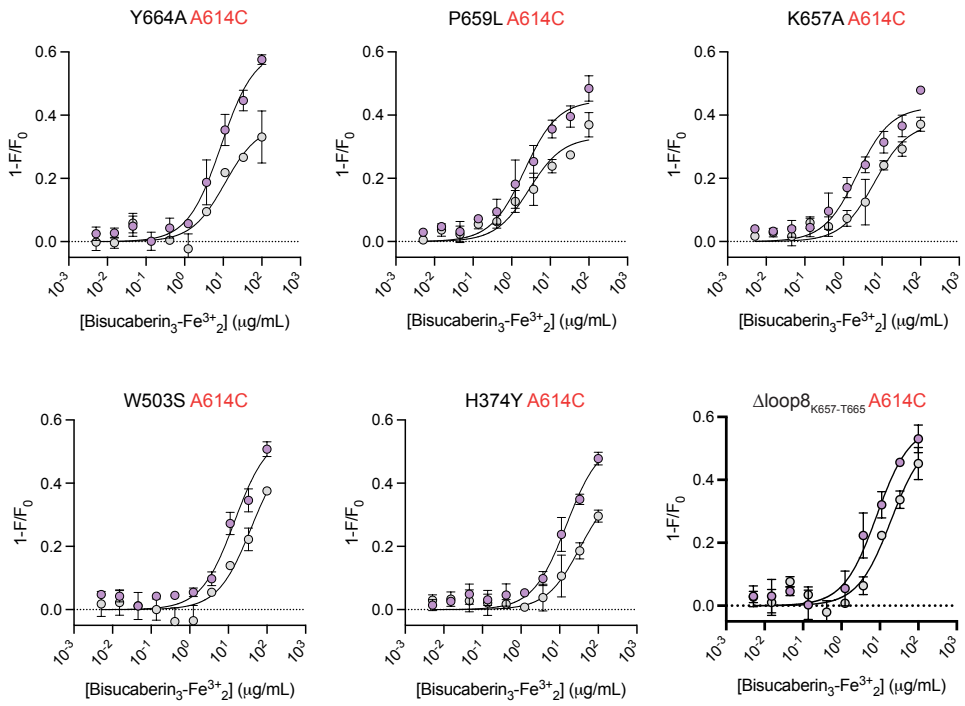

Supplementary Figure 7. Fluorescence quenching of labeled FoxA and FoxA mutants by bisucaberin with and without thiocillin. Results are averaged from three independent biological replicates.

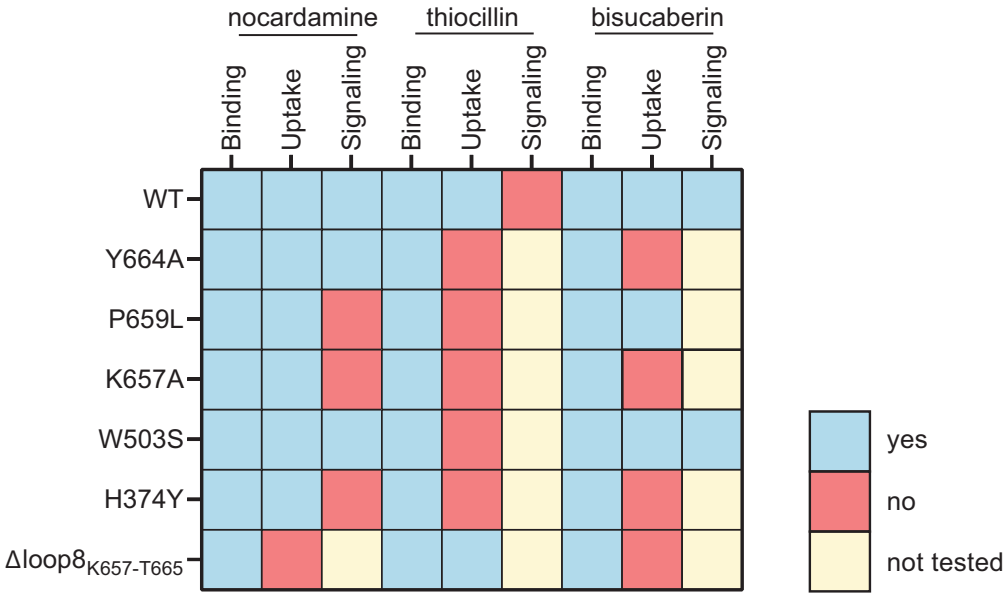

Supplementary Figure 8. Summary of phenotypes of FoxA mutants. Mutations are listed on the left and their effects on ligand binding, uptake, and signaling are indicated. Blue boxes indicate that the phenotype was observed. Red boxes indicate that the phenotype was not observed or disrupted. Yellow boxes indicate that the phenotype was not tested for a particular mutation. If uptake was not observed, then signaling was not tested. Signaling for P659L was not tested since the V5 tag was not detected even *in trans*.

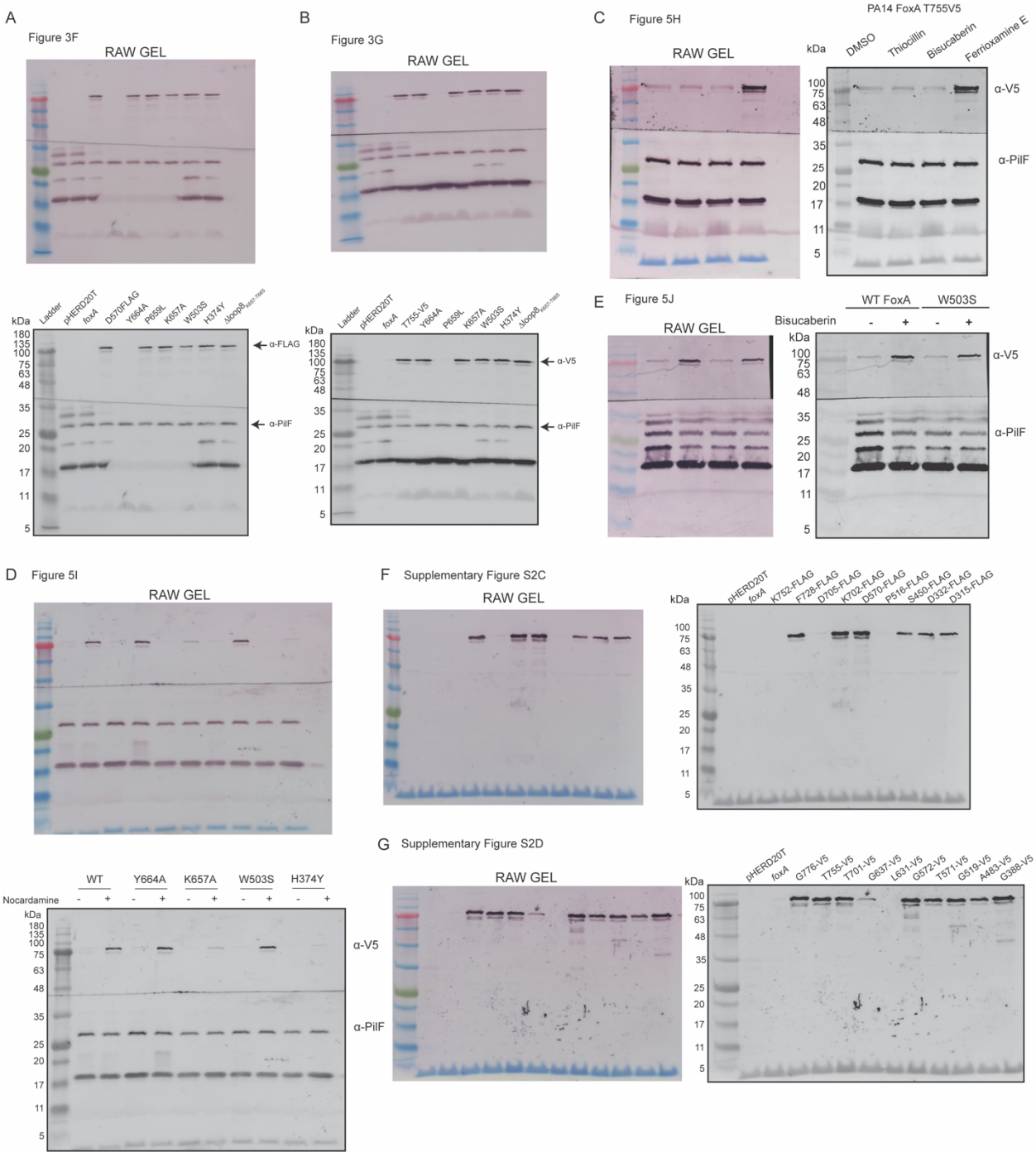

Supplementary Figure 9. Raw and labeled blots. (A) Fig. 3F, (B) Fig. 3G, (C) Fig. 5H, (D) Fig. 5I, (E) Fig. 5J, (H) SI Appendix Fig. S2C, and I) SI Appendix Fig. S2D. Raw blots are shown above (A, B, D) or left (C, E-G) and labeled blots below or right. Raw blots were converted to grey scale and labeled.

Supplementary Table 1. FoxA data collection and refinement statistics

	FoxA dataset* (PDBID: 8B43)
Data collection	
Beamline	PETRA III, P13
Space group	$P3_221$
Cell dimensions	
a, *b*, *c* (Å)	95.4, 95.4, 177.98
α, β, γ (°)	90, 90, 120
Resolution (Å)	82.628-2.49 (2.8-2.49)
R_{pim}	0.043 (0.506)
R_{meas}	0.185 (1.97)
$I / \sigma I$	16 (1.8)
$CC_{1/2}$	0.99 (0.727)
Completeness (%) spherical ellipsoidal	 60.5 (10.3) 92.5 (74.4)
Redundancy	18.1 (14.5)
Refinement	
Resolution (Å)	2.49
No. reflections	20915 (1045)
R_{work} / R_{free}	0.22/0.259
No. atoms	5509
Protein	5324
Ligand/ion	185
B-factors	
Protein	60.51
Ligand/ion	69.24
R.m.s. deviations	
Bond lengths (Å)	0.013
Bond angles (°)	1.809
Ramachandran (%) Favored regions Allowed regions Outliers	 94.07 5.78 0.15

*Values in parentheses are for highest-resolution shell.

Supplementary Table 2. Summary of K_d values from WT and mutants treated with nocardamine and thiocillin

*Values are averaged from three independent biological replicates

		-TC	+TC
	FoxA	K_d (ng/mL)	K_d (ng/mL)
Nocardamine-Fe^{3+}	A614C	6.0 ± 0.62*	12 ± 1.8
	Y664A	20 ± 1.8	62 ± 9.7
	P659L	46 ± 11	309 ± 186
	K657A	38 ± 8.3	198 ± 94
	W503S	12 ± 1.7	37 ± 9.7
	H374Y	168 ± 20	898 ± 215
	ΔL8	85 ± 20	105 ± 32

Supplementary Table 3. List of Strains

P. aeruginosa strains	Reference
PA14	1
PA14 Δ*foxA*	This study
PA14 Δ*foxA* pHERD20T	This study
PA14 Δ*foxA* pHERD20T-*foxA*	This study
PA14 Δ*foxA* pHERD20T-*foxA* Y664A	This study
PA14 Δ*foxA* pHERD20T-*foxA* P659L	This study
PA14 Δ*foxA* pHERD20T-*foxA* K657A	This study
PA14 Δ*foxA* pHERD20T-*foxA* W503S	This study
PA14 Δ*foxA* pHERD20T-*foxA* H374Y	This study
PA14 Δ*foxA* pHERD20T-*foxA* ΔL8 K657-T665	This study
PA14 Δ*foxA* pHERD20T-*foxA* D570 FLAG	This study
PA14 Δ*foxA* pHERD20T-*foxA* Y664A D570FLAG	This study
PA14 Δ*foxA* pHERD20T-*foxA* P659L D570FLAG	This study
PA14 Δ*foxA* pHERD20T-*foxA* K657A D570FLAG	This study
PA14 Δ*foxA* pHERD20T-*foxA* W503S D570FLAG	This study
PA14 Δ*foxA* pHERD20T-*foxA* H374Y D570FLAG	This study
PA14 Δ*foxA* pHERD20T-*foxA* ΔL8 K657-T665 D570FLAG	This study
PA14 Δ*foxA* pHERD20T-*foxA* T755V5	This study
PA14 ΔfoxA pHERD20T-foxA Y664A T755V5	This study
PA14 ΔfoxA pHERD20T-foxA P659L T755V5	This study
PA14 ΔfoxA pHERD20T-foxA K657A T755V5	This study
PA14 ΔfoxA pHERD20T-foxA W503S T755V5	This study
PA14 ΔfoxA pHERD20T-foxA H374Y T755V5	This study
PA14 ΔfoxA pHERD20T-foxA ΔL8 K657-T665 T755V5	This study

PA14 Δ*foxA* pHERD20T-*foxA* A614C	This study
PA14 P_x-*gfp*	This study
PA14 P_{foxA}-*gfp*	This study
PA14 P_{foxA}-*gfp* FoxA Y664A (Chromosomal)	This study
PA14 P_{foxA}-*gfp* FoxA P659L (Chromosomal)	This study
PA14 P_{foxA}-*gfp* FoxA K657A (Chromosomal)	This study
PA14 P_{foxA}-*gfp* FoxA W503S (Chromosomal)	This study
PA14 P_{foxA}-*gfp* FoxA H374Y (Chromosomal)	This study
PA14 P_x-*gfp* FoxA Y664A (Chromosomal)	This study
PA14 P_x-*gfp* FoxA P659L (Chromosomal)	This study
PA14 P_x-*gfp* FoxA K657A (Chromosomal)	This study
PA14 P_x-*gfp* FoxA W503S (Chromosomal)	This study
PA14 P_x-*gfp* FoxA H374Y (Chromosomal)	This study
PA14 FoxA Y664A (Chromosomal)	This study
PA14 FoxA P659L (Chromosomal)	This study
PA14 FoxA K657A (Chromosomal)	This study
PA14 FoxA W503S (Chromosomal)	This study
PA14 FoxA H374Y (Chromosomal)	This study
PA14 FoxA T755V5 (Chromosomal)	This study
PA14 FoxA Y664A T755V5 (Chromosomal)	This study
PA14 FoxA P659L T755V5 (Chromosomal)	This study
PA14 FoxA K657A T755V5 (Chromosomal)	This study
PA14 FoxA W503S T755V5 (Chromosomal)	This study
PA14 FoxA H374Y T755V5 (Chromosomal)	This study
PA14 Δ*pvdA* Δ*pchA*	2
PA14 Δ*pvdA* Δ*pchA* Δ*46640*	This study
PA14 Δ*pvdA* Δ*pchA* Δ*foxA*	This study
PA14 Δ*pvdA* Δ*pchA* Δ*foxA* pHERD20T	This study
PA14 Δ*pvdA* Δ*pchA* Δ*foxA* pHERD20T-*foxA*	This study
PA14 Δ*pvdA* Δ*pchA* Δ*foxA* pHERD20T-*foxA* Y664A	This study
PA14 Δ*pvdA* Δ*pchA* Δ*foxA* pHERD20T-*foxA* P659L	This study
PA14 ΔpvdA ΔpchA ΔfoxA pHERD20T-foxA K657A	This study
PA14 Δ*pvdA* Δ*pchA* Δ*foxA* pHERD20T-*foxA* W503S	This study
PA14 Δ*pvdA* Δ*pchA* Δ*foxA* pHERD20T-*foxA* H374Y	This study
PA14 Δ*pvdA* Δ*pchA* Δ*foxA* pHERD20T-*foxA* Δloop 8 T665-K657	This study
PA14 Δ*pvdA* Δ*pchA* FoxA T755V5 (Chromosomal)	This study
PA14 Δ*pvdA* Δ*pchA* FoxA W503S T755V5 (Chromosomal)	This study
PA14 Δ*foxA* pHERD20T-*foxA* Y664Q	This study
PA14 Δ*foxA* pHERD20T-*foxA* Y664S	This study
PA14 Δ*foxA* pHERD20T-*foxA* P659E	This study
PA14 Δ*foxA* pHERD20T-*foxA* K657Q	This study

PA14 Δ*foxA* pHERD20T-*foxA* K657T	This study
PA14 Δ*foxA* pHERD20T-*foxA* W503G	This study
PA14 Δ*foxA* pHERD20T-*foxA* W503T	This study
PA14 Δ*foxA* pHERD20T-*foxA* 802FLAG	This study
PA14 Δ*foxA* pHERD20T-*foxA* 776FLAG	This study
PA14 Δ*foxA* pHERD20T-*foxA* 771FLAG	This study
PA14 Δ*foxA* pHERD20T-*foxA* 752FLAG	This study
PA14 Δ*foxA* pHERD20T-*foxA* 728FLAG	This study
PA14 Δ*foxA* pHERD20T-*foxA* 705FLAG	This study
PA14 Δ*foxA* pHERD20T-*foxA* 702FLAG	This study
PA14 Δ*foxA* pHERD20T-*foxA* 685FLAG	This study
PA14 Δ*foxA* pHERD20T-*foxA* 637FLAG	This study
PA14 Δ*foxA* pHERD20T-*foxA* 613FLAG	This study
PA14 Δ*foxA* pHERD20T-*foxA* 570FLAG	This study
PA14 Δ*foxA* pHERD20T-*foxA* 521FLAG	This study
PA14 Δ*foxA* pHERD20T-*foxA* 516FLAG	This study
PA14 Δ*foxA* pHERD20T-*foxA* 451FLAG	This study
PA14 Δ*foxA* pHERD20T-*foxA* 450FLAG	This study
PA14 Δ*foxA* pHERD20T-*foxA* 355FLAG	This study
PA14 Δ*foxA* pHERD20T-*foxA* 332FLAG	This study
PA14 Δ*foxA* pHERD20T-*foxA* 315FLAG	This study
PA14 Δ*foxA* pHERD20T-*foxA* 776V5	This study
PA14 Δ*foxA* pHERD20T-*foxA* 775V5	This study
PA14 Δ*foxA* pHERD20T-*foxA* 771V5	This study
PA14 Δ*foxA* pHERD20T-*foxA* 752V5	This study
PA14 Δ*foxA* pHERD20T-*foxA* 711V5	This study
PA14 Δ*foxA* pHERD20T-*foxA* 701V5	This study
PA14 Δ*foxA* pHERD20T-*foxA* 637V5	This study
PA14 Δ*foxA* pHERD20T-*foxA* 631V5	This study
PA14 Δ*foxA* pHERD20T-*foxA* 571V5	This study
PA14 Δ*foxA* pHERD20T-*foxA* 519V5	This study
PA14 Δ*foxA* pHERD20T-*foxA* 483V5	This study
PA14 Δ*foxA* pHERD20T-*foxA* 388V5	This study
PA14 Δ*foxA* pHERD20T-*foxA* 382V5	This study
PA14 Δ*foxA* pHERD20T-*foxA* 381V5	This study
PA14 Δ*foxA* pHERD20T-*foxA* V667C	This study
PA14 Δ*foxA* pHERD20T-*foxA* S666C	This study
PA14 Δ*foxA* pHERD20T-*foxA* T665C	This study
PA14 Δ*foxA* pHERD20T-*foxA* F663C	This study
PA14 Δ*foxA* pHERD20T-*foxA* N662C	This study
PA14 Δ*foxA* pHERD20T-*foxA* D661C	This study
PA14 Δ*foxA* pHERD20T-*foxA* Q660C	This study
PA14 Δ*foxA* pHERD20T-*foxA* S656C	This study

PA14 Δ*foxA* pHERD20T-*foxA* A655C	This study
PA14 Δ*foxA* pHERD20T-*foxA* P621C	This study
PA14 Δ*foxA* pHERD20T-*foxA* A620C	This study
PA14 Δ*foxA* pHERD20T-*foxA* L619C	This study
PA14 Δ*foxA* pHERD20T-*foxA* P618C	This study
PA14 Δ*foxA* pHERD20T-*foxA* T617C	This study
PA14 Δ*foxA* pHERD20T-*foxA* G616C	This study
PA14 Δ*foxA* pHERD20T-*foxA* A614C	This study
PA14 Δ*foxA* pHERD20T-*foxA* A613C	This study
PA14 Δ*foxA* pHERD20T-*foxA* Y611C	This study
PA14 Δ*foxA* pHERD20T-*foxA* P608C	This study
PA14 Δ*foxA* pHERD20T-*foxA* A614C Y664A	This study
PA14 Δ*foxA* pHERD20T-*foxA* A614C P659L	This study
PA14 Δ*foxA* pHERD20T-*foxA* A614C K657A	This study
PA14 Δ*foxA* pHERD20T-*foxA* A614C W503S	This study
PA14 Δ*foxA* pHERD20T-*foxA* A614C H374Y	This study
PA14 Δ*foxA* pHERD20T-*foxA* A614C ΔLoop 8 T665-K657	This study
E. coli strains	
DH5α pHERD20T	This study
DH5α pHERD20T-*foxA*	This study
DH4α pHERD20T-*foxA* Y664A	This study
DH4α pHERD20T-*foxA* P659L	This study
DH4α pHERD20T-*foxA* K657A	This study
DH4α pHERD20T-*foxA* W503S	This study
DH4α pHERD20T-*foxA* H374Y	This study
DH4α pHERD20T-*foxA* ΔL8 K657-T665	This study
DH4α pHERD20T-*foxA* D570 FLAG	This study
DH4α pHERD20T-*foxA* Y664A D570FLAG	This study
DH4α pHERD20T-foxA P659L D570FLAG	This study
DH4α pHERD20T-*foxA* K657A D570FLAG	This study
DH4α pHERD20T-*foxA* W503S D570FLAG	This study
DH4α pHERD20T-*foxA* H374Y D570FLAG	This study
DH4α pHERD20T-*foxA* ΔL8 K657-T665 D570FLAG	This study
DH4α pHERD20T-*foxA* T755V5	This study
DH4α pHERD20T-*foxA* Y664A T755V5	This study
DH4α pHERD20T-*foxA* P659L T755V5	This study
DH4α pHERD20T-*foxA* K657A T755V5	This study
DH4α pHERD20T-*foxA* W503S T755V5	This study
DH4α pHERD20T-*foxA* H374Y T755V5	This study
DH4α pHERD20T-*foxA* ΔL8 K657-T665 T755V5	This study
DH4α pHERD20T-*foxA* A614C	This study
DH4α P_x-*gfp*	This study

DH4α P_{foxA}-*gfp*	This study
DH4α pHERD20T-*foxA* Y664Q	This study
DH4α pHERD20T-*foxA* Y664S	This study
DH4α pHERD20T-*foxA* P659E	This study
DH4α pHERD20T-*foxA* K657Q	This study
DH4α pHERD20T-*foxA* K657T	This study
DH4α pHERD20T-*foxA* W503G	This study
DH4α pHERD20T-*foxA* W503T	This study
DH4α pHERD20T-*foxA* 802FLAG	This study
DH4α pHERD20T-*foxA* 776FLAG	This study
DH4α pHERD20T-*foxA* 771FLAG	This study
DH4α pHERD20T-*foxA* 752FLAG	This study
DH4α pHERD20T-*foxA* 728FLAG	This study
DH4α pHERD20T-*foxA* 705FLAG	This study
DH4α pHERD20T-*foxA* 702FLAG	This study
DH4α pHERD20T-*foxA* 685FLAG	This study
DH4α pHERD20T-*foxA* 637FLAG	This study
DH4α pHERD20T-*foxA* 613FLAG	This study
DH4α pHERD20T-*foxA* 570FLAG	This study
DH4α pHERD20T-*foxA* 521FLAG	This study
DH4α pHERD20T-*foxA* 516FLAG	This study
DH4α pHERD20T-*foxA* 451FLAG	This study
DH4α pHERD20T-*foxA* 450FLAG	This study
DH4α pHERD20T-*foxA* 355FLAG	This study
DH4α pHERD20T-*foxA* 332FLAG	This study
DH4α pHERD20T-*foxA* 315FLAG	This study
DH4α pHERD20T-*foxA* 776V5	This study
DH4α pHERD20T-*foxA* 775V5	This study
DH4α pHERD20T-*foxA* 771V5	This study
DH4α pHERD20T-*foxA* 752V5	This study
DH4α pHERD20T-*foxA* 711V5	This study
DH4α pHERD20T-*foxA* 701V5	This study
DH4α pHERD20T-*foxA* 637V5	This study
DH4α pHERD20T-*foxA* 631V5	This study
DH4α pHERD20T-*foxA* 571V5	This study
DH4α pHERD20T-*foxA* 519V5	This study
DH4α pHERD20T-*foxA* 483V5	This study
DH4α pHERD20T-*foxA* 388V5	This study
DH4α pHERD20T-*foxA* 382V5	This study
DH4α pHERD20T-*foxA* 381V5	This study
DH4α pHERD20T-*foxA* V667C	This study
DH4α pHERD20T-*foxA* S666C	This study
DH4α pHERD20T-*foxA* T665C	This study

DH4α pHERD20T-*foxA* F663C	This study
DH4α pHERD20T-*foxA* N662C	This study
DH4α pHERD20T-*foxA* D661C	This study
DH4α pHERD20T-*foxA* Q660C	This study
DH4α pHERD20T-*foxA* S656C	This study
DH4α pHERD20T-*foxA* A655C	This study
DH4α pHERD20T-*foxA* P621C	This study
DH4α pHERD20T-*foxA* A620C	This study
DH4α pHERD20T-*foxA* L619C	This study
DH4α pHERD20T-*foxA* P618C	This study
DH4α pHERD20T-*foxA* T617C	This study
DH4α pHERD20T-*foxA* G616C	This study
DH4α pHERD20T-*foxA* A614C	This study
DH4α pHERD20T-*foxA* A613C	This study
DH4α pHERD20T-*foxA* Y611C	This study
DH4α pHERD20T-*foxA* P608C	This study
DH4α pHERD20T-*foxA* A614C Y664L	This study
DH4α pHERD20T-*foxA* A614C P659L	This study
DH4α pHERD20T-*foxA* A614C K657A	This study
DH4α pHERD20T-*foxA* A614C W503S	This study
DH4α pHERD20T-*foxA* A614C H374Y	This study
DH4α pHERD20T-*foxA* A614C ΔLoop 8 T665-K657	This study
SM10 pEX18Gm-Δ*foxA*	This study
SM10 pEX18Gm-*foxA* Y664L	This study
SM10 pEX18Gm-*foxA* P659L	This study
SM10 pEX18Gm-*foxA* K657A	This study
SM10 pEX18Gm-*foxA* W503S	This study
SM10 pEX18Gm-*foxA* H374Y	This study
SM10 pEX18Gm-*foxA* Y664L T755V5	This study
SM10 pEX18Gm-*foxA* P659L T755V5	This study
SM10 pEX18Gm-*foxA* K657A T755V5	This study
SM10 pEX18Gm-*foxA* W503S T755V5	This study
SM10 pEX18Gm-*foxA* H374Y T755V5	This study
SM10 pEX18Gm-ΔPA14_46640	This study

Supplementary Table 4. List of Primers

FoxA point mutation primers

Mutations		**Primer sequences**	
#	**Mutation**	**Forward (5'->3')**	**Reverse (5'->3')**
1	Y805A	CCTGGACTTCTGCGCATTCGGCGA	TCGCCGAATGCGCAGAAGTCCAGG
2	Q441A	GTAGGCGTAGACTGCAGACAGGTC	GACCTGTCTGCAGTCTACGCCTAC

3	H374L	ACGGGGGATATCTTGGCGGCGTAC	GTACGCCGCCAAGATATCCCCCGT
4	T245A	ACAGCGGTGCCTTCAGCTCGATGC	ACAGCGGTGCCTTCAGCTCGATGC
5	Y218V	AACCGCTACGACGTCGTGGTGATG	CATCACCACGACGTCGTAGCGGTT
6	F803A	CAGCCTGGATGCATGCTACTTCGG	CCGAAGTAGCATGCATCCAGGCTG
7	Y443L	GCAAGTACTAGCCTACGGCTGGAG	CTCCAGCCGTAGGCTAGTACTTGC
8	Y373A	CAACGGGGGTGCACACGGCGGCGT	ACGCCGCCGTGTGCACCCCCGTTG
9	F246A	GGTACCGCCTCTTCGATGCAGGTC	GACCTGCATCGAAGAGGCGGTACC
10	S247A	GGTACCTTCGCATCGATGCAGGTC	GACCTGCATCGATGCGAAGGTACC
11	S243A	CCATGGGCGACGCAGGAACCTTCA	TGAAGGTTCCTGCGTCGCCCATGG
12	D230V	ACAACAGCGTGGTTAACATCTACC	GGTAGATGTTAACCACGCTGTTGT
13	S228V	ACAACGTTGTGGACAACATCTACC	GGTAGATGTTGTCCACAACGTTGT
14	N227D	GCTTCGCCGACGACAGCGTGGACA	TGTCCACGCTGTCGTCGGCGAAGC
15	N227A	GCTTCGCCGACGCGTCCGTGGACA	TGTCCACGGACGCGTCGGCGAAGC
16	D217A	AACCGCTATGCATACGTGGTGATG	CATCACCACGTATGCATAGCGGTT
17	Y216L	AATCGATTGGACTACGTGGTGATG	CATCACCACGTAGTCCAATCGATT
18	R215V	CGCCTCCAACGTTTACGACTACGT	ACGTAGTCGTAAACGTTGGAGGCG
19	N214A	CGGCGCCAGGGCCCGCTACGACTA	TAGTCGTAGCGGGCCCTGGCGCCG
20	S213A	AGGTCGCGGCCGCCAACCGCTACG	CGTAGCGGTTGGCGGCCGCGACCT
21	P659L	GCCTCCAAGGAGCTGCAGGACAAC	GTTGTCCTGCAGCTCCTTGGAGGC
22	N662A	GAGCCCCAGGATGCATTCTACACC	GGTGTAGAATGCATCCTGGGGCTC
23	Y664A	AGGACAACTTCGCGACGTCGGTCG	CGACCGACGTCGCGAAGTTGTCCT
24	K752A	AGACCTGGGCGGACGCAGAA	TTCTGCGTCCGCCCAGGTCT
25	F663A	AAGGAGCCCCAGGACAACGCGTAC	GTACGCGTTGTCCTGGGGCTCCTT
26	D661A	CCAGGCCAACTTCTACACCTCGGT	ACCGAGGTGTAGAAGTTGGCCTGG
27	Q660A	CGCAGACAACTTCTACACCTCGGT	ACCGAGGTGTAGAAGTTGTCTGCG
28	D226A	GATGCGCGGCTTCGCCGCAAAC	GTTTGCGGCGAAGCCGCGCATC
29	D661C	CTCCAAGGAGCCCCAGTGCAACTT	AAGTTGCACTGGGGCTCCTTGGAG
30	G244A	CATGGGCGACAGCGCTACCTTCA	TGAAGGTAGCGCTGTCGCCCATG
31	Y611A	ACCCGAACGCCGCATCCGACGCCT	AGGCGTCGGATGCGGCGTTCGGGT
32	N609A	ACCCGGCAGCCTATTCCGACGCCT	AGGCGTCGGAATAGGCTGCCGGGT
33	R272A	GTGCTCTACGGCGCAAGCCTGCCG	CGGCAGGCTTGCGCCGTAGAGCAC
34	D242A	TCAAGGCCATGGGCGCAAGCGGTA	TACCGCTTGCGCCCATGGCCTTGA
35	K238A	TCGACGGCCTCGCAGCCATGGGC	GCCCATGGCTGCGAGGCCGTCGA
36	P608A	GTCGTTCAACGCAAACGCCTATTC	GAATAGGCGTTTGCGTTGAACGAC
37	S273A	GCTCTACGGCCGTGCACTGCCGG	CCGGCAGTGCACGGCCGTAGAGC
38	P275A	TCTACGGCCGTAGCCTGGCAGGCG	CGCCTGCCAGGCTACGGCCGTAGA
39	M240A	CGGTCTCAAGGCCGCAGGCGAC	GTCGCCTGCGGCCTTGAGACCG
40	N607A	GTCGTTCGCACCGAACGCCTATTC	GAATAGGCGTTCGGTGCGAACGAC
41	S615C	TTCCGACGCCTGCGGCACGCCCCT	AGGGGCGTGCCGCAGGCGTCGGAA
42	S573C	GCAGCACCGGCTGCAAGGCCGACG	CGTCGGCCTTGCAGCCGGTGCTGC
43	S703C	CATCACCTACACCAAGTGCCTGGA	TCCAGGCACTTGGTGTAGGTGATG
44	S450C	CTACGGCTGGAGCGCCTGCGAGC	GCTCGCAGGCGCTCCAGCCGTAG
45	S384C	GACGGCACCCTGTGCCACCACAAC	GTTGTGGTGGCACAGGGTGCCGTC

46	T571C	GCAGCTGCGGCAGCAAGGCCGACG	CGTCGGCCTTGCTGCCGCAGCTGC
47	T755C	AACTGCTTGCGGGTGCCGGACTAC	GTAGTCCGGCACCCGCAAGCAGTT
48	T382C	CGACGGCTGCCTGTCGCACCACAAC	GTTGTGGTGCGACAGGCAGCCGTCG
49	T617C	GGCTGTCCCCTGGCGCCCACCGA	TCGGTGGGCGCCAGGGGACAGCC
50	S612C	ATTGCGACGCCTCCGGCACGC	GCGTGCCGGAGGCGTCGCAAT
51	D613C	TCAACCCGAACGCCTATTCCTGCG	CGCAGGAATAGGCGTTCGGGTTGA
52	D661C	CCCAGTGCAACTTCTACAC	GTGTAGAAGTTGCACTGGG
53	H374Y	GGGCTACTATGGCGGCGTAC	GTACGCCGCCATAGTAGCCC
54	S666A	TACACCGCAGTCGGCGAAGTGC	GCACTTCGCCGACTGCGGTGTA
55	T665A	TACGCATCGGTCGGCGAAGTGC	GCACTTCGCCGACCGATGCGTA
56	Y218S	AACCGCTACGACAGTGTGGTGATG	CATCACCACACTGTCGTAGCGGTT
57	Y218D	AACCGCTACGACGATGTGGTGATG	CATCACCACATCGTCGTAGCGGTT
58	Y218F	AACCGCTACGACTTCGTGGTGATG	CATCACCACGAAGTCGTAGCGGTT
59	Y218K	AACCGCTACGACAAGGTGGTGATG	CATCACCACCTTGTCGTAGCGGTT
60	D230A	ACAACAGCGTGGCAAACATCTACC	GGTAGATGTTTGCCACGCTGTTGT
61	D230K	ACAACAGCGTGTTTAACATCTACC	GGTAGATGTTAAACACGCTGTTGT
62	D230F	ACAACAGCGTGTTCAACATCTACC	GGTAGATGTTGAACACGCTGTTGT
63	P527D	TCAGCTATTTCCGAGACGACA	TGTCGTCTCGGAAATAGCTGA
64	W503S	ACCGTGGTCGACTCTCGTTCC	GGAACGAGAGTCGACCACGGT
65	P527F	TCAGCTATTTCTTGGACGACA	TGTCGTCCAAGAAATAGCTGA
66	P621C	CACGCCCCTGGCGTGTACC	GGTACACGCCAGGGGCGTG
67	A620C	CACGCCCCTGTGTCCCACC	GGTGGGACACAGGGGCGTG
68	L619C	CACGCCCTGTGCGCCCACC	GGTGGGCGCACAGGGCGTG
69	P618C	CACGTGTCTGGCGCCCACC	GGTGGGCGCCAGACACGTG
70	G244F	CATGGGCGACAGCTTCACCTTCA	TGAAGGTGAAGCTGTCGCCCATG
71	G616C	TATTCCGACGCCTCCTGTACGC	GCGTACAGGAGGCGTCGGAATA
72	A614C	TATTCCGACTGCTCCGGCACGC	GCGTGCCGGAGCAGTCGGAATA
73	Y611C	TCAACCCGAACGCCTGTTCCGACG	CGTCGGAACAGGCGTTCGGGTTGA
74	A610C	TCAACCCGAACTGCTATTCCGACG	CGTCGGAATAGCAGTTCGGGTTGA
75	N609C	TCAACCCGTGCGCCTATTCCGACG	CGTCGGAATAGGCGCACGGGTTGA
76	A655C	AAACGTCTGCTCCAAGGAGCC	GGCTCCTTGGAGCAGACGTTT
77	S656C	AAACGTCGCCTGCAAGGAGCC	GGCTCCTTGCAGGCGACGTTT
78	Q660C	CTCCAAGGAGCCCTGCGACAACTT	AAGTTGTCGCAGGGCTCCTTGGAG
79	N662C	CTCCAAGGAGCCCCAGGACTGCTT	AAGCAGTCCTGGGGCTCCTTGGAG
80	F663C	ACAACTGCTACACCTCGGTCGGCG	CGCCGACCGAGGTGTAGCAGTTGT
81	T665C	ACAACTTCTACTGCTCGGTCGGCG	CGCCGACCGAGCAGTAGAAGTTGT
82	S666C	ACAACTTCTACACCTGCGTCGGCG	CGCCGACGCAGGTGTAGAAGTTGT
83	V667C	ACAACTTCTACACCTCGTGCGGCG	CGCCGCACGAGGTGTAGAAGTTGT
Deletion primers			
		Forward (5'->3')	Reverse (5'->3')
	WT *foxA* PA14	CAATTCTAGATTCAACGACTCCAAC GGATTCC	CAGTAAGCTTGTAGCCAGACCGACA TAGCG

	PfoxA	CAATTCTAGATGGGTGAGGGTGGTCGCCGCCTGA	CAATGCATGCTCATAGTTAATTTCTCCTCTTTGAACGGAATCCGTTGGAGTCGTTG
Δ*foxA*	Part 1	CAATGAATTCTGCAACTGAACACCGACAGCGCGG	CAATTCTAGAGAACGGAATCCGTTGGAGTCGTT
	Part 2	CAATTCTAGATCCTGGTTCTGCTGCACCGCTAT	CAATAAGCTTTACTGCAAGCGGTAGAAACGCTCT
Δ*pvdA*	Part 1	GCCGAATTCCATTATCGGGAGCTGCTGCGATTC	CAATGGATCCTTCCAGTTCCTCTGGATTGGCCCC
	Part 2	CAATGGATCCACGCAGGGCGTTTTCGTTGCATGT	CAATAAGCTTGAAGTGGCTGGAGGTATCCACCGT
Δ*pchA*	Part 1	CAATGAATTCTTCCGTAGCTGGAGCGAACGCCTG	TCGACGACGACATTCCGTTCTAATCATGCGGCACCCCGTGTCTGGCG
	Part 2	CGCCAGACACGGGGTGCCGCATGATTAGAACGGAATGTCGTCGTCGA	CAATAAGCTTGTGACCAGCATTCGCCTGCCGCTC
Δ*46640*	Part 1	AATGAATTCGCACCTGCGCCTCGGACTGGC	ATGCCTGCCCATGACAACGGGTCTCGATTTCCTATGCAGGTT
	Part 2	AACCTGCATAGGAAATCGAGACCCGTTGTCATGGGCAGGCAT	CATAAGCTTGGCAATGCTGCTGACGAGATCGT

FLAG and V5 tag primers

Tag	Forward (5'->3')	Reverse (5'->3')
D315FLAG	GACTACAAAGACGATGACGACAAGGAGGAGAAGCGCATCGCCTACC	CTTGTCGTCATCGTCTTTGTAGTCGAGCGGCCCGCTGAAAT
D332FLAG	GACTACAAAGACGATGACGACAAGACCCAGTTCGATCACGTCAAGGA	CTTGTCGTCATCGTCTTTGTAGTCCGAGCCCTTGCCGAGA
D355FLAG	GACTACAAAGACGATGACGACAAGGACACCACCCTGACCCTGCA	CTTGTCGTCATCGTCTTTGTGTCGCTGAAGTCGATGGCCAG
D403FLAG	GACTACAAAGACGATGACGACAAGGACTTCGACCGCACCCAGC	CTTGTCGTCATCGTCTTTGTAGTCCTTGCTCGGCTCGCCA
D421FLAG	GACTACAAAGACGATGACGACAAGGACGTCTGGTCGGCGCGG	CTTGTCGTCATCGTCTTTGTAGTCGATGCGGTGCTCCAGCT
S450FLAG	GACTACAAAGACGATGACGACAAGGAGCCGAACAAGCTGAACCGCTAC	CTTGTCGTCATCGTCTTTGTAGTCGCTGGCGCTCCAGCCGTA
E451FLAG	GACTACAAAGACGATGACGACAAGGAGCCGAACAAGCTGAACCGCTAC	CTTGTCGTCATCGTCTTTGTAGTCGCTGGCGCTCCAGCCGTA
P516FLAG	GACTACAAAGACGATGACGACAAGGTCTACGGCGACGACGCCATC	CTTGTCGTCATCGTCTTTGTAGTCCGGGTTGAACGCGTCCAGC
D521FLAG	GACTACAAAGACGATGACGACAAGGCCATCAGCTATTTCCCGGACGACA	CTTGTCGTCATCGTCTTTGTAGTCGTCGCCGTAGACCGG
D528FLAG	GACTACAAAGACGATGACGACAAGGACAACCACACCCGCCGCCTG	CTTGTCGTCATCGTCTTTGTAGTCCGGGAAATAGCTGATGGCG
D549FLAG	GACTACAAAGACGATGACGACAAGCAGTGGCGCTTCTCGCTCG	CTTGTCGTCATCGTCTTTGTGTCGATGTCGATCAGGTCCTGG
S570FLAG	GACTACAAAGACGATGACGACAAGACCGGCAGCAAGGCCGACGA	CTTGTCGTCATCGTCTTTGTAGTCGCTGCGGTTCTTGTCGGTGAC
F592FLAG	GACTACAAAGACGATGACGACAAGGACAACGGCCTGGCGCCC	CTTGTCGTCATCGTCTTTGTAGTCGTCGAACAGGTACAGCGCGC
D593FLAG	GACTACAAAGACGATGACGACAAGAACGGCCTGGCGCCCTAC	CTTGTCGTCATCGTCTTTGTGTCGAACAGGTACAGCGCGC
D613FLAG	GACTACAAAGACGATGACGACAAGGACGCCTCCGGCACGCCCCT	CTTGTCGTCATCGTCTTTGTAGTCGGAATAGGCGTTCGGGTT
A647FLAG	GACTACAAAGACGATGACGACAAGAGCAACAGCTTCTACACCGCCTCG	CTTGTCGTCATCGTCTTTGTAGTCGCCCGGCGCCTGGAACTT

D685FLAG	GACTACAAAGACGATGACGACAAGAACCTGAAGCTGCTCGGCAGC	CTTGTCGTCATCGTCTTTGTGTCGCTGAGCTGGGTATGGG
K702FLAG	GACTACAAAGACGATGACGACAAGTCGCTGGACGGCAACCAG	CTTGTCGTCATCGTCTTTGTAGTCCTTGGTGTAGGTGATGTCGGTG
D705FLAG	GACTACAAAGACGATGACGACAAGGGCAACCAGGGCCATACGCC	CTTGTCGTCATCGTCTTTGTAGTCCAGCGACTTGGTGTAGGT
F728FLAG	GACTACAAAGACGATGACGACAAGGACGCCGGCCCGCTCAGC	CTTGTCGTCATCGTCTTTGTAGTCGAAGGCATAGTCGGCCC
D751FLAG	GACTACAAAGACGATGACGACAAGGAAAACACCTTGCGGGTGC	CTTGTCGTCATCGTCTTTGTGTCCGCCCAGGTCTCGCC
K752FLAG	GACTACAAAGACGATGACGACAAGGAAAACACCTTGCGGGTGCCG	CTTGTCGTCATCGTCTTTGTAGTCCTTGTCCGCCCAGGTCTCG
D771FLAG	GACTACAAAGACGATGACGACAAGCTCGGCAAGCTCGGCCTGA	CTTGTCGTCATCGTCTTTGTGTCGTAACCGATCCGCGCG
G776FLAG	GACTACAAAGACGATGACGACAAGCTGAAAGGCCTGGACGTCAGC	CTTGTCGTCATCGTCTTTGTAGTCGCCGAGCTTGCCGAGGTC
D802FLAG	GACTACAAAGACGATGACGACAAGTTCTGCTACTTCGGCGAGAAGCGC	CTTGTCGTCATCGTCTTTGTAGTCCAGGCTGTAGCAGGACG
T333V5	GGTAAGCCTATCCCTAACCCTCTCCTCGGTCTCGATTCTACCCCGCTGGAAGCGGAAG	GGTAGAATCGAGACCGAGGAGAGGGTTAGGGATAGGCTTACCGTCGGCGAGCAGCCGGG
G381V5	AAGCCTATCCCTAACCCTCTCCTCGGTCTCGATTCTACCCTGTCGCACCACAACG	GGTAGAATCGAGACCGAGGAGAGGGTTAGGGATAGGCTTGCCGTCGGCCGGTACGCC
T382V5	GGCAAGCCTATCCCTAACCCTCTCCTCGGTCTCGATTCTACCCTGTCGCACCACAACGG	AGAATCGAGACCGAGGAGAGGGTTAGGGATAGGCTTGCCGTCGGCCGGTACGC
G388V5	AAGCCTATCCCTAACCCTCTCCTCGGTCTCGATTCTACGCGGCACATCTCCCGCGAG	CGTAGAATCGAGACCGAGGAGAGGGTTAGGGATAGGCTTGCCGTTGTGGTGCGACAGGGT
G482V5	AAGCCTATCCCTAACCCTCTCCTCGGTCTCGATTCTACGGCGGCGCGCCACACCCT	CGTAGAATCGAGACCGAGGAGAGGGTTAGGGATAGGCTTGCCGGTGGCGAATTCGGC
G519V5	AAGCCTATCCCTAACCCTCTCCTCGGTCTCGATTCTACGGACGACGCCATCAGCTATTTC	CGTAGAATCGAGACCGAGGAGAGGGTTAGGGATAGGCTTGCCGTAGACCGGGTTGAACGC
T571V5	GGTAAGCCTATCCCTAACCCTCTCCTCGGTCTCGATTCTACCGGCAGCAAGGCCGA	AGAATCGAGACCGAGGAGAGGGTTAGGGATAGGCTTACCGTAGGTGATGTCGGTGTAGGTG
G572V5	AAGCCTATCCCTAACCCTCTCCTCGGTCTCGATTCTACGAGCAAGGCCGACGACGACT	CGTAGAATCGAGACCGAGGAGAGGGTTAGGGATAGGCTTGCCGGTGCTGCGGTTCTTGTC
G637V5	AAGCCTATCCCTAACCCTCTCCTCGGTCTCGATTCTACGAGCAACAGCTTCTACACCGCC	CGTAGAATCGAGACCGAGGAGAGGGTTAGGGATAGGCTTGCCCGGCGCCTGGAACTT
T701V5	GGTAAGCCTATCCCTAACCCTCTCCTCGGTCTCGATTCTACCAAGTCGCTGGACGGCAAC	AGAATCGAGACCGAGGAGAGGGTTAGGGATAGGCTTACCGTAGGTGATGTCGGTGTAGGT
G706V5	AAGCCTATCCCTAACCCTCTCCTCGGTCTCGATTCTACGAACCAGGGCCATACGCCGAAC	CGTAGAATCGAGACCGAGGAGAGGGTTAGGGATAGGCTTGCCGTCCAGCGACTTGGTGTAG
T711V5	GGTAAGCCTATCCCTAACCCTCTCCTCGGTCTCGATTCTACGCCGAACCAGGCGCC	AGAATCGAGACCGAGGAGAGGGTTAGGGATAGGCTTACCATGGCCCTGGTTGCCGTCCA

G731V5	AAGCCTATCCCTAACCCTCTCCTCGGTCTCGATTCTACGCCGCTCAGCGGTCTGAGC	CGTAGAATCGAGACCGAGGAGAGGGTTAGGGATAGGCTTGCCGGCGTCGAAGGCATAG
T755V5	GGTAAGCCTATCCCTAACCCTCTCCTCGGTCTCGATTCTACCTTGCGGGTGCCGGACTACA	AGAATCGAGACCGAGGAGAGGGTTAGGGATAGGCTTACCGTTTTCCTTGTCCGCCCAGGT
G776V5	AAGCCTATCCCTAACCCTCTCCTCGGTCTCGATTCTACGCTGAAAGGCCTGGACGTCAGC	CGTAGAATCGAGACCGAGGAGAGGGTTAGGGATAGGCTTGCCGAGCTTGCCGAGGTC

GFP promoter assay primers		
	Forward (5'-->3')	Reverse (5'-->3')
P_{foxA}-*gfp*	CAATGCATGCTCATAGTTAATTTCTCCTCTTTGAACGGAATCCGTTGGAGTCGTTG	CAATTCTAGATGGGTGAGGGTGGTCGCCGCCTGA

SI References

1. Liberati NT, Urbach JM, Miyata S, et al. An ordered, nonredundant library of *Pseudomonas aeruginosa* strain PA14 transposon insertion mutants. *Proc Natl Acad Sci* 2006; 103: 2833–8.
2. Chan DCK, Burrows LL. *Pseudomonas aeruginosa* FpvB is a high-affinity transporter for xenosiderophores ferrichrome and ferrioxamine B. *Mbio.* 2022 Dec 12:e03149-22.

Chapter Six: Nutrient Limitation Sensitizes *P. aeruginosa* to Vancomycin

Preface

The work presented in the following chapter has been accepted in *ACS Infectious Diseases.*

Chan D. C. K., Dykema, K., Fatima, M., Harvey, H., Qaderi, I., and Burrows L. L. (2023). Nutrient limitation sensitizes *Pseudomonas aeruginosa* to vancomycin.

D.C.K.C. and L.L.B. designed the experiments and wrote the draft. D.C.K.C. performed the fluorescence microscopy, silver stain, western blot, GFP-promoter assays, phage plaque assays, and clinical isolate screening experiments. K.D. and D.C.K.C. conducted the transposon mutant screen. D.C.K.C. designed primers and D.C.K.C. and K.D. made the mutants. D.C.K.C. and K.D. conducted the checkerboards, antibiotic susceptibility assays, and raised spontaneous resistant mutants. M.F. assisted with the primary screen for antibiotics with increased activity under low-nutrient conditions. H.H. made the *pilA* mutant, isolated phages from environmental samples, and assisted with phage plaquing and silver stain assays. I.Q. purified phage P2B9 for phage studies.

This manuscript is available as a preprint at https://doi.org/10.1101/2023.04.10.536232.

Abstract

Traditional antibacterial screens rely on growing bacteria in nutrient-replete conditions which are not representative of the natural environment or sites of infection. Instead, screening in more physiologically relevant conditions may reveal novel activity for existing antibiotics. Here, we screened a panel of antibiotics reported to lack activity against the opportunistic Gram-negative bacterium, *Pseudomonas aeruginosa,* under low-nutrient and low-iron conditions, and discovered that the glycopeptide vancomycin inhibited growth of *P. aeruginosa* at low micromolar concentrations through its canonical mechanism of action, disruption of peptidoglycan cross-linking. Spontaneous vancomycin-resistant mutants had activating mutations in the sensor kinase of the two-component CpxSR system, which induced cross-resistance to almost all classes of β-lactams, including the siderophore antibiotic cefiderocol. Other mutations that conferred vancomycin resistance mapped to WapR, an α-1,3-rhamnosyltransferase involved in lipopolysaccharide core biosynthesis. A WapR P164T mutant had a modified LPS profile compared to wild type that was accompanied by increased susceptibility to select bacteriophages. We conclude that screening in nutrient-limited conditions can reveal novel activity for existing antibiotics and lead to discovery of new and impactful resistance mechanisms.

The outer membrane (OM) of Gram-negative bacteria provides intrinsic resistance to many antibiotics by reducing uptake. With some exceptions, the OM excludes large and charged molecules with a size-exclusion limit of ~600 Da[1]. The OM of the Gram-negative opportunistic pathogen *P. aeruginosa* is considered particularly impenetrable, up to 100-fold less permeable compared to that of *Escherichia coli*[2]. This characteristic, coupled with multiple efflux systems which extrude molecules that enter the cell, make *P. aeruginosa* infections difficult to treat. A better understanding of how antibiotics cross the OM may be informative for the development of new strategies to increase drug uptake.

A major contributor to OM impermeability is lipopolysaccharide (LPS), found in the outer leaflet. LPS is composed of a lipid A anchor, an inner and outer core oligosaccharide, and O-antigen of varying length and chemical composition. LPS contributes to membrane stability[3], motility[4,5], biofilm formation[6–8], and antibiotic resistance[9]. LPS is highly negatively charged due to the presence of phosphate groups on lipid A and the inner core region[10]. Divalent cations such as Mg^{2+} and Ca^{2+} are essential to neutralize the negative charge and maintain barrier integrity[11]. Some antibiotics, such as cationic peptides colistin and polymyxin B, can compete with divalent cations for LPS binding, leading to OM permeabilization[11,12]. The macrolide, azithromycin, acts through a similar mechanism against *P. aeruginosa*[13]. However, bacteria can modify their LPS composition to gain resistance. In *P. aeruginosa,* mutations in the sensor kinase of the two-component PmrAB system leads to activation of multiple genes, including the *arn* operon which catalyzes the covalent addition of 4-amino-4-deoxy-L-arabinose to lipid A[10]. This addition of sugars reduces the binding of cationic antimicrobial peptides. In *E. coli*, mutations in the O-antigen ligase *waaL* lead to incorporation of peptidoglycan precursors that bind vancomycin to prevent entry of the antibiotic into the cell[14]. LPS also serves as a primary receptor for many

bacteriophages. In response, bacteria can modify their LPS composition to prevent phage attachment[15,16]. Phages can counter resistance by encoding enzymes that modify host LPS, to facilitate their own uptake or that of related phages. Overall, LPS composition plays an important role in antibiotic and phage susceptibility.

Once an antibiotic gets inside the cell, bacteria respond to the resulting stress in ways that are not yet fully understood. For example, multiple two-component regulatory systems can be activated in response to specific stimuli[17–20]. Typical two-component systems are composed of a sensor kinase and a response regulator. The sensor can have both kinase (activating) and phosphatase (deactivating) activities that control the phosphorylation state of the response regulator. The response regulator binds upstream of various genes to modulate their expression. Among the best-characterized two-component systems is CpxA-CpxR in *E. coli*, which is activated in response to misfolded proteins in the periplasm[21], upon overexpression of NlpE[22], or loss of the L,D-transpeptidase LdtD[23]. *P. aeruginosa* has an orthologous system – CpxSR[24]; however, the exact repertoire of genes regulated by CpxR and the effects downstream of its activation are not yet fully understood. Activation of the Cpx system is involved in antibiotic resistance through the regulation of porin[25] and efflux pump expression[26], plus other mechanisms that remain to be discovered.

We previously discovered that the thiopeptide antibiotics, thiostrepton and thiocillin, cross the OM of *P. aeruginosa* using siderophore transporters that are upregulated in low-iron media[27–30]. The thiopeptides synergized with the FDA-approved iron chelator deferasirox (DSX). Prior to our work, the thiopeptides were considered to lack antipseudomonal activity[31,32] because susceptibility assays are typically conducted in nutrient-replete media. These findings suggested there may be other large natural product antibiotics that could cross the OM in nutrient-depleted

conditions. In this work, we screened existing antibiotics reported to have poor or no activity against *P. aeruginosa* in low-nutrient conditions. We found that the glycopeptide vancomycin had low micromolar activity against *P. aeruginosa* and that its activity was iron- and copper-dependent. Analysis of vancomycin-resistant mutants revealed mutations that activated CpxSR, concomitantly inducing resistance to β-lactam antibiotics. Further, we identified a mutation in a LPS glycosyltransferase that decreased susceptibility to vancomycin and azithromycin, another large natural product antibiotic, but unexpectedly increased susceptibility to select bacteriophages. These data provide insight on the mechanism of vancomycin uptake in *P. aeruginosa* and describe resistance mechanisms that can promote changes in resistance to other drug classes or therapeutic alternatives, with implications for uptake of antibiotics across the OM barrier and effective treatment of *P. aeruginosa* infections.

Results

Vancomycin inhibits *P. aeruginosa* growth in an iron and copper-dependent manner

To identify natural products besides the thiopeptides with possible antipseudomonal activity, we screened 21 commercially available natural product antibiotics at 10μg/mL for activity against *P. aeruginosa* PA14 in nutrient-limited 10:90 (10% lysogeny broth: 90% phosphate-buffered saline) medium in the presence of the iron chelator, deferasirox (64μg/mL) (**Fig. 1A, Supplementary Table S1**). The 21 antibiotics were selected because they were 1) reported to lack antimicrobial activity against *P. aeruginosa* and 2) had a molecular weight >600 kDa, precluding their passive diffusion through porins[33,34]. Six of the 21 compounds inhibited the growth of *P. aeruginosa* in 10:90 (**Supplementary Table S1**). We focused here on vancomycin because it is used clinically to treat *Staphylococcus aureus* infections that are often associated with *P.*

aeruginosa in the cystic fibrosis lung[35–38]. The mechanism of action of vancomycin has also been extensively studied using Gram positive species.

We first confirmed that vancomycin had activity in combination with other iron chelators using the synthetic 3-hydroxypyridin-4-one polymeric iron chelator DIBI (Denying Iron to Bacterial Infections) that is unable to enter cells due to its high molecular weight (~9,000 kDa)[39]. Similar to the results with DSX, vancomycin synergized with DIBI, further supporting the connection between iron limitation and antibiotic activity (**Fig. 1B**). Vancomycin alone had a minimal inhibitory concentration (MIC) of 16 μg/mL (11 μM) in 10:90, but the addition of 8.3 μg/mL of DIBI reduced the MIC of vancomycin to 4 μg/mL. DIBI alone has a MIC of 63 μg/mL (7 μM) in 10:90. Since the thiopeptides thiostrepton and thiocillin can cross the OM using siderophore transporters, we tested synergy between vancomycin and DIBI against a *tonB1* transposon mutant. The TonB1-ExbBD complex energizes uptake of ligands through OM siderophore transporters and *tonB1* mutants are thiopeptide-resistant[29]. Susceptibility of the *tonB1* mutant to the combination of vancomycin + DIBI was similar to that of the wild type (WT), suggesting that vancomycin uptake did not rely on TonB1-dependent transporters or that loss of *tonB1* was insufficient to reduce activity (**Fig. 1C**). Since vancomycin susceptibility was iron-dependent, we tested the effects of adding back various metal salts, including $FeCl_3$, $CuCl_2$, $MgCl_2$, and $CaCl_2$ into 10:90. We predicted that $FeCl_3$ would antagonize vancomycin susceptibility because of the observed sensitization by iron chelators. Further, we predicted that $MgCl_2$ and $CaCl_2$ may have a similar effect because the divalent cations stabilize the highly negative charge of the LPS and thus OM integrity. As expected, iron supplementation antagonized vancomycin susceptibility (**Fig. 1D**). Interestingly, copper supplementation also resulted in antagonism (**Fig. 1E**), but neither $MgCl_2$ and $CaCl_2$ antagonized vancomycin susceptiblity to the same extent

(**Supplementary Fig. S1**). These results suggest that vancomycin susceptibility is mainly Fe^{3+} and Cu^{2+} dependent and that the antibiotic was not simply entering the cell due to compromised OM integrity in 10:90.

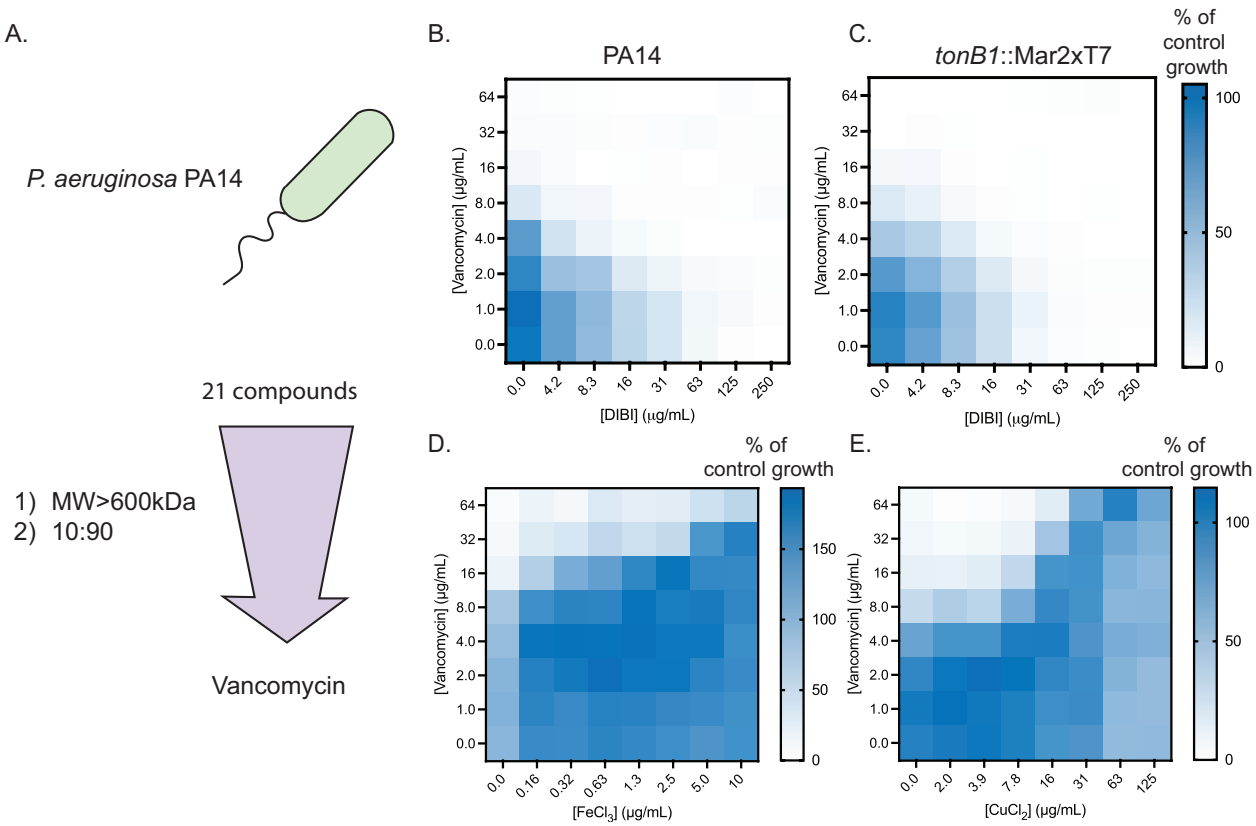

Figure 1. Vancomycin inhibits *P. aeruginosa* under nutrient-limited conditions. **A.** Schematic for screening compounds against *P. aeruginosa*. Checkerboard assays with vancomycin + DIBI against **B.** PA14 and **C.** *tonB1*::Mar2xT7. The darker the shade of blue, the more growth observed. White squares indicate a lack of growth observed. Checkerboard assays with vancomycin and **D.** $FeCl_3$ and **E.** $CuCl_2$. All checkerboards were averaged from three independent biological replicates.

Activity is vancomycin-specific and not due to decreased outer membrane integrity

We verified that the susceptibility to vancomycin was not associated with membrane permeabilization (**Fig. 2A**). 1-N-phenylnaphtylamide (NPN) is a weakly fluorescent dye that poorly permeates the OM; however, upon permeabilization of the OM, the dye binds to phospholipids and strongly fluoresces. Polymyxin B, which disrupts the OM, increased

fluorescence whereas vancomycin or piperacillin had no effect on fluorescence compared to the vehicle control.

We next tested if other glycopeptides could inhibit *P. aeruginosa* growth in 10:90 (**Fig. 2B**). Teicoplanin, oritavancin, and dalbavancin all lacked activity up to 64 μg/mL (**Fig. 2C**). We also tested FITC-vancomycin, a fluorescent derivative, and saw no inhibition (**Fig. 2D**). Using microscopy we saw no fluorescence in cells, indicating that the fluorescent analog could likely not cross the OM (**Fig. 2E**). As controls, we included methicillin-resistant *S. aureus* MRSA USA 300 which was labeled as expected with FITC-vancomycin (**Supplementary Fig. S2**). These results show that the activity is vancomycin-specific and sensitive to structural modifications.

Vancomycin is primarily bacteriostatic against *P. aeruginosa* but bactericidal during early exponential phase (**Supplementary Fig. S3A**). At 1X MIC (16 μg/mL), where no growth was observed, cells grew similarly to the WT until early exponential phase, when there was a decrease in OD_{600}, indicative of bactericidal activity. Time-kill curves showed that at 1X MIC, there was a 1 log increase in CFU/mL compared to the starting inoculum after 24 h (**Supplementary Fig. 3B**). At 4X MIC, vancomycin was bactericidal up to 8 h; however, regrowth occurred by 24 h. These results suggest that while vancomycin has activity under low-nutrient conditions, *P. aeruginosa* can develop resistance. Therefore, we investigated whether vancomycin was acting through its canonical mechanism of action, how it was taken up, and how *P. aeruginosa* could become resistant.

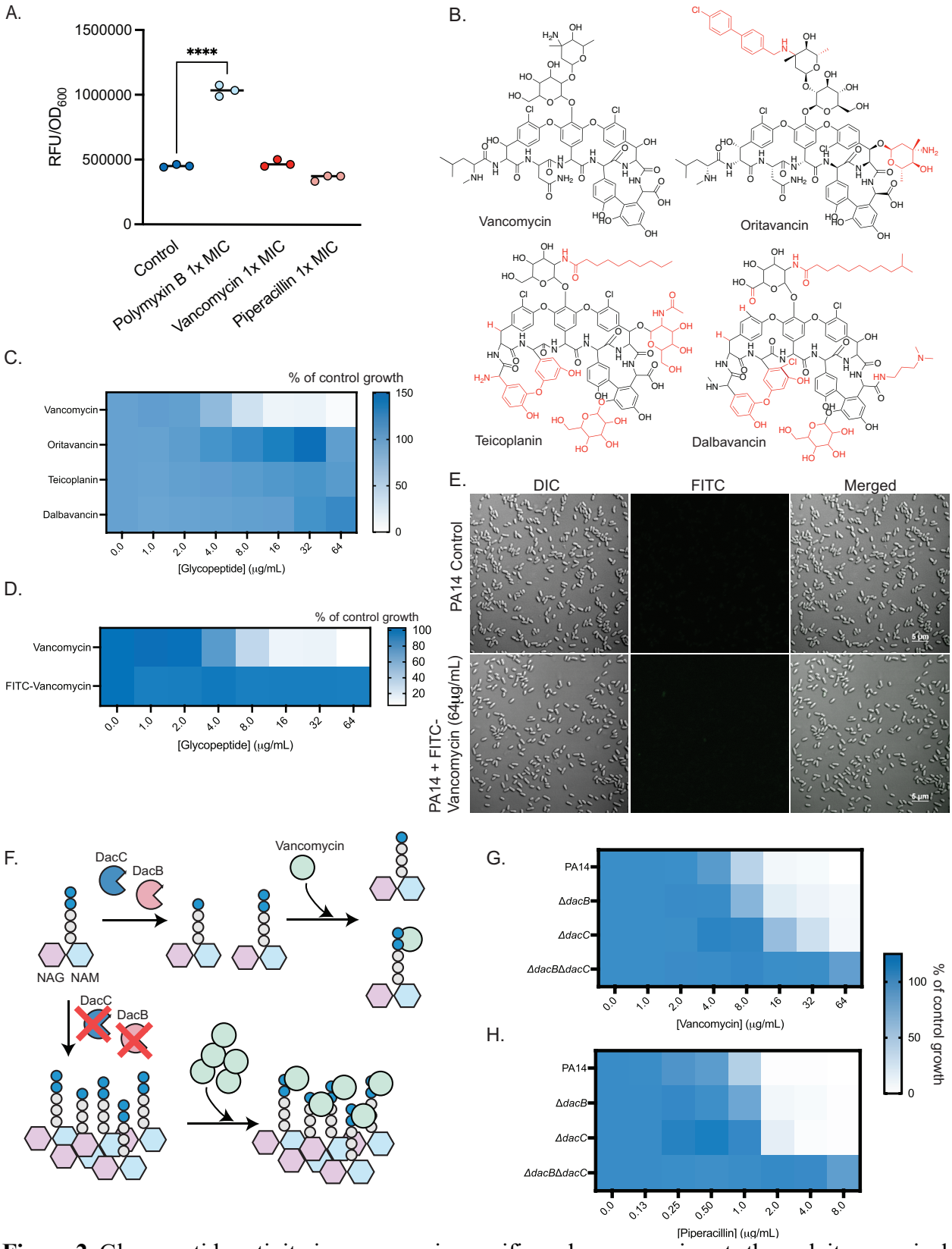

Figure 2. Glycopeptide activity is vancomycin specific and vancomycin acts through its canonical mechanism of action. **A.** NPN assay with PA14 in 10:90 with polymyxin B (1X MIC = 1μg/mL),

vancomycin (1X MIC = 16μg/mL), and piperacillin (1X MIC = 8μg/mL). NPN fluorescence was measured with excitation at 350nm and emission at 420nm. Values for individual biological replicates are shown. Statistical analysis was calculated using a one-way ANOVA followed by Dunnett's multiple comparison test. ****, $p<0.0001$. **B.** Structures of vancomycin, oritavancin, teicoplanin, and dalbavancin. Structural compared to vancomycin are highlighted in red. **C.** MIC assay with vancomycin and the three glycopeptides against PA14 in 10:90. **D.** MIC assay with FITC-vancomycin against PA14 in 10:90. **E.** Representative fluorescent microscopy images of cells treated with FITC-vancomycin. Scale bar = 5μm. **F.** Schematic for vancomycin (green circle) binding to the D-Ala-D-Ala moiety of the pentapeptide of lipid II. DacB and DacC remove the terminal D-Ala from the pentapeptide stem to form the tetrapeptide. The cell has both penta- and tetrapeptides and vancomycin can bind to the pentapeptides through H-bonding with the D-Ala-D-Ala residues. In the absence of DacB and DacC, the pool of pentapeptides increases, thus more vancomycin is required to inhibit transpeptidation. MIC assays of PA14, *ΔdacB, ΔdacC*, and *ΔdacBΔdacC treated* with **G.** vancomycin and **H.** piperacillin. All MIC assays were conducted in 10:90 and averaged from three independent biological replicates.

Loss of DacB and DacC leads to vancomycin resistance

Vancomycin binds the D-Ala-D-Ala moiety of peptidoglycan pentapeptide stems, resulting in decreased crosslinking and impairment of cell wall integrity[40]. Therefore, we predicted that mutations that increase pentapeptide levels would result in decreased susceptibility to vancomycin. Previous studies reported that loss of the D,D-carboxypeptidases, DacB (penicillin binding protein 5, PBP5) and DacC (PBP4), increased the pool of pentapeptides in *P. aeruginosa* (**Fig. 2F**)[41]. Deletion of *dacB* also upregulates expression of the chromosomally-encoded beta-lactamase, AmpC, increasing the MIC for beta lactams such as piperacillin although the degree of AmpC stimulation depends on the strain[42,43]. Consistent with these data, MICs for both vancomycin and piperacillin increased in a *dacB dacC* double mutant, suggesting that vancomycin was acting through its expected mechanism of action (**Fig. 2GH**).

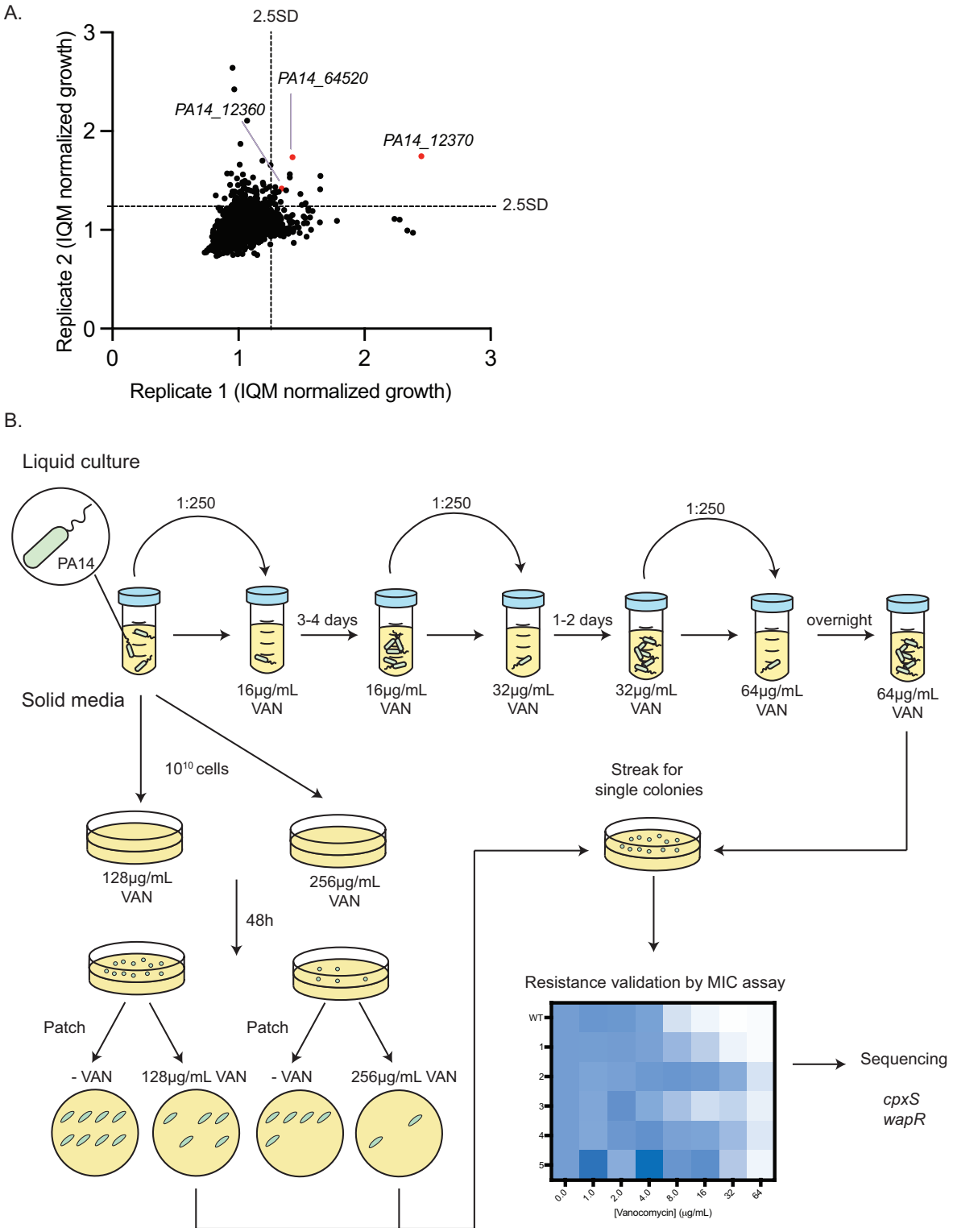

Figure 3. Identifying genes important for vancomycin resistance. **A.** Replica plot of interquartile-mean normalized growth of the PA14 transposon library screened at 64µg/mL vancomycin in 10:90. Mutants with growth >2.5 standard deviations (SD) above the mean were considered as resistant. Validated resistant mutants are highlighted in red and labeled with their gene name. **B.**

Schematic for raising spontaneous vancomycin-resistant mutants in liquid and solid media – Vancomycin (VAN).

Spontaneous vancomycin resistant mutants harbour mutations in the CpxSR two-component system

To understand potential mechanisms of uptake and resistance to vancomycin in *P. aeruginosa*, we screened a library of non-redundant *P. aeruginosa* Mar2xT7 transposon insertion mutants at 64 μg/mL vancomycin (4X MIC) to identify mutants with increased resistance (**Fig. 3A**). Only three mutants were reproducibly resistant: *PA14_64520*, *PA14_12360*, and *PA14_12370*, each with MICs of 64 μg/mL. *PA14_64520* encodes a putative bacterioferritin contributing to iron homeostasis. *PA14_12360* and *PA14_12370* are tandem uncharacterized genes, suggesting a potential interaction between their protein products or possible polar effects on *PA14_12370* from the transposon insertion in *PA14_12360*. The relationship between the products of these genes and their relation to vancomycin uptake or mechanisms of resistance was unclear; therefore, we also raised spontaneously vancomycin-resistant mutants in both liquid (up to 64 μg/mL) and solid medium formats (128-256 μg/mL) (**Fig. 3B**). We sequenced the vancomycin-resistant mutants arising from liquid cultures, which all mapped to the two-component system sensor CpxS, causing a T163P mutation. Interestingly, all mutants raised on solid medium with 256 μg/mL vancomycin also had mutations in *cpxS*, suggesting that the CpxSR system is required for high level vancomycin resistance. In *E. coli,* at least 10 mutations in the CpxS ortholog, CpxA, have been shown to be activating mutations. We aligned the AlphaFold2 structural models of CpxA and CpxS, which showed that CpxS T163P is located at transmembrane helix 2, a position similar to those of 5 CpxA activating mutations (**Fig. 4AB**). All the other

mutations identified are also located in positions similar to known CpxA activating mutations (**Fig. 4C**).

We focused on CpxS T163P because it was recovered from both liquid and solid medium cultures. The CpxS T163P mutant was regenerated in a WT background via allelic exchange and we confirmed that it was resistant to vancomycin (**Fig. 4D**) with an MIC > 64μg/mL. We also complemented a *cpxS*::Mar2xT7 mutant with WT PA14 CpxS or CpxS T163P and tested for vancomycin susceptibility (**Supplementary Fig. S4**). The *cpxS* mutant had WT susceptibility to vancomycin with a MIC of 16 μg/mL. Expression of CpxS T163P, but not empty vector or WT CpxS, restored resistance (MIC = 64 μg/mL). In *E. coli*, mutations in the CpxAR system can be activating or repressing; therefore, to learn whether CpxS T163P is an activating mutation, we examined the expression of GFP under the control of the CpxR-responsive *mexA* promoter (**Fig. 4E**). MexA is the periplasmic component of the MexAB-OprM efflux pump, and a previous study showed that CpxR binds upstream of *mexA* at a conserved CpxR box binding motif[26]. We compared the expression of GFP in WT PA14 and the CpxS T163P mutant using either a promoterless reporter or a reporter under control of P_{mexA}. GFP expression was significantly higher in CpxS T163P compared to the WT or a promoterless control, suggesting that CpxS T163P is an activating mutation.

To confirm that the effect of the CpxS T163P mutation was mediated via the response regulator CpxR, we deleted *cpxR* from WT and CpxS T163P and tested susceptibility to vancomycin (**Fig. 4D**). Δ*cpxR* had WT susceptibility to vancomycin. Further, loss of Δ*cpxR* in the CpxS T163P mutant increased susceptibility to vancomycin to WT levels, suggesting that CpxS T163P activates CpxR to confer resistance. We could also complement the Δ*cpxR* mutants with *cpxR in trans* on an arabinose-inducible plasmid with a gentamicin resistance maker, pBADGr,

which restored resistance to vancomycin in the CpxS T163P mutant even without the addition of arabinose, suggesting that low level expression from the leaky promoter was sufficient (**Fig. 4F**). Expression of CpxR *in trans* in Δ*cpxR* increased the MIC slightly in the presence of arabinose (0.05%), suggesting that there is also a dosage-dependent effect even without CpxS activation (**Fig. 4G**), consistent with limited kinase-independent activation of response regulators by small-molecule phosphodonors[44,45].

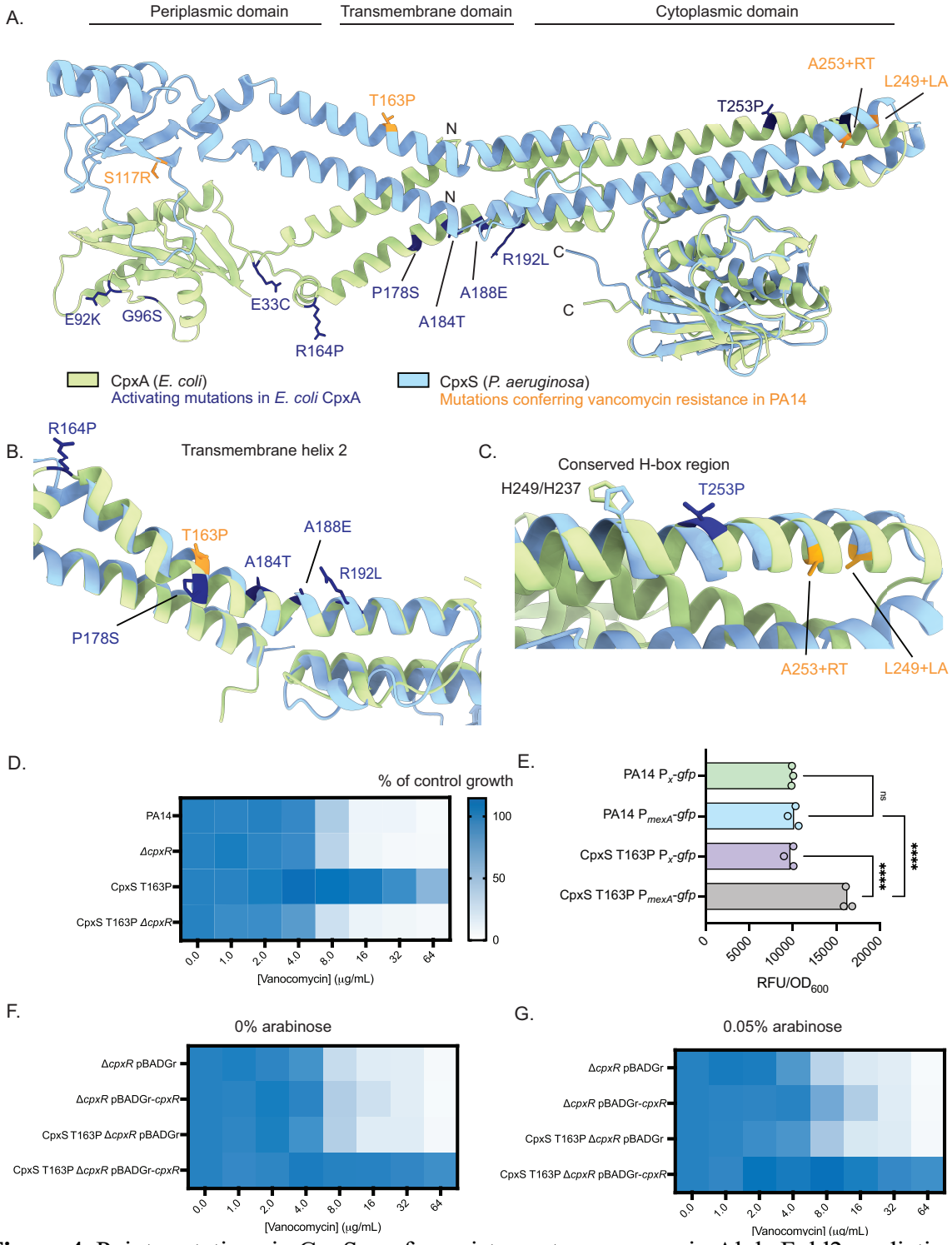

Figure 4. Point mutations in CpxS confer resistance to vancomycin.AlphaFold2 predictions of *E. coli* CpxA (green) and *P. aeruginosa* CpxS (blue) overlayed. Activating mutations in *E. coli* CpxA are highlighted in dark blue whereas mutations in CpxS in spontaneous vancomycin-resistant mutants are indicated in orange. Structural alignment of **B.** transmembrane helix 2 and **C.** transmembrane helix 1 near the conserved H-box region between CpxA (green) and CpxS (blue). **D.** MIC assay of PA14, *ΔcpxR*, CpxS T163P, and CpxS T163P *ΔcpxR* treated with vancomycin.

E. GFP-reporter assay of PA14 WT versus CpxS T163P using a promoterless control or P_{mexA} to drive GFP expression ns: not significant; ****: p<0.0001. Statistics were calculated by one-way ANOVA followed by Dunnett's multiple comparison test in Prism. Individual values for each biological replicate are shown. *ΔcpxR* and CpxS T163P *ΔcpxR* complemented with empty vector (pBADGr) or a WT copy of *cpxR*, and treated with vancomycin in 10:90 **F.** with no arabinose or **G.** 0.05% arabinose. All assays were conducted in 10:90 and results shown are averaged from three independent biological replicates.

Next, we tested whether activation of the CpxSR response was responsible for observed antagonism between vancomycin + copper and vancomycin + iron. We conducted checkerboard assays with CpxS T163P, Δ*cpxR,* and CpxS T163P Δ*cpxR* challenged with vancomycin + $CuCl_2$ and vancomycin + $FeCl_3$ (**Supplementary Figure S5**). WT, Δ*cpxR,* and CpxS T163P Δ*cpxR* showed similar profiles of antagonism. CpxS T163P was resistant to vancomycin, but had increased sensitivity to copper compared to other strains. These results suggest that copper and iron antagonize vancomycin activity independently of the CpxSR two-component system.

Activation of CpxS confers resistance to multiple classes of β-lactams

In *E. coli*, CpxA has been implicated in resistance to multiple classes of antibiotics[46–48]; therefore, we tested whether CpxS T163P conferred resistance to antibiotics besides vancomycin. The penicillins, monobactams, and cephalosporins showed 4-fold or greater increases in MIC for CpxS T163P compared to the WT (**Fig. 5A**). The mutant also had an elevated MIC of 8-fold for the siderophore antibiotic cefiderocol compared to WT. However, there was no change in MIC for the penems (meropenem and imipenem). Similarly, compounds that inhibit early steps of peptidoglycan synthesis (e.g. D-cycloserine and fosfomycin) or classes of antibiotics with non-cell wall targets showed no change or only a 2-fold change in MIC. These results suggest that CpxS T163P primarily impacts the periplasmic steps of peptidoglycan synthesis, where vancomycin and β-lactams act. In *E. coli,* CpxA activation induces changes in cell wall cross-linking and expression

of L,D-transpeptidases, which may contribute to resistance[23]. Additionally, the mechanism of resistance may be independent of MexAB-OprM, despite its upregulation in the CpxS T163P mutant, because the MICs for other classes of antibiotics that are substrates for efflux pumps were unchanged. CpxS T163P and WT had similar susceptibility to polymyxin B, suggesting that OM integrity was not impacted.

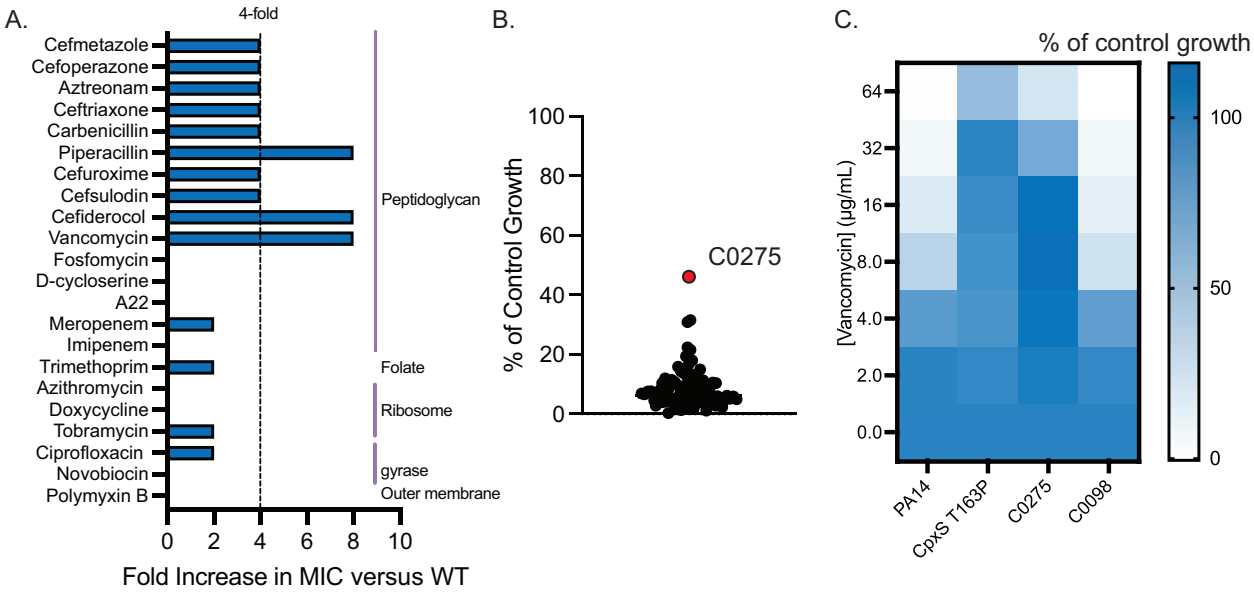

Figure 5. CpxSR activation confers resistance to β-lactams. **A.** Fold change in MIC of PA14 versus CpxS T163P for the panel of antibiotics tested. Fold changes 4-fold or more are considered resistant. **B.** Screening of the WCC *P. aeruginosa* clinical isolate panel for susceptibility to 64µg/mL vancomycin in 10:90. C0275, a resistant clinical isolate, is highlighted in red. **C.** MIC assay of PA14, CpxS T163P, C0275, and C0098 treated with vancomycin in 10:90. Results for all assays are averaged from three independent biological replicates.

Our data suggested that various CpxS point mutations can activate the CpxSR system. This led us to hypothesize that clinical isolates of *P. aeruginosa* may harbour mutations in CpxS that differ depending on their diversity, prior antibiotic exposure, and the site of infection. We used vancomycin resistance at 64 µg/mL (4x MIC of WT) (**Fig. 5B**) as a filter to uncover potential CpxS-activating mutations in a set of 96 clinical isolates. One isolate C0275 had ~40% of control growth even at 64 µg/mL vancomycin whereas most isolates had <20% of control growth, which

was not observable by eye. C0275 had a MIC for vancomycin >64 μg/mL, similar to CpxS T163P, whereas WT PA14 had a MIC of 16 μg/mL. C0098 was used as a control and had similar susceptibility to WT PA14 (**Fig. 5C**). All the clinical isolates had CpxS sequences similar to those of WT PA14 or PAO1, suggesting that there are other resistance mechanisms that could contribute to the elevated vancomycin MIC in C0275.

A WapR P164T vancomycin-resistant mutant has altered LPS composition and increased phage sensitivity in nutrient-limited media

We also investigated another spontaneously-resistant mutant raised on 10:90 solid medium containing 128 μg/mL vancomycin. This isolate had a mutation in *wapR* leading to a P164T substitution. WapR is an enzyme involved in LPS core oligosaccharide biosynthesis that adds a L-rhamnose (α-1,3-linked) to the outer core to provide an attachment site for O-antigen polymerization. Mutants lacking WapR synthesize rough LPS without O-antigen. To understand the effects of the Pro to Thr mutation, we searched the AlphaFold2 structure of WapR using the Dali server[49,50]. The best matched identified was a chrondroitin polymerase from *E. coli* K4 (KfoC; PDB: 2Z86)[51]. KfoC is a bifunctional glycosyltransferase that catalyzes the elongation of the chrondroitin chain involved in the synthesis of the extracellular layer of the bacterial capsule. WapR aligned with the A2 domain of K4CP bound to uridine-diphosphate glucuronic acid (UDP-GluUA) (**Fig. 6A**). WapR P164 is located in the region that aligns with the K4CP binding cavity for UDP-GluUA, suggesting that the mutation in WapR may affect its function as an L-rhamnosyltransferase (**Fig. 6B**).

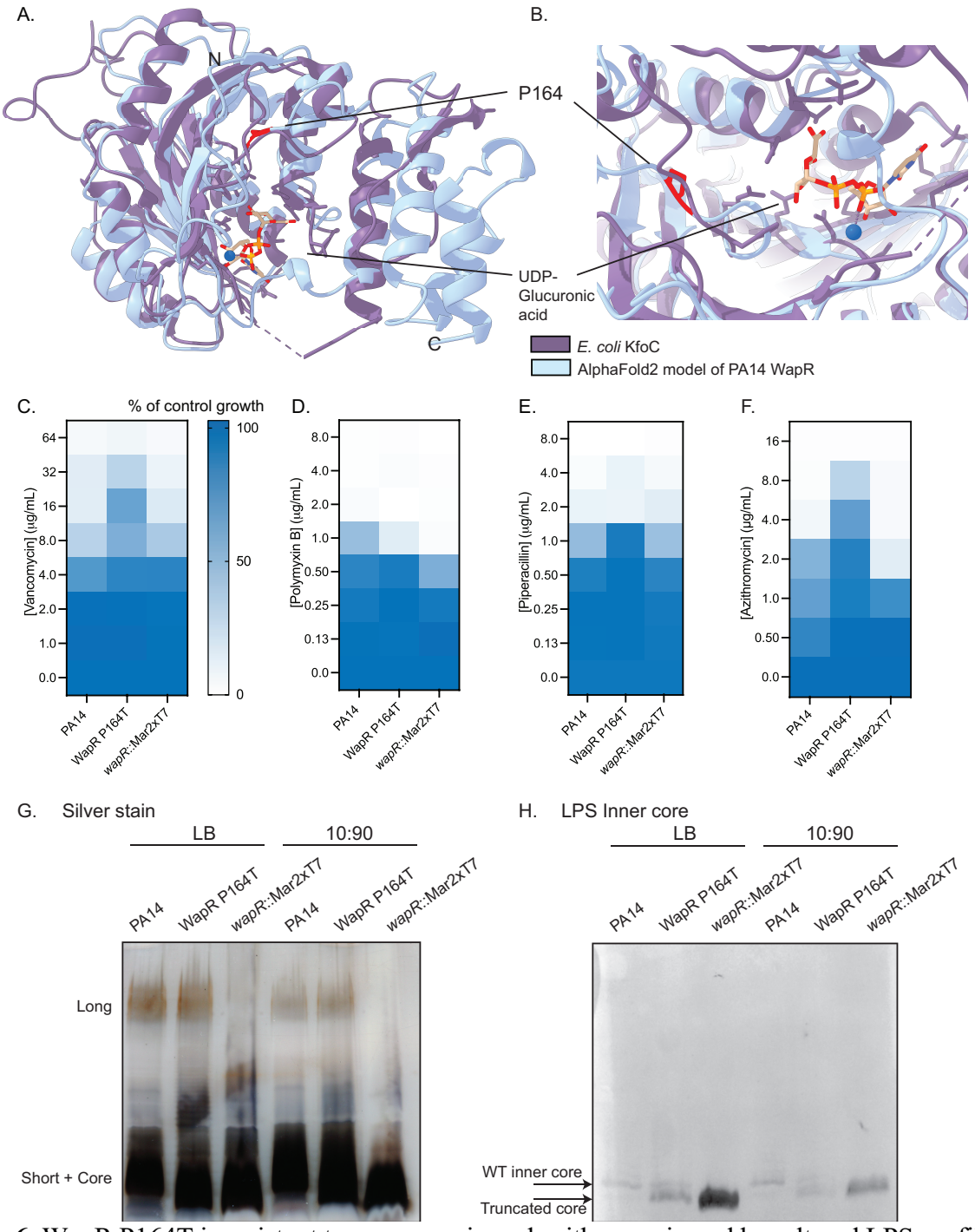

Figure 6. WapR P164T is resistant to vancomycin and azithromycin and has altered LPS profiles. **A.** Overlay of the A2 domain of *E. coli* K4 KfoC (purple) (PDB: 2Z86) and an AlphaFold2 model of PA14 WapR (blue). UDP-glucuronic acid, which binds to KfoC, is highlighted in beige with heteroatoms coloured differently. The blue sphere is Mn^{2+}. P164 is highlighted in blue. **B.** A zoomed-in view of the UDP-glucuronic acid binding site of KfoC overlayed with WapR. P164 is highlighted in red. MIC assays of PA14, WapR P164T, and *wapR*::Mar2xT7 treated with **C.** vancomycin, **D.** polymyxin B, **E.** piperacillin, and **F.** azithromycin. Results are averaged from

three independent biological replicates. **G.** Silver stain of proteinase K-treated crude lysates for LPS from PA14, WapR P164T, and *wapR*::Mar2xT7. The three strains were grown on LB and 10:90 agar plates. **H.** Western blot of LPS preparations probed with the monoclonal antibody 5c-7-4 (LPS inner core specific).

To test this hypothesis, we tested the susceptibility of WT PA14, WapR P164T, and a *wapR* transposon mutant (*wapR*::Mar2xT7) to vancomycin (**Fig. 6C**). As expected, the WapR P164T mutant had a MIC 4-fold greater than that of the WT. Surprisingly, susceptibility of *wapR*::Mar2xT7 was similar to WT. This result suggests that the WapR P164T mutant may not be a loss-of-function mutation. As a control, we also tested susceptibility of the mutants to polymyxin B (to assess OM integrity) and piperacillin (for peptidoglycan-acting antibiotics) and saw no differences (**Fig. 6DE**). LPS structure modulates antibiotic resistance[10]; therefore, we tested other high-molecular weight antibiotics identified from our initial screen as having activity under nutrient-limited conditions using PA14, WapR P164T, and the *wapR* mutant (**Fig 6F**). Interestingly, the WapR P164T mutant was also 4-fold more resistant to azithromycin compared to the WT, similar to vancomycin. These results suggest that this mutation can also confer resistance to other classes of antibiotics in a LPS-dependent manner.

To further confirm that WapR P164T was not an inactivating mutation, we isolated crude LPS preparations for the three strains grown in LB or 10:90, separated the samples by SDS-PAGE, and visualized LPS by silver staining (**Fig. 6G**). The LPS profile of cells grown in LB were similar to in 10:90 although there appeared to be less long-chain O antigen in 10:90. However in both conditions, WapR P164T makes long-chain length O-antigen that was comparable to the WT while no polymers in that range were present for *wapR*::Mar2xT7. The *wapR*::Mar2xT7 mutant also failed to make short chain length LPS, consistent with previous reports[52]. Additionally, there were differences in the migration pattern of the short + core LPS (**Fig. 6H**). The LPS profiles of the WapR P164T and *wapR*::Mar2xT7 mutants showed that there were bands corresponding to the

LPS core region that migrated faster compared to the WT. This observation is consistent with the fact that WapR modifies the LPS core. Therefore, we probed phenol/ethyl ether-extracted LPS preparations with monoclonal antibody 5c-7-4 that recognizes the inner core. For the WT, a single band was present, whereas the *wapR* transposon mutant had a single band of decreased molecular weight, corresponding to a truncated core, consistent with previous observations[53]. However, two bands were seen for the WapR P164T mutant – one higher molecular weight band corresponding to the WT core and a lower molecular weight band corresponding to the *wapR*::Mar2xT7 mutant truncated core. No differences were seen between cells grown in LB or 10:90. Together, these results suggest that the WapR P164T mutation leads to an heterogenous core phenotype, between WT and the *wapR*::Mar2xT7 mutant.

The O antigen is important for antibiotic resistance, but also acts as a receptor for phages to recognize suitable host cells. We tested PA14, WapR P164T, and *wapR*::Mar2xT7 for their susceptibilities to LPS-specific phages P2B9, D6, and E6 (**Fig. 7**). As a control, we also tested three phages (B6, P2A3, and P2F10) that use type IV pili as a receptor, using a Δ*pilA* mutant which is unable to make the major pilin subunit as a negative control (**Fig. 7, Supplementary Figure S6**). We spotted increasing dilutions of each phage on bacterial lawns grown on LB agar and looked for differences in susceptibility. All 6 phages plaqued on WT PA14. When the same set of phages was spotted on WapR P164T, we saw a similar susceptibility pattern to the WT; however, the plaques were clearer and larger. *wapR*::Mar2xT7 was resistant to phages P2B9, D6, and E6, but susceptible to the pilus-specific phages, B6, P2A3, and P2F10, consistent with the requirement for O-antigen binding for infection. The Δ*pilA* mutant was susceptible to phages P2B9, D6, and E6 but resistant to B6, P2A3, and P2F10. The larger plaque sizes for WapR P164T appear to be an LPS-independent phenomenon because the same phenotype was also observed for pilus-

dependent phage B6. We also tested the CpxS T163P mutant for phage susceptibility. The titres were similar but the plaques were more turbid compared to WT, suggesting that CpxS activation may impact the efficiency of phage replication.

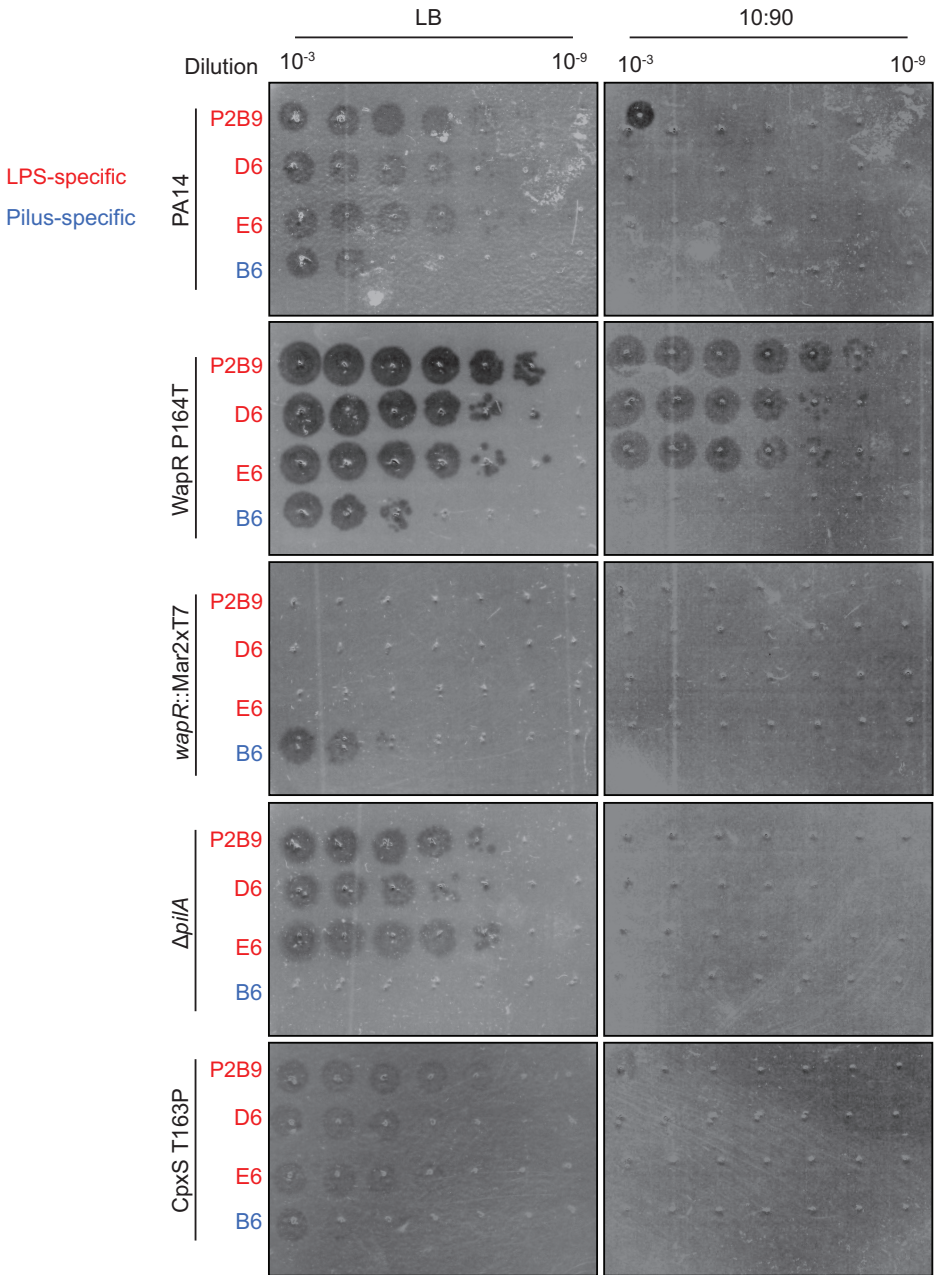

Figure 7. WapR P164T has larger plaques in LB and increased phage susceptibility in 10:90. Phage plaquing assays with PA14, WapR P164T, *wapR*::Mar2xT7, ΔpilA, and CpxS T163P in LB and 10:90 agar. Each strain was treated with increasing dilutions of the LPS-specific phages (highlighted in red): P2B9, D6, and E6 and the pilus-specific phage (highlighted in blue) B6. Three biological replicates were conducted and representative plaquing assays are shown.

Despite the differences in plaque sizes between WapR P164T and WT, there were no differences in susceptibility. However, these initial phage assays were conducted in nutrient-replete LB whereas our antibiotic susceptibility assays were done in 10:90. Therefore, we repeated the phage susceptibility assays in 10:90 agar. Interestingly, on that medium PA14 was resistant to LPS-specific phages D6 and E6 and had a 10^5-fold decrease in susceptibility to P2B9. However, this was not the case for the WapR P164T mutant. We observed similar plaquing and susceptibility patterns of the LPS-specific phages on WapR P164T in LB and 10:90, although it became resistant to pilus-specific phage B6. The *wapR*::Mar2xT7, Δ*pilA,* and CpxS T163P mutants were resistant to all phages tested when grown on 10:90. The differences in phage susceptibility were not due to differences in growth as all strains grew similarly in 10:90 (**Supplementary Fig. S7**). Altogether, these results show that the WapR P164T mutant has altered LPS composition and differences in susceptibility to vancomycin, azithromycin, and phages in rich versus nutrient-limited media.

Discussion

We found that *P. aeruginosa* is sensitized to the large natural product antibiotic vancomycin when grown in nutrient-limited conditions that may be more representative of the host environment[54]. Vancomycin activity was antagonized by various metals such as iron and copper, but calcium and magnesium – which help to stabilize the negative charge of the OM – were less important for resistance. One potential explanation for the antagonism between vancomycin and copper is that vancomycin can chelate the metal[55,56]. The functional groups that participate in chelation overlap with those that participate in H-bonding with the D-Ala-D-Ala pentapeptide. Thus, complex formation with copper may inhibit uptake and/or interaction of vancomycin with its target. Copper antagonism of vancomycin activity was independent of the CpxSR pathway,

consistent with the chelation hypothesis, although further investigation to support this conclusion is necessary (**Supplementary Fig. S5**). The antagonism of vancomycin activity by iron also suggests that there are alternate mechanisms of resistance yet to be identified but confirms that iron limitation potentiates vancomycin activity.

Our screen of the *P. aeruginosa* PA14 transposon library to identify genes involved in vancomycin resistance yielded only three mutants in poorly-characterized genes. This result suggested that inactivating mutations are not the primary mechanism of *P. aeruginosa* resistance to vancomycin. Instead, isolation of spontaneously-resistant mutants led to the identification of multiple point mutations in CpxS, suggesting that the sensor can be activated through specific substitutions such as T163P, similar to CpxA in *E. coli*[57]. Vancomycin resistance conferred by CpxS T163P was dependent on CpxR, as *cpxR* deletion reduced susceptibility to WT levels.

Detailed examination of the consequences of CpxSR activation will be necessary to understand the transcriptional responses that result in vancomycin resistance. For example, activation of CpxSR may increase the expression of L,D-transpeptidases, implicated in β-lactam resistance because they bypass the effects of D,D-transpeptidase inhibition[58]. In *P. aeruginosa*, 3,3-crosslinking of peptidoglycan catalyzed by L,D-transpeptidases increases in low-nutrient conditions[59] In *E. coli,* activation of the CpxS homologue CpxA increases expression of L,D-transpeptidase LdtD[23]. The L,D-transpeptidases are not well characterized in *P. aeruginosa,* although there are some candidates (e.g. PA14_27180 and PA14_54810) predicted to have the YkuD-like fold characteristic of this family[60]. In *E. coli*, CpxR also indirectly decreases expression of *dacC* and genes involved in LPS biosynthesis[61]; but whether this changes pentapeptide levels is unclear. Some CpxA-activating mutants have increased abundance whereas others do not[23].

Overall, changes in peptidoglycan composition and remodeling may be one way to confer resistance to both vancomycin and β-lactams.

Interestingly, activation of CpxSR through the T163P mutation did not increase resistance to other classes of antibiotics. In *E. coli* CpxAR is involved in fosfomycin resistance, by repressing transporters of the antibiotic[46]. These results suggest that the regulatory consequences of activation differ between the two species. *P. aeruginosa* CpxS T163P was identified previously, in a study investigating the efficacy of sequential antibiotic treatment protocols[24]. They found that pre-treating cells with carbenicillin for 15 min increased susceptibility to gentamicin compared to treatment with gentamicin alone. However, among the mutations that conferred resistance to this combination was CpxS T163P, which based on our work may have resulted in increased carbenicillin resistance.

Our finding that CpxS mutations confer resistance to β-lactams including the recently FDA-approved siderophore-cephalosporin cefiderocol, but not the penems, has significant implications for the treatment of *P. aeruginosa* infections. The target of β-lactams are the PBPs; however, the penem subclass also inhibits the L,D-transpeptidases, which may explain why the CpxS T163P mutant remains susceptible to meropenem and imipenem[58]. Further investigation into the mechanism will be informative. These results, when combined with studies to find additional CpxS-activating mutations, could help guide antibiotic selection for treatment of *P. aeruginosa* infections. For example, in polymicrobial infections, methicillin-resistant *Staphylococcus aureus* (MRSA) is often associated with *P. aeruginosa* in chronic wounds and the lungs of cystic fibrosis patients, and vancomycin is used in the treatment of MRSA[54,62–64]. However, this work shows that vancomycin can also inhibit *P. aeruginosa* under nutrient limiting conditions and select for mutations in CpxS that confer multidrug resistance. Further studies examining the effects of

vancomycin on cocultures will be informative to see if this phenomenon could be clinically relevant. We note that the utility of vancomycin in cystic fibrosis lung infections caused by P. aeruginosa may be limited due to increased iron concentrations in that environment[65–69].

Previous work on *E. coli* showed that cold stress, rather than nutrient limitation, sensitized cells to vancomycin and that truncations in the LPS core restored resistance[70]. They hypothesized that cold stress negatively affected OM integrity, leading to increased susceptibility to vancomycin, while mutants in LPS biosynthesis were better at maintaining the barrier. Resistance was correlated with truncations with the LPS core or production of heterogenous LPS populations. In contrast, our work showed that *wapR*::Mar2xT7, which fails to produce short or long-chain LPS (**Fig. 6G**) and has a truncated core (**Fig. 6H**), had WT levels of vancomycin susceptibility. These results suggest that in *P. aeruginosa,* core truncations alone were insufficient to confer resistance. However, intermediate LPS profiles, as seen with WapR P164T, correlated with resistance. *P. aeruginosa* makes two distinct O-antigens, called A-band or common polysaccharide antigen (CPA), and B-band or O-specific antigen (OSA). However, PA14 has a single amino acid substitution G20R in *wbpX* that abolishes CPA production[8]. Therefore, only OSA is produced by the wild type. Another possibility is that the OSA is differentially attached to the core compared to WT LPS. More detailed studies of LPS composition in these strains will help to clarify the mechanism of resistance. Interestingly, WapR P164T was also more resistant to the macrolide antibiotic, azithromycin. Like vancomycin, the activity of azithromycin on *P. aeruginosa* is nutrient dependent and it directly interacts with LPS by displacing divalent cations[13,71]. However, since the WapR P164T mutant and WT were equally susceptible to polymyxin B, resistance is likely not due to altered OM integrity.

Interestingly, one study reported that a single amino acid mutation in the *E. coli* O-antigen ligase WaaL conferred vancomycin resistance in both WT and mutants with defects in the OM[14]. Resistance was due to modification of LPS with peptidoglycan subunits that bound vancomycin and reduced its uptake[14]. However, this does not appear to be the case with WapR P164T, as we saw no labeling with FITC-vancomycin. WapR P164T was less susceptible to vancomycin and azithromycin, but more susceptible to LPS-specific phages in nutrient-limited 10:90. This combination of phenotypes may be due to altered LPS composition, changes in levels of expression, or exposure of secondary phage receptors. Further investigation into the effects of nutrient limitation on phage replication cycle and burst size will be informative in understanding the mechanism for the observed differences in phage susceptibility. These observations are important considerations for the use of phages as antibiotic alternatives, as many sites of infection can be limiting for key nutrients such as iron[72].

Conclusion

In conclusion, we showed that vancomycin – but not other glycopeptides – has antimicrobial activity against *P. aeruginosa* in low-nutrient conditions. Vancomycin-resistant mutants harboured activating mutations in CpxS that also conferred resistance to β-lactams, including cefiderocol, but not the penems. A mutation in WapR which conferred resistance to vancomycin and azithromycin but increased susceptibility to phages under nutrient-limited conditions was also identified. Our study highlights how screening in low-nutrient conditions can reveal novel activity for existing antibiotics and shows how investigation of resistance mechanisms may help to guide antibiotic therapies for *P. aeruginosa*.

Methods

Media and Growth Conditions

All bacteria were cultured overnight in lysogeny broth (LB) at 37°C with 200rpm shaking. Strains with pBADGr and P-*gfp*, cultures were supplemented with 15μg/mL gentamicin. Subcultures (1:500 dilution of overnight cultures) were grown in 10:90 supplemented with or without gentamicin for 3-4hr until at least OD_{600} at 37°C with 200rpm shaking. Arabinose was made as a 20% stock solution in 10:90 and filtered through 0.2μm filters (Fisher Scientific) before diluting into 10:90 for growth assays.

Bacterial strains, phage, and plasmids

Bacterial strains, phage, and plasmids are listed in **Supplementary Table S2**.

Molecular Biology

See **Supplementary Table S3** for all primers used in this study. All procedures were conducted as previously described[28,30].

Compounds

Supplementary Table S4 lists all compounds used in this study. All antibiotic powders were stored at 4°C. Stock solutions were stored at -20°C. Compounds were solubilized in dimethyl sulfoxide or DI H_2O for assays.

MIC and Checkerboards assays

Broth microdilution MIC assays and checkerboards were conducted as previously described[27–30].

NPN assay

The NPN assay was conducted as previously described with modifications[73]. Briefly, overnight cultures of PA14 in LB were subcultured (1:500 dilution) into 50mL of 10:90 and incubated for 3hrs at 37°C with shaking (200 rpm). Cells were harvested by centrifugation at 3,000G for 5min and washed three times with PBS. Cells were resuspended in 10:90 to a final OD_{600} of 0.1 with 5 μM of carbonyl cyanide m-chlorophenyl hydrazone and 15 μM of NPN. Cells were aliquoted into 96-well black plates with flat clear bottoms (Corning). Antibiotics or vehicle controls were added at 75x the final concentration and fluorescence was read immediately on a BioTek Neo plate reader at excitation and emission wavelengths of 350 nm and 420 nm respectively.

Fluorescence microscopy

Microscopy was conducted as previously described[28,30]. Briefly, overnight cultures of PA14 were subcultured in fresh 10:90 (1:500 dilution) and grown at 37°C with shaking (200RPM) for 3-4 hours. Cells were harvested by centrifugation and washed 3X with 1X PBS then incubated with 10μM FITC-vancomycin for 30min at 37°C with shaking (200 rpm). Cells were harvested by centrifugation and washed 3X with 1X PBS before spotting on a 1% agarose pad in 10:90 and imaged with a Nikon A1 confocal microscope through a Plan Apo 60x (NA=1.40) oil objective and acquired with Nikon NIS Elements Advanced Research (V. 5.11.01 64-bit). MRSA USA 300 was grown, labeled, and imaged under the same conditions.

Transposon library screening and WCC vancomycin susceptibility testing.

All mutants from the non-redundant PA14 transposon insertion library[74] were transferred into 96-well plates containing 150 µL/well liquid LB media and incubated for 16 h at 37ºC with shaking at 200 rpm. Each mutant was then diluted 1:200 into 10:90 deferrated using FEC-1[75] to keep the iron concentration consistent between batches of media and incubated for a further 4 h. Mutants were then diluted 1:200 into deferrated 10:90 LB containing 64 µg/mL vancomycin (two replicates) and media without vancomycin (one replicate). Plates were incubated for 16 h at 37ºC with shaking at 200 rpm, then OD_{600} for each well was recorded. OD_{600} values were normalized to the interquartile mean of each plate and each well position[76]. Growth of >2.5 SD above the mean in the presence of vancomycin was considered a hit. The *P. aeruginosa* WCC was tested in a similar manner except untreated 10:90 was used.

Spontaneous vancomycin-resistant *P. aeruginosa*

Spontaneously resistant mutants were selected in liquid and solid media. For liquid media, a PA14 overnight culture was diluted 1:500 into 5 mL cultures of 10:90 LB media containing 16 µg/mL vancomycin, or equivalent volumes of sterile H_2O. The cultures were incubated at 37ºC with 200 rpm shaking and inspected daily. When turbidity (growth) was observed, the culture was diluted 1:250 into fresh media containing 2x concentration of compounds. The DIBI concentration was held at 16 µg/mL as higher concentrations prevented growth. Cultures were passaged until growth was observed at 64 µg/mL vancomycin then streaked on LB agar. Single colonies were selected and their genomic DNA sequenced.

For solid media, 10^7 cells of PA14 subcultured in 10:90 were plated onto 10:90 + 1.5% agar containing 128 and 256 µg/mL in triplicates. Plates were incubated at 37°C for 48h where

colonies appeared. Sixteen colonies in total from the 128 and 256 μg/mL plates were patched onto fresh 10:90 plates with and without vancomycin. For example, a colony that grew from a plate containing 128 μg/mL vancomycin would be patched onto a plate without vancomycin and a plate containing 128 μg/mL vancomycin. Mutants that grew on both plates were streaked for single colonies for MIC testing to confirm resistance to vancomycin (>= 4-fold MIC). This process was repeated for the Δ*cpxR* mutant.

Genomic DNA isolation and sequencing

Genomic DNA of vancomycin-resistant mutants was isolated using Promega Wizard Genomic Isolation Kit. Samples were sent to SeqCenter (Pittsburgh, USA) for Illumina sequencing. FASTA files were processed using FASTQ Groomer, Trimmomatic, FASTQ-interlacer, and FASTQ de-interlacer. Mutations were identified using breseq by comparing to the reference genome (accession number GCF_000404265.1)[77].

LPS isolation (whole cell and phenol/ethyl ether extraction)

LPS from PA14, WapR P164T, and *wapR*::Mar2xT7 were isolated as previously described with some modifications[78]. Cells from overnight cultures in LB or 10:90 1.5% agar plates were collected and resuspended in PBS. The OD_{600} was standardized to 2.0 and cells collected again by centrifugation. Cells were resuspended in 150 μL of lysing buffer (2% SDS, 4% 2-mercaptoethanol, 10% glycerol, 0.1M Tris-HCl, pH 6.8) and boiled for 10 min. After cooling to room temperature, proteinase K (NEB) (10 μl of 20mg/mL) was added and incubated at 60°C for 1 h. Proteinase K-treated preparations were used for silver staining.

For LPS core samples detected by Western blot, prewarmed phenol solution (60°C) containing 90% phenol (Sigma), 0.1% 2-mercaptoethanol, and 0.2% 8-hydroxyquinoline (Sigma) was added to each lysate (1:1 v/v phenol:lysate) and incubated for 15 min at 60°C. The tubes were then incubated on ice for 10 min before centrifugation (21,000 x g for 5 min). The top aqueous layer was transferred to a fresh tube and 500 μL of ethyl ether solution containing 20 mM Tris-HCl, 1 mM EDTA, pH 8.0 was added. Tubes were centrifuged for 1 min at 21,000 x g and the top ethyl ether layer was removed by aspiration. An equal volume of 2X SDS-PAGE loading buffer was added. All LPS samples were stored at -20°C.

SDS-PAGE and Western blot

SDS-PAGE and Western blot were conducted as previously described[28,30] with some modifications. For the detection of inner LPS core, isolated LPS was separated on a 15% SDS-PAGE gel at 90V for 10 min followed by 200V for 1h. After transferring the LPS to a nitrocellulose membrane and blocking for 1h with 5% skim milk, the blot was incubated overnight with mAb 5c-7-4 (specific for the inner core; 1:100 dilution in PBS)[79]. Isolated LPS was also separated on a 12.5% SDS-PAGE gel at 120V for 1.5hr with the same transferring and blocking steps. The next morning, the blot was washed 3x with PBS for 5 min/wash and incubated with 1:500 α-mouse-alkaline phosphatase in PBS for 1 h. The blot was washed 3x with PBS for 5 min/wash and rinsed briefly with DI H_2O before detection with BCIP and NBT. Bands appeared after 5-15 mins and imaged with an Azure 400 imaging system.

Silver stain

Silver stain was conducted as previously described with modifications[78]. Four µL of each LPS preparation were loaded onto a 12.5% polyacrylamide gel and separated for 1.5hr at 120V. The gel was then incubated in EtOH:acetic acid (40%:10%) overnight on a shaking platform at room temperature. The next morning cells were treated with periodic acid solution (40% ethanol: 10% acetic acid: 0.7% periodic acid) for 30 min then washed 3x with DI H_2O for 10 min each. Silver stain solution (2mL NH_4OH, 28mL 0.1M NaOH, 115mL DI H_2O) was added and the gel incubated for 30 min. The gel was then washed two times (6 min/wash). Overwashing led to destaining of the high molecular weight LPS. Gels were developed immediately with developing solution (100 µL 37% formaldehyde, 10 mg citric acid, 200 mL DI H_2O) until bands could be visualized. Development was stopped by putting the gel in 10% acetic acid. Gels were imaged using an Azure 400 imaging system.

Phage isolation, purification, and plaquing assays

Environmental phage lysates isolated and amplified using *P. aeruginosa* PA14 were serially diluted (10^{-1} to 10^{-8}) in phage buffer (68 mM NaCl, 10 mM Tris-HCl (7.5), 10 mM $MgSO_4$, 10 mM $CaCl_2$). Five microlitres of each dilution was spotted onto the prepared plates. Phage spots were air dried for 10 min with the lid on. Plates were incubated inverted for 18 h at 37°C. Phage lysate dilutions that produced visible plaques were used for phage plaque purification. Ten microlitres of serially diluted phage lysate and 100 µL of culture were added to 10 ml of top agar (0.6% agar) and poured onto pre-set 1% LB-agar. Plates were incubated inverted for 18 h at 37°C. Plates that had 2-30 plaques were used for plaque purification. A pipette was used to touch the centre of a plaque, followed by resuspension in 100 µL of phage buffer. This process was repeated 2-3 times or until uniform plaque morphology was observed.

Phage plaque assays were conducted as previously described[80]. Briefly, bacteria were grown at 37°C overnight then subcultured in LB or 10:90 (1:100 dilution) and cultured until the OD_{600} reached 0.3 for LB and 0.2 for 10:90. One hundred μL of the LB subculture or 200 μL of the 10:90 culture was mixed with 10 mL of LB + 0.6% agar or 10:90 + 0.6% agar. Phage stocks were serially diluted 10-fold in phage buffer (68 mM NaCl, 10 mM Tris-HCl (7.5), 10 mM $MgSO_4$, 10 mM $CaCl_2$) and 5 μL of each dilution was spotted. Plates were allowed to dry with the lid on for 10 min, inverted, and incubated at 37°C overnight. The next day plates were imaged. Each experiment was repeated at least three times, representative plates are shown.

Structural comparisons and phylogenetic analyses

High confidence structural models of CpxA, CpxS, and WapR were generated using AlphaFold2[50]. The AlphaFold2 model of WapR was used to look for similar proteins using Dali[49]. The structure of KfoC was retrieved from the Protein Data Bank (PDB: 2Z86)[51]. Structural alignments were conducted using ChimeraX[81].

Acknowledgments

We thank Dr. Bruce Holbein (Fe Pharmaceuticals) for providing DIBI and FEC-1 and Dr. Joseph Lam for anti-LPS core mAb 5c-7-4. This work was supported by a Natural Sciences and Engineering Research Council (NSERC) Discovery Grant RGPIN-2021-04237 to LLB. LLB holds a Tier 1 Canada Research Chair in Microbe-Surface Interactions. DCKC holds a Canadian Institute of Health Research (CIHR) Canada Graduate Scholarship – Doctoral program (CGS-D), and IQ holds a CIHR Masters award (CGS-M). KD held a NSERC Undergraduate Student Research Award.

References

(1) van den Berg, B.; Prathyusha Bhamidimarri, S.; Dahyabhai Prajapati, J.; Kleinekathöfer, U.; Winterhalter, M. Outer-Membrane Translocation of Bulky Small Molecules by Passive Diffusion. *Proc. Natl. Acad. Sci.* **2015**, *112* (23), E2991–E2999. https://doi.org/10.1073/pnas.1424835112.
(2) Yoshimura, F.; Nikaido, H. Permeability of *Pseudomonas aeruginosa* Outer Membrane to Hydrophilic Solutes. *J. Bacteriol.* **1982**, *152* (2), 636–642.
(3) Kucharska, I.; Liang, B.; Ursini, N.; Tamm, L. K. Molecular Interactions of Lipopolysaccharide with an Outer Membrane Protein from *Pseudomonas aeruginosa* Probed by Solution NMR. *Biochemistry* **2016**, *55* (36), 5061–5072. https://doi.org/10.1021/acs.biochem.6b00630.
(4) Toguchi, A.; Siano, M.; Burkart, M.; Harshey, R. M. Genetics of Swarming Motility in *Salmonella enterica* Serovar Typhimurium: Critical Role for Lipopolysaccharide. *J. Bacteriol.* **2000**, *182* (22), 6308–6321.
(5) Bowden, M. G.; Kaplan, H. B. The Myxococcus Xanthus Lipopolysaccharide O-Antigen Is Required for Social Motility and Multicellular Development. *Mol. Microbiol.* **1998**, *30* (2), 275–284. https://doi.org/10.1046/j.1365-2958.1998.01060.x.
(6) Penterman, J.; Nguyen, D.; Anderson, E.; Staudinger, B. J.; Greenberg, E. P.; Lam, J. S.; Singh, P. K. Rapid Evolution of Culture-Impaired Bacteria during Adaptation to Biofilm Growth. *Cell Rep.* **2014**, *6* (2), 293–300. https://doi.org/10.1016/j.celrep.2013.12.019.
(7) Murphy, K.; Park, A. J.; Hao, Y.; Brewer, D.; Lam, J. S.; Khursigara, C. M. Influence of O Polysaccharides on Biofilm Development and Outer Membrane Vesicle Biogenesis in *Pseudomonas aeruginosa* PAO1. *J. Bacteriol.* **2014**, *196* (7), 1306–1317. https://doi.org/10.1128/JB.01463-13.
(8) Hao, Y.; Murphy, K.; Lo, R. Y.; Khursigara, C. M.; Lam, J. S. Single-Nucleotide Polymorphisms Found in the MigA and WbpX Glycosyltransferase Genes Account for the Intrinsic Lipopolysaccharide Defects Exhibited by *Pseudomonas aeruginosa* PA14. *J. Bacteriol.* **2015**, *197* (17), 2780–2791. https://doi.org/10.1128/JB.00337-15.
(9) Wang, J.; Ma, W.; Fang, Y.; Liang, H.; Yang, H.; Wang, Y.; Dong, X.; Zhan, Y.; Wang, X. Core Oligosaccharide Portion of Lipopolysaccharide Plays Important Roles in Multiple Antibiotic Resistance in *Escherichia coli*. *Antimicrob. Agents Chemother. 65* (10), e00341-21. https://doi.org/10.1128/AAC.00341-21.
(10) Chen, H. D.; Groisman, E. A. The Biology of the PmrA/PmrB Two-Component System: The Major Regulator of Lipopolysaccharide Modifications. *Annu. Rev. Microbiol.* **2013**, *67* (1), 83–112. https://doi.org/10.1146/annurev-micro-092412-155751.
(11) Sun, J.; Rutherford, S. T.; Silhavy, T. J.; Huang, K. C. Physical Properties of the Bacterial Outer Membrane. *Nat. Rev. Microbiol.* **2022**, *20* (4), 236–248. https://doi.org/10.1038/s41579-021-00638-0.
(12) Manioglu, S.; Modaresi, S. M.; Ritzmann, N.; Thoma, J.; Overall, S. A.; Harms, A.; Upert, G.; Luther, A.; Barnes, A. B.; Obrecht, D.; Müller, D. J.; Hiller, S. Antibiotic Polymyxin Arranges Lipopolysaccharide into Crystalline Structures to Solidify the Bacterial Membrane. *Nat. Commun.* **2022**, *13* (1), 6195. https://doi.org/10.1038/s41467-022-33838-0.
(13) Imamura, Y.; Higashiyama, Y.; Tomono, K.; Izumikawa, K.; Yanagihara, K.; Ohno, H.; Miyazaki, Y.; Hirakata, Y.; Mizuta, Y.; Kadota, J.; Iglewski, B. H.; Kohno, S. Azithromycin Exhibits Bactericidal Effects on *Pseudomonas aeruginosa* through Interaction with the Outer

Membrane. *Antimicrob. Agents Chemother.* **2005**, *49* (4), 1377–1380. https://doi.org/10.1128/AAC.49.4.1377-1380.2005.
(14) Grabowicz, M.; Andres, D.; Lebar, M. D.; Malojčić, G.; Kahne, D.; Silhavy, T. J. A Mutant *Escherichia coli* That Attaches Peptidoglycan to Lipopolysaccharide and Displays Cell Wall on Its Surface. *eLife* **2014**, *3*, e05334. https://doi.org/10.7554/eLife.05334.
(15) Lam, J. S.; Taylor, V. L.; Islam, S. T.; Hao, Y.; Kocíncová, D. Genetic and Functional Diversity of *Pseudomonas aeruginosa* Lipopolysaccharide. *Front. Microbiol.* **2011**, *2*, 118. https://doi.org/10.3389/fmicb.2011.00118.
(16) Huszczynski, S. M.; Lam, J. S.; Khursigara, C. M. The Role of *Pseudomonas aeruginosa* Lipopolysaccharide in Bacterial Pathogenesis and Physiology. *Pathogens* **2019**, *9* (1), 6. https://doi.org/10.3390/pathogens9010006.
(17) Kilmury, S. L. N.; Burrows, L. L. Type IV Pilins Regulate Their Own Expression via Direct Intramembrane Interactions with the Sensor Kinase PilS. *Proc. Natl. Acad. Sci.* **2016**, *113* (21), 6017–6022. https://doi.org/10.1073/pnas.1512947113.
(18) Francis, V. I.; Stevenson, E. C.; Porter, S. L. Two-Component Systems Required for Virulence in *Pseudomonas aeruginosa*. *FEMS Microbiol. Lett.* **2017**, *364* (11), fnx104. https://doi.org/10.1093/femsle/fnx104.
(19) Kilmury, S. L. N.; Burrows, L. L. The *Pseudomonas aeruginosa* PilSR Two-Component System Regulates Both Twitching and Swimming Motilities. *mBio* **2018**, *9* (4), e01310-18. https://doi.org/10.1128/mBio.01310-18.
(20) Wang, B. X.; Cady, K. C.; Oyarce, G. C.; Ribbeck, K.; Laub, M. T. Two-Component Signaling Systems Regulate Diverse Virulence-Associated Traits in *Pseudomonas aeruginosa*. *Appl. Environ. Microbiol.* **2021**, *87* (11), e03089-20. https://doi.org/10.1128/AEM.03089-20.
(21) Isaac, D. D.; Pinkner, J. S.; Hultgren, S. J.; Silhavy, T. J. The Extracytoplasmic Adaptor Protein CpxP Is Degraded with Substrate by DegP. *Proc. Natl. Acad. Sci.* **2005**, *102* (49), 17775–17779. https://doi.org/10.1073/pnas.0508936102.
(22) Raivio, T. L.; Leblanc, S. K. D.; Price, N. L. The *Escherichia coli* Cpx Envelope Stress Response Regulates Genes of Diverse Function That Impact Antibiotic Resistance and Membrane Integrity. *J. Bacteriol.* **2013**, *195* (12), 2755–2767. https://doi.org/10.1128/JB.00105-13.
(23) Bernal-Cabas, M.; Ayala, J. A.; Raivio, T. L. The Cpx Envelope Stress Response Modifies Peptidoglycan Cross-Linking via the l,d-Transpeptidase LdtD and the Novel Protein YgaU. *J. Bacteriol.* **2015**, *197* (3), 603–614. https://doi.org/10.1128/JB.02449-14.
(24) Roemhild, R.; Gokhale, C. S.; Dirksen, P.; Blake, C.; Rosenstiel, P.; Traulsen, A.; Andersson, D. I.; Schulenburg, H. Cellular Hysteresis as a Principle to Maximize the Efficacy of Antibiotic Therapy. *Proc. Natl. Acad. Sci. U. S. A.* **2018**, *115* (39), 9767–9772. https://doi.org/10.1073/pnas.1810004115.
(25) Batchelor, E.; Walthers, D.; Kenney, L. J.; Goulian, M. The *Escherichia coli* CpxA-CpxR Envelope Stress Response System Regulates Expression of the Porins OmpF and OmpC. *J. Bacteriol.* **2005**, *187* (16), 5723–5731. https://doi.org/10.1128/JB.187.16.5723-5731.2005.
(26) Tian, Z.-X.; Yi, X.-X.; Cho, A.; O'Gara, F.; Wang, Y.-P. CpxR Activates MexAB-OprM Efflux Pump Expression and Enhances Antibiotic Resistance in Both Laboratory and Clinical NalB-Type Isolates of *Pseudomonas aeruginosa*. *PLoS Pathog.* **2016**, *12* (10), e1005932. https://doi.org/10.1371/journal.ppat.1005932.
(27) Ranieri, M. R. M.; Chan, D. C. K.; Yaeger, L. N.; Rudolph, M.; Karabelas-Pittman, S.; Abdo, H.; Chee, J.; Harvey, H.; Nguyen, U.; Burrows, L. L. Thiostrepton Hijacks Pyoverdine

Receptors To Inhibit Growth of *Pseudomonas aeruginosa*. *Antimicrob. Agents Chemother.* **2019**, *63* (9), e00472-19. https://doi.org/10.1128/AAC.00472-19.
(28) Chan, D. C. K.; Burrows, L. L. *Pseudomonas aeruginosa* FpvB Is a High-Affinity Transporter for Xenosiderophores Ferrichrome and Ferrioxamine B. *mBio* **2022**, *0* (0), e03149-22. https://doi.org/10.1128/mbio.03149-22.
(29) Chan, D. C. K.; Burrows, L. L. Thiocillin and Micrococcin Exploit the Ferrioxamine Receptor of *Pseudomonas aeruginosa* for Uptake. *J. Antimicrob. Chemother.* **2021**, *76* (8), 2029–2039. https://doi.org/10.1093/jac/dkab124.
(30) Chan, D. C. K.; Josts, I.; Koteva, K.; Wright, G. D.; Tidow, H.; Burrows, L. L. Interactions of TonB-Dependent Transporter FoxA with Siderophores and Antibiotics That Affect Binding, Uptake, and Signal Transduction. *Proc. Natl. Acad. Sci.* **2023**, *120* (16), e2221253120. https://doi.org/10.1073/pnas.2221253120.
(31) Su, T. L. Micrococcin. An Antibacterial Substance Formed by a Strain of Micrococcus. *Br. J. Exp. Pathol.* **1948**, *29* (5), 473–481.
(32) Kelly, J.; Kutscher, A. H.; Tuoti, F. Thiostrepton, a New Antibiotic: Tube Dilution Sensitivity Studies. *Oral Surg. Oral Med. Oral Pathol.* **1959**, *12* (11), 1334–1339. https://doi.org/10.1016/0030-4220(59)90222-1.
(33) Nikaido, H. Molecular Basis of Bacterial Outer Membrane Permeability Revisited. *Microbiol. Mol. Biol. Rev.* **2003**, *67* (4), 593–656. https://doi.org/10.1128/MMBR.67.4.593-656.2003.
(34) O'Shea, R.; Moser, H. E. Physicochemical Properties of Antibacterial Compounds: Implications for Drug Discovery. *J. Med. Chem.* **2008**, *51* (10), 2871–2878. https://doi.org/10.1021/jm700967e.
(35) Ahlgren, H. G.; Benedetti, A.; Landry, J. S.; Bernier, J.; Matouk, E.; Radzioch, D.; Lands, L. C.; Rousseau, S.; Nguyen, D. Clinical Outcomes Associated with Staphylococcus Aureus and *Pseudomonas aeruginosa* Airway Infections in Adult Cystic Fibrosis Patients. *BMC Pulm. Med.* **2015**, *15* (1), 67. https://doi.org/10.1186/s12890-015-0062-7.
(36) Limoli, D. H.; Yang, J.; Khansaheb, M. K.; Helfman, B.; Peng, L.; Stecenko, A. A.; Goldberg, J. B. Staphylococcus Aureus and *Pseudomonas aeruginosa* Co-Infection Is Associated with Cystic Fibrosis-Related Diabetes and Poor Clinical Outcomes. *Eur. J. Clin. Microbiol. Infect. Dis.* **2016**, *35* (6), 947–953. https://doi.org/10.1007/s10096-016-2621-0.
(37) Maliniak, M. L.; Stecenko, A. A.; McCarty, N. A. A Longitudinal Analysis of Chronic MRSA and *Pseudomonas aeruginosa* Co-Infection in Cystic Fibrosis: A Single-Center Study. *J. Cyst. Fibros.* **2016**, *15* (3), 350–356. https://doi.org/10.1016/j.jcf.2015.10.014.
(38) Hubert, D.; Réglier-Poupet, H.; Sermet-Gaudelus, I.; Ferroni, A.; Bourgeois, M. L.; Burgel, P.-R.; Serreau, R.; Dusser, D.; Poyart, C.; Coste, J. Association between Staphylococcus Aureus Alone or Combined with *Pseudomonas aeruginosa* and the Clinical Condition of Patients with Cystic Fibrosis. *J. Cyst. Fibros.* **2013**, *12* (5), 497–503. https://doi.org/10.1016/j.jcf.2012.12.003.
(39) Ang, M. T. C.; Gumbau-Brisa, R.; Allan, D. S.; McDonald, R.; Ferguson, M. J.; Holbein, B. E.; Bierenstiel, M. DIBI, a 3-Hydroxypyridin-4-One Chelator Iron-Binding Polymer with Enhanced Antimicrobial Activity †Electronic Supplementary Information (ESI) Available. CCDC 1812776 and 1830658. For ESI and Crystallographic Data in CIF or Other Electronic Format See DOI: 10.1039/C8md00192h. *MedChemComm* **2018**, *9* (7), 1206–1212. https://doi.org/10.1039/c8md00192h.

(40) Walsh, T. R.; Howe, R. A. The Prevalence and Mechanisms of Vancomycin Resistance in *Staphylococcus Aureus*. *Annu. Rev. Microbiol.* **2002**, *56* (1), 657–675. https://doi.org/10.1146/annurev.micro.56.012302.160806.
(41) Ropy, A.; Cabot, G.; Sánchez-Diener, I.; Aguilera, C.; Moya, B.; Ayala, J. A.; Oliver, A. Role of *Pseudomonas aeruginosa* Low-Molecular-Mass Penicillin-Binding Proteins in AmpC Expression, β-Lactam Resistance, and Peptidoglycan Structure. *Antimicrob. Agents Chemother.* **2015**, *59* (7), 3925–3934. https://doi.org/10.1128/AAC.05150-14.
(42) Torrens, G.; Hernández, S. B.; Ayala, J. A.; Moya, B.; Juan, C.; Cava, F.; Oliver, A. Regulation of AmpC-Driven β-Lactam Resistance in *Pseudomonas aeruginosa*: Different Pathways, Different Signaling. *mSystems* **2019**, *4* (6), e00524-19. https://doi.org/10.1128/mSystems.00524-19.
(43) Zamorano, L.; Moyá, B.; Juan, C.; Oliver, A. Differential β-Lactam Resistance Response Driven by AmpD or DacB (PBP4) Inactivation in Genetically Diverse *Pseudomonas aeruginosa* Strains. *J. Antimicrob. Chemother.* **2010**, *65* (7), 1540–1542. https://doi.org/10.1093/jac/dkq142.
(44) Barbieri, C. M.; Mack, T. R.; Robinson, V. L.; Miller, M. T.; Stock, A. M. Regulation of Response Regulator Autophosphorylation through Interdomain Contacts. *J. Biol. Chem.* **2010**, *285* (42), 32325–32335. https://doi.org/10.1074/jbc.M110.157164.
(45) Boll, J. M.; Hendrixson, D. R. A Specificity Determinant for Phosphorylation in a Response Regulator Prevents in Vivo Cross-Talk and Modification by Acetyl Phosphate. *Proc. Natl. Acad. Sci.* **2011**, *108* (50), 20160–20165. https://doi.org/10.1073/pnas.1113013108.
(46) Kurabayashi, K.; Hirakawa, Y.; Tanimoto, K.; Tomita, H.; Hirakawa, H. Role of the CpxAR Two-Component Signal Transduction System in Control of Fosfomycin Resistance and Carbon Substrate Uptake. *J. Bacteriol.* **2014**, *196* (2), 248–256. https://doi.org/10.1128/JB.01151-13.
(47) Mahoney, T. F.; Silhavy, T. J. The Cpx Stress Response Confers Resistance to Some, but Not All, Bactericidal Antibiotics. *J. Bacteriol.* **2013**, *195* (9), 1869–1874. https://doi.org/10.1128/JB.02197-12.
(48) Masi, M.; Pinet, E.; Pagès, J.-M. Complex Response of the CpxAR Two-Component System to β-Lactams on Antibiotic Resistance and Envelope Homeostasis in Enterobacteriaceae. *Antimicrob. Agents Chemother.* **2020**, *64* (6), e00291-20. https://doi.org/10.1128/AAC.00291-20.
(49) Holm, L. Dali Server: Structural Unification of Protein Families. *Nucleic Acids Res.* **2022**, *50* (W1), W210–W215. https://doi.org/10.1093/nar/gkac387.
(50) Jumper, J.; Evans, R.; Pritzel, A.; Green, T.; Figurnov, M.; Ronneberger, O.; Tunyasuvunakool, K.; Bates, R.; Žídek, A.; Potapenko, A.; Bridgland, A.; Meyer, C.; Kohl, S. A. A.; Ballard, A. J.; Cowie, A.; Romera-Paredes, B.; Nikolov, S.; Jain, R.; Adler, J.; Back, T.; Petersen, S.; Reiman, D.; Clancy, E.; Zielinski, M.; Steinegger, M.; Pacholska, M.; Berghammer, T.; Bodenstein, S.; Silver, D.; Vinyals, O.; Senior, A. W.; Kavukcuoglu, K.; Kohli, P.; Hassabis, D. Highly Accurate Protein Structure Prediction with AlphaFold. *Nature* **2021**, *596* (7873), 583–589. https://doi.org/10.1038/s41586-021-03819-2.
(51) Osawa, T.; Sugiura, N.; Shimada, H.; Hirooka, R.; Tsuji, A.; Shirakawa, T.; Fukuyama, K.; Kimura, M.; Kimata, K.; Kakuta, Y. Crystal Structure of Chondroitin Polymerase from *Escherichia coli* K4. *Biochem. Biophys. Res. Commun.* **2009**, *378* (1), 10–14. https://doi.org/10.1016/j.bbrc.2008.08.121.
(52) Kocíncová, D.; Ostler, S. L.; Anderson, E. M.; Lam, J. S. Rhamnosyltransferase Genes MigA and WapR Are Regulated in a Differential Manner To Modulate the Quantities of Core

Oligosaccharide Glycoforms Produced by *Pseudomonas aeruginosa*. *J. Bacteriol.* **2012**, *194* (16), 4295–4300. https://doi.org/10.1128/JB.05741-11.
(53) Poon, K. K. H.; Westman, E. L.; Vinogradov, E.; Jin, S.; Lam, J. S. Functional Characterization of MigA and WapR: Putative Rhamnosyltransferases Involved in Outer Core Oligosaccharide Biosynthesis of *Pseudomonas aeruginosa*. *J. Bacteriol.* **2008**, *190* (6), 1857–1865. https://doi.org/10.1128/JB.01546-07.
(54) Nelson, C. E.; Huang, W.; Zygiel, E. M.; Nolan, E. M.; Kane, M. A.; Oglesby, A. G. The Human Innate Immune Protein Calprotectin Elicits a Multimetal Starvation Response in *Pseudomonas aeruginosa*. *Microbiol. Spectr.* **2021**, *9* (2), e00519-21. https://doi.org/10.1128/Spectrum.00519-21.
(55) Kucharczyk, M.; Brzezowska, M.; Maciąg, A.; Lis, T.; Jeżowska-Bojczuk, M. Structural Features of the Cu2+–Vancomycin Complex. *J. Inorg. Biochem.* **2008**, *102* (4), 936–942. https://doi.org/10.1016/j.jinorgbio.2007.12.014.
(56) Świątek, M.; Valensin, D.; Migliorini, C.; Gaggelli, E.; Valensin, G.; Jeżowska-Bojczuk, M. Unusual Binding Ability of Vancomycin towards Cu2+ Ions. *Dalton Trans.* **2005**, No. 23, 3808. https://doi.org/10.1039/b508662k.
(57) Raivio, T. L.; Silhavy, T. J. Transduction of Envelope Stress in *Escherichia coli* by the Cpx Two-Component System. *J. Bacteriol.* **1997**, *179* (24), 7724–7733. https://doi.org/10.1128/jb.179.24.7724-7733.1997.
(58) Hugonnet, J.-E.; Mengin-Lecreulx, D.; Monton, A.; den Blaauwen, T.; Carbonnelle, E.; Veckerlé, C.; Brun, Y., V.; van Nieuwenhze, M.; Bouchier, C.; Tu, K.; Rice, L. B.; Arthur, M. Factors Essential for L,D-Transpeptidase-Mediated Peptidoglycan Cross-Linking and β-Lactam Resistance in *Escherichia coli*. *eLife* **2016**, *5*, e19469. https://doi.org/10.7554/eLife.19469.
(59) Anderson, E. M.; Shaji Saji, N.; Anderson, A. C.; Brewer, D.; Clarke, A. J.; Khursigara, C. M. *Pseudomonas aeruginosa* Alters Peptidoglycan Composition under Nutrient Conditions Resembling Cystic Fibrosis Lung Infections. *mSystems 7* (3), e00156-22. https://doi.org/10.1128/msystems.00156-22.
(60) Bielnicki, J.; Devedjiev, Y.; Derewenda, U.; Dauter, Z.; Joachimiak, A.; Derewenda, Z. S. B. Subtilis YkuD Protein at 2.0 Å Resolution: Insights into the Structure and Function of a Novel, Ubiquitous Family of Bacterial Enzymes. *Proteins* **2006**, *62* (1), 144–151. https://doi.org/10.1002/prot.20702.
(61) Dbeibo, L.; van Rensburg, J. J.; Smith, S. N.; Fortney, K. R.; Gangaiah, D.; Gao, H.; Marzoa, J.; Liu, Y.; Mobley, H. L. T.; Spinola, S. M. Evaluation of CpxRA as a Therapeutic Target for Uropathogenic *Escherichia coli* Infections. *Infect. Immun.* **2018**, *86* (3), e00798-17. https://doi.org/10.1128/IAI.00798-17.
(62) DeLeon, S.; Clinton, A.; Fowler, H.; Everett, J.; Horswill, A. R.; Rumbaugh, K. P. Synergistic Interactions of *Pseudomonas aeruginosa* and Staphylococcus Aureus in an In Vitro Wound Model. *Infect. Immun.* **2014**, *82* (11), 4718–4728. https://doi.org/10.1128/IAI.02198-14.
(63) Murdoch, C. C.; Skaar, E. P. Nutritional Immunity: The Battle for Nutrient Metals at the Host–Pathogen Interface. *Nat. Rev. Microbiol.* **2022**, *20* (11), 657–670. https://doi.org/10.1038/s41579-022-00745-6.
(64) P. Skaar, E.; Raffatellu, M. Metals in Infectious Diseases and Nutritional Immunity. *Metallomics* **2015**, *7* (6), 926–928. https://doi.org/10.1039/C5MT90021B.
(65) Stites, S. W.; Plautz, M. W.; Bailey, K.; O'brien-Ladner, A. R.; Wesselius, L. J. Increased Concentrations of Iron and Isoferritins in the Lower Respiratory Tract of Patients with Stable

Cystic Fibrosis. *Am. J. Respir. Crit. Care Med.* **1999**, *160* (3), 796–801. https://doi.org/10.1164/ajrccm.160.3.9811018.
(66) Reid, D. W.; Lam, Q. T.; Schneider, H.; Walters, E. H. Airway Iron and Iron-Regulatory Cytokines in Cystic Fibrosis. *Eur. Respir. J.* **2004**, *24* (2), 286–291. https://doi.org/10.1183/09031936.04.00104803.
(67) Stites, S. W.; Walters, B.; O'Brien-Ladner, A. R.; Bailey, K.; Wesselius, L. J. Increased Iron and Ferritin Content of Sputum From Patients With Cystic Fibrosis or Chronic Bronchitis. *CHEST* **1998**, *114* (3), 814–819. https://doi.org/10.1378/chest.114.3.814.
(68) Gifford, A. h.; Miller, S. d.; Jackson, B. p.; Hampton, T. h.; O'Toole, G. a.; Stanton, B. a.; Parker, H. w. Iron and CF-Related Anemia: Expanding Clinical and Biochemical Relationships. *Pediatr. Pulmonol.* **2011**, *46* (2), 160–165. https://doi.org/10.1002/ppul.21335.
(69) Reid, D. W.; Carroll, V.; O'May, C.; Champion, A.; Kirov, S. M. Increased Airway Iron as a Potential Factor in the Persistence of *Pseudomonas aeruginosa* Infection in Cystic Fibrosis. *Eur. Respir. J.* **2007**, *30* (2), 286–292. https://doi.org/10.1183/09031936.00154006.
(70) Stokes, J. M.; French, S.; Ovchinnikova, O. G.; Bouwman, C.; Whitfield, C.; Brown, E. D. Cold Stress Makes *Escherichia coli* Susceptible to Glycopeptide Antibiotics by Altering Outer Membrane Integrity. *Cell Chem. Biol.* **2016**, *23* (2), 267–277. https://doi.org/10.1016/j.chembiol.2015.12.011.
(71) Belanger, C. R.; Lee, A. H.-Y.; Pletzer, D.; Dhillon, B. K.; Falsafi, R.; Hancock, R. E. W. Identification of Novel Targets of Azithromycin Activity against *Pseudomonas aeruginosa* Grown in Physiologically Relevant Media. *Proc. Natl. Acad. Sci. U. S. A.* **2020**, *117* (52), 33519–33529. https://doi.org/10.1073/pnas.2007626117.
(72) Chibani-Chennoufi, S.; Bruttin, A.; Dillmann, M.-L.; Brüssow, H. Phage-Host Interaction: An Ecological Perspective. *J. Bacteriol.* **2004**, *186* (12), 3677–3686. https://doi.org/10.1128/JB.186.12.3677-3686.2004.
(73) Loh, B.; Grant, C.; Hancock, R. E. Use of the Fluorescent Probe 1-N-Phenylnaphthylamine to Study the Interactions of Aminoglycoside Antibiotics with the Outer Membrane of *Pseudomonas aeruginosa*. *Antimicrob. Agents Chemother.* **1984**, *26* (4), 546–551. https://doi.org/10.1128/AAC.26.4.546.
(74) Liberati, N. T.; Urbach, J. M.; Miyata, S.; Lee, D. G.; Drenkard, E.; Wu, G.; Villanueva, J.; Wei, T.; Ausubel, F. M. An Ordered, Nonredundant Library of *Pseudomonas aeruginosa* Strain PA14 Transposon Insertion Mutants. *Proc. Natl. Acad. Sci. U. S. A.* **2006**, *103* (8), 2833–2838. https://doi.org/10.1073/pnas.0511100103.
(75) Feng, M.; Mei, J.; Hu, S.; Janney, S.; Carruthers, J.; Holbein, B.; Huber, A.; Kidby, D. Selective Removal of Iron from Grape Juice Using an Iron(III) Chelating Resin. *Sep. Purif. Technol.* **1997**, *11* (2), 127–135. https://doi.org/10.1016/S1383-5866(97)00010-5.
(76) Mangat, C. S.; Bharat, A.; Gehrke, S. S.; Brown, E. D. Rank Ordering Plate Data Facilitates Data Visualization and Normalization in High-Throughput Screening. *J. Biomol. Screen.* **2014**, *19* (9), 1314–1320. https://doi.org/10.1177/1087057114534298.
(77) Deatherage, D. E.; Barrick, J. E. Identification of Mutations in Laboratory Evolved Microbes from Next-Generation Sequencing Data Using Breseq. *Methods Mol. Biol. Clifton NJ* **2014**, *1151*, 165–188. https://doi.org/10.1007/978-1-4939-0554-6_12.
(78) Marolda, C. L.; Lahiry, P.; Vinés, E.; Saldías, S.; Valvano, M. A. Micromethods for the Characterization of Lipid A-Core and O-Antigen Lipopolysaccharide. In *Glycobiology Protocols*; Brockhausen, I., Ed.; Methods in Molecular Biology; Humana Press: Totowa, NJ, 2007; pp 237–252. https://doi.org/10.1385/1-59745-167-3:237.

(79) Kocíncová, D.; Hao, Y.; Vinogradov, E.; Lam, J. S. Evidence That WapB Is a 1,2-Glucosyltransferase of *Pseudomonas aeruginosa* Involved in Lipopolysaccharide Outer Core Biosynthesis ▿ . *J. Bacteriol.* **2011**, *193* (11), 2708–2716. https://doi.org/10.1128/JB.00032-11.
(80) *Pseudomonas aeruginosa defends against phages through type IV pilus glycosylation | Nature Microbiology*. https://www.nature.com/articles/s41564-017-0061-y (accessed 2023-02-21).
(81) Goddard, T. D.; Huang, C. C.; Meng, E. C.; Pettersen, E. F.; Couch, G. S.; Morris, J. H.; Ferrin, T. E. UCSF ChimeraX: Meeting Modern Challenges in Visualization and Analysis. *Protein Sci.* **2018**, *27* (1), 14–25. https://doi.org/10.1002/pro.3235.

Supplementary Information

Derek C. K. Chan, Katherine Dykema, Mahrukh Fatima, Hanjeong Harvey, Ikram Qaderi, and Lori L. Burrows

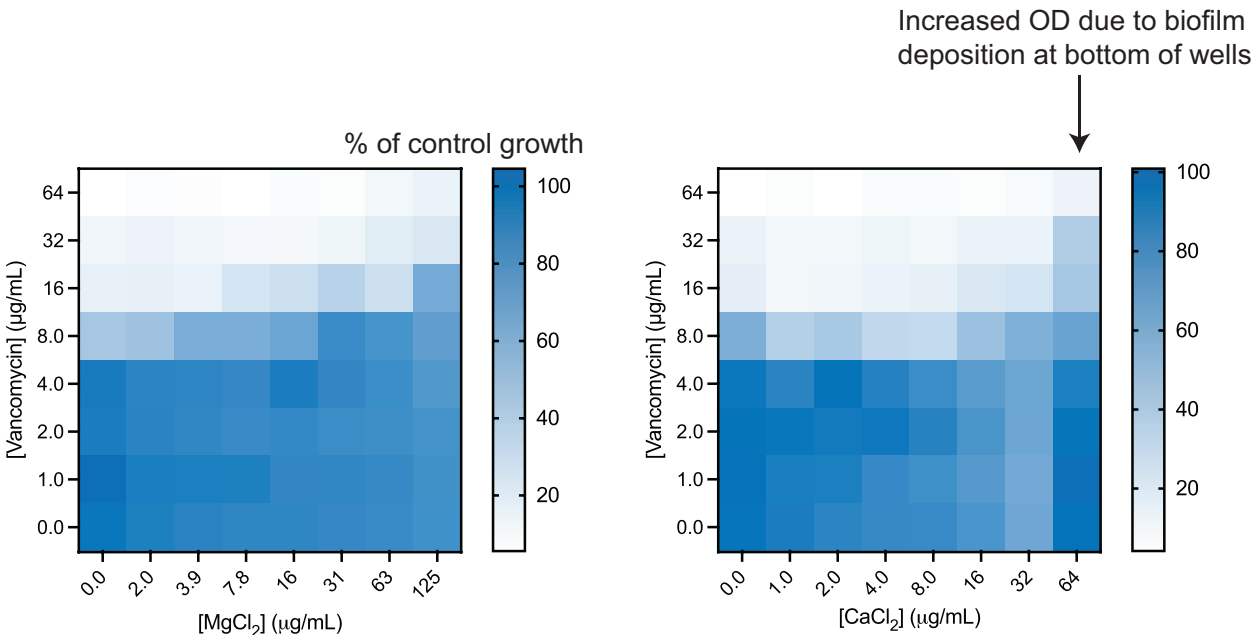

Supplementary Figure S1. Checkerboard assays of vancomycin with $MgCl_2$ and $CaCl_2$ against PA14. Results are averaged from three independent biological replicates.

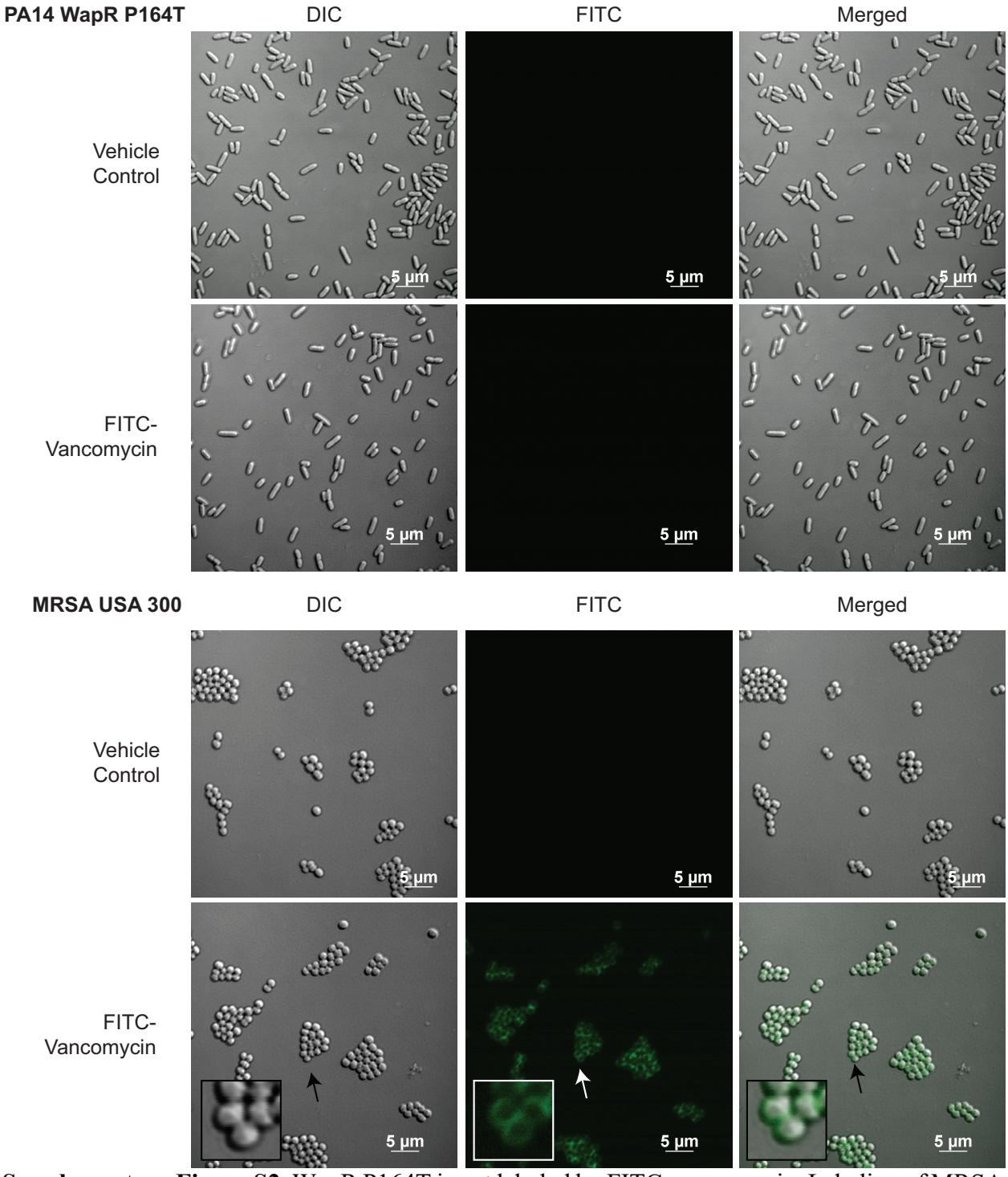

Supplementary Figure S2. WapR P164T is not labeled by FITC-vancomycin. Labeling of MRSA USA 300 is shown as a positive control. Representative images are shown. Scale bar is indicated.

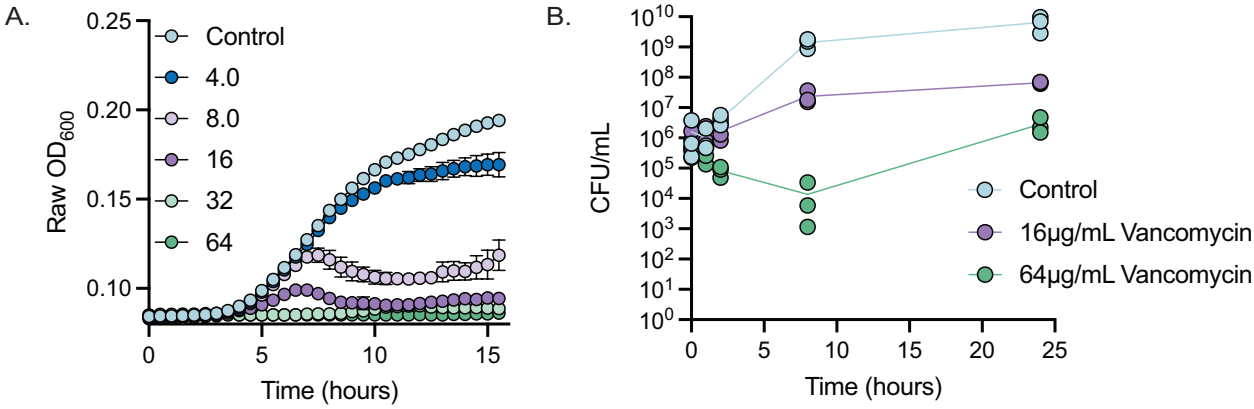

Supplementary Figure S3. A. Growth curves with PA14 treated with increasing concentrations of vancomycin (µg/mL) and **B.** time-kill kinetics of vancomycin at 1X MIC (16µg/mL) and 4X MIC (64µg/mL) in 10:90. All results are averaged from three independent biological replicates. Individual biological replicates are shown for the time-kill kinetics. Cells were grown in 10:90 for all assays.

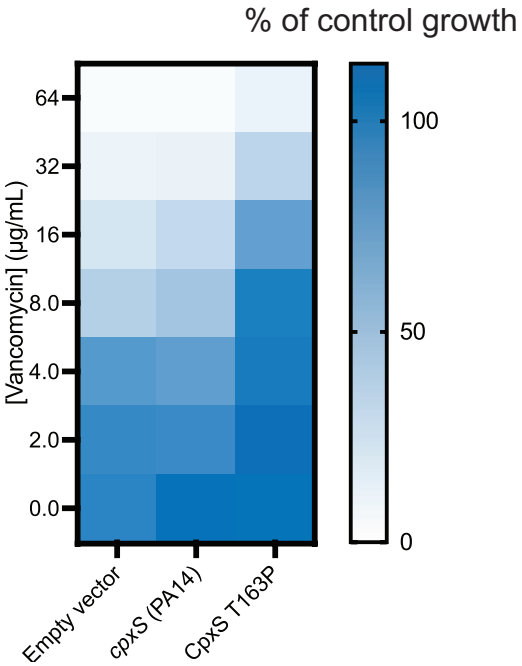

Supplementary Figure S4. Vancomycin MIC assays with PA14 *cpxS*::Mar2xT7 with empty vector, expressing WT PA14 *cpxS*, and CpxS T163P in 10:90 + 0.25% arabinose. Results are averaged from three independent biological replicates.

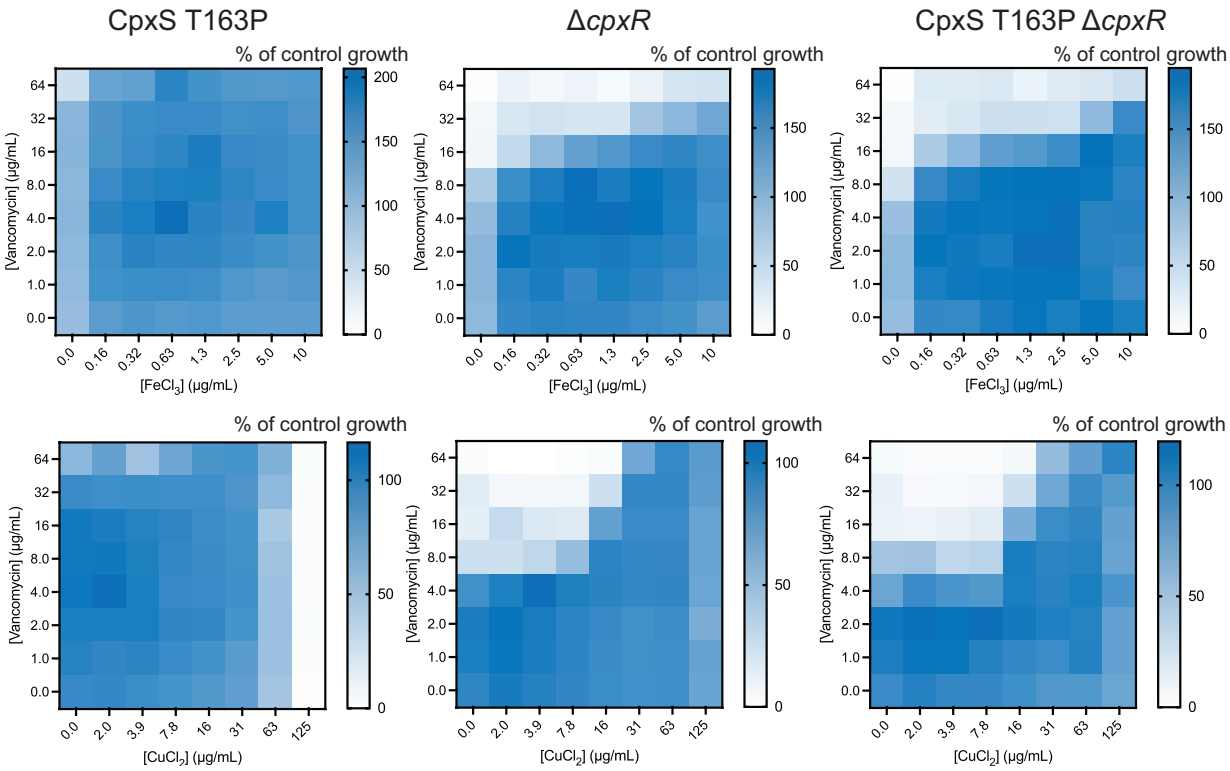

Supplementary Figure S5. Checkerboard assays of vancomycin with $FeCl_3$ and $CuCl_2$ against Δ*cpxR*, CpxS T163P, and CpxS T163P Δ*cpxR*. Results are averaged from three independent biological replicates.

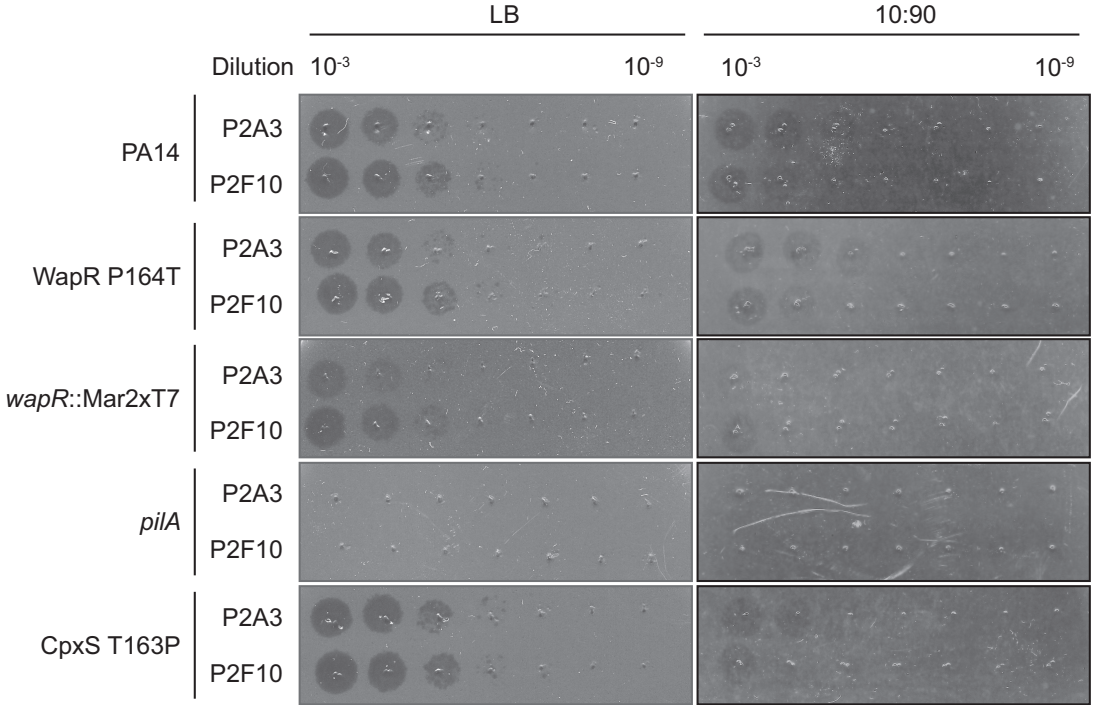

Supplementary Figure S6. WapR P164T mutant is not sensitized to pilus-specific phages in LB or 10:90.

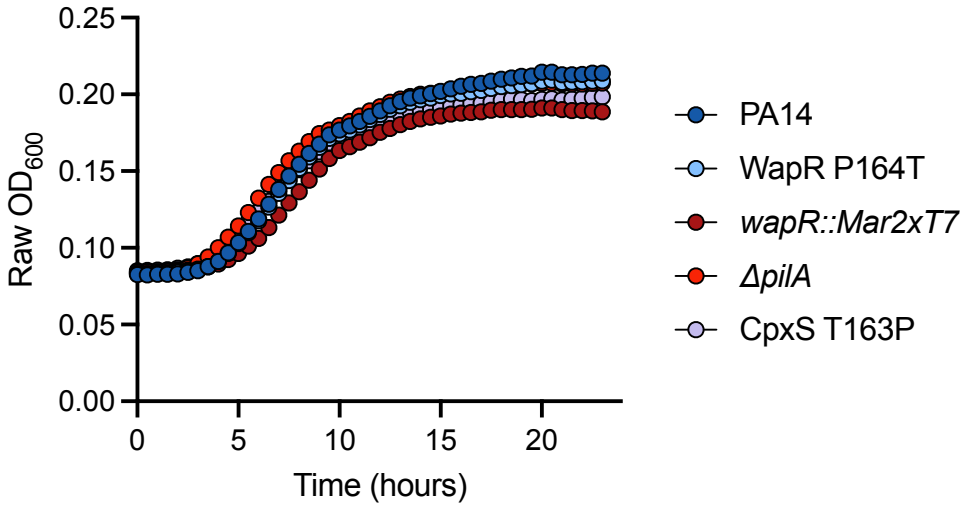

Supplementary Figure S7. Growth curves of PA14, WapR P164T, *wapR*::Mar2xT7, Δ*pilA*, and CpxS T163P in 10:90. Results are averaged from three independent biological replicates.

Supplementary Table S1. List of Compounds in the Initial Screen

Compound	Activity against PA14	Molecular Weight (g/mol)
A54556A	N	718.8
Actagardin	N	1754
Actinomycin D	Y	1255.4
Amphomycin	N	1290.4
Aspartocin D	N	1276.4
Azithromycin	Y	749
Boromycin	N	879.9
Capreomycin	N	668.7
Echinomycin	Y	1101.3
Feglymycin	N	1900.9
Fidaxomicin	N	1058.1
Gramicidin	N	1882.3
Luzopeptin A	N	1343.3
Nosiheptide	Y	1222.4
Quinaldopeptin	Y	1243.3
Quinupristin	N	1022.2
Sandramycin	Y	1221.3
Siamycin	N	2163.5
Streptogramin B	N	867

Telomycin	N	1272.3
Thiocoraline	N	1157.4
Tunicamycin	N	816.9
Virginiamycin	N	1349.5
Vancomycin	Y	1449.3

Y: has antimicrobial activity against *P. aeruginosa* PA14 in the screen (highlighted blue)
N: lacks antimicrobial activity against *P. aeruginosa* PA14 in the screen (highlighted red)

Supplementary Table S2. Strains used in this study

Strain	**Source**
PA14	1
PA14 Δ*cpxR*	This study
PA14 CpxS T163P	This study
PA14 CpxS T163P Δ*cpxR*	This study
PA14 Δ*cpxR* pBADGr	This study
PA14 Δ*cpxR* pBADGr-*cpxR*	This study
PA14 CpxS T163P Δ*cpxR* pBADGr	This study
PA14 CpxS T163P Δ*cpxR* pBADGr-*cpxR*	This study
PA14 WapR P164T	This study
PA14 *wapR*::Mar2xT7	1
PA14 *cpxS*::Mar2xT7	1
PA14 *cpxS*::Mar2xT7 pHERD20T	This study
PA14 *cpxS*::Mar2xT7 pHERD20T-$cpxS_{PA14}$	This study
PA14 *cpxS*::Mar2xT7 pHERD20T-$cpxS_{PA14}$ T163P	This study
PA14 Δ*pilA*	This study
PA14 Δ*dacB*	This study
PA14 Δ*dacC*	This study
PA14 Δ*dacB* Δ*dacC*	This study
PA14 P_x-*gfp*	2
PA14 P_{mexA}-*gfp*	This study
PA14 CpxS T163P P_x-*gfp*	This study
PA14 CpxS T163P P_{mexA}-*gfp*	This study
P. aeruginosa C0275	3
P. aeruginosa C0098	3
MRSA USA300	Brown Lab

Supplementary Table S3. Primers used in this study. Restriction sites are bolded and underlined.

Primer	Forward 5' → 3'	Reverse 5' → 3'
cpxR deletion upstream	CCT**GGATCC**GTGGTCTTCACCT ATCCGAACTTCTGG	TCAGTGGCTGTAGTAGTAGCCGC GGCAGAGCTCCCGGTCATCG
cpxR deletion downstream	CGATGACCGGGAGCTCTGCCGC GGCTACTACTACAGCCACTGA	CCT**TCTAGA**TCCTGTTGAATCGC ATGTCGGG
CpxS T163P chromosomal mutation upstream	CAT**GAATTC**GGCCCGACATGC GATTCAACAG	TGGTGGTGCTGCCTCTGTTCA

CpxS T163P chromosomal mutation downstream	TGAACAGAGGCAGCACCACCA	CCC**AAGCTT**TTATTCGGTCGCCTTGCGCC
cpxR complementation	CGT**GAATTC**CGACAGCGACGCGAATGGATC	GCT**AAGCTT**GCTTGGGTAAAGACCTTGTGTCGG
dacB chromosomal deletion upstream	CGT**TCTAGA**AGCAATTGGCCTGGTTATCTGCATGA	TTCGTACTGCGCCTTATTTCCGCGTAATGAAGAACCCTTGAAGACGGAGGGTAG
dacB chromosomal deletion downstream	CTACCCTCCGTCTTCAAGGGTTCTTCATTACGCGGAAATAAGGCGCAGTACGAA	CAC**AAGCTT**AGGAGCGGGTGGTGGTCAAG
dacC chromosomal deletion upstream	GCT**TCTAGA**GACTATTCCCGTCCGCATCGC	GGTCGGTCAGTTGAACAAACCGTAGAAATTCCCTGCGTGAGTAGGCGC
dacC chromosomal deletion downstream	GCGCCTACTCACGCAGGGAATTTCTACGGTTTGTTCAACTGACCGACC	CAG**AAGCTT**TGCTCGATCCGGCTGACCA
P_{mexA}-*gfp*	CCA**TCTAGA**GCTCGCGGATCTTCCGGGT	CAAT**GCATGC**TCAGCGAAAGCGGCCGATGCA
cpxS amplification	CAT**GAATTC**GGCCCGACATGCGATTCAACAG	CCC**AAGCTT**TTATTCGGTCGCCTTGCGCC
pilA chromosomal deletion upstream	TCGA**GGATCC**GCATCACGATCTTCTC	TAC**CTGCAG**TCGCAACCACGATCATCAG
pilA chromosomal deletion downstream	AC**CTGCAG**ATATGCCTGCCCTGACTGCA	CTGG**AAGCTT**CCGGCGGAATCAACG

Supplementary Table S4. Compounds used in this study

Vendor/Source	**Compound**
Bioshop	Kanamycin
Bioshop	Gentamicin
Bioshop	Arabinose
AK Scientific	Carbenicillin
AK Scientific	Vancomycin
AK Scientific	Imipenem
AK Scientific	Meropenem
AK Scientific	Tobramycin
AK Scientific	Azithromycin
AK Scientific	$CuCl_2$
Sigma	FITC-vancomycin
Sigma	Polymyxin B
Sigma	Cefmetazole
Sigma	Cefoperazone
Sigma	Aztreonam
Sigma	Ceftriaxone
Sigma	Piepracillin
Sigma	Cefuroxime
Sigma	Cefsulodin
Sigma	A22
Sigma	Fosfomycin
Sigma	Doxycycline
Sigma	Ciprofloxacin

Sigma	Novobiocin
Cayman Chemicals	D-cycloserine
Cayman Chemicals	Dalbavancin
Cayman Chemicals	Oritavancin
Cayman Chemicals	Teicoplanin
Cayman Chemicals	CCCP
Cayman Chemicals	Nosiheptide
Cayman Chemicals	Actinomycin D
Cayman Chemicals	Echinomycin
Cayman Chemicals	Virginiamycin
Cayman Chemicals	Amphomycin
Cayman Chemicals	Capreomycin
Cayman Chemicals	Fidaxomicin
Cayman Chemicals	A54556A
Cayman Chemicals	Streptogramin B
Cayman Chemicals	Quinupristin
Cayman Chemicals	Gramicidin
Cayman Chemicals	Tunicamycin
Cayman Chemicals	Telomycin
Cayman Chemicals	Boromycin
Cayman Chemicals	Siamycin
Cayman Chemicals	Astagardin
Cayman Chemicals	Thiocoraline
Cayman Chemicals	Luzopeptin A
Cayman Chemicals	Feglymicin
Cayman Chemicals	Sandramycin
Cayman Chemicals	Quinaldopeptin
Cayman Chemicals	Aspartocin D
Fisher Scientific	NPN
Fisher Scientific	$FeCl_3$
DIBI	Dr. Bruce Holbein (Fe Pharmaceuticals)
FEC-1 (insoluble DIBI analog to remove iron from media)	Dr. Bruce Holbein (Fe Pharmaceuticals)
MedChemExpress	Cefiderocol

Supplementary References

1. Liberati, N. T.; Urbach, J. M.; Miyata, S.; Lee, D. G.; Drenkard, E.; Wu, G.; Villanueva, J.; Wei, T.; Ausubel, F. M. An Ordered, Nonredundant Library of *Pseudomonas aeruginosa* Strain PA14 Transposon Insertion Mutants. *Proc. Natl. Acad. Sci. U. S. A.* **2006**, *103* (8), 2833–2838.
2. Chan, D. C. K.; Josts, I.; Koteva, K.; Wright, G. D.; Tidow, H.; Burrows, L. L. A Single Extracellular Loop of FoxA Controls Ligand Specificity, Uptake, and Signaling in *Pseudomonas aeruginosa*. bioRxiv November 18, 2022, p 2022.11.18.517105.
3. Ranieri, M. R. M.; Chan, D. C. K.; Yaeger, L. N.; Rudolph, M.; Karabelas-Pittman, S.; Abdo, H.; Chee, J.; Harvey, H.; Nguyen, U.; Burrows, L. L. Thiostrepton Hijacks Pyoverdine Receptors To Inhibit Growth of *Pseudomonas aeruginosa*. *Antimicrob. Agents Chemother.* **2019**, *63* (9), e00472-19.

Chapter Seven: Discussion and future directions

The OM of Gram-negative bacteria provides intrinsic resistance to multiple classes of antibiotics by blocking the uptake of large, hydrophobic, and charged molecules. This phenomenon reduces the treatment options available for Gram-negative infections. The Trojan Horse strategy to deliver drugs across the OM is a promising approach to address this problem. In Chapters 2 and 4, we described the discovery that the thiopeptide class of antibiotics has activity against *P. aeruginosa* due to their ability to hijack the FpvA, FpvB, and FoxA siderophore transporters under iron-limited conditions. The thiopeptides have narrow spectrum activity against *P. aeruginosa* and some other Pseudomonads as described in Chapter 4. These results suggest that other classes of natural products may have activity against other Gram-negative bacterial pathogens under more physiologically relevant growth conditions than MHB or LB. Therefore, future screens for molecules with antimicrobial activity against these pathogens should be conducted under nutrient-limited conditions. In a pilot screen was described in Chapter 6, we discovered that vancomycin has activity against *P. aeruginosa*, supporting the hypothesis that screening under nutrient limitation mimics physiologically conditions which improves uptake of existing antibiotics. Future work will focus on screening a larger set of compounds, which may yield new antimicrobial compounds and new strategies to promote drug uptake across the OM. This strategy is applicable to Gram-negative bacteria such as *A. baumannii,* where a nutrient-limited screen led to the discovery that the rifamycin derivative, rifabutin, is a substrate of the TBDT FhuE and has increased activity under low-iron due to increased expression of the transporter[1].

The work in Chapter 3 suggested a novel strategy to expand our knowledge of the range of ligands that can be taken up by a single transporter. The traditional strategy for identifying potential ligands of TBDTs involves aligning their sequences to those of transporters with known ligands.

However, this is an inefficient approach, because while some TBDTs share over 60% sequence similarity, they take up different ligands. Instead, we suggest using a competition-based approach. The susceptibility to an antimicrobial that uses a particular TBDT can be measured in the presence of increasing concentrations of various siderophores to look for growth recovery through competition for the transporter. Siderophores that antagonize activity are potential substrates of the transporter of interest. This approach can be expanded to TBDTs in other bacterial species and with other functions. Additionally, this approach is not limited to antibacterial compounds, but also applicable to phages and bacteriocins. One such example is pyocin SX2, which requires the uncharacterized TBDT PA0434 (PA14_05640) for activity[2]. Screening for substrates that antagonize pyocin activity may reveal its function. Overall, expanding our knowledge on the repertoire of substrates that can be taken up through various TBDTs will provide increased flexibility in the design of novel antibiotic conjugates.

While Chapter 3 focused primarily on investigating the interactions between FpvB and TS, we also looked at how TS interacts with FpvA. Unfortunately, even after identifying important sites for interaction through docking and site-directed mutagenesis and mutagenizing sites important for pyoverdine uptake, we identified no residues that specifically abrogated TS uptake. This result suggests that uptake of TS through FpvA may rely on multiple interactions and that loss of only one at a time is insufficient to prevent uptake. However, using TS may be a viable strategy as single amino acid mutations in FpvA do not confer resistance. We were also unable to identify mutations in *fpvA* in TS-resistant mutants *in vitro,* suggesting that there is a low frequency of mutation in this gene. FpvA is the main transporter for the endogenously-produced high affinity siderophore, pyoverdine, and mutations in this gene compromise iron uptake in nutrient-limited conditions. Loss of *tonB1*, TBDTs for endogenous siderophores such as FpvA, and even some

xenosiderophore transporters can reduce bacterial fitness *in vivo*, which supports our observations[3–5]. These data further support the use of Trojan Horse antibiotics that target FpvA because 1) endogenous transporters are highly expressed, which promotes antibiotic uptake, 2) selective pressure from the antibiotic to inactivate the transporter would reduce bacterial fitness, and 3) narrow-spectrum antibiotics would have reduced side effects on the microbiota compared to broad-range antibiotics.

Targeting transporters that have signaling capabilities could also enhance antibiotic uptake. In Chapter 5, we showed that TC can bind to and be taken up through FoxA. Unlike siderophores bisucaberin and nocardamine however, TC did not trigger a signalling response. Therefore, the design of future siderophore-antibiotic conjugates should take into consideration the self-promoted uptake pathway to further increase drug accumulation inside cells. Previous work showed that plant metabolites containing catechol groups could stimulate the expression of *piuA* and *pirA* to promote the uptake of three siderophore-antibiotics: cefiderocol, MC-1, and BAL30072[6]. However, whether the antibiotic themselves can promote their own uptake is not clear, although select plant phenols with catechol groups induce expression of PiuA and PirA, suggesting that there is redundancy in substrate uptake and downstream signaling[6]. This work also demonstrates the potential of conjugating antibiotics to plant metabolites that stimulate TBDT expression to promote uptake. Many of these metabolites are small aromatic compounds and may be easier to manipulate through medicinal chemistry compared to other natural products.

Investigating thiopeptide uptake across the IM

One of the remaining questions regarding thiopeptide uptake is how they cross the IM. Since the target of the thiopeptides is the ribosome in the cytoplasm, they must cross the IM. In

Chapter 1, we originally hypothesized that because TS is a peptide antibiotic, it may use peptide transport systems. The Npp, Dpp, and Spp systems are known to take up other peptide antibiotics such as pacidamycin, microcin C, and blasticidin[7]. However, mutants defective in these systems were equally susceptible to TS compared to the WT, suggesting that either TS uses different transporters, or it is recognized by multiple redundant IM transporters. One of the differences is that that the thiopeptides are cyclic whereas the latter peptide antibiotics are all linear – this difference may explain why the thiopeptides do not appear to depend on the Dpp, Npp, and Spp peptide transport systems.

An alternative strategy is to use a comparative genomics approach to predict the potential IM thiopeptide transporter based on data for other antimicrobials. For example, uptake pathway of the lassopeptide microcin J25 in *E. coli* is one of the best characterized. It involves initial uptake through the OM using the TBDT FhuA[8,9] followed by uptake through the IM using ATP-Binding Cassette (ABC) transporter protein SbmA[10]. SbmA is important for activity of microcin B17, bleomycin, antisense peptide nucleic acid oligomers, eukaryotic proline-rich antimicrobial peptides, pyrrhococicin, and arasin[11–15]. Interestingly, it was hypothesized that the thiazole rings of bleomycin were recognized by SbmA[12] and we hypothesized that a SbmA homolog in *P. aeruginosa* may be responsible for thiopeptide transport through the IM since thiopeptides are also decorated with thiazoles. However, a BLAST search (E value cut off of $1e^{-4}$) yielded no similar proteins. A similar approach was used to show that the lassopeptide ubonodin targets RNA polymerase of *Burkholderia* spp. using the PupB TBDT, which recognizes the siderophore pseudobactin, for entry[16]. Interestingly, pseudobactin is structurally similar to pyoverdine. To identify the IM protein for ubonodin uptake, the authors conducted a BLAST search using the amino acid sequence of SbmA, which yielded the uncharacterized IM ABC transporter YddA.

YddA was only 25% identical in sequence to SbmA over ~50% of the protein because YddA has an additional cytoplasmic nucleotide binding domain. Despite the low similarity, a *yddA* mutant was resistant to ubonodin, suggesting it is required to transport the lassopeptide into the cytoplasm. Since our efforts to identify a SbmA homolog in *P. aeruginosa* were unsuccessful, we conducted a BLAST search using YddA which yielded 46 hits. Future work will focus on testing mutants lacking each transporter for their susceptibility to TS compared to the WT with the goal of identifying a mutant that is less susceptible to TS.

Some bacteriocins, which are proteinaceous toxins, like the colicins and pyocins, have evolved to use TBDTs to cross the OM. These toxins are multidomain in nature and harbour a receptor binding domain that contains a TonB-like box, a variable cytotoxic domain, and an immunity protein[17–19]. The toxin component can function as a nuclease, DNAse, protein synthesis inhibitor, have peptidoglycan-degrading activity, or disrupt the IM by pore formation. The receptor domain is recognized by an OM, which then interacts with TonB as it transverses through the OM. In *P. aeruginosa,* pyocin S2 exploits FpvA[18] for entry whereas pyocin G uses the Hur TBDT for hemin[20] and pyocins SX1 and SX2 use the uncharacterized TBDT PA0434 (PA14_05640)[2]. Many of these toxins needed to cross the IM to reach their cytoplasmic targets and use an IM transporter. For example, pyocin G, SX1, and SX2 and some colicins are imported via the IM transporter FtsH[2,20,21]. FtsH also has protease activity that processes the toxins by proteolytic cleavage, which releases the cytotoxic domain from the rest of the toxin for import into the cytoplasm[22]. It seems unlikely that thiopeptides would require proteolytic processing to be imported into the cytoplasm as crystal structures of thiopeptides bound to the ribosome show that the full structure interacts with the complex[23] although TS fragments have antibacterial activity. However, it has not been confirmed if the fragments act through the same mechanism[24]. Nonetheless, since there are so

many examples of toxins using FtsH for entry into the cytoplasm, it would be worth testing a *ftsH* mutant for TS and TC susceptibility. Another possibility that has not been considered is that TS and TC may use different IM transporters since their OM transporters (FpvA and FpvB vs FoxA) are also different.

Alternatively, we could raise spontaneously resistant TS mutants to identify the potential IM transporter. In Chapter 3, we raised TS-resistant mutants in liquid media and only identified a mutation in *fpvB* that abolished expression and a missense mutation *tonB1*. While informative, these mutations only supported our previous observation that FpvB and TonB1 are important for TS activity[25,26]. The disadvantage of using liquid media is that the fittest mutants are likely to be selected whereas mutants that may be less fit, but are also TS-resistant, may be missed. Therefore, future efforts should focus on raising mutants on low-iron solid media and a Δ*foxA* Δ*fiuA* background could be used to minimize identifying mutations in *fpvB*. In Chapter 3 we showed that Δ*foxA* Δ*fpvB* and Δ*fiuA* Δ*fpvB* mutants are unable to grow in the presence of ferrioxamine B and ferrichrome respectively; therefore, patching TS-resistant mutants on low-iron media with either siderophore will prevent the growth of mutants with loss of function or expression mutations in *fpvB* and will help identify mutations in other genes.

Uncovering new substrates for TBDTs

Our work in Chapters 3 and 5 suggested that siderophore transporters are promiscuous and can take up multiple ligands. FpvB takes up TS (FpvA), ferrioxamine B (FoxA), ferrichrome (FiuA), and pyoverdine (FpvA). FoxA takes up thiocillin, nocardamine, ferrioxamine B, and bisucaberin (Chapter 3, Figure 6). These findings are consistent with previous reports that single TBDT deletion mutations are not sufficient to reveal the identities of all the transporters that a

particular ligand can use due to potential redundancy[27,28]. Further, the growth conditions that might lead to expression of uncharacterized transporters are unknown, making it hard to assess their potential substrate repertoires. To overcome these limitations, we created a panel of PA14 strains each overexpressing one of the 35 predicted TBDTs of *P. aeruginosa,* plus the TonB1, TonB2, and TonB3 proteins, and named it the Surface Receptor (SURFAR) Platform. The transporters are overexpressed using the arabinose inducible plasmid pHERD20T. Using this platform, we can screen for antimicrobial compounds that use multiple transporters to enter the cell. Understanding how antibiotics cross the OM is essential and can give insight into possible resistance mechanisms. For example, antibiotics that use a single transporter may have higher frequencies of resistance if mutation of a single transporter is sufficient to prevent drug uptake. Meanwhile, antibiotics that can use multiple transporters would be less prone to selecting for resistance. The platform can also be applied to study phage and bacteriocin uptake (Figure 1). We validated the platform by testing TS and TC at sub-MIC levels. As expected, overexpressing FpvA or FpvB sensitized cells to TS. Surprisingly, overexpressing FoxA and ChtA (PA14_61850) also sensitized cells, suggesting that TC may use an additional transporter besides FoxA for uptake. This result was not seen in the initial thiopeptide screen where WT cells were treated with DSX and a thiopeptide, suggesting that FoxA is the dominant TC transporter or that PA14_61850 may not be expressed in 10:90. However, these results further support that TBDTs are promiscuous and using the SURFAR Platform can inform us of other uptake pathways. An example of its utility is an ongoing collaboration with the Brown and Magolan labs, who designed a novel siderophore-monobactam based on a screen conducted in serum[29]. The SURFAR Platform is being used to characterize the uptake pathway for their lead compound, MLLB-22043.

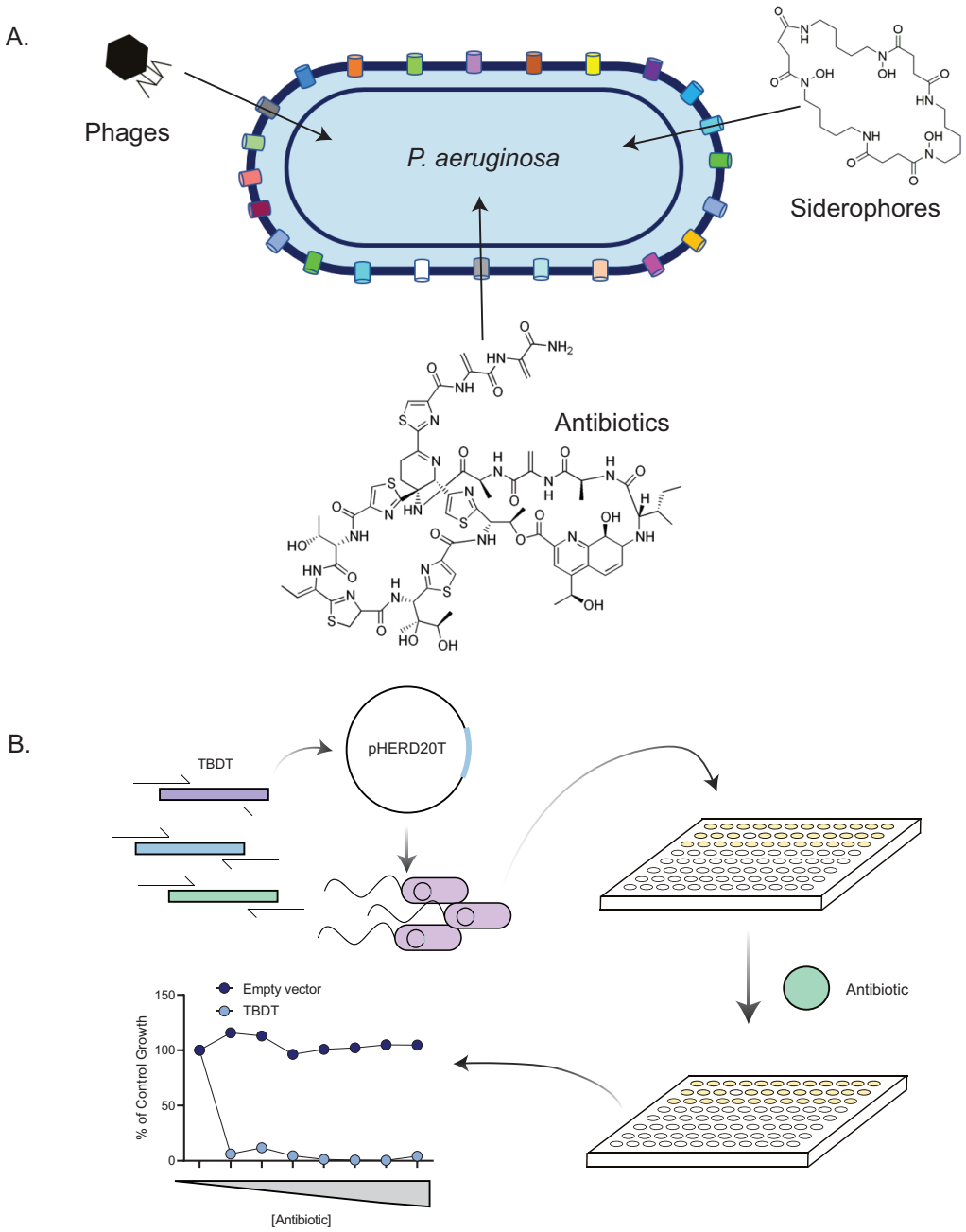

Figure 1. The SURFAR Platform. A) The SURFAR Platform can be used to study phage, siderophore, and antibiotic uptake in *P. aeruginosa*. B) Screening schematic for the platform.

The current limitation of this platform is that it was built in a WT background that still encodes all 35 transporters; therefore, we can only study compounds that inhibit growth. However, we are working to expand the SURFAR platform by generating a mutant lacking all transporters then complemented with one of 35 TBDTs. This strategy has been employed to study *E. coli* efflux

pump substrates and *P. aeruginosa* porin substrates[30,31]. Using this background would allow us to identify the functions of the unknown TBDTs and further understand the range of substrates that can be taken up by each TBDT without the interference from other transporters. As shown in Chapters 3 and 5, if a transporter or multiple transporters for a siderophore are deleted, supplementing the growth media with the siderophore will inhibit growth because it cannot be taken up. Complementing the mutant with a TBDT that can recognize the siderophore will restore growth, allowing us to study uptake of compounds that lack inhibitory activity against WT cells. So far, we have so far knocked out 9 out of 35 transporters and have made deletion constructs for the remaining 26.

An advantage of the SURFAR Platform is that TBDTs that are not normally expressed under normal conditions can be studied. However, one aspect that requires further investigation is the toxicity that results from overexpressing some transporters (PA14_21730, 15070, 47380, 29350, 01870, and 47800) but not others, which may be due to expression under noninducing conditions. OprC (PA14_15070), is a copper transporter that is toxic when overexpressed[32]. It was hypothesized that toxicity may be due to increased accumulation of copper in cells. Further evidence supporting this argument came from inductively coupled plasma mass spectrometry measurements of copper concentrations in an *oprC* mutant and an OprC-overexpressing mutant showed that the overexpression strain contained significantly more copper[32]. However, overexpression of an inactive OprC variant unable to bind copper also induced toxicity, suggesting that the phenomenon is not due to copper accumulation. The results instead suggest that OprC overexpression may be due to altered membrane integrity. This can be tested using the dye NPN, as described in Chapter 6. OM perturbation allows the poorly permeable dye to accumulate in cells and strongly fluoresce. Overall, the reason why some TBDTs induce toxicity all remains unknown;

however, some TBDTs have been crystallized with LPS[33,34]. It is possible that overexpression of some TBDTs may lead to modifications to the LPS or its arrangement that disrupts OM integrity. Measurements of polymyxin B susceptibility will also be informative as strains with a defective OM would be more susceptible to cationic antimicrobial peptides. Nonetheless, the platform is still informative for studying uptake, as expression of most transporters is possible.

So far, TBDTs have only been considered as import transporters. This is not surprising since all known TBDT substrates are imported into the cell. However, a TBDT that exports a protease important in *Myxococcus xanthus* fruiting body maturation was recently reported[35]. This is the first example where a substrate is exported and may explain the function of some uncharacterized TBDTs. It may also help to explain why overexpression of some TBDTs is toxic. Metabolites and proteins that are secreted in the extracellular milieu from TBDT overexpression strains can be analyzed by mass spectrometry for differences compared to empty vector controls. This approach may help reveal the roles of the uncharacterized TBDTs in *P. aeruginosa*.

In conclusion, the information presented in this work corrected the assumption that thiopeptide antibiotics lacked antimicrobial activity against *P. aeruginosa*. The results emphasize the importance of screening in physiologically relevant conditions such as sites of infection. Antimicrobial substrates of various TBDTs can be used as tools to probe the spectrum of substrates that can be taken up through various transporters in different Gram-negative pathogens and can guide the design of novel antibiotic conjugates to treat bacterial infections.

References

(1) Luna, B.; Trebosc, V.; Lee, B.; Bakowski, M.; Ulhaq, A.; Yan, J.; Lu, P.; Cheng, J.; Nielsen, T.; Lim, J.; Ketphan, W.; Eoh, H.; McNamara, C.; Skandalis, N.; She, R.; Kemmer, C.; Lociuro, S.; Dale, G. E.; Spellberg, B. A Nutrient-Limited Screen Unmasks Rifabutin Hyperactivity for Extensively Drug-Resistant *Acinetobacter baumannii*. *Nat Microbiol* **2020**, *5* (9), 1134–1143. https://doi.org/10.1038/s41564-020-0737-6.

(2) Premsuriya, J.; Mosbahi, K.; Atanaskovic, I.; Kleanthous, C.; Walker, D. Mechanism of Targeted Killing of *P. aeruginosa* by Pyocins SX1 and SX2. bioRxiv March 14, 2023, p 2022.10.27.514055. https://doi.org/10.1101/2022.10.27.514055.

(3) Minandri, F.; Imperi, F.; Frangipani, E.; Bonchi, C.; Visaggio, D.; Facchini, M.; Pasquali, P.; Bragonzi, A.; Visca, P. Role of Iron Uptake Systems in *Pseudomonas aeruginosa* Virulence and Airway Infection. *Infect Immun* **2016**, *84* (8), 2324–2335. https://doi.org/10.1128/IAI.00098-16.

(4) Takase, H.; Nitanai, H.; Hoshino, K.; Otani, T. Requirement of the *Pseudomonas aeruginosa* TonB Gene for High-Affinity Iron Acquisition and Infection. *Infect Immun* **2000**, *68* (8), 4498–4504.

(5) Turner, K. H.; Everett, J.; Trivedi, U.; Rumbaugh, K. P.; Whiteley, M. Requirements for *Pseudomonas aeruginosa* Acute Burn and Chronic Surgical Wound Infection. *PLOS Genetics* **2014**, *10* (7), e1004518. https://doi.org/10.1371/journal.pgen.1004518.

(6) Luscher, A.; Gasser, V.; Bumann, D.; Mislin, G. L. A.; Schalk, I. J.; Köhler, T. Plant-Derived Catechols Are Substrates of TonB-Dependent Transporters and Sensitize *Pseudomonas aeruginosa* to Siderophore-Drug Conjugates. *mBio 13* (4), e01498-22. https://doi.org/10.1128/mbio.01498-22.

(7) Pletzer, D.; Braun, Y.; Dubiley, S.; Lafon, C.; Köhler, T.; Page, M. G. P.; Mourez, M.; Severinov, K.; Weingart, H. The *Pseudomonas aeruginosa* PA14 ABC Transporter NppA1A2BCD Is Required for Uptake of Peptidyl Nucleoside Antibiotics. *J Bacteriol* **2015**, *197* (13), 2217–2228. https://doi.org/10.1128/JB.00234-15.

(8) Destoumieux-Garzón, D.; Duquesne, S.; Peduzzi, J.; Goulard, C.; Desmadril, M.; Letellier, L.; Rebuffat, S.; Boulanger, P. The Iron–Siderophore Transporter FhuA Is the Receptor for the Antimicrobial Peptide Microcin J25: Role of the Microcin Val11–Pro16 β-Hairpin Region in the Recognition Mechanism. *Biochem J* **2005**, *389* (Pt 3), 869–876. https://doi.org/10.1042/BJ20042107.

(9) Mathavan, I.; Zirah, S.; Mehmood, S.; Choudhury, H. G.; Goulard, C.; Li, Y.; Robinson, C. V.; Rebuffat, S.; Beis, K. Structural Basis for Hijacking Siderophore Receptors by Antimicrobial Lasso Peptides. *Nat Chem Biol* **2014**, *10* (5), 340–342. https://doi.org/10.1038/nchembio.1499.

(10) Salomón, R. A.; Farías, R. N. The Peptide Antibiotic Microcin 25 Is Imported through the TonB Pathway and the SbmA Protein. *J Bacteriol* **1995**, *177* (11), 3323–3325.

(11) Laviña, M.; Pugsley, A. P.; Moreno, F. Identification, Mapping, Cloning and Characterization of a Gene (SbmA) Required for Microcin B17 Action on *Escherichia coli* K12. *J Gen Microbiol* **1986**, *132* (6), 1685–1693. https://doi.org/10.1099/00221287-132-6-1685.

(12) Yorgey, P.; Lee, J.; Kördel, J.; Vivas, E.; Warner, P.; Jebaratnam, D.; Kolter, R. Posttranslational Modifications in Microcin B17 Define an Additional Class of DNA Gyrase Inhibitor. *Proc Natl Acad Sci U S A* **1994**, *91* (10), 4519–4523. https://doi.org/10.1073/pnas.91.10.4519.

(13) Ghosal, A.; Vitali, A.; Stach, J. E. M.; Nielsen, P. E. Role of SbmA in the Uptake of Peptide Nucleic Acid (PNA)-Peptide Conjugates in *E. coli*. *ACS Chem Biol* **2013**, *8* (2), 360–367. https://doi.org/10.1021/cb300434e.
(14) Mattiuzzo, M.; Bandiera, A.; Gennaro, R.; Benincasa, M.; Pacor, S.; Antcheva, N.; Scocchi, M. Role of the *Escherichia coli* SbmA in the Antimicrobial Activity of Proline-Rich Peptides. *Mol Microbiol* **2007**, *66* (1), 151–163. https://doi.org/10.1111/j.1365-2958.2007.05903.x.
(15) Narayanan, S.; Modak, J. K.; Ryan, C. S.; Garcia-Bustos, J.; Davies, J. K.; Roujeinikova, A. Mechanism of *Escherichia coli* Resistance to Pyrrhocoricin. *Antimicrob Agents Chemother* **2014**, *58* (5), 2754–2762. https://doi.org/10.1128/AAC.02565-13.
(16) Do, T.; Thokkadam, A.; Leach, R.; Link, A. J. Phenotype-Guided Comparative Genomics Identifies the Complete Transport Pathway of the Antimicrobial Lasso Peptide Ubonodin in Burkholderia. *ACS Chem. Biol.* **2022**, *17* (8), 2332–2343. https://doi.org/10.1021/acschembio.2c00420.
(17) Cascales, E.; Buchanan, S. K.; Duché, D.; Kleanthous, C.; Lloubès, R.; Postle, K.; Riley, M.; Slatin, S.; Cavard, D. Colicin Biology. *Microbiol Mol Biol Rev* **2007**, *71* (1), 158–229. https://doi.org/10.1128/MMBR.00036-06.
(18) White, P.; Joshi, A.; Rassam, P.; Housden, N. G.; Kaminska, R.; Goult, J. D.; Redfield, C.; McCaughey, L. C.; Walker, D.; Mohammed, S.; Kleanthous, C. Exploitation of an Iron Transporter for Bacterial Protein Antibiotic Import. *Proceedings of the National Academy of Sciences* **2017**, *114* (45), 12051–12056. https://doi.org/10.1073/pnas.1713741114.
(19) Hilsenbeck, J. L.; Park, H.; Chen, G.; Youn, B.; Postle, K.; Kang, C. Crystal Structure of the Cytotoxic Bacterial Protein Colicin B at 2.5 A Resolution. *Mol Microbiol* **2004**, *51* (3), 711–720. https://doi.org/10.1111/j.1365-2958.2003.03884.x.
(20) Atanaskovic, I.; Mosbahi, K.; Sharp, C.; Housden, N. G.; Kaminska, R.; Walker, D.; Kleanthous, C. Targeted Killing of *Pseudomonas aeruginosa* by Pyocin G Occurs via the Hemin Transporter Hur. *J Mol Biol* **2020**, *432* (13), 3869–3880. https://doi.org/10.1016/j.jmb.2020.04.020.
(21) Walker, D.; Mosbahi, K.; Vankemmelbeke, M.; James, R.; Kleanthous, C. The Role of Electrostatics in Colicin Nuclease Domain Translocation into Bacterial Cells. *Journal of Biological Chemistry* **2007**, *282* (43), 31389–31397. https://doi.org/10.1074/jbc.M705883200.
(22) Chauleau, M.; Mora, L.; Serba, J.; de Zamaroczy, M. FtsH-Dependent Processing of RNase Colicins D and E3 Means That Only the Cytotoxic Domains Are Imported into the Cytoplasm. *J Biol Chem* **2011**, *286* (33), 29397–29407. https://doi.org/10.1074/jbc.M111.242354.
(23) Harms, J. M.; Wilson, D. N.; Schluenzen, F.; Connell, S. R.; Stachelhaus, T.; Zaborowska, Z.; Spahn, C. M. T.; Fucini, P. Translational Regulation via L11: Molecular Switches on the Ribosome Turned On and Off by Thiostrepton and Micrococcin. *Molecular Cell* **2008**, *30* (1), 26–38. https://doi.org/10.1016/j.molcel.2008.01.009.
(24) Nicolaou, K. C.; Zak, M.; Rahimipour, S.; Estrada, A. A.; Lee, S. H.; O'Brate, A.; Giannakakou, P.; Ghadiri, M. R. Discovery of a Biologically Active Thiostrepton Fragment. *J. Am. Chem. Soc.* **2005**, *127* (43), 15042–15044. https://doi.org/10.1021/ja0552803.
(25) Ranieri, M. R. M.; Chan, D. C. K.; Yaeger, L. N.; Rudolph, M.; Karabelas-Pittman, S.; Abdo, H.; Chee, J.; Harvey, H.; Nguyen, U.; Burrows, L. L. Thiostrepton Hijacks Pyoverdine Receptors To Inhibit Growth of *Pseudomonas aeruginosa*. *Antimicrobial Agents and Chemotherapy* **2019**, *63* (9), e00472-19. https://doi.org/10.1128/AAC.00472-19.

(26) Chan, D. C. K.; Burrows, L. L. Thiocillin and Micrococcin Exploit the Ferrioxamine Receptor of *Pseudomonas aeruginosa* for Uptake. *Journal of Antimicrobial Chemotherapy* **2021**, *76* (8), 2029–2039. https://doi.org/10.1093/jac/dkab124.
(27) Normant, V.; Josts, I.; Kuhn, L.; Perraud, Q.; Fritsch, S.; Hammann, P.; Mislin, G. L. A.; Tidow, H.; Schalk, I. J. Nocardamine-Dependent Iron Uptake in *Pseudomonas aeruginosa*: Exclusive Involvement of the FoxA Outer Membrane Transporter. *ACS Chem Biol* **2020**, *15* (10), 2741–2751. https://doi.org/10.1021/acschembio.0c00535.
(28) Chan, D. C. K.; Burrows, L. L. *Pseudomonas aeruginosa* FpvB Is a High-Affinity Transporter for Xenosiderophores Ferrichrome and Ferrioxamine B. *mBio* **2022**, *0* (0), e03149-22. https://doi.org/10.1128/mbio.03149-22.
(29) Weber, B. S.; De Jong, A. M.; Guo, A. B. Y.; Dharavath, S.; French, S.; Fiebig-Comyn, A. A.; Coombes, B. K.; Magolan, J.; Brown, E. D. Genetic and Chemical Screening in Human Blood Serum Reveals Unique Antibacterial Targets and Compounds against Klebsiella Pneumoniae. *Cell Reports* **2020**, *32* (3), 107927. https://doi.org/10.1016/j.celrep.2020.107927.
(30) Teelucksingh, T.; Thompson, L. K.; Zhu, S.; Kuehfuss, N. M.; Goetz, J. A.; Gilbert, S. E.; MacNair, C. R.; Geddes-McAlister, J.; Brown, E. D.; Cox, G. A Genetic Platform to Investigate the Functions of Bacterial Drug Efflux Pumps. *Nat Chem Biol* **2022**, *18* (12), 1399–1409. https://doi.org/10.1038/s41589-022-01119-y.
(31) Ude, J.; Tripathi, V.; Buyck, J. M.; Söderholm, S.; Cunrath, O.; Fanous, J.; Claudi, B.; Egli, A.; Schleberger, C.; Hiller, S.; Bumann, D. Outer Membrane Permeability: Antimicrobials and Diverse Nutrients Bypass Porins in *Pseudomonas aeruginosa*. *Proc Natl Acad Sci U S A* **2021**, *118* (31), e2107644118. https://doi.org/10.1073/pnas.2107644118.
(32) Bhamidimarri, S. P.; Young, T. R.; Shanmugam, M.; Soderholm, S.; Baslé, A.; Bumann, D.; Berg, B. van den. Acquisition of Ionic Copper by the Bacterial Outer Membrane Protein OprC through a Novel Binding Site. *PLOS Biology* **2021**, *19* (11), e3001446. https://doi.org/10.1371/journal.pbio.3001446.
(33) Ferguson, A. D.; Hofmann, E.; Coulton, J. W.; Diederichs, K.; Welte, W. Siderophore-Mediated Iron Transport: Crystal Structure of FhuA with Bound Lipopolysaccharide. *Science* **1998**, *282* (5397), 2215–2220. https://doi.org/10.1126/science.282.5397.2215.
(34) D Ferguson, A.; Welte, W.; Hofmann, E.; Lindner, B.; Holst, O.; Coulton, J. W.; Diederichs, K. A Conserved Structural Motif for Lipopolysaccharide Recognition by Procaryotic and Eucaryotic Proteins. *Structure* **2000**, *8* (6), 585–592. https://doi.org/10.1016/S0969-2126(00)00143-X.
(35) Gómez-Santos, N.; Glatter, T.; Koebnik, R.; Świątek-Połatyńska, M. A.; Søgaard-Andersen, L. A TonB-Dependent Transporter Is Required for Secretion of Protease PopC across the Bacterial Outer Membrane. *Nat Commun* **2019**, *10* (1), 1360. https://doi.org/10.1038/s41467-019-09366-9.